Report no. changed (Mar 2006): SR-124-UU

SACLANTCEN REPORT
serial no.: SR-124

SACLANT UNDERSEA RESEARCH CENTRE

REPORT

THE GIN SEA

Review of physical oceanography and literature from 1972

T.S. Hopkins

July 1988

The SACLANT Undersea Research Centre provides the Supreme Allied Commander Atlantic (SACLANT) with scientific and technical assistance under the terms of its NATO charter, which entered into force on 1 February 1963. Without prejudice to this main task—and under the policy direction of SACLANT—the Centre also renders scientific and technical assistance to the individual NATO nations.

Report no. changed (Mar 2006): SR-124-UU

This document is released to a NATO Government at the direction of SACLANT Undersea Research Centre subject to the following conditions:

- The recipient NATO Government agrees to use its best endeavours to ensure that the information herein disclosed, whether or not it bears a security classification, is not dealt with in any manner (a) contrary to the intent of the provisions of the Charter of the Centre, or (b) prejudicial to the rights of the owner thereof to obtain patent, copyright, or other like statutory protection therefor.

- If the technical information was originally released to the Centre by a NATO Government subject to restrictions clearly marked on this document the recipient NATO Government agrees to use its best endeavours to abide by the terms of the restrictions so imposed by the releasing Government.

Page count for SR-124
(excluding covers)

Pages	Total
i–v	5
1–190	190
	195

SACLANT Undersea Research Centre
Viale San Bartolomeo 400
19026 San Bartolomeo (SP), Italy

tel: 0187 540 111
telex: 271148 SACENT I

NORTH ATLANTIC TREATY ORGANIZATION

Report no. changed (Mar 2006): SR-124-UU

SACLANTCEN SR-124

THE GIN SEA

Review of physical oceanography and literature from 1972

T.S. Hopkins

The content of this document pertains to work performed under Project 04 of the SACLANTCEN Programme of Work. The document has been approved for release by The Director, SACLANTCEN.

Peter C. Wille
Director

Report no. changed (Mar 2006): SR-124-UU

intentionally blank page

Report no. changed (Mar 2006): SR-124-UU

SACLANTCEN SR-124

THE GIN SEA

Review of physical oceanography and literature from 1972

T.S. Hopkins

Abstract: A synthesis and review of the physical oceanography of the GIN Sea (Greenland, Iceland, and Norwegian Seas) is presented. An accompanying bibliography complete from 1972 is included. Emphasis is placed on describing the GIN Sea as a major semi-enclosed basin that plays a function unique among the world's ocean: by providing a strong two-way advective exchange between the ice-covered Polar Sea and the North Atlantic Ocean and at the same time acting as the primary site for Northern Hemisphere bottom water formation. The water masses for the GIN Sea are defined, in a manner as consistent as possible with the literature. The large scale oceanographic and meteorological factors influencing the water mass formation and circulation are described. A sample calculation of the various horizontal and vertical thermohaline-driven exchanges is given.

Keywords: Arctic Ocean o Barents Sea Opening o bathymetry o Bering Strait o circulation o Denmark Strait o Fram Strait o GIN Sea o Greenland Basin o Greenland Sea o Greenland-Scotland Continental Ridge o ice o Iceland-Færo Ridge o Færœse Channel o Iceland Sea o Kolbeinsey Ridge o meteorology o modelling o Mohn Ridge o nordic seas o North Atlantic Ocean o North Sea o Norwegian Basin o Norwegian Sea o oceanography o Polar Sea o water masses

Report no. changed (Mar 2006): SR-124-UU

Contents

Acknowledgement: The author would like to express his appreciation to the Applied Oceanography Group Leader, Henk G. Mulder, for his support in the completion of this research. Also, the author would like to specifically thank Despina Grillaki for her work in categorising the published works in the Annex, Clotilde Pedenovi for assembling the bibliography, and Giuliano Tognarini for the preparation of figures. The author is grateful to Steve Piacsek and Germana Peggion for their contributions to the modelling section and to Harold Dooley, Peter Minnett and Henk Mulder for their helpful criticisms of the text.

Report no. changed (Mar 2006): SR-124-UU

1. Introduction

1.1. PURPOSE OF REVIEW

In the spring of 1984 the Applied Oceanography Group at SACLANTCEN commenced a broad-based oceanographic programme in the Greenland-Iceland-Norwegian (GIN) Sea. An initial phase of this programme has been the preparation of this review, which is intended to provide an assessment of existing knowledge and activity in the region. This assessment has assisted us in designing our observational and modelling programs, the details of which can be found in AOG/SACLANTCEN programme documents. In some sense the present document may also be considered as an update of a previous review conducted for SACLANTCEN in 1974 by **Trangeled**.

Our intent has been to provide a text which both summarizes and synthesizes the observations, analyses, and the knowledge derived therefrom. We do not claim to present a synthesis evenly distributed among all oceanographic topics: the emphasis is on the general nature of the physical oceanography of the GIN-Sea region. For reasons of readability, not every specific work since 1972 is referenced within the text; however, a complete as possible list is included in the Bibliography. Where there seem to be omissions it must be noted that at the time of writing considerable material was not available because it was in preparation, or in press. Some of this category of material is referred to in the text as 'personal communication'.

1.2. HISTORICAL SUMMARY

The **Trangeled** series (1974) gives an historical summary of the GIN Sea activities up to approximately 1973, and we saw no reason to repeat his work in the present document. Table A.1 gives a list of major expeditions in the GIN Sea after 1972. Many of the recent analyses have made use of the data and/or conclusions resulting from these expeditions. For the purpose of this oceanographic synthesis, no distinction has been made with historical sequence of the works reviewed. The reader should also note that the bibliography serves both as a list of references for works cited in the text and as a bibliography for the period 1972–1985.

2. Bathymetry

The bathymetry of a region plays a vital role in the dynamics of its circulations. The geographic setting and the bathymetric connections with other oceanic regions act to determine its thermohaline characteristics. The geomorphology directs and limits its circulation.

The bathymetry of the GIN Sea is complicated and most of it only recently charted. Consequently, certain features and their nomenclature are differently cited in the literature. The purpose of this section is primarily to introduce the nomenclature and terminology used in this report and in the process to cite the major relevant features. More detailed information can be found in specific works, such as **Stocks** (1950), **Balaksin** (1959), **Eggvin** (1963), **Johnson** and **Eckhoff** (1966), **Joseph** (1967), **Beal** (1968), **Perry** (1986) and **Vogt** (1986). Major bathymetric features and land masses are indicated in Fig. 2.1. Additional place names used in the text are separately described or illustrated.

The GIN Sea as referred to herein is the collective waters of the Greenland, Iceland and Norwegian Seas but it has also been collectively referred to as the Norwegian Sea (**Helland-Hansen** and **Nansen**, 1909) or the Nordic Seas (**Hurdle**, 1986). The GIN Sea together with the Polar Sea constitute the Arctic Ocean. The Arctic Ocean is connected to the Pacific Ocean by the continental Bering Sea through the Bering Strait, and to the Atlantic Ocean by sixteen restricted passages through the Canadian Arctic Archipelago to the northwest of Greenland, and by a sequence of three continental ridges to the southeast of Greenland known collectively as the Greenland-Scotland Ridge. The latter connection is approximately an order of magnitude wider than the other two. We have considered the GIN Sea to be within the Arctic Ocean, contrary to its historical geographic inclusion in the Atlantic Ocean, because in a geomorphological sense the bottom is continuously oceanic in crust and in depth through the connecting passage of Fram Strait, whereas the connection through the Greenland-Scotland Ridge is over a continental ridge. Also, the deep thermohaline circulation that we subsequently describe closely links the GIN Sea to the Arctic Ocean. The Polar Sea has two major basins, the Canadian and the Eurasian Basins separated by the Lomonosov Ridge; the two are roughly equivalent in volume (Fig. 2.2) with the Eurasian Basin being slightly deeper and and smaller in volume. The Polar Sea has five continental shelf seas: the Barents, Kara, Laptev, East Siberian, and Chukchi Seas. Only the Barents Sea is shared with the GIN Sea through what we have referred to as the Barents Sea Opening; this major opening connects to the Polar Sea through openings between Spitsbergen and Franz Josef Land and between Franz Josef Land and Novaya Zemlya, both with sills of $\sim$ 200-m depth, the Barents Sea Opening also connects to the Kara Sea via the Karskiye Vorota Proliv Strait with a $\sim$ 75-m sill depth.

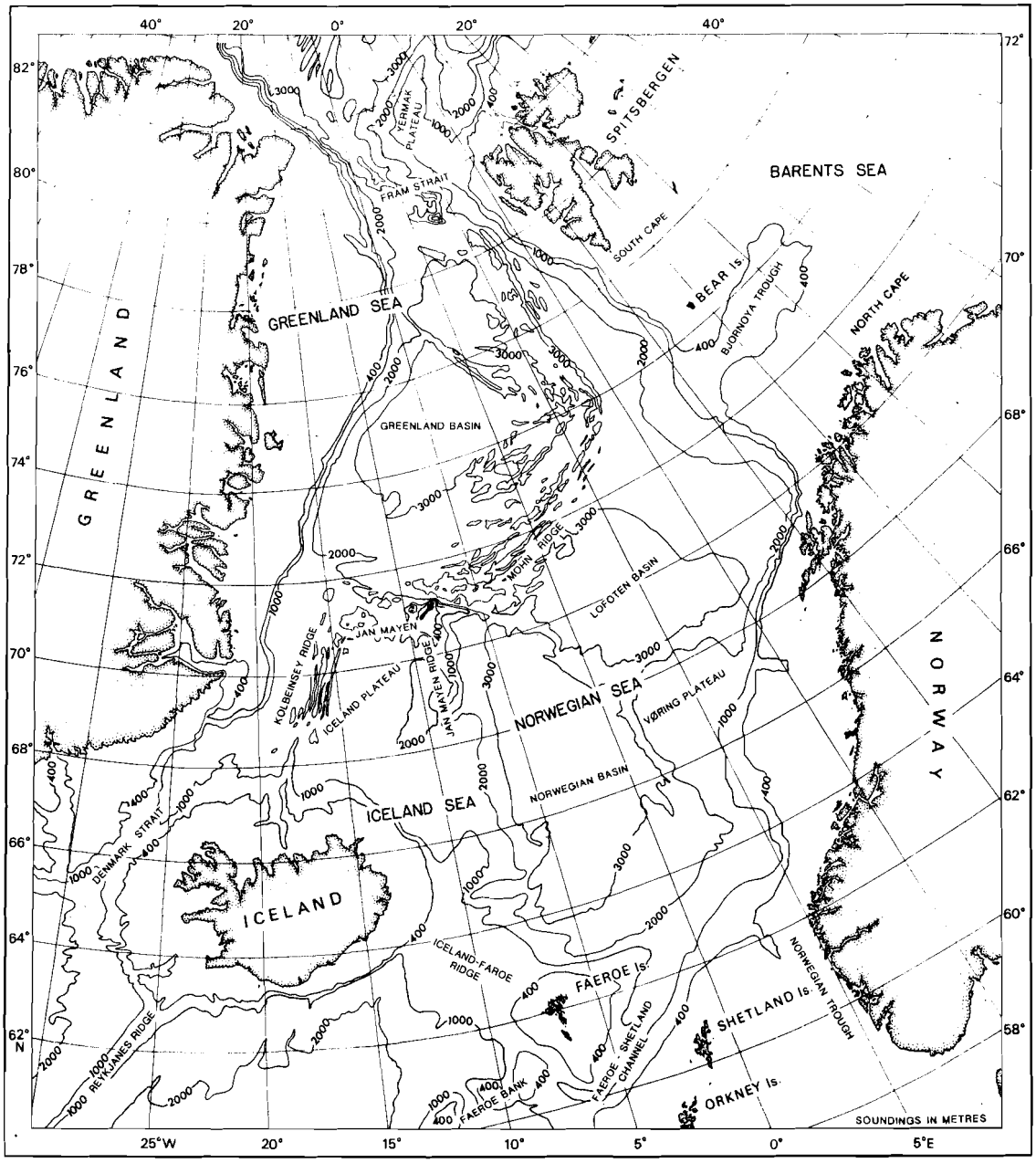

Fig. 2.1. The bathymetry and place names of major features in the GIN Sea area. Depth contours are in meters. Projection is polar-steric, redrawn from **Perry, Fleming, Cherkis, Feden** and **Vogt** (1980). Place names not found on this chart are identified in other figures of the text.

The GIN Sea is about one third of the volume of the Polar Sea (Fig. 2.2) and it also comprises two major basins: the Greenland and Greater Norwegian Basins, separated by a mid-ocean ridge. The Greenland Basin is defined to the east by Greenland, to the west and south by the Mohn Ridge, and to the north by Fram Strait. It has two depressions separated by the Greenland Fracture Zone, of which the northern one is smaller and shallower ($\sim$ 3200 m in depth) than the southern one ($\sim$ 3600 m in depth). The Greenland Sea comprises the waters of the Greenland Basin. The Norwegian Greater Basin comprises a deep depression ($\sim$ 3600 m in depth) of the Norwegian Basin (lying between Jan Mayen Island and the Færœ Islands), a slightly shallower basin ($\sim$ 3200 m in depth) to the north (but to the east of the Mohn Ridge and called the Lofoten Basin) and the Iceland Plateau ($\sim$ 1800 m in depth), which is subdivided into two smaller depressions west and east of Kolbeinsey Ridge.

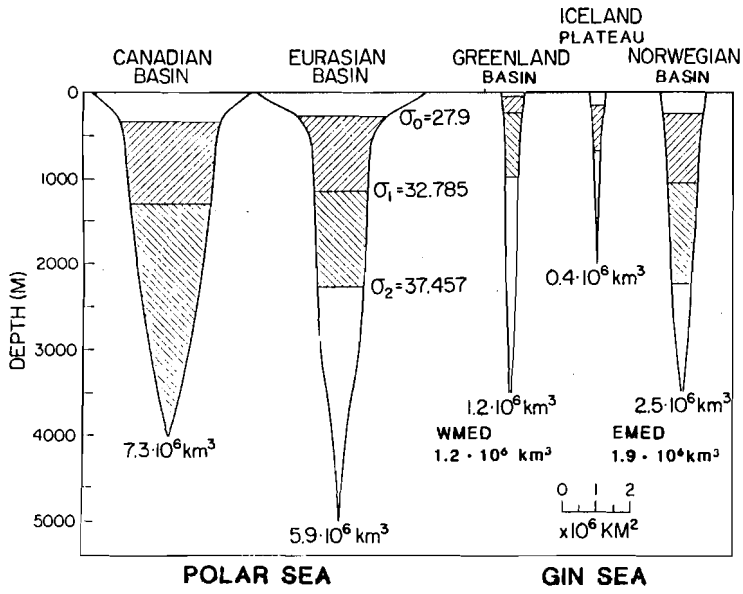

Fig. 2.2. Hypsography of the Arctic Ocean from **Aagaard, Swift,** and **Carmack** (1985). Horizontal coordinate is the area corresponding to the depth interval. Areas were computed from the following, isobaths: 200, 500, 1000, 1500, 2000, 2500, 3000, 3500 and 4000 m. The horizontal bars represent the mean depths within each basin of isopycnal surfaces (indicated by the σ-values) separating the upper, intermediate, and two categories of deep waters. The total volume for each basin is given below the individual hypsographic curves. Those of the Western Mediterranean (WMED) and Eastern Mediterranean (EMED) are annotated for comparison.

The Lofoten Basin is defined to the south by the Jan Mayen fracture zone that extends from Jan Mayen Island to the Vøring Plateau. At a depth of $\sim$ 2400 m the Lofoten Basin extends northward on the eastern side of the Mohn Ridge. The Norwegian Sea consists of the waters between the continental shelves of Norway and Spitsbergen to the east, and the Mohn Ridge and Jan Mayen Ridge to the west. The Iceland Plateau is partly separated from the rest of the Norwegian Basin by the Jan Mayen Ridge that extends southward from that Island. The Iceland Sea is roughly defined as the waters west of Jan Mayen Ridge (at $\sim$ 7°W).

The mid-ocean ridge system continues from the Reykjanes Ridge through Iceland and into the GIN Sea, where it takes the composite form of the Kolbeinsey Ridge and the Mohn Ridge. These two ridges have numerous unnamed transverse gaps, some of which are very important in the exchange of waters between and within basins, e.g. the broad saddle (at a depth of $\sim$ 2400 m) across the Mohn Ridge at $\sim$ 75°30′ N and the two gaps north and south of Kolbeinsey Ridge that lie directly northeast of Jan Mayen Island. The western depression of the Iceland Plateau and the southern depression of the Greenland Basin are connected (at a depth of $\sim$ 1600 m) between the Greenland continental slope and the westernmost portion of the Mohn Ridge by the Greenland-Jan Mayen Gap.

The GIN Sea has six open boundaries through which important exchanges occur. Fram Strait is the only oceanic boundary and it exchanges with the Polar Sea; three of the boundaries exchange with the Atlantic Ocean over the continental Greenland-Scotland Ridge, and the remaining two exchange with the continental shelf seas, the Barents Sea in conjunction with the Polar Sea, and the North Sea in conjunction with the Atlantic Ocean. We have prepared Figs. 2.3a–f to assist in comparing the dimensions of these six openings. Because the sill depth does not always lie on the narrowest cross-section, we have included the projected sill areas for comparison. The projected sill area is the minimum bathymetric crossection projected onto a straight transect. Further particulars of each opening are given in Sect. 5.

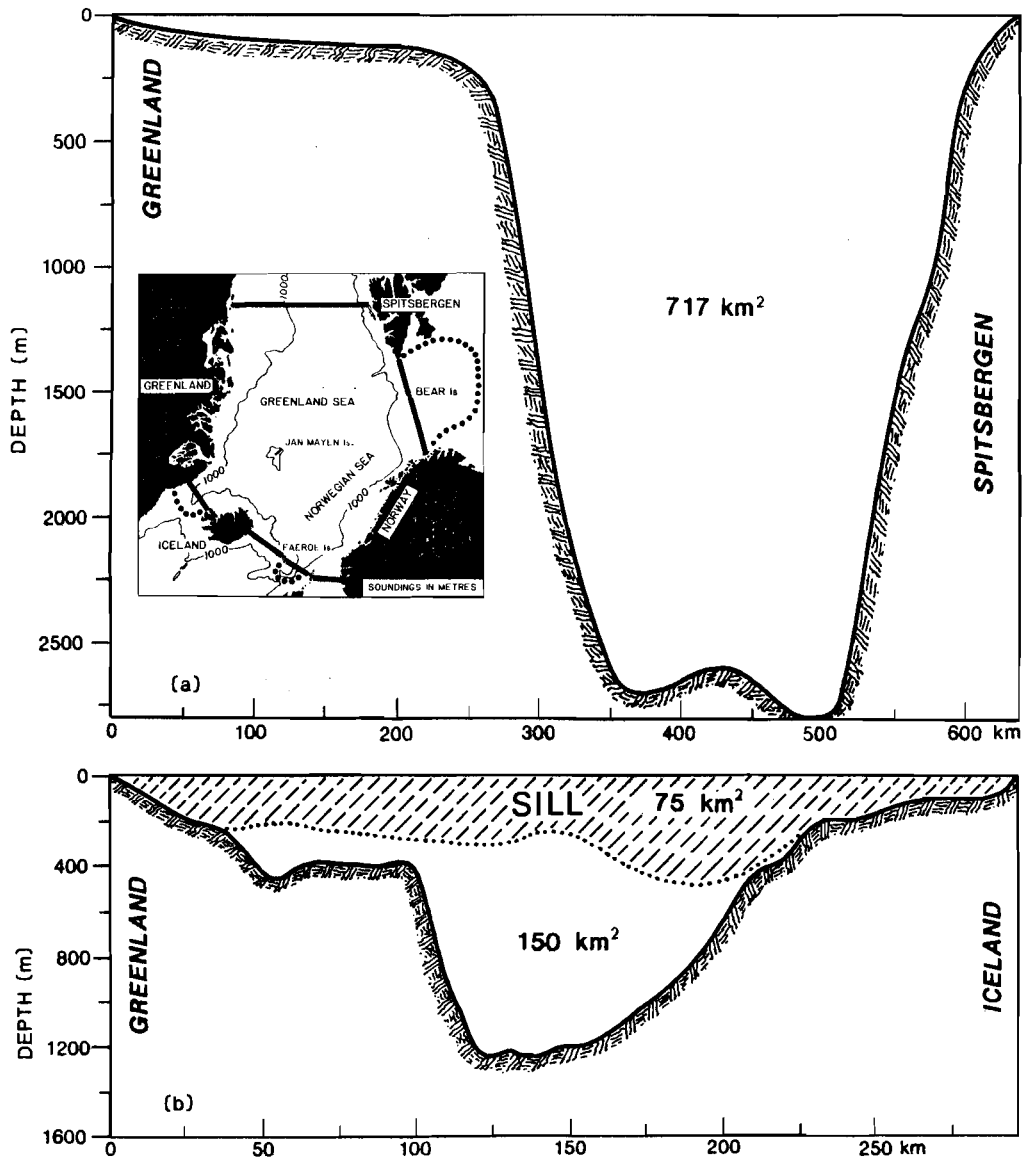

Fig. 2.3. The cross-sectional profiles of the GIN Sea openings. (a) Fram Strait with locator map, (b) Denmark Strait. The hatched profiles are the projected areas across the sills.

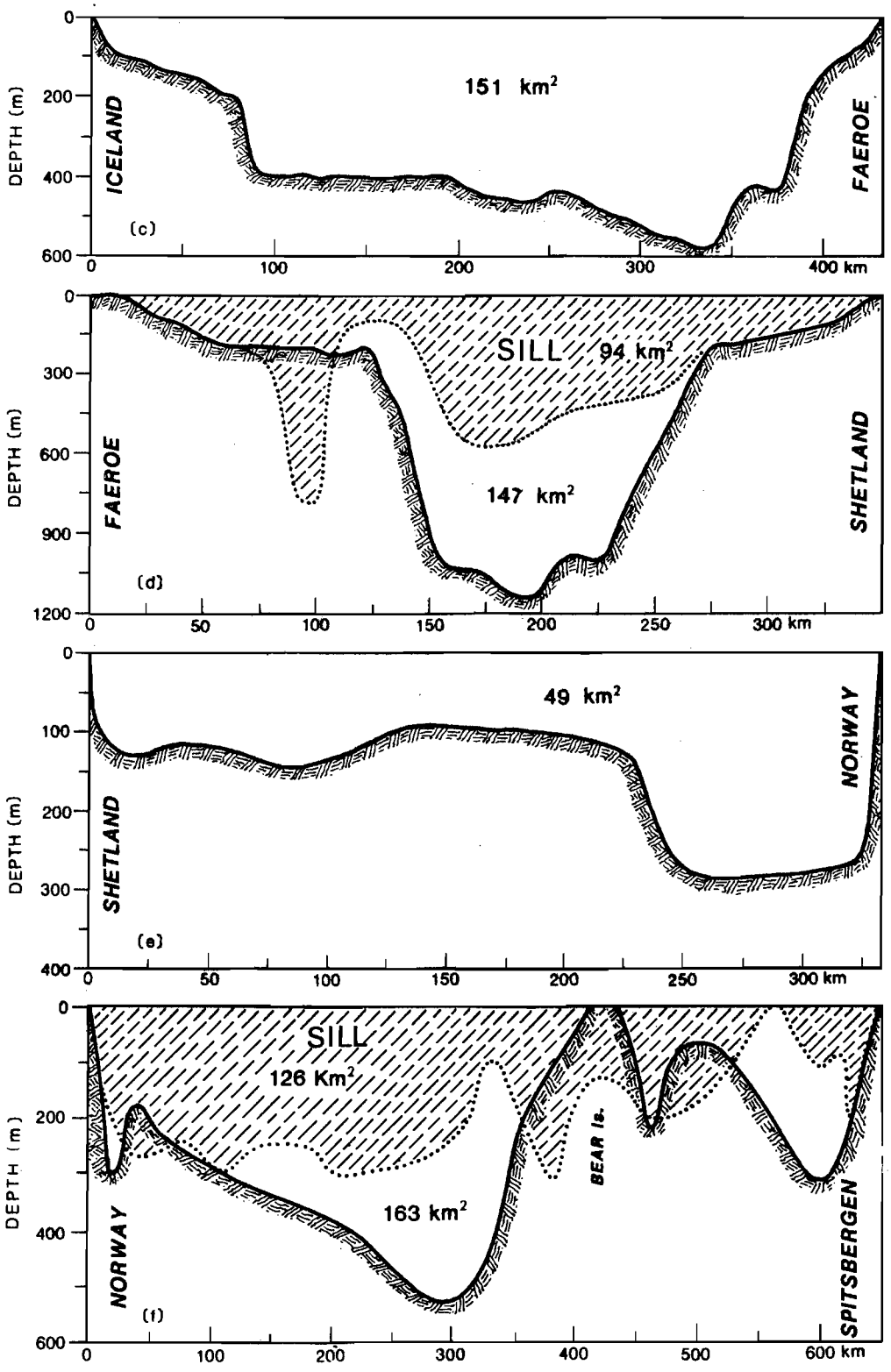

Fig. 2.3 (cont.). (c) Iceland-Færœ Ridge, (d) Færœse Channel, (e) North Sea Entrance and (f) Barents Sea Opening. The hatched profiles are the projected areas across the sills.

3. Meteorology

The following brief description of the GIN Sea meteorology is included as reference information for the discussions pertaining to momentum, heat, and mass exchange with the atmosphere. The climatology of the region has not often been described separately, as in **Gathman** (1986) or **Puls** and **Meincke** (1975); more frequently it has been included in descriptions and atlases of the Polar region (e.g. **Orvig**, 1970 and **Gorshkov**, 1983) or the North Atlantic region (e.g. **Meserve**, 1974). Synoptic data sources are available, for example, through the Norwegian Meteorological Office, the UK Meteorological Office, (Bracknell), the Koninklijk Nederlands Meteorologisch Institut (KNMI), and the US Fleet Weather service.

3.1. PRESSURE AND WIND

The GIN Sea does not conveniently lie within one of the world's climatic regions. In fact, its meridional extent, from $\sim 60°$ to $\sim 80°$N, is bifurcated by the 70°N latitude which nominally divides the region of polar easterlies from that of the westerlies. This division would be better described as running northeastward from Iceland to Bear Island, as indicated by the mean position of the Arctic front in Fig. 3.1a, and which, we note, approximately separates the Norwegian Sea from the Greenland and Iceland Seas.

Before remarking further on this division of climate, we look first at the atmospheric surface pressure field for the northernmost latitudes. The prominent features are: (1) two lows pressure cells, the Icelandic and the Aleutian, located at approximately the latitude of 60°N in the North Atlantic and North Pacific, respectively; and (2) two highs pressure cells, the Siberian and McKenzie, located at approximately the latitude of 70°N but connected somewhat by a ridge over the Canadian Basin. The distribution of these four cells is not symmetrical about the North Pole, such that the GIN Sea region is primarily influenced by the Icelandic Low and secondarily by the high pressures over the Polar Sea. The strong pressure gradients around Greenland are considered spurious in the sense that they are not entirely indicative of geostrophic air flow but are somewhat a static artifact of the the anomolously cold temperatures over Greenland.

During winter the Icelandic Low is most intense and it is most extensive: the 1010 mb isobar encompasses all of the Barents Sea and much of the Eurasian Basin nearly to the North Pole, Fig. 3.2b. The warm ocean temperatures underneath the Icelandic Low help sustain that feature by heating the atmosphere and causing a sea surface air convergence. Hence, the configuration of the Icelandic Low tends to be elongated to the northeast over the warm Norwegian Atlantic Current. The sea temperature

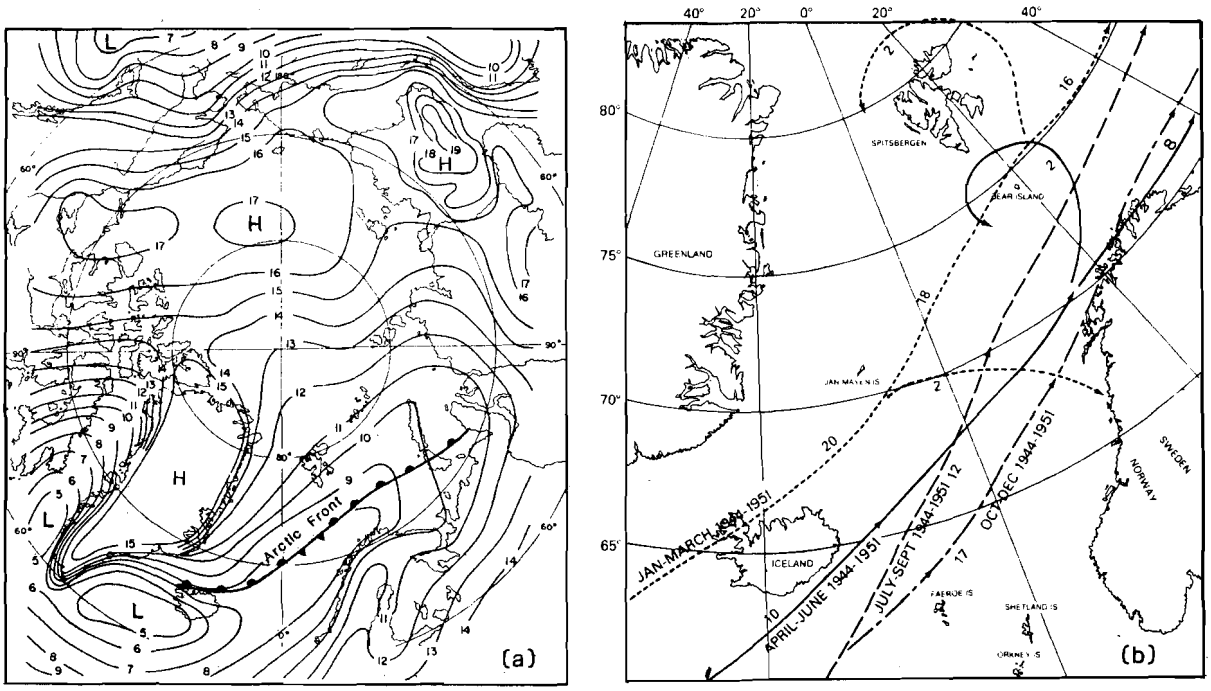

Fig. 3.1. (a) Annual mean air pressure (mbar), from **Vowinckel** and **Orvig** (1970). The position of the arctic front is from (b) The mean tracks of low-pressure centres (severe storms). The numbers along the tracks indicate the relative frequency of the storms. [From **Gathman** (1986).]

gradients, between the waters north and south of Iceland, are greatest during winter (as in Fig. 4.5a,d below), and contribute to the seasonal intensity of the Icelandic Low. The trough, or the elongated portion of the low, is not synoptic over a month but is the result of a mean of higher frequency cyclonic disturbances traveling along its axis (Fig. 3.1b). In this trough, the mean wind speeds are greatest (Fig. 3.2c) but, because of variablity, the resultant winds (Fig. 3.2a) are much less and spatially incoherent. On the southeastern portion of the trough the winds are more consistently from the southwest. To the north of the low, the increasing pressures drive polar easterlies that are fairly steady, and prevail in the region to the north and west of a line connecting northwestern Iceland to Bear Island (Fig. 3.2a).

The winter situation lasts through March when the Icelandic Low rapidly begins to fill and the Polar High to build, Fig. 3.3b. The easterlies extend further southward, i.e. to a line from Iceland to North Cape (Fig. 3.3a). Over the Norwegian Sea the incidence of cyclones is diminished and their mean track is shifted to the southeast (Fig. 3.1b). Both the mean and the resultant wind speed of the southwesterlies decrease over the Norwegian Sea while they remain nearly the same over the Greenland Sea (Figs. 3.3c and 3.3a, respectively). In July the atmospheric pressure

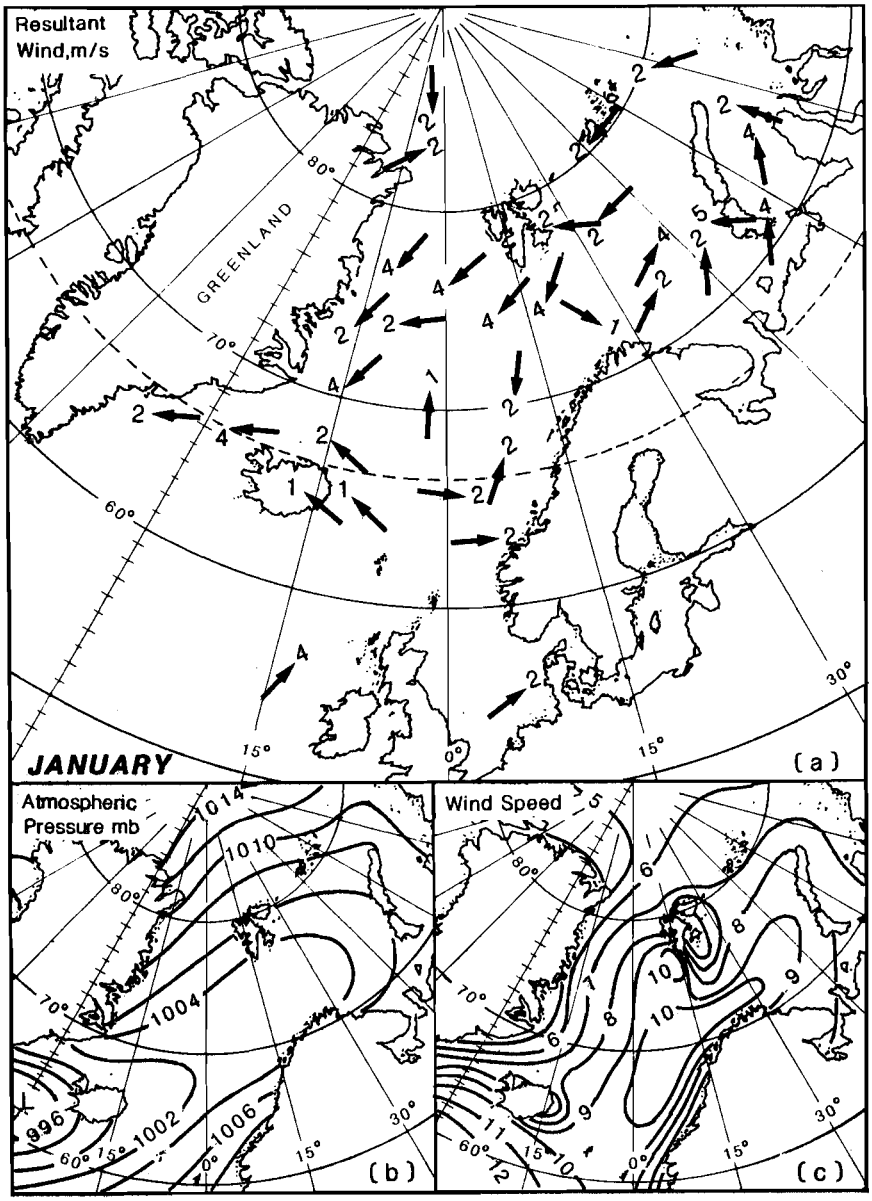

Fig. 3.2. (a) The resultant wind vectors at the ocean surface for January. Arrows labeled 1 represent resultant speeds < 1 m/s, those with 2 represent 1 to 3 m/s, those with 4 represent 3–5 m/s, and those with 5 represent > 5 m/s; (b) The mean atmospheric pressure (mbar) for January; (c) The average wind speed for January. [Redrawn from **Gorshkov** (1983).]

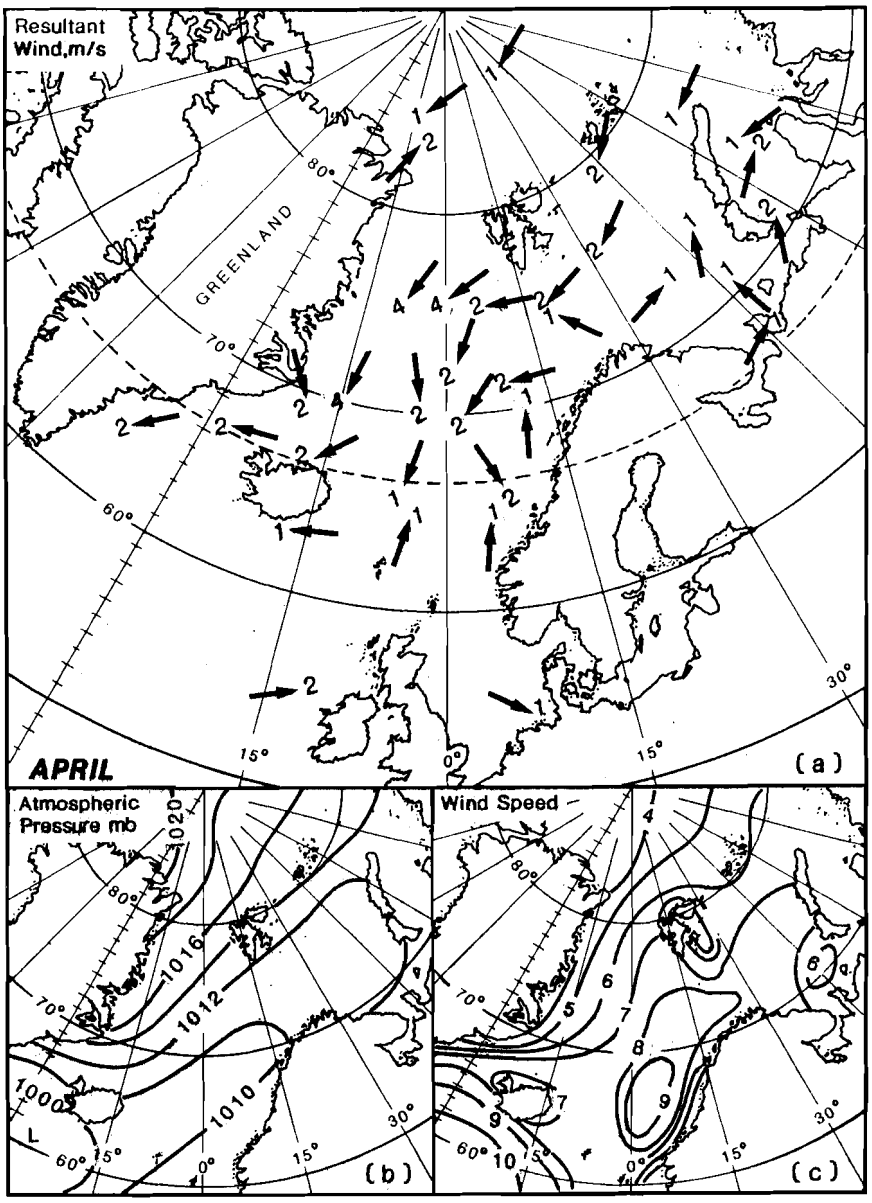

Fig. 3.3. (a) The resultant wind vectors at the ocean surface for April. Arrows labeled 1 represent resultant speeds < 1 m/s, those with 2 represent 1 to 3 m/s, those with 4 represent 3–5 m/s, and those with 5 represent > 5 m/s; (b) The mean atmospheric pressure (mbar) for April; (c) The average wind speed for April. [Redrawn from **Gorshkov** (1983).]

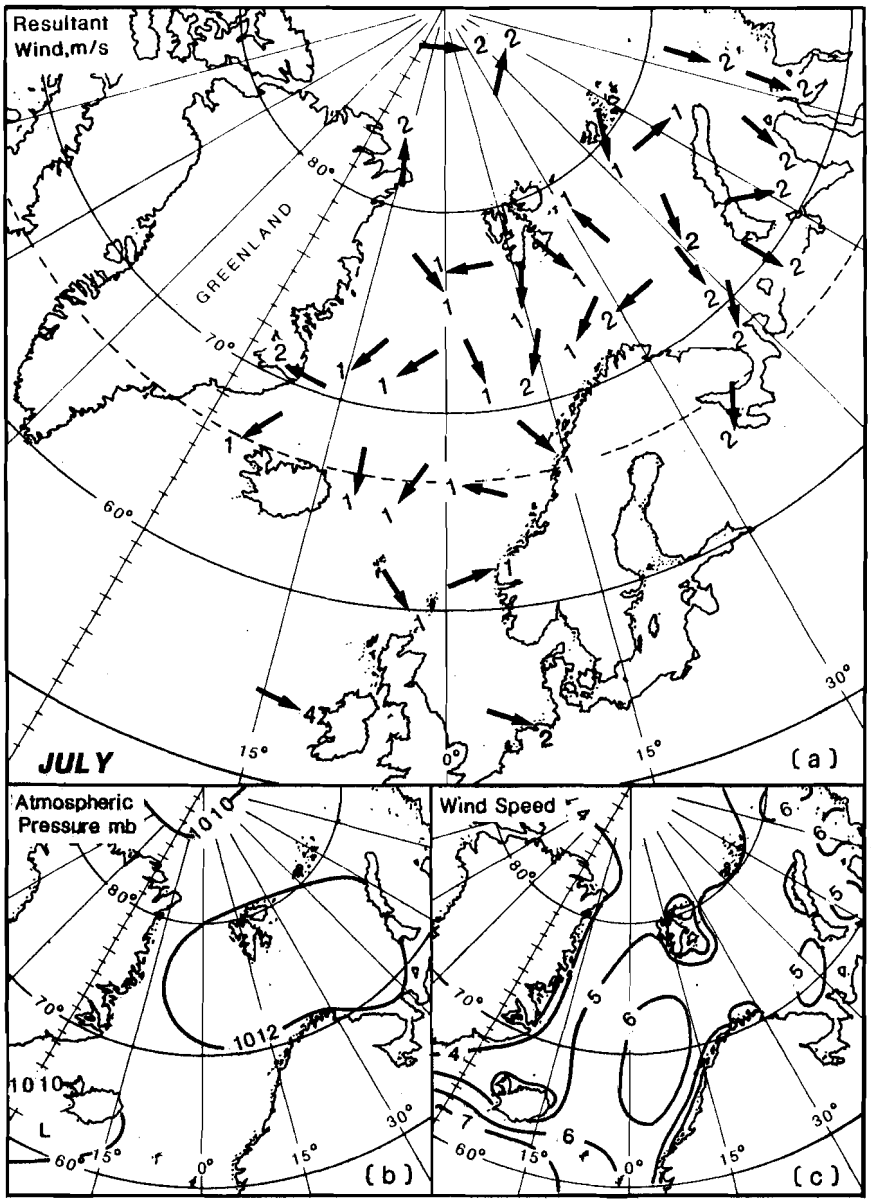

Fig. 3.4. (a) The resultant wind vectors at the ocean surface for July. Arrows labeled 1 represent resultant speeds < 1 m/s, those with 2 represent 1 to 3 m/s, those with 4 represent 3–5 m/s, and those with 5 represent > 5 m/s; (b) The mean atmospheric pressure (mbar) for July; (c) The average wind speed for July. [Redrawn from **Gorshkov** (1983).]

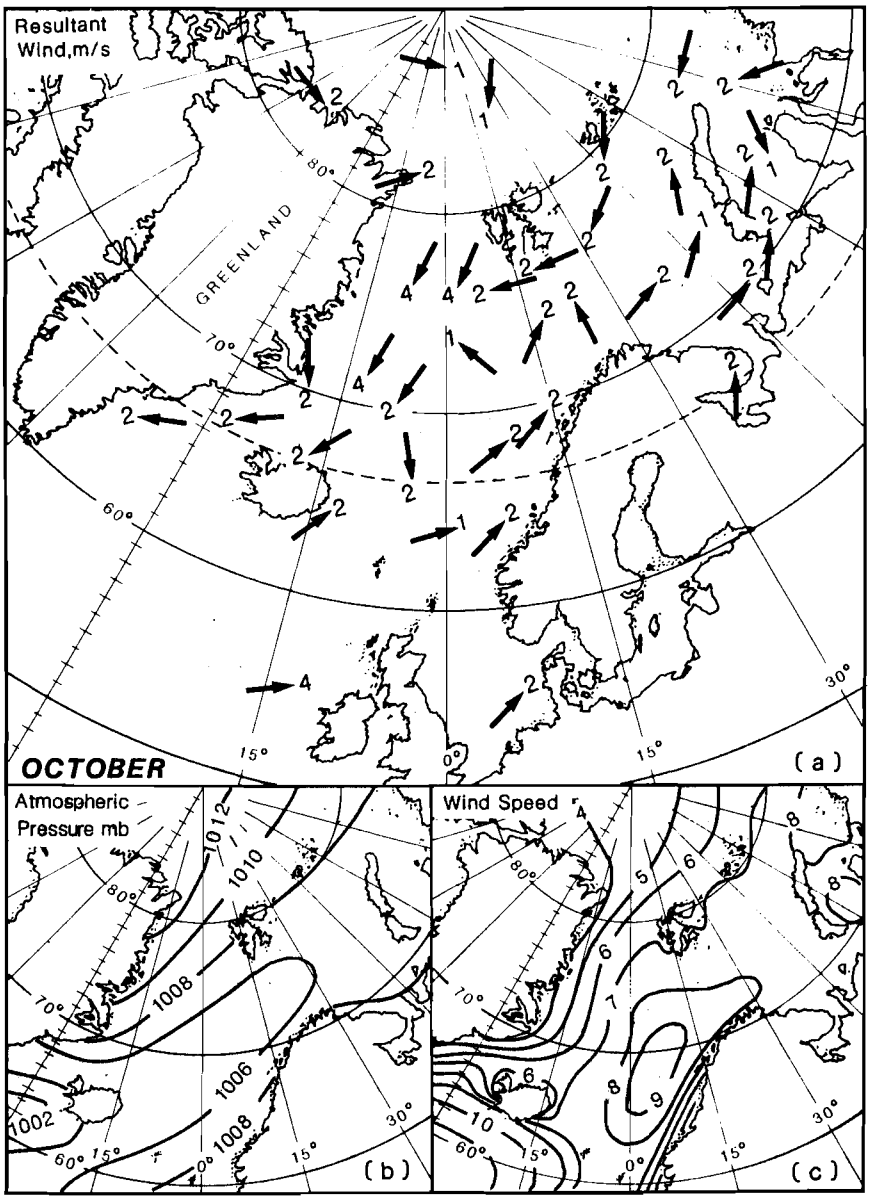

Fig. 3.5. (a) The resultant wind vectors at the ocean surface for October. Arrows labeled 1 represent resultant speeds < 1 m/s, those with 2 represent 1 to 3 m/s, those with 4 represent 3–5 m/s, and those with 5 represent > 5 m/s; (b) The mean atmospheric pressure (mbar) for October; (c) The average wind speed for October. [Redrawn from **Gorshkov** (1983).]

gradients are minimal. The Icelandic Low remains as a weak low, and is separated from another weak low over the North Pole by a weak high centered over Bear Island (Fig. 3.4b). Spatial coherence in the resultant wind field is weak (Fig. 3.4a) with the strongest winds still occurring over the Lofoten Basin and in the North Atlantic (Fig. 3.4c).

During fall, the Polar High continues to build and to move toward a position over the Canadian Basin (Fig. 3.5b). As a result a greater and more extensive pressure gradient develops over the northern GIN Sea which resembles that of spring and drives northeasterly winds over the Greenland (Fig. 3.5a) and Eurasian Seas. During the fall-winter transition, the mean pressure gradient strengthens slightly over the GIN Sea with most of the with high latitude changes occurring in the building toward the winter maxima of the Siberian and McKenzie Highs. During fall, the Icelandic Low deepens towards its winter minimum. The incidence of cyclones over the Norwegian Sea increases as do the mean and resultant winds, Figs. 3.1b and 3.5a,c, respectively.

Thus the mean winds and their seasonality differ significantly between the northwest and southeast sectors of the GIN Sea. To the northwest, the mean wind speed is $\sim$ 5 m/s with a light seasonal signal ± 1 m/s from winter to summer. Spatial coherence and consistency are likely to be greatest in the spring and fall (northeasterlies). During winter, there is a greater tendency or incidence of cyclonic storms intruding from the south. To the southeast, the winds are dominated by the frequent (Fig. 3.1b) cyclonic storms emanating from the Icelandic Low and traveling towards the Barents Sea. These produce greater mean speeds $\sim$ 8 m/s but with considerable temporal variability and with spatial scales less than the dimension of the Norwegian Sea. The seasonal cycle is strong with a maximum in early winter, and minimum in early summer.

3.2. HEAT AND WATER EXCHANGE

Quantitative assessments of the heat and water exchange with the atmosphere for the GIN Sea are among the least reliable of any region of the world ocean, particularly when judged relative to the thermohaline importance of that Sea. Data come from scant shore-based meteorological observations, which often are not representative of offshore conditions, from ship data, which are not spatially or temporally synoptic, and from some remotely-sensed observations. An important exception is the Ocean Weather Station *'M'*, which has recorded meteorological and oceanographic information since 1948 at approximately 66°N and 2°E over the Norwegian continental slope (**Mosby**, 1950), but which can not serve as representative of the entire GIN Sea. In fact when treated as an integral surface for ocean-atmoshere exchange, the GIN Sea presents large non-uniformities (incident radiation and albedo) due to its meridional extent, its different climatology (anticyclonic and cyclonic conditions),

and its partial ice coverage (differing exchange processes). Any assessment of the net heat exchange must involve estimates of advective heat transfer, which for the GIN Sea is anomalously large (see Subsect. 5.4).

Vowinckel and **Orvig** (1970) have compared the relative heat exchange components for Arctic ice-open water and Polar ice-cover conditions, summarized in Table 3.1. Over ice-covered regions, the reflection of incoming radiation is much increased, and the amount of incident radiation is less due to the higher latitude. In partial compensation for the reduced incoming radiation is a reduction in the loss in the net back radiation over the ice-covered regions. Furthermore, because the ice acts to insulate the ocean from the atmosphere, the evaporative and sensible heat losses are also reduced. Thus, the exchange of radiation between the ocean and atmosphere is more nearly in balance in the Polar ice-covered regions than in the Arctic ice-free regions, which as a consequence require considerably more advective heat (Q_v), as shown in Table 3.1. We note that the term Q_o represents the heat received at the surface which, in the case of ice cover, is much less than the heat adsorbed by the underlying water where the opacity of the ice and its low conductivity cause additional reductions in the amount of incoming heat. These differences result in a profound difference in the degree of vertical heat exchange forced by the surface boundary condition between the ice-free and ice-covered regions of the Arctic.

Table 3.1

Relative components of major heat exchange terms expressed as percentage of the total annual radiation available at the top of the atmosphere[1]

	Incoming				Surface losses			Subsurface gain[2]
	Q_o	Q_r	Q_s	Q_a	Q_b	Q_e	Q_h	Q_v
Arctic (ice free)	37	11	37	15	28	20	12	23
Polar (ice covered)	23	30	33	14	24	2	3	6

[1] Notation: Q_o= net incoming at surface, Q_r= atmospheric reflected, Q_s= atmospheric scattered, Q_a= atmospheric absorbed, Q_b= net back, Q_e= evaporative, Q_h= sensible, Q_v= net heat, or equal to heat supplied by ocean.

[2] Subsurface gain is the difference between the incoming and the surface losses.

The values of Table 3.1 are annual averages. The most important temporal change is in that of the incoming radiation, since for latitudes $\sim 70°$N the sun is above the horizon during summer and below it during winter. The Q_r and Q_s terms also have

a seasonal variation because both phenomena of reflection and scattering depend on the sun's elevation. The surface losses are dependent on prevailing weather conditions. Particularly important is the dependence in Q_b on atmospheric water vapor. As **Vowinckel** and **Orvig** (1970) point out, the presence of clouds at such high latitudes has a significantly different effect from winter to summer. That is, for clear winter skies, the lack of atmospheric water vapor makes the net loss due to Q_b more than the increase in Q_o; whereas, clear summer skies make the net gain greater because the gain realized by a larger Q_o is greater than the loss of a smaller Q_b. Hence, cloudy summers and clear winters are detrimental to the net gain of heat by the ocean. Also, winter anticyclonic conditions increase the evaporative and sensible heat losses. Since these turbulent exchange terms, both Q_e and Q_h, dependent on the sea-air temperature difference, we expect the greatest heat losses to occur where the waters of the Norwegian Atlantic Current under the winter anyticyclonic conditions.

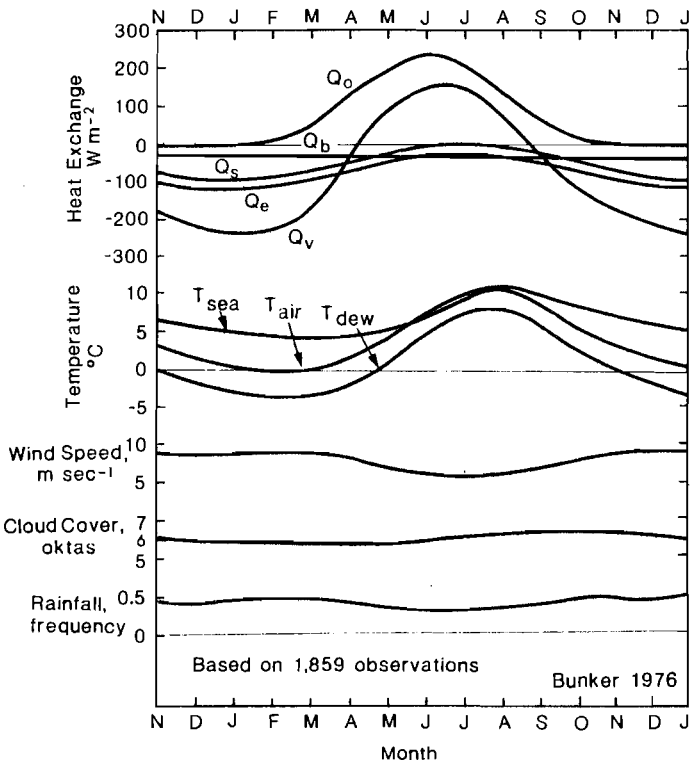

Fig. 3.6. The annual cycle of indicated parameters over the Norwegian Sea area, 71°N, 17°E [from **Bunker** (1976)]. The heat exchange parameters are defined in the text.

Estimates of the various terms for the GIN Sea are available from several sources. The rates of air-sea exchange processes of the region have been estimated by **Bunker** (1976) from an analysis of ships' observations. The seasonal variability is shown in Fig. 3.6. The net heat budget (Q_v) is positive for less than five months from April to mid-August. A winter minimum in mid-January and a summer maximum in mid-June causes the spring transition to be sharper than that of fall. The mean back radiation shows little variation because of correspondingly little variation in reported cloud cover. The evaporative and sensible heat terms have winter maxima due to the larger winter differences in sea, air, and dew-point temperatures. **Bunker** (1976) found a region of maximum evaporation (< 100 cm/yr) centered over the Lofoten Basin, which amounts to less than a third of the evaporative heat loss maximum found in the North Atlantic (centered over the Gulf Stream at $\sim 38°$N and 65°W).

The analysis of **Bunker** (1976) was focused in the North Atlantic and showed only enough spatial resolution in the GIN Sea to indicate the northwest-southeast differences. **Esbensen** and **Kushnir** (1981) prepared the heat budget terms for the global ocean at approximately $5° \times 5°$ resolution for use in global numerical models. They used the marine observations of the US National Climatic Center and an atlas of cloudiness prepared by **Berliand** and **Strokina** (1960). As with **Bunker** the resolution in the GIN Sea is limited.

The treatments of **Vowinckel** and **Orvig** (1970) and **Gorshkov** (1983) both focus on the Arctic Ocean and therefore provide better spatial resolution in the GIN Sea region. Both of these rely less on ship observations, and more on other data sources. All analyses differ somewhat, dependent on data and method (see also, **Fletcher**, 1966; **Scor Working Group 58**, 1979). The figures presented below were chosen from the **Gorshkov** (1983) atlas on the basis of completeness not necessarily on accuracy.

The amount of short wave solar radiation available at the surface differs considerably from the simple meridional dependence that dominates the amount of ratiation at the top of the atmosphere. In Fig. 3.7a,b,c are shown the distributions of Q_o for annual, February, and August averages, respectively. For the annual and August averages the combined effects of cloud cover and solar elevation are evident, i.e. a broad minimum over the northeastern GIN and Barents Seas. North of 70°N, the August cloudiness is actually greater than that of February, as Fig. 3.8 shows. However this does not produce a high-latitude minimum in August because there the trasmissivity of the clouds is greater (**Vowinckel** and **Orvig**, 1970). The February reduction in cloud cover is an indication of the dominance of anticyclonic easterly weather conditions at the more northern latitudes. Because the February solar input is so low, the absorbed radiation is not correspondingly increased (Fig. 3.6b).

In addition to the short-wave radiation, the surface is also heated by long-wave radiation emitted from the atmosphere. This 'counter' radiation should be considered as a separate heat source. It is not directly coupled to the diurnal and seasonal solar cycles; and at high latitudes it is significantly larger than the solar input, for

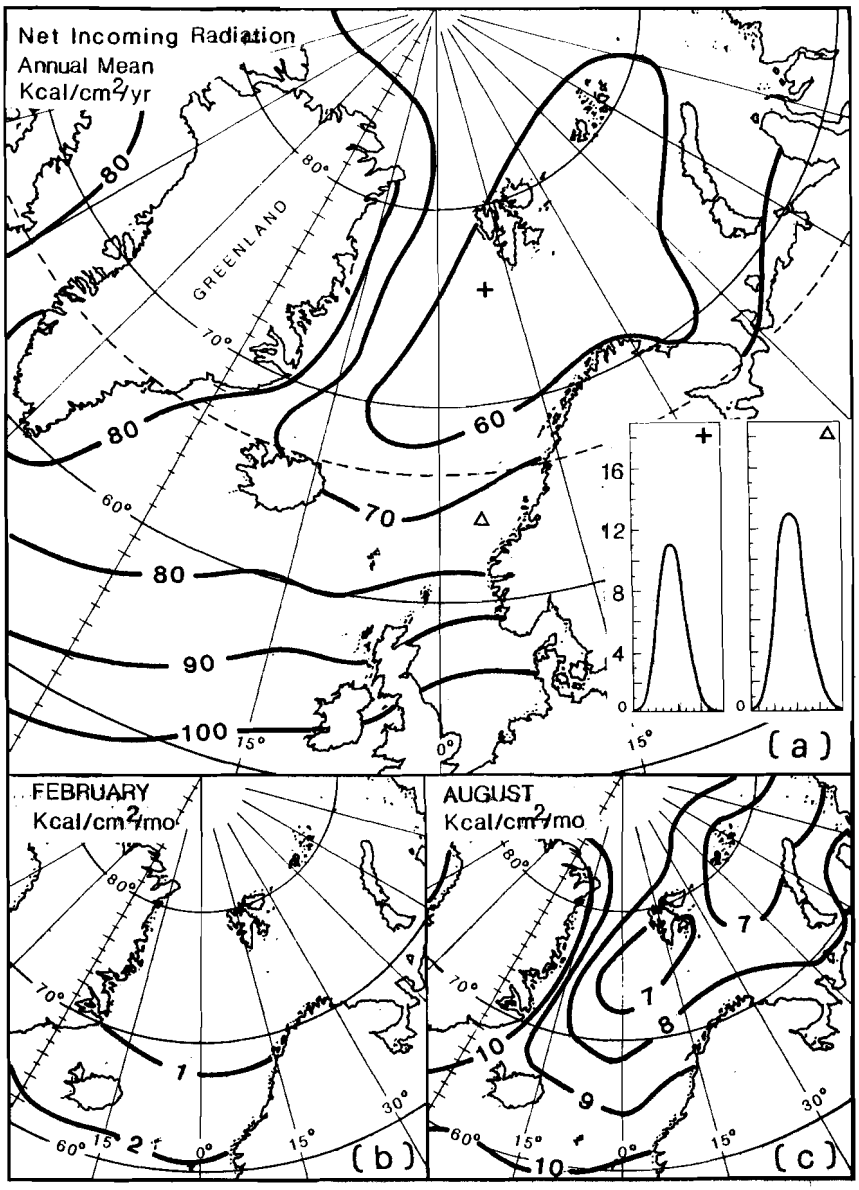

Fig. 3.7. The distribution of the net incoming radiation, Q_o, for (a) annual mean, (b) monthly mean of February and (c) end of August. The annual cycle for two locations (indicated by the symbols + and △) are shown in the inserted panels. The vertical axis is in kcal/cm^2/yr and the horizontal axis in months. Note, 60 kcal/cm^2/yr corresponds to $\sim$ 80 W^2/m^2 and 8 kcal/cm^2/mo corresponds to $\sim$ 130 W^2/m^2. [From **Gorshkov** (1983).]

example, for the GIN Sea the annual average ratio is about 4 : 1 and even in June it is about 2 : 1 (**Vowinckel** and **Orvig**, 1970). Instead of being considered separately, it is commonly combined with the long wave heat emitted from the sea surface to form a net 'back' radiation, Q_b. Both of these emissions follow the Stefan-Boltzman black-body radiation dependence of the fourth power of the temperature. In the case of the radiation from the sea, the estimation is simplified by the fact that the sea-surface temperature can be easily measured and averaged over monthly-or-less time scales. On the other hand, the atmospheric temperature is not only more difficult to measure but the counter radiation has a strong nonlinear dependence on the amount of water vapor and carbon dioxide. The atmospheric water vapor content is difficult to measure and average. Furthermore, the counter radiation has a dependence on cloud type, height and cover; it is also difficult to measure and data are practically nonexistent during periods of darkness. As a result, Q_b is estimated via empirical formula (e.g. **Lind** and **Katsaros**, 1982) with an accuracy which deteoriates with the sparseness of the data.

Figure 3.9a,b,c show the distributions of Q_b for the annual, February, and August averages, respectively. The term is larger for clear sky conditions (counter radiation reduced) and smaller for cloudy conditions; it is greater over Greenland and is less over the Norwegian Sea (cf. Fig. 3.8). The warmer surface temperatures during the less cloudy conditions of February cause a Q_b maximum over the West Spitsbergen Current (Fig. 3.9b). (We note that the **Gorshkov** values are over twice that of **Vowinckel** and **Orvig**.) Regardless of the amount, the cloud cover of the Norwegian sea insulates that region reducing Q_b, whereas the incidence of anticyclonic weather over the warm-water regions of the Greenland Sea allows significant long-wave radiation losses.

The evaporation and sensible heat loss terms are also difficult to measure and average. Both depend directly on the sea-air temperature difference and indirectly on the wind. Q_e depends also on the water vapor pressure at the sea surface. The role of the wind is to increase the flow of air over the surface particularly under unstable conditions when the convective upward component prevents a sea-air equilibration in both temperature and water vapor content. Thus there is an implicit dependency on the wind direction rendering less accurate the use of averaged winds in empirical formulae. Furthermore, the relationship between water vapor content and temperature is not linear so that the two terms have different dependencies over an area. In practice, the value of Q_h is often taken as a fixed proportion of Q_e with the Bowen's ratio (**Bowen**, 1926) because over much of the world's ocean Q_e is greater. **Zaitsev** (1960) took this ratio to be 0.8. The ratio implied in Table 3.1 above is 0.6. During conditions of ice cover, the value of Q_h can be greater than that of Q_e, although, as seen in Table 3.1, both of time terms are reduced to relative unimportance.

These turbulent-exchange terms, Q_e and Q_h, have been observed to play important roles in water mass formation through the extraction of heat and water in areas

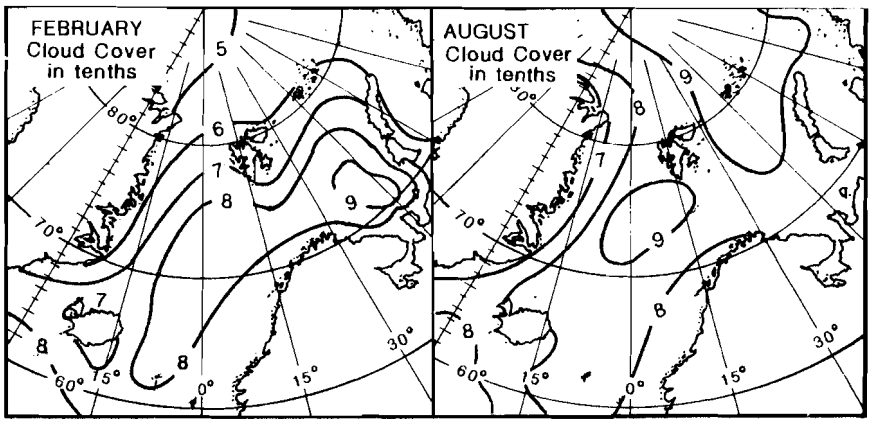

Fig. 3.8. The average cloud cover for the months of February and August. [From **Gorshkov** (1983).]

exposed to cold and dry westerlies flowing off the continents as, for example, in the northwestern Pacific, northwestern Atlantic, and northwestern Mediterranean. In all of these cases, strong buoyancy extraction occurs first in a coastal zone, as the continental air encounters the ocean surface, and secondly in an offshore zone where the somewhat modified air encounters warm oceanic features, e.g. as the Gulf Stream, etc. (cf. **Bunker**, 1976; **Hopkins** and **Garfield**, 1979). While for the most part the GIN Sea has anomalously warm water for its latitude, the weather patterns there do not generate the same type of situations of extraordinarily high evaporative and sensible heat fluxes. The primary exception occurs during the occasion of Siberian easterlies encountering the warm waters of Atlantic origin.

The annual, February, and August distributions of evaporative heat loss is shown in Fig. 3.10a,b,c, and of sensible heat loss in Fig. 3.11a,b,c, respectively. The annual distributions are both biased toward their winter values, with maxima centered over the warmer waters of Atlantic origin, compare Figs. 3.10a and 3.11a with 3.10b and 3.11b. Although the water temperatures do decrease to the north (Fig. 4.5a,d), both Q_e and Q_h tend to have larger values to the north where occurs an increased incidence of easterly winds, i.e. with colder, drier air. In August, evaporation is low and fairly uniform and the sensible heat exchange is virtually zero. **Gorshkov** uses a nonconstant Bowen's ratio, one which is maximum in the fall at ~ 0.9 and minimum in the summer at ~ 0.5.

The net exchange of heat is expressed by the sum of the above terms. The distribution of this sum for the **Gorshkov** data is shown in Fig. 3.12a,b,c for the annual average, February, and August, respectively. On an annual basis, the entire GIN Sea is a region of heat loss, except for the inshore portions over the Greenland Shelf.

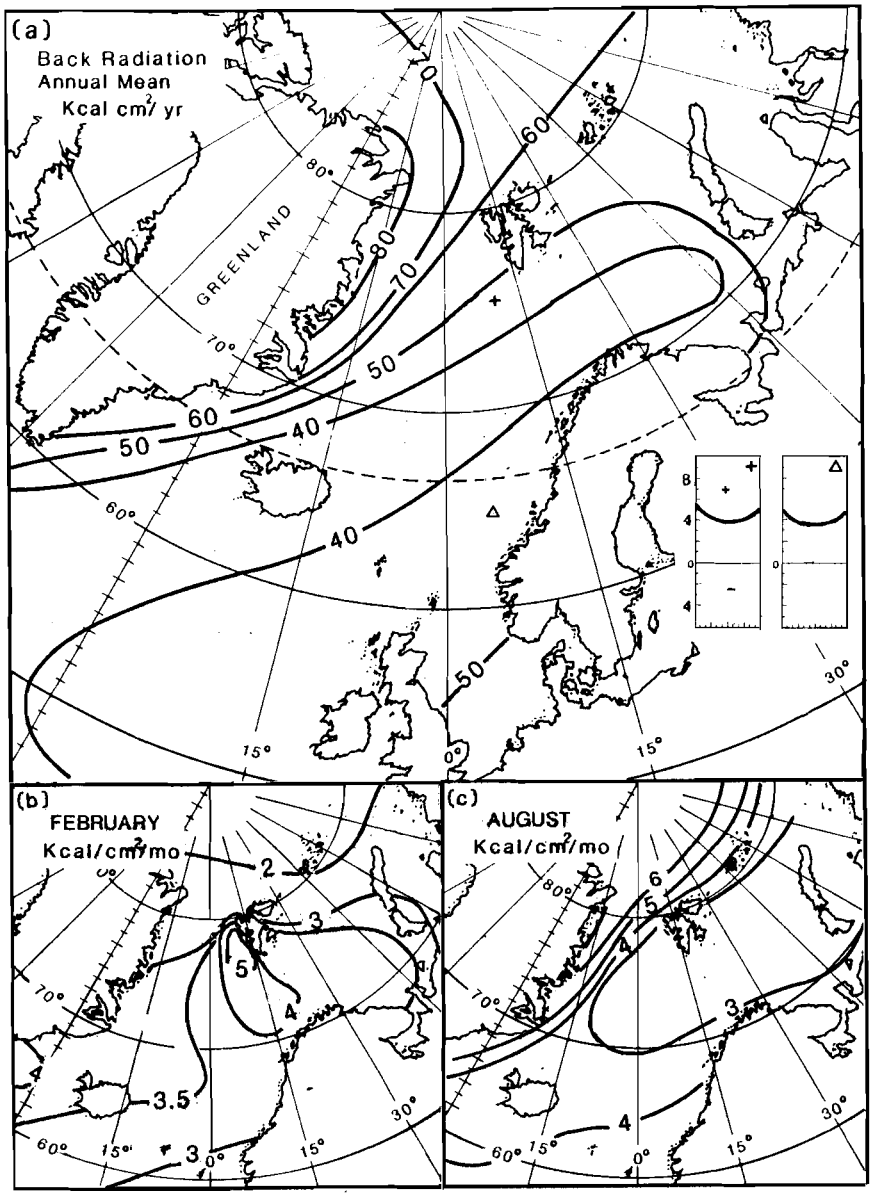

Fig. 3.9. The distribution of the net back radiation, Q_b, for (a) annual mean, (b) monthly mean of February and (c) end of August. The annual cycles for two locations (indicated by the symbols + and △) are shown in the inserted panels. The vertical axis is in kcal/cm^2/mo and the horizontal axis is in months. [From **Gorshkov** (1983).]

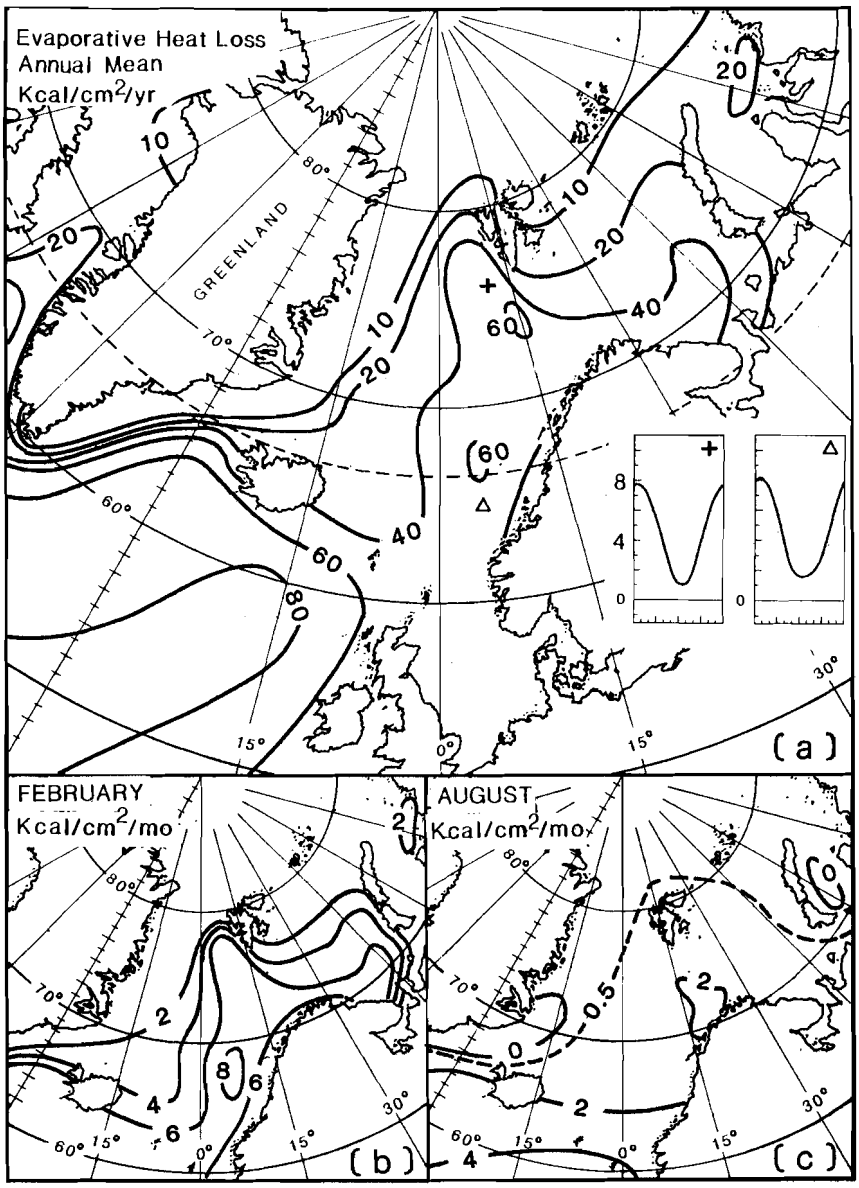

Fig. 3.10. The distribution of the evaporative heat loss, Q_e, for (a) annual mean, (b) monthly mean of February and (c) end of August. The annual cycles for two locations (indicated by the symbols + and △) are shown in the inserted panels. The vertical axis is in kcal/cm^2/mo and the horizontal axis is in months. [From **Gorshkov** (1983).]

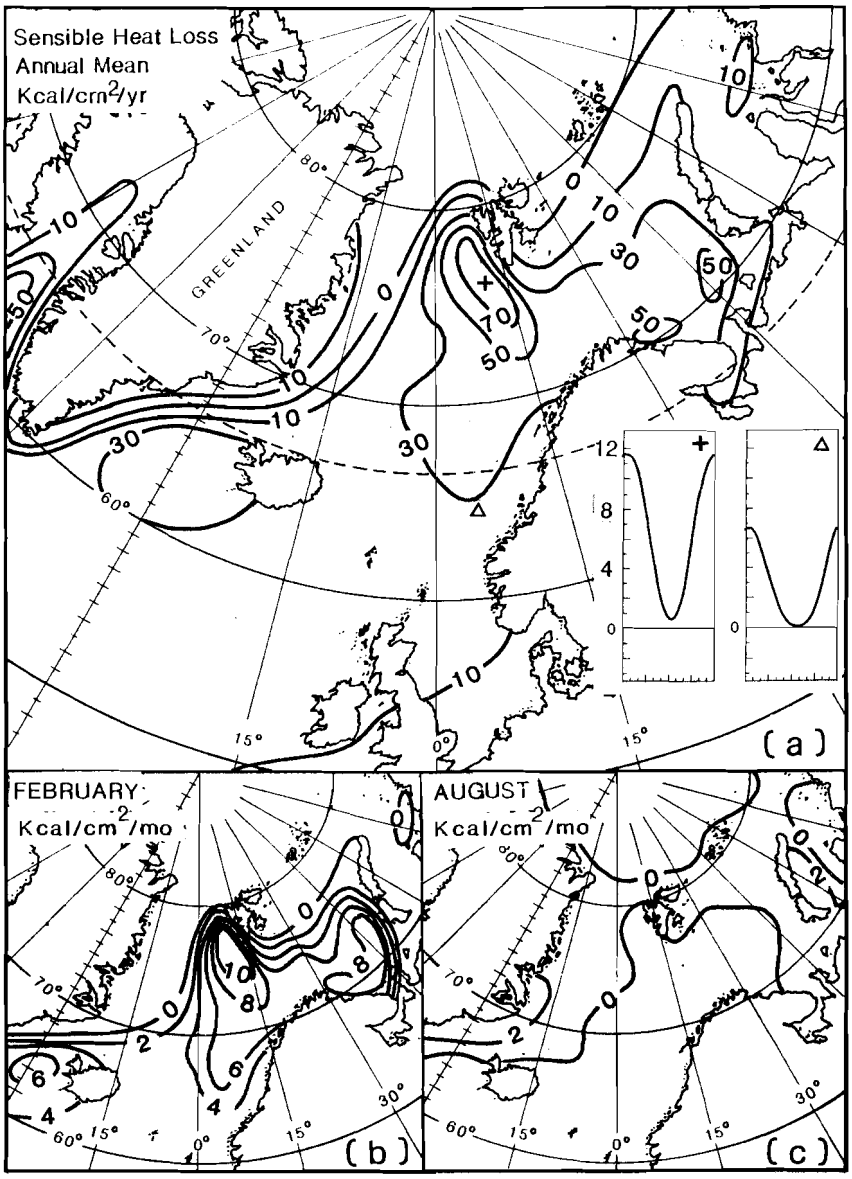

Fig. 3.11. The distribution of the sensible heat loss, Q_h, for (a) annual mean, (b) monthly mean of February and (c) end of August. The annual cycles for two locations (indicated by the symbols + and △) are shown in the inserted panels. The vertical axis is in kcal/cm^2/mo and the horizontal axis is in months. [From **Gorshkov** (1983).]

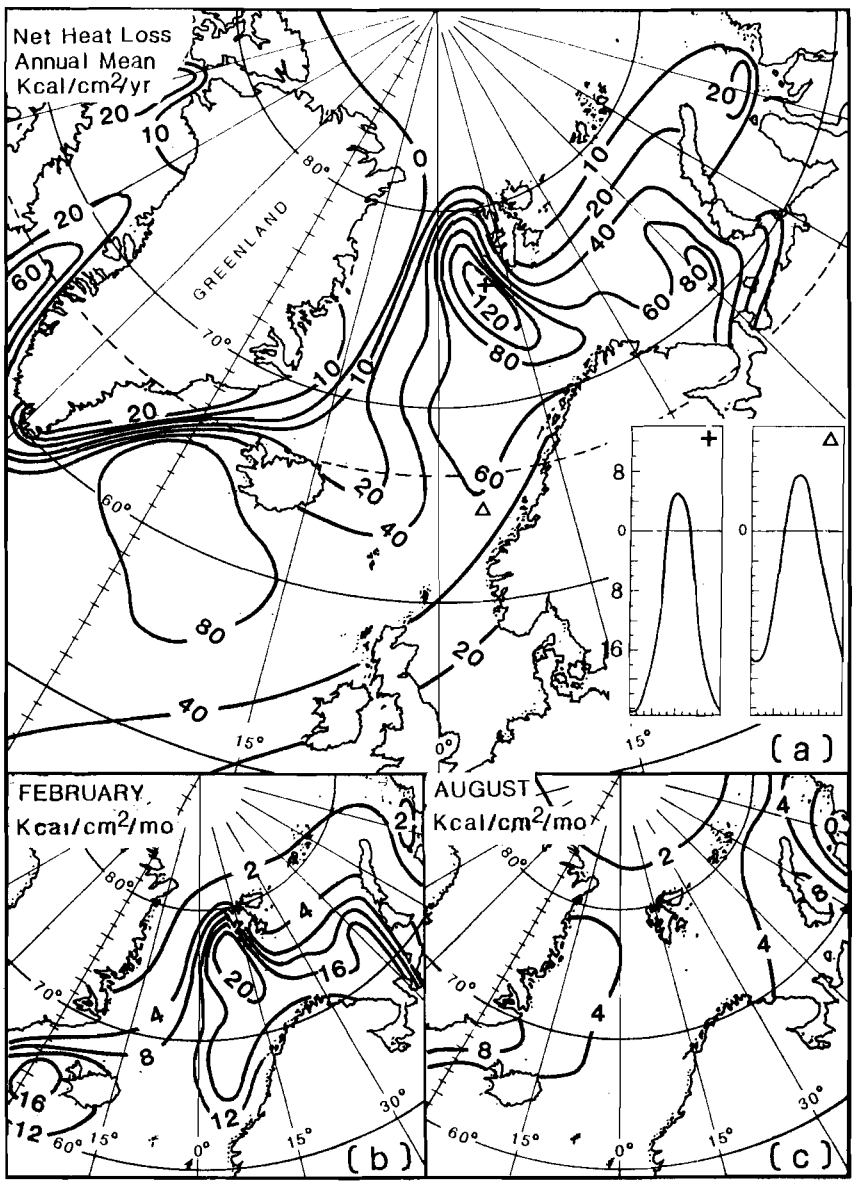

Fig. 3.12. The distribution of the net available heat, $-Q_v$, for (a) annual mean, (b) monthly mean of February and (c) end of August. The annual cycles for two locations (indicated by the symbols + and △) are shown in the inserted panels. The vertical axis is in kcal/cm^2/mo and the horizontal axis is in months. [From **Gorshkov** (1983).]

The area of maximum loss is situated to the east and south of Spitsbergen, being the result of a combination of high values for the back radiation, evaporative, and sensible heat losses during easterly wind events. The maximum February values of $\sim 350 \mathrm{W/m^2}$ are equivalent to a $\Delta T \sim 2$ K/month loss in temperature for the surface 100 m of water during February. Without an adequate advective source of heat, this area would certainly be a site of deep water production.

Finally, in Fig. 3.13a,b we present the precipitation and the sum of precipitation minus evaporation ($E - P$) for the annual distributions. The annual precipitation increases fairly linearly from the southeast ($\sim$ 160 cm) to the northwest ($\sim$ 30 cm). Also amplitude of the seasonal cycle diminishes northward and shifts from late spring (south) to early spring (north), as shown in the inserts of Fig. 3.13a. These values are greater by about a third than those of **Mosby** (1962) who used a value of 60 cm for the entire region. In either case the volume input is less than 0.1 Sv. More significant, perhaps, are the $E - P$ maxima, which are indicated in two areas: east of Spitsbergen and in the Barents Sea, Fig. 3.13b. These are of sufficient magnitude to cause significant local salting. For example, for February in the area off Spitsbergen, if we take $P = 3$ cm and $E = 12$ cm, the resulting salinity increase of an 100 m thick water column would be $S = 0.03$ ppt.

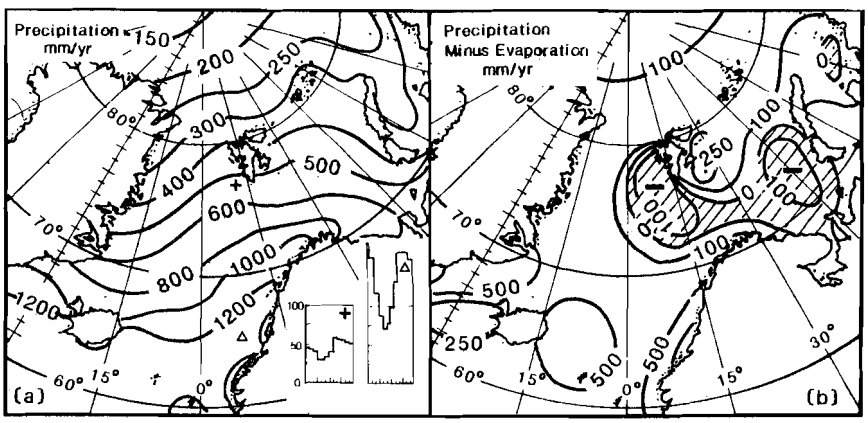

Fig. 3.13. The annual distributions of (a) precipitation and (b) precipitation minus evaporation expressed in mm/yr [from **Gorshkov** (1983)]. The annual cycles for two locations are shown in the inserted panels. The distribution for evaporation alone is given in Fig. 3.10 where $Q_e =$ 60 kcal/cm^2/yr corresponds to $\sim$ 1000 mm/yr.

3.3. ICE

A physical oceanographic description of the GIN Sea would be incomplete without some treatment of its ice cover. In general the presence of ice alters several important physical processes: the sea-atmosphere exchange of momentum, heat, and water; the control of the upper layer buoyancy through the melting/freezing cycle; the advective fluxes of heat and salt of surface currents; and the reflection and scatering of energy, including sound. The topic is well reviewed elsewhere (e.g. **Wadhams**, 1986) and will be only summarized here relevant to the rest of the text.

■ *3.3.1. Ice characteristics*

Ice in the GIN Sea occurs mostly in the form of pack ice. Primarily, this is multi-year ice which originated over the Siberian continental shelf, drifted across the Pole, and exited the Polar Sea via the East Greenland Current (EGC) **Weeks** (1986). The pack ice itself is interspersed with quantities of first-year (or recently formed ice), the amount of which varies with season. Pack ice is typically 3–4 m thick, whereas first-year ice may be 0.02 to 2 m thick (**Weeks**, 1986). The results from submarine sonar profiling have reveled significant erosion in the keel drafts in the transit from Fram to Denmark Straits (e.g. **Kozo** and **Tucker**, 1974; **Wadhams**, 1980).

Other general categories of ice type encountered in the GIN Sea are icebergs, ice islands, landfast ice, and ice of the marginal ice zone. Icebergs are of glacial origin, and thus they are considered as non-marine or as a source of runoff in the water budget of a region. They are essentially chunks of ice discharged to sea by a parent glacier. Along the northern portion of the Greenland coast, icebergs are often grounded, or trapped, so that the main source of icebergs to the EGC is further south where the conditions for escape are more favorable, e.g. Scoresby Sound.

Landfast is multi-year sea ice that forms along the coasts and is grounded in the shallow ($\sim$ 20 m deep) nearshore zone. The nearshore bathymetry of east Greenland is too steep for extensive landfast ice developement, unlike the north coast of Greenland and much of the coasts of the Polar Sea (e.g. **Koch**, 1945). Chunks of landfast ice that become detached are called sikussak, meaning 'ice like ocean ice' in Eskimo. These often drift towards Fram Strait and enter the EGC. The sikussak are undeformed, of exceptional thickness (up to 10 or 12 m), and have rather low salinities ($S \sim 2$ ppt). A cycle of melting, refreezing, and snow accumulation causes slow accretion: **Walker** and **Wadhams** (1979) estimated 65 years to reach a 12-m thickness. Ice islands are large tabular ice sheets of equilibrium thickness (20 to 50 m) which have broken off from the Polar ice shelf. Recent ice islands that entered the EGC were: the '$T2$' of 697 km^2 circa 1951, the *Arlis II* of 14.5 km^2 circa 1965, and the '$WH-2$' of 68 km^2 circa 1973 (**Wadhams**, 1986).

The boundary between the pack ice and the open waters, referred to as the marginal ice zone (MIZ), may be on the order of 100 km. The ice composition differs from the interior pack ice, for example, consisting of various ice forms of pancake ice

(0.3–2 m thick), ice cakes (1.8–20 m thick) and floes (20–100 m thick). The size and frequency of multi-year ice increases towards the interior. First-year ice fragmented or cemented together (breccia) are common (**Kozo** and **Tucker**, 1974). This compositional difference is a result of the fact that the MIZ is a complex dynamic transition-region that serves to buffer incident energy (e.g. waves) from the main ice pack. It is also the main region of ice growth and decay, being thus subject to the variability in the physical and thermohaline driving forces (see **Wadhams**, 1986).

Satellite observations have shown the leads, or openings, in the ice pack to be more frequent and wider in the EGC than in the Polar Sea (**Wadhams**, 1986). Large leads are called polynyas and are generally produced by surface transport divergences, for example, as occurring to the lee of an island or promontory. They vary in scale and duration: along the Greenland coast of dimension tens of kilometers whereas south and west of Franz Josef Land on the order of hundreds of kilometers.

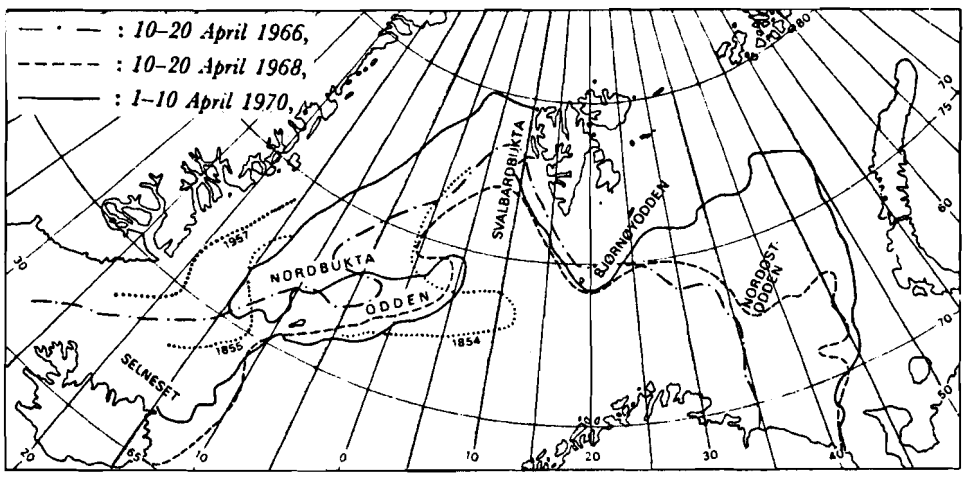

Fig. 3.14. The ice-edge limits under extreme conditions showing several of the named promontories. The dashed-and-dotted line is for April 1966, the dashed line is for 10–20 April 1968, and the continuous line is for 1–10 April 1970. The dotted lines are ship observations in April 1854, 1855, and 1957. [From **Wadhams** (1986); **Vinje** (1977b).]

■ *3.3.2. Ice cover*

The ice cover has been occasionally recorded for the last millenium (e.g. **Bergthorsson**, 1969) and much more systematically recorded for montly summaries for the last 90 years (e.g. **Vilmundarson**, 1972). Recently, satellite imagery has provided synoptic capacity to observe the ice cover and other properties (e.g. **Thomas**, 1986 or

Vinje, 1977a). The large-scale configuration of the sea-ice boundary in the GIN Sea is shown in Fig. 3.14. Ice is found to the west along Greenland, to the south along the north coast of Iceland, and to the northeast in the vicinity of Spitsbergen. These three areas are distinguished because in each instance ice cover there is somewhat separately controlled, i.e. by the East Greenland Current, by the Icelandic Low (atmospheric), and by the East Spitsbergen Current. This fact has frustrated attempts to determine an 'ice index' (an empirical criterion for the ice cover extent during any season, e.g. **Meinardus**, 1906) appropriate to the entire GIN Sea. Also shown in Fig. 3.14 are the more prominent features, with their names.

A number of researchers have noted that the year-to-year variability exceeds the interannual trends. **Vinje** 1977b has provided monthly depictions of the ice cover from the decade 1966–75, from which the March, June, September, and December cases are presented in Fig. 3.15. These, together with Fig. 3.14, give an impression of the seasonal, annual, and interannual variability of the ice cover. One can note from Fig. 3.15a (March) that the area of maximum extent is more than double that of the minimum extent, and that the width of the area enclosed by the extremes varies with time as well as position. The Isodden (ice promontory) and Nordbukta (the bight to the north of it) are features known to whalers and sealers that are manifested in the mean winter condition but not necessarily every year (Fig. 3.15). In early April 1970, they were extremely well developed (Fig. 3.14), as opposed to not at all in March 1975 (Fig. 3.15). The maximum recorded eastward extension of the Isodden occured in 1854 and the minimum extension occured 103 years later in 1957. However, the 1957 minimum was not much different than the minimum which occured one year after the 1854 maximum, of 1855.

The 1975 ice boundary demonstrates this variability (the dashed line in Fig. 3.15) from March to June the ice edge retreated along Greenland but remained nearly fixed in the Bjornoyodden, south of Spitsbergen. From June to September, it retreated both in the Denmark Strait and in the region east of Spitsbergen but remained in nearly the same location along Greenland. In contrast to what occurred to the north, the ice limit in Denmark Strait was less than the ten-year minimum in March, while in June it was close to the maximum, indicating unusually rapid spring growth that year. **Kagan** (1977) reports the amplitude of the year-to-year variation in Denmark Strait is $\sim$ 50% of its seasonal range, which is with the position 400–500 km being most extensive in April and least so in September.

■ *3.3.3. Causes of variability*

An explanation for the fact, that greater variability is often observed between successive years rather than in interannual trends, is partly found in self-regulatory aspect of the annual cycle: a greater winter areal coverage leads to a greater summer melt (**Vowinckel**, 1964). Additional self-regulation occurs through the difficult to evaluate atmospheric feedbacks, wherein the ice, by insulating the air from the sea, reduces the heat lost from the sea to the atmosphere (Table 3.1). The consequence of this is additional ocean heat available for melting the ice. Also, the cooled atmosphere

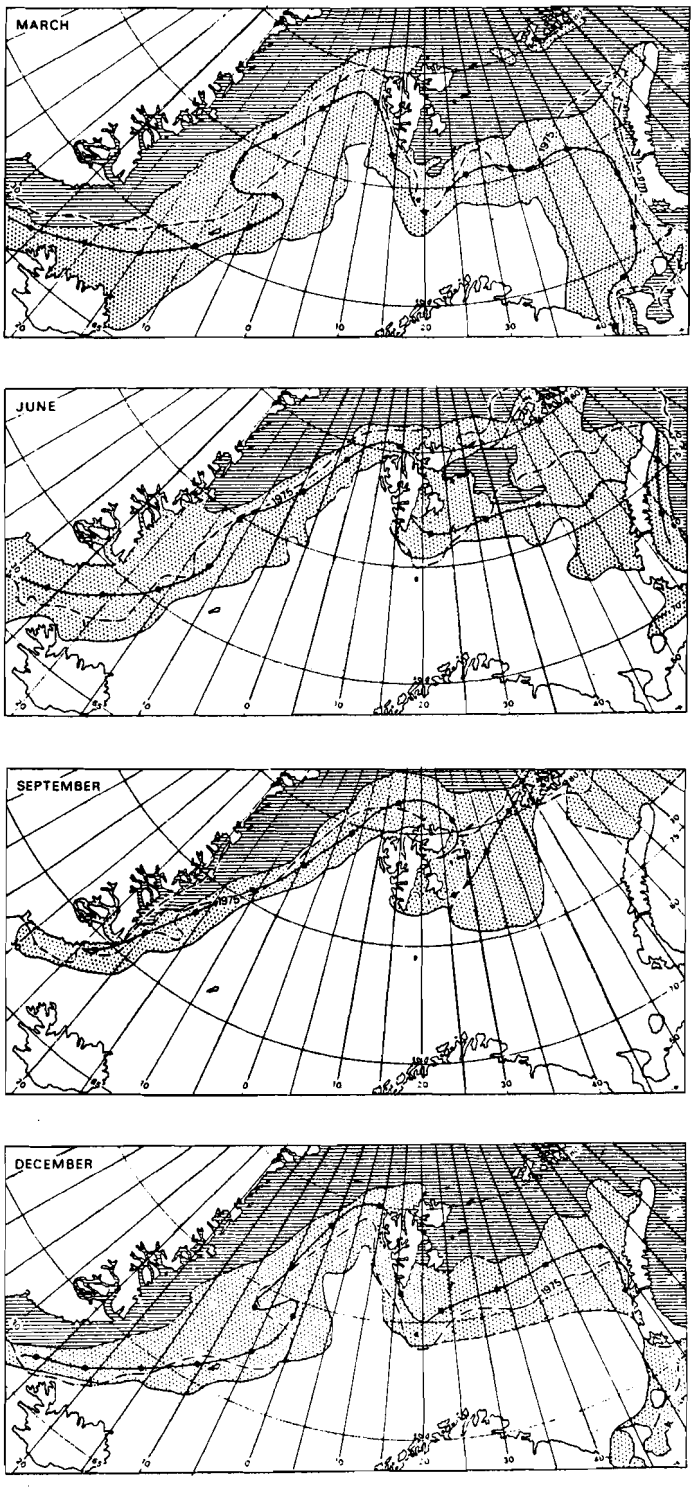

Fig. 3.15. The mean and extreme ice limits for the month-ends of March, June, September, and December for the years 1966 through 1975. The range of extreme limits for the 3/8 ice is indicated by the dotted area, with the hatched area being where there was never less than 3/8 sea ice and the white area of the sea being where there was never more than 3/8 ice at the end of the given month during the decade. The thick black line is the median of these limits and the dashed line is the 1975 limit. [From **Vinje** (1977b).]

leads to a positive atmospheric pressure anomaly and contributes to wind changes that effect the ice this distribution.

Air temperature is the most obvious parameter with which to seek correlations with ice cover. The long-term climatic trend of the 'little ice age', from circa 1450 to 1830, resulted in a $\sim$ 1 K decrease in annual mean temperature at Iceland (**Batten, Rapp,** and **Warshaw,** 1976). The winters were longer and colder but the summer temperatures remained about the same and no interannual accumulative trend in ice cover occurred. A similar response has occurred during the recent shorter-term climatic cycles of approximately the same amplitude. These were a warming from the 1890's to the late 1930's, then cooling through the 1960's, and warming through the 1970's, and again cooling to present (**Stefansson,** 1969; **Batten,** 1976; **Malmberg,** 1984). However for application to the GIN Sea, simple correlations with air temperature are often masked by the dominance of advective heat. This has lead others to seek other relationships to indicate ice cover, as water mass properties, currents, or their atmospheric forcing.

Skov (1970) considered the year-to-year variability in ice cover to be primarily due to variability in current transport. In fact, he showed a good inverse relationship between the temperature south of Iceland and the ice cover in Denmark Strait. The assumption being that the existence of warmer, more saline waters south of Iceland implies a greater convergence of the North Atlantic waters, carried by the Irminger Current, against the Greenland-Iceland Ridge and hence a retardation of the southern extension of the EGC carrying potentially ice producing waters in to the Strait (see Subsect. 5.3.2).

The role of currents in controlling the ice cover is two-fold: the advection of warm, salty waters inhibits ice formation and the advection of cold, less saline waters fosters it. Svalbardbukta (Fig. 3.14) is an example of the former; one can note its conformance to the West Spitsbergen Current and its greater extent in December relative to March (Subsect. 5.2.2). The Selneset is an example of the latter, its development being linked to amount of Greenland Polar Water advected eastward and incorporated into the Icelandic Current (Subsect. 5.2.4). Some of this eastward advection may even be ice itself, but the important additional point is the accompanying reduction in surface salinity. **Dickson, Lamb, Malmberg,** and **Colebrook** (1975) and **Malmberg** (1984) have pointed out that surface waters with salinities less than $S = 34.7$ ppt in the Iceland Sea can produce ice cover whereas waters with salinities above this value, on cooling to the freezing point, would be dense enough to induce a convective overturn. Figure 3.16 shows this correlation. **Weyl** (1966) suggested that the lower salinities were a result of increased precipitation, preferrably under conditions of light winds, rather than eastward extensions of the EGC low-salinity waters. Such a distinction is difficult to confirm observationally (**Skov,** 1970). However, surface tongues of low-salinity waters north of Iceland, of what ever origin, have been observed to proceed short-term rapid advances of the ice edge (e.g. **Einarsson,** 1972).

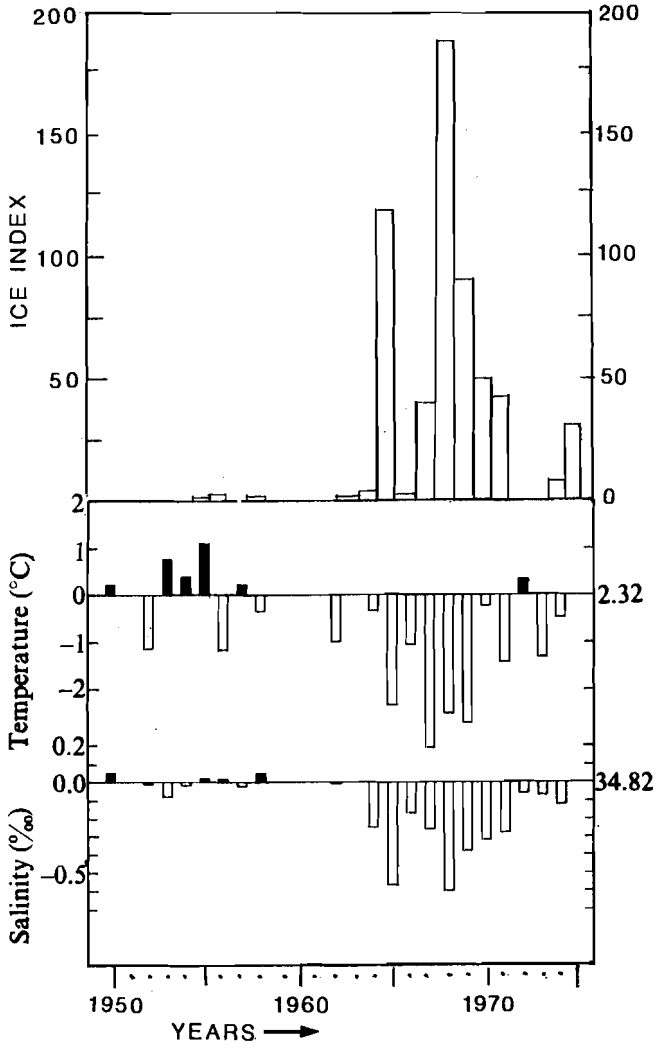

Fig. 3.16. The 'ice index' (the product of the number of weeks with ice per year and the number of North Icelandic coastal areas near which it was observed) and the corresponding temperature and salinity deviations based on the 25-m values from the area 67°–69°N and 11°–15°W in June relative to the mean of the same data, 1950–1980. On the left is indicated the deviation and on the right the mean value. [Adapted from **Malmberg** (1984).]

In looking for correlations with currents, it is logical to pursue correlations with winds and/or atmospheric pressure differences. In the most straightforward causal relation, the wind-driven frictional transport can induce ice cover through advection of ice itself. For example, by applying **Zubov**'s (1945) formula for wind transport of ice, **Vowinckel** (1964) showed that the wind transport amounted to about a third of the transport of ice into the GIN Sea through Fram Strait. The entire southward ice movement along the Greenland continental shelf is assisted by this mechanism via the northerly winds, prevailing from the north whether they are being driven by the Greenland High pressure system or by the cyclones passing to the south of them.

Aagaard (1972) argued a causal relationship between the anomalous ice years (Icelandic Sea) during the mid-to-late sixties and an eastward extension of the Greenland High, i.e. that enhanced northerly winds drove a greater ice transport through and in the EGC system. In fact, the positive pressure anomaly along the Greenland coast was $\sim$ 10 mb from 1965–70 relative to the 1900–1939 average **Dickson, Lamb, Malmberg** and **Colebrook** (1975). However, **Einarsson** (1969) found that extensive ice cover in Icelandic waters was not well correlated with that in the rest of the Greenland Sea (also as in Fig. 3.15). The implication of this is that factors enchancing ice cover in the north, as for example greater EGC transport, do not necessarily enhance ice cover in the southern iceland Sea. This follows if we assume the Icelandic Low, and whatever other large-scale forcing drives the Icelandic Sea–North Atlantic exchange, are conditions somewhat independent of those which force the flow to the north.

Additionally, the EGC is not entirely a one-season system (Subsect. 5.2.3), i.e. entering arctic ice does not necessarily reach Denmark Strait in one winter season. Consequently, winter ice in the southern sector is to some degree uncoupled from the same winter's Arctic ice input. In **Einarsson**'s (1972) estimate of the ice budget of the southern EGC, he estimated that there was a net annual production of ice, i.e. 9.2×10^5 km^2 was imported from north of 76°N, 4.5×10^5 km^2 was formed locally 2.6×10^5 km^2 was melted locally, and 11.1×10^5 km^2 was exported southward to the North Atlantic. Considering the input draft to be $\sim$ 3 m and the output $\sim$ 2.25 m (from **Wadhams**, 1986), the net local production is 8% of the input. In our thermohaline budget (Subsect. 5.4), we assume 60% loss between the volume of ice entering via Fram Strait and that exiting via Denmark Strait.

4. Water masses

The waters of the ocean are not randomly distributed with respect to temperature (T) and salinity (S) such that a space defined by these two variables is not evenly filled. We define a water type as occupying a particular location in this space, i.e. a specific value for both T and S. Similarly, we define an area of this space, or envelope of water types, as a water mass. Unfortunately the specification of a water mass remains somewhat arbitrary and a function of method. One of the more rigorous methods relies on 'volumetric T-S analysis', in which the volumes for unit water types are calculated and then grouped into water masses. This technique was used in both the Greenland and Iceland Seas by **Carmack** (1972) and **Swift** (1980), respectively. In a large system such as the GIN Sea, the water mass definitions often vary dependent on the sub-region and/or the purpose of the analysis. Therefore, the water masses definitions which we suggest below might differ from those used in former publications. We have attempted to make them amenable to a discussion of the entire Sea. Some of the more conventional water mass acronyms were slightly modified to simplify or to avoid ambiguity between names beginning with the same letter. Tables 4.1a–d specify the various water masses* and Fig. 4.1 identifies schematically their locations. In an accompanying illustration, we present for comparison the annual mean cross-sections (Fig. 4.2a,b) of **Koltermann** and **Machoczek** (1985).

The water masses found in the GIN Sea arise from two parent water masses: the Polar Water (PW) from the Polar Sea, which is cold and of low salinity, and the North Atlantic Water (NAtW) from the North Atlantic, which is warm and of high salinity. We do not discuss the PW and NAtW water masses in detail since they originate outside the GIN Sea, but we refer to them often in a general sense.

The basic division in the GIN Sea between water masses occurs longitudinally in salinity, and vertically (and meridionally) in temperature. The result is a water mass segregation east–west across the basin by salinity and vertically by temperature. The waters of each of the three major seas of the GIN Sea occupy different but overlapping regions in T-S space. This is shown schematically in Fig. 4.3, where the Iceland Sea evolves out of the Atlantic water via the Norwegian and Greenland Seas in that sequence.

The general vertical differentiation (surface, intermediate, and deep) can be made on the basis of density, as shown in Fig. 4.4. In the winter time many of the surface water types converge with those of the intermediate water types. Because of geographic variation, the choice of a single density value will not always serve to divide surface waters from intermediate waters. For this reason, we have allowed the σ_0 values to

* In these tables a range of temperature and salinity has been given wherever possible; otherwise, single values of temperature and salinity indicate core water type.

Table 4.1a
Water mass definitions: Atlantic Waters

Water mass	Symbol	Water type (°C, ppt)	Comments
Surface Water	SW	$\sigma_0 < 27.75$ summer $\sigma_0 < 27.9$ winter	Upper layer waters with exposure to atmosphere
North Atlantic Water	NAtW	$T > 8, S > 35.3$	Surface waters of the North Atlantic current and/or the Irminger current
FærœAtlantic Water	FAtW	$T > 7, S > 35.2$	Slightly modified NAtW found south or the Iceland-Færœ-Ridge front and around the Faeroe Islands
Irminger Atlantic Water	IrAtW	$T > 5, S > 35.0$	Modified NAtW in and entering the Denmark Strait as a part of the North Irminger current
Norwegian Atlantic Water	NwAtW	$T > 2, S > 35.0$	Waters of the Norwegian Atlantic current and its branches
Intermediate Water	IW	$27.75 < \sigma_0 < 28.05$ $\sigma_1 < 32.785$	Transitional waters between surface and deep waters; may be exposed to atmosphere and may be at the bottom
Atlantic Intermediate Water	AtIW	$T > 0, S < 34.9$	Intended to represent the more saline components of the IW
Greenland Atlantic Intermediate Water	GAtIW	$T = 2$–4, $S = 35.0$–35.15	AtIW in the Greenland sea originating from the east via modification of NwAtW in the Norwegian Atlantic and West Spitsbergen currents
Return Atlantic Intermediate Water	rAtIW	$T = 0$–2.0, $S = 34.9$–35.0	AtIW within the East Greenland current system

Table 4.1a (continued)

Water mass	Symbol	Water type (°C, ppt)	Comments
Intermediate Water (continued)	IW	$27.75 < \sigma_0 < 28.05$ $\sigma_1 < 32.785$	Transitional waters between surface and deep waters; may be exposed to atmosphere and may be at the bottom
Jan Mayen Atlantic Intermediate Water	JMAtIW	$T = 0$–0.5, $S = 34.9$–35.0	AtIW in the Jan Mayen current emanating from the rAtIW in the East Greenland current
Iceland Atlantic Intermediate Water	IAtIW	$T = 0$–0.5, $S = 34.9$–35.0	IW in the Icelandic Sea originating from local production from NwAtW or advection from rAtIW; correspond to the 'lower' IW component described by **Swift** and **Aagaard** (1981)
Deep Water	DW		Generic meaning waters of or in the deep ocean; to indicate the presence in bottom-most layer the term Bottom Water is often use
North Atlantic Bottom Water	NAtBW	$\sigma_0 > 27.8$ $\sigma_2 \sim 37.1$	Used in text to indicate the densest water of the North Atlantic (see e.g. **Swift**, 1984) to which the various overflows from the GIN Sea contribute; commonly abbreviated as NABW in the literature

range from $\sigma_0 = 27.75$ to $\sigma_0 = 27.90$, the latter being the value cited by **Aagaard**, **Swift** and **Carmack** (1985). These authors also use the σ_1 value of $\sigma_1 = 32.785$ (the density at a depth of 1000 m) to separate the intermediate and deep waters, which we have also done. This approach is more useful for distinguishing between the low temperatures found in the GIN Sea, where the isolines of σ_0 and σ_1 are no longer parallel. This means, for example, that of two water types with the same density at the surface, the colder one would be the more dense at a depth of 1000 m.

Table 4.1b
Water mass definitions: Polar Waters

Water mass	Symbol	Water type (°C, ppt)	Comments
Surface Water			
Polar Water	PW	Freezing to 2 33.0 to 34.4	Intended to include surface water of the Polar Sea and most particularly that available for entry to the GIN Sea
Greenland Polar Water	GPW	$T < 5, S < 34.4$	Surface water of the East Greenland current (median value 33.7); low in silicate $\sim 8\ \mu g - at/l$, high in tritium ~ 20 T.U.
Jan Mayen Polar Water	JMPW	$T = -1$, $S = 34.6$	GPW mixed with ArSW and found in the surface portion of the Jan Mayen current
Intermediate Water			
Polar Intermediate Water	PIW	$T < 0$, $S =< 34.4$–34.7	Salinity minimum water under the GPW
Polar Atlantic Intermediate Water	PAtIW	$T > 0$, $S = 34.9$–35.0	AtIW within the Polar Basins north of Fram Strait
Deep Water			
Eurasian Basin Deep Water	EADW	$T = -0.8$, $S = 34.93$	Silicate $\sim 10\ \mu g - at/l$
Canadian Basin Deep Water	CDW	$T = -0.5$, $S = 34.95$	Silicate $\sim 13\ \mu g - at/l$

Table 4.1c
Water mass definitions: Arctic Waters

Water mass	Symbol	Water type (°C, ppt)	Comments
Arctic Surface Water	ArSW		Generic meaning in/of the surface waters of the GIN Sea
Greenland Arctic Surface Water	GArSW	Freezing to 5 34.7–34.9	Surface waters of the Greenland Sea not otherwise specified, i.e. Greenland Sea gyre
Iceland Arctic Surface Water	IArSW	Freezing to 8 34.7–34.9	Surface waters of the Iceland Sea not otherwise specified
Icelandic Current Water	ICW	T = 1–4, S = 34.6–34.9	Surface waters of the Icelandic current; water type can vary along σ_t = 27.7 depending on admixture of GPW or IrAtW
Intermediate Water			Generic meaning for intermediate water formed in GIN Sea
Greenland Arctic Intermediate Water	GArIW	$T < 2, S$ = 34.7–34.9	Subsurface IW in the Greenland Sea; year crop more saline and less abundant than in Iceland Sea
Iceland Arctic Intermediate Water	IArIW	$T < 2$, S = 34.7–34.9	Subsurface IW in the Iceland Sea corresponds to 'upper' IW component described by **Swift and Aagaard** (1981)
Norwegian Arctic Intermediate Water	NwArIW	$T = 0.5, S = 34.88$	ArIW under the NwAtW in the Norwegian Sea
Icelandic Current Intermediate Water	ICIW	T = 0–3, S = 34.75–34.9	IW formed within the Icelandic current system; referred to as North Icelandic winter water (**Stefansson**, 1962)

Table 4.1c (continued)

Water mass	Symbol	Water type (°C, ppt)	Comments
Deep Water			
Greenland Sea Deep Water	GDW	$T = -1.25, S = 34.89$	Deep water of the Greenland Sea below 2000 m; commonly abbreviated as GSDW in the literature
Norwegian Sea Deep Water	NwDW	$T \sim -1.05, S \sim 34.91$	Deep water of the Norwegian Sea below 2500 m; commonly abbreviated as NSDW in the literature
Upper Norwegian Deep Water	uNwDW	$T = -0.5, S = 34.92$	Deep water of the Norwegian Sea above 2500 m

4.1. SURFACE WATERS

■ *4.1.1. Norwegian Atlantic Water (NwAtW)*

Warm, high-salinity water in the GIN Sea has its origin in the North Atlantic. The main source of this water is an inflow through the Færœse Channel which then continues northward to Spitsbergen and into the Polar Basin. Atlantic Water also enters the GIN Sea through the Denmark Strait but becomes mixed and does not form a discrete internal water mass. The NwAtW is dynamically constrained to remain within the eastern half of the Sea as part of the Norwegian Atlantic Current (NwAtC) system. **Helland-Hansen** and **Nansen** (1909) defined this water as simply having $S > 35$ ppt regardless of its temperature. Since we intend it to be considered as a surface water mass, we exclude those water types cooler than $T = 2\,°C$ which would give it a density within the intermediate water range, or those fresher than 35 ppt which might indicate substantial admixtures of Polar or Shelf waters.

An example of the NwAtW distribution is given in Fig. 4.5, where the GIN Sea surface contours of the T, S, and σ_t have been plotted from the sequence of cruises of the International Geophysical Year (**Dietrich**, 1969). The 35 ppt contour has been hatched for identification purposes, as it is considered the best indicator of the NwAtW rather than temperture (which has a 3 K to 6 K seasonal variation at the surface). The contours demonstrate a unique characteristic of the GIN Sea: its lower

Table 4.1d
Water mass definitions: Shelf waters

Water mass	Symbol	Water type (°C, ppt)	Comments
Shelf Water	ShW		Generic for waters of continental shelf regions
Northern North Sea Water	nNSW	$T = 7$–9, $S = 35.2$–35.3	Water found east of Scotland
Norwegian Shelf Water	NwSW	$T = 2$–13, $S = 32$–35	Waters of the Norwegian Shelf
Barents Sea Water	BrW		Waters of the Barents Sea
(1) Barents Atlantic Water	BrAtW	$T = 2$–$5, S > 34.8$	BrW originating from NwAtW
(2) Barents Polar Water	BrPW	$-1 > T > -3$, $S =< 34.4$	BrW originating from PW
(3) Barents Bottom Water	BrBW	$T = 0$–$1, S > 35.0$	BrAtW cooled and found at bottom depths
Eastern Icelandic Shelf Water	eIShW	$T < 7$, $S = 34.45$–34.65	Locally freshened, coastal water of the Icelandic current primarily on or from eastern Icelandic shelf

spatial variability in the summer, which is in contrast to other northern hemispheric regions. With regard to density, the compensation for the west to east increase in salinity by an west to east increase in temperature is much more in summer than during in winter.

The lateral extent of the NwAtW in winter is greater than in summer, a difference which is more pronounced at the surface than at subsurface depths. It is not yet known if there exists a repeatable seasonal pattern to the NwAtW volume. Obviously the contours of Fig. 4.5 are not synoptic in time and thus may be in error with regard to seasonal differences. Also, we now know that there is considerable structure at smaller spatial scales which would create an alias in attempts to portray the horizontal structure. Climatological averages, such as those of **Koltermann** and **Machoczek** (1985) provide a smoother picture by filtering out the seasonal effect, for example as shown in Fig. 4.6. Such averages also smooth the important interseasonal variations.

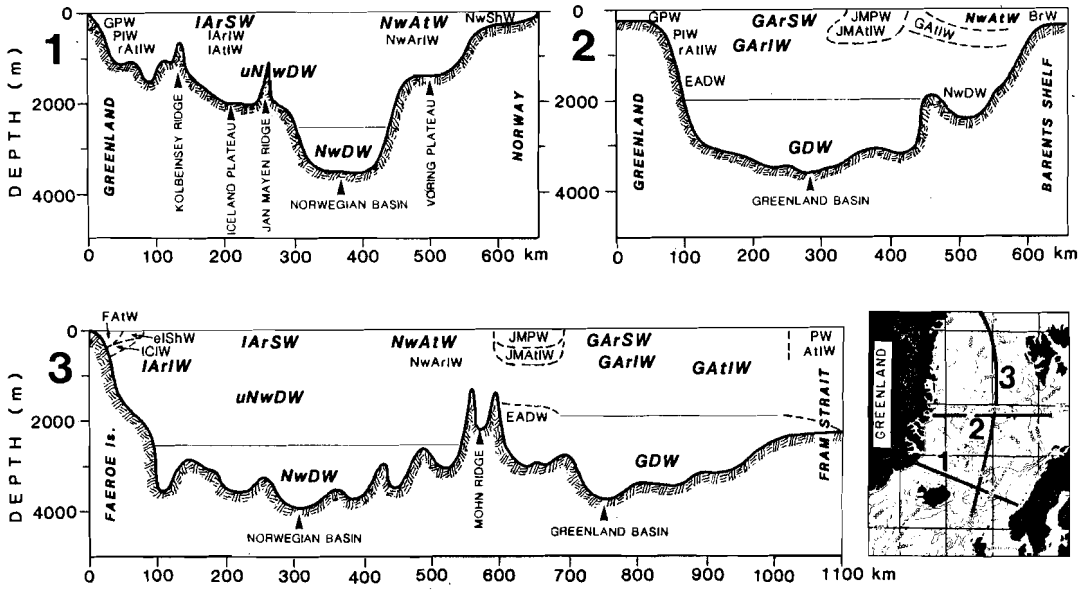

Fig. 4.1. Schematic location of the various GIN Sea water masses across three sections. Bathymetry is to scale but the depths of the water masses area are only approximate. Dotted lines indicate variability in the position or the presence of a water mass. Bold letters indicate major water masses. Abbreviations are given in Table 3.1.

Table 3.1.

A look at the cross-sections of this same (IGY) data set (Fig. 4.7) shows the cross-sectional area of the NwAtW varying with regard to size as it proceeds northward. We expect a general northward loss of salt and heat, and such a trend can be detected. However it is obscured somewhat by considerable variations attributable to along-stream convergences/divergences or to non-synoptic observational errors. The total volume of the NwAtW for this particular case is approximately 0.3×10^6 km^3 for winter and 0.4×10^6 km^3 for summer, corresponding to 7 and 10% of the GIN Sea volume, i.e. approximately the same as the 7% figure given by **Mosby** (1972). The core of the NwAtW can be identified by a salinity maximum, which varies in depth between the surface and a depth of 300 m. Noticeable too in Fig. 4.7 is a tendency for core splitting to occur where the NwAtW spreads westward roughly between 66° and 72°N. The deeper portions of the NwAtW are less in salinity (and temperature), the most obvious explanation for which would be that of mixing with the less saline, deeper and intermediate waters. However, recent evidence, such as the persistence northward of the underlying salinity minimum layer and the results of the thermohaline balances (Subsect. 5.4), indicates very little vertical exchange between NwAtW and deeper waters. These deeper, less saline, cold water types may be formed initially at the confluence of the entering Atlantic and Icelandic Current waters. The northward water-type evolution of the NwAtW is an extremely impor-

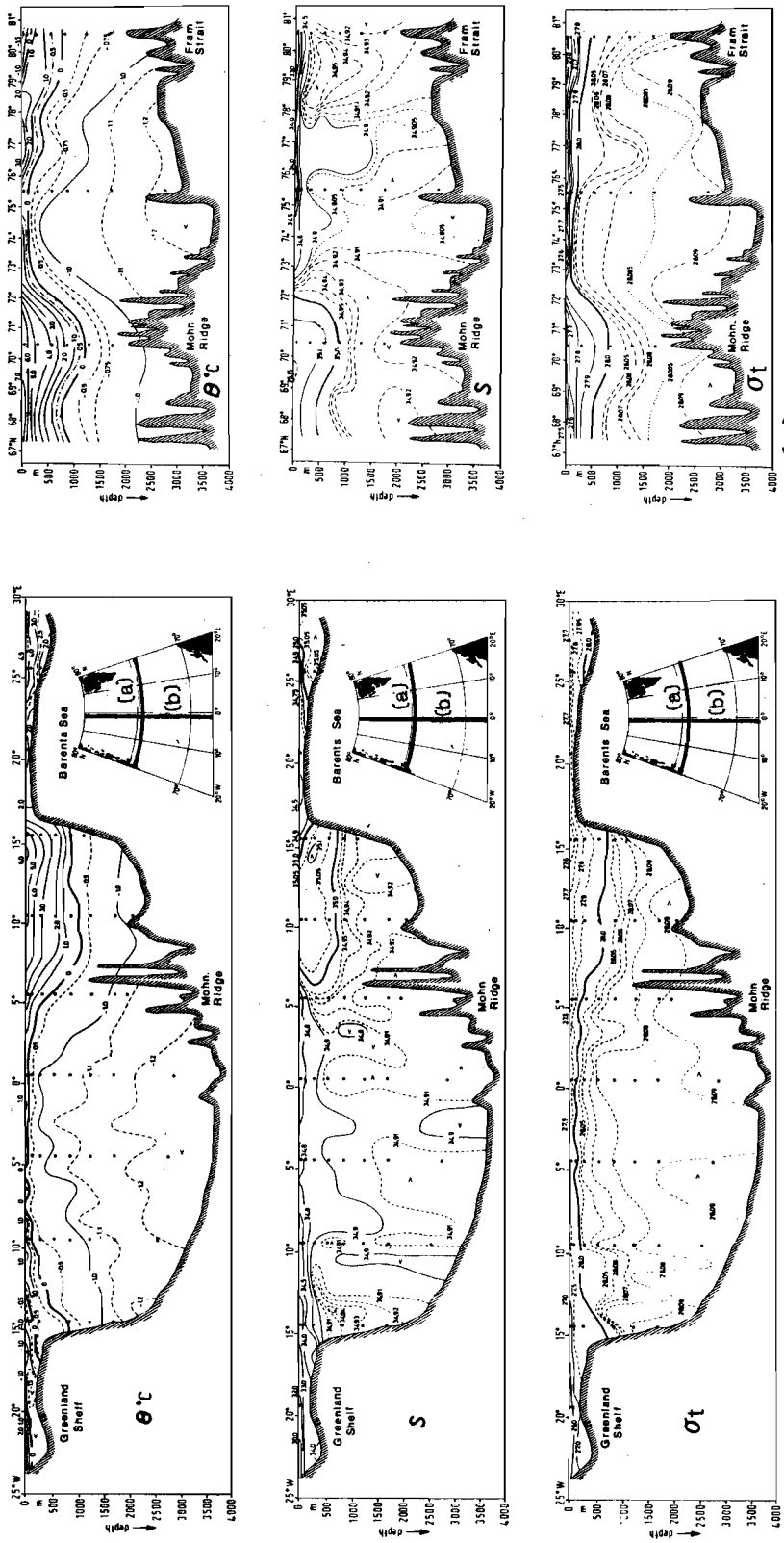

Fig. 4.2. (a) Latitudinal (74°N) cross section of the Greenland and northern Norwegian Seas, and (b) Meridional (0°W) cross section of the Greenland and northern Norwegian Seas. [From **Koltermann** and **Machoczek** (1985).]

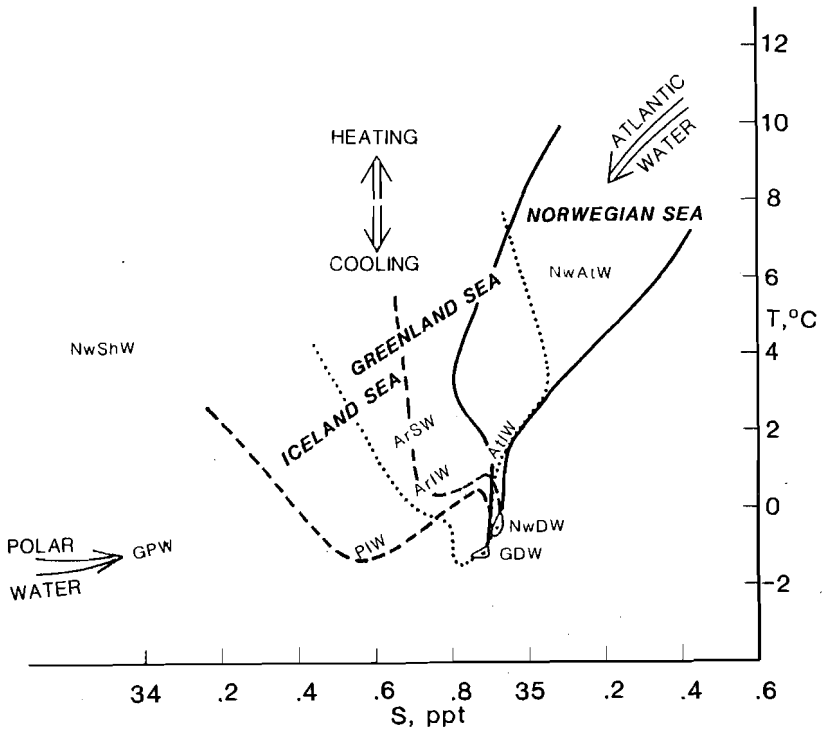

Fig. 4.3. Schematic T-S diagram showing the evolutionary sequence of the GIN Sea water masses.

tant feature of the GIN Sea thermohaline dynamics. At its southern entry point it is too buoyant (due to its heat content) to mix convectively or isopycnally with local waters. At its northern exit point this is no longer the case, and it submerges around 78°N. The enroute process is often referred to as a 'preconditioning' phase, that is, one in which a water mass loses buoyancy prior to undergoing the convective mixing requisite to deep water production. To demonstrate this evolution, we have prepared Fig. 4.8 which shows the northward T-S trend of the NwAtW core. This evolution is not isopycnal, but results in density increasing downstream to the north. This can be attributed to a much greater loss of heat to the atmosphere than a decrease in salt concentration due to greater precipitation than evaporation or due to lateral mixing. Note that the T-S regression does not extend linearly to the deep water type, and so additional heat extraction without loss of salt is required to convert NwAtW to deep water even at its northernmost extremity.

■ *4.1.2. Greenland Polar Water (GPW)*

Polar Water enters the GIN Sea as a surface water mass in a southward flowing boundary current along the eastern continental margin of Greenland. As such it constitutes an input analogous to the Atlantic Water, but we shall demonstrate that its influence on the system is much less than that of NwAtW, primarily be-

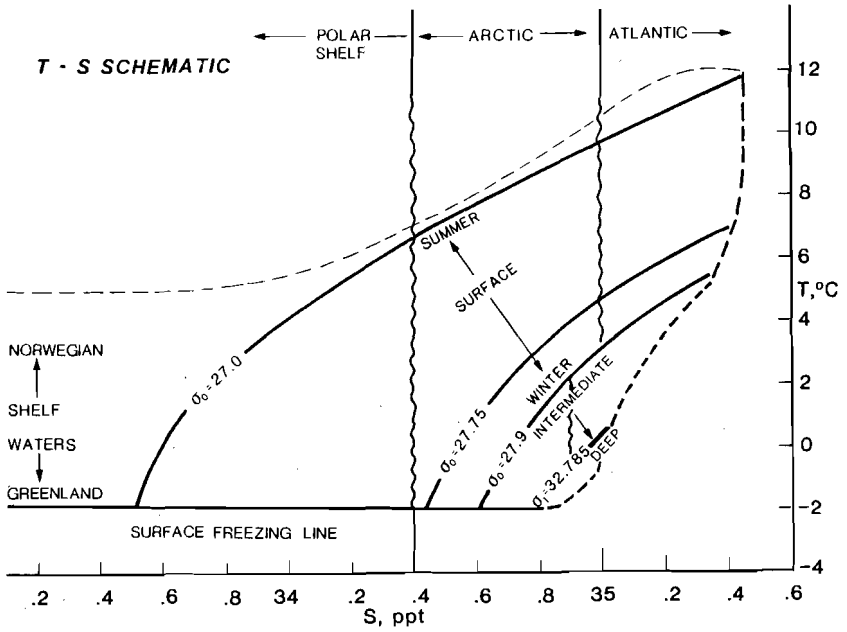

Fig. 4.4. Schematic T-S diagram showing the water-type limits for the surface, intermediate, and deep water masses of the GIN Sea.

cause its salinity is too low to permit any water-type evolution that would result in a water mass sufficiently dense to sink or to move isopycnally into the deep interior of the Greenland or Iceland Seas. In fact, this entering water shows little water-type evolution along its $\sim$ 1600 km path southward along the East Greenland continental margin. The entering Polar Water generally has salinities less than 34.5 ppt and temperatures less than 0 °C. This is the water type that **Aagaard** and **Coachman** (1968) used to distinguish between waters of polar origin and resident Greenland Sea waters. However, we consider that a salinity of 34.4 ppt is a more representative upper bound for the entire GIN Sea. **Swift** (1980) uses this salinity delineation in his Iceland Sea T-S analysis. The temperatures of the GPW range from the freezing point temperature ($T \sim -1.7$ °C) to summer surface maximums of up to 5 °C. We define the GPW as 5 °C, $S < 34.4$ ppt, and note that its water-type median is around (−1 °C, 33.7 ppt).

The salinities vary down to minima of 29 ppt, and typically the GPW is underlain by a strong halocline, which is an advected feature originating in the Polar Sea but maintained locally along the Greenland Shelf through ice melt. Ice import estimates (e.g. **Mosby**, 1962) are about 0.1 Sv, or 3.000 km^3/yr. The total volume of the GPW is of the order of 4×10^4 km^3. The water type of the ice is (−10 °C, 3 ppt) so

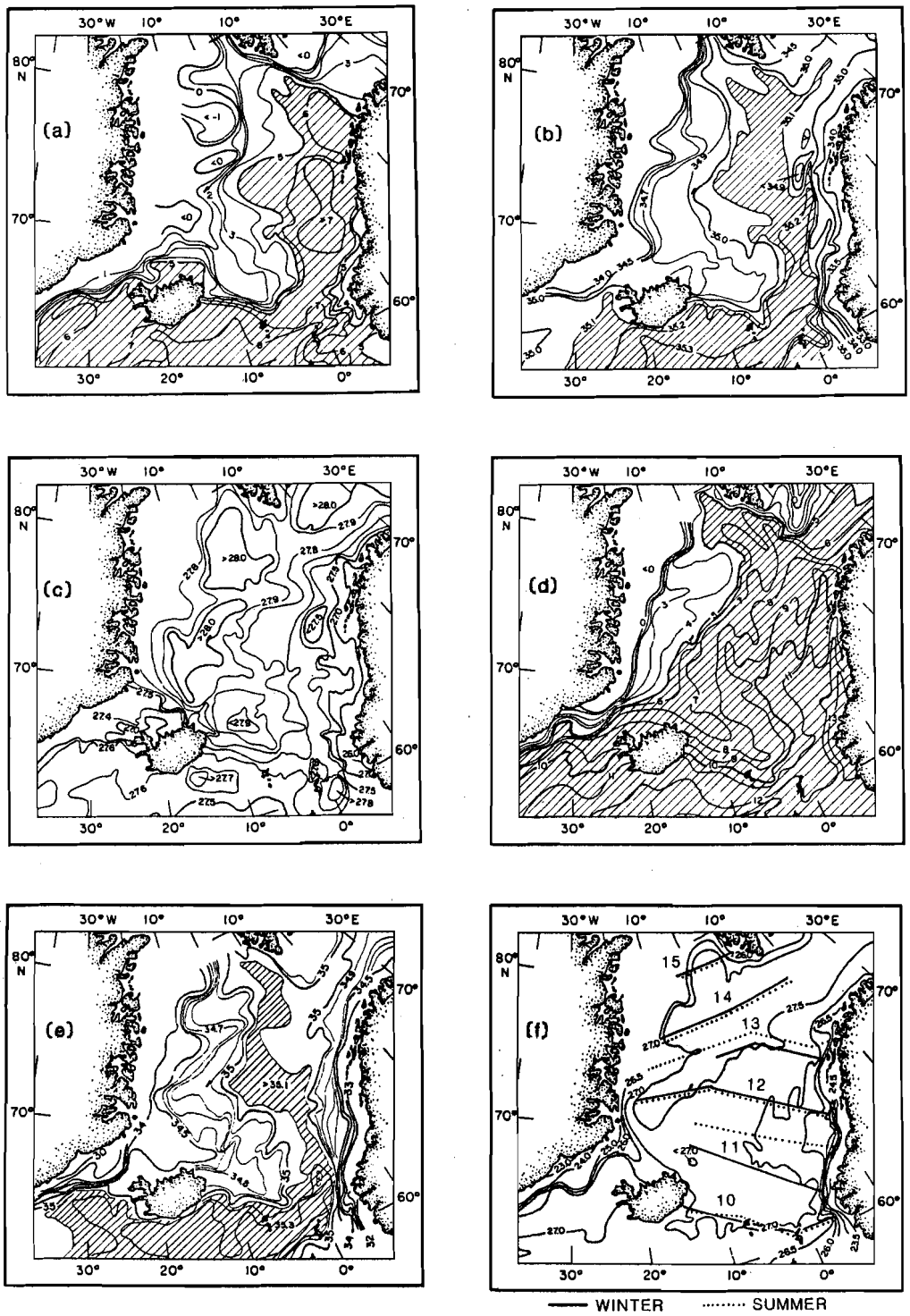

Fig. 4.5a–f. Surface contours of T, S, and σ_t for the GIN Sea [from **Dietrich** (1969)]. (a) temperature, winter; (b) salinity, winter; (c) σ_t, winter; (d) temperature, summer; (e) salinity, summer; and (f) σ_t, summer. Also numbered sections on (f) correspond to those of Fig. 4.6. Data are from the 'Polar Front' surveys of the International Geophysical year 1957–1958. The summer composite extended into autumn and the winter into spring, see cruise list in **Trangeled** (1974).

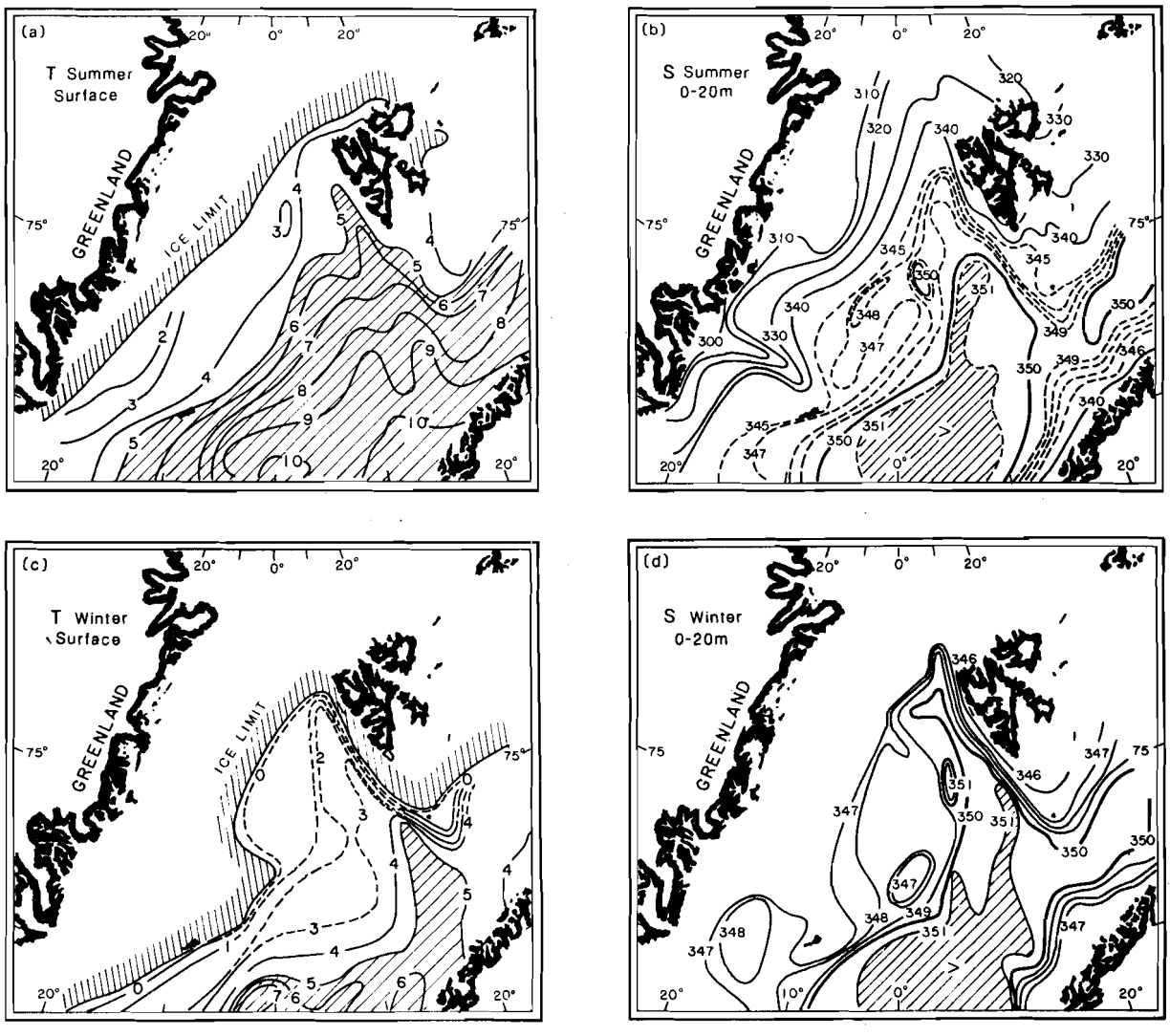

Fig. 4.6a–d. Climatological averages of (a) temperature at the surface (June–November), (b) salinity from 0–20 m, (June–November), (c) temperature at surface (December–May) and (d) salinity from 0–20 m (December–May) in the GIN Sea north of 69°N. [From **Koltermann** and **Machoczek** (1985).]

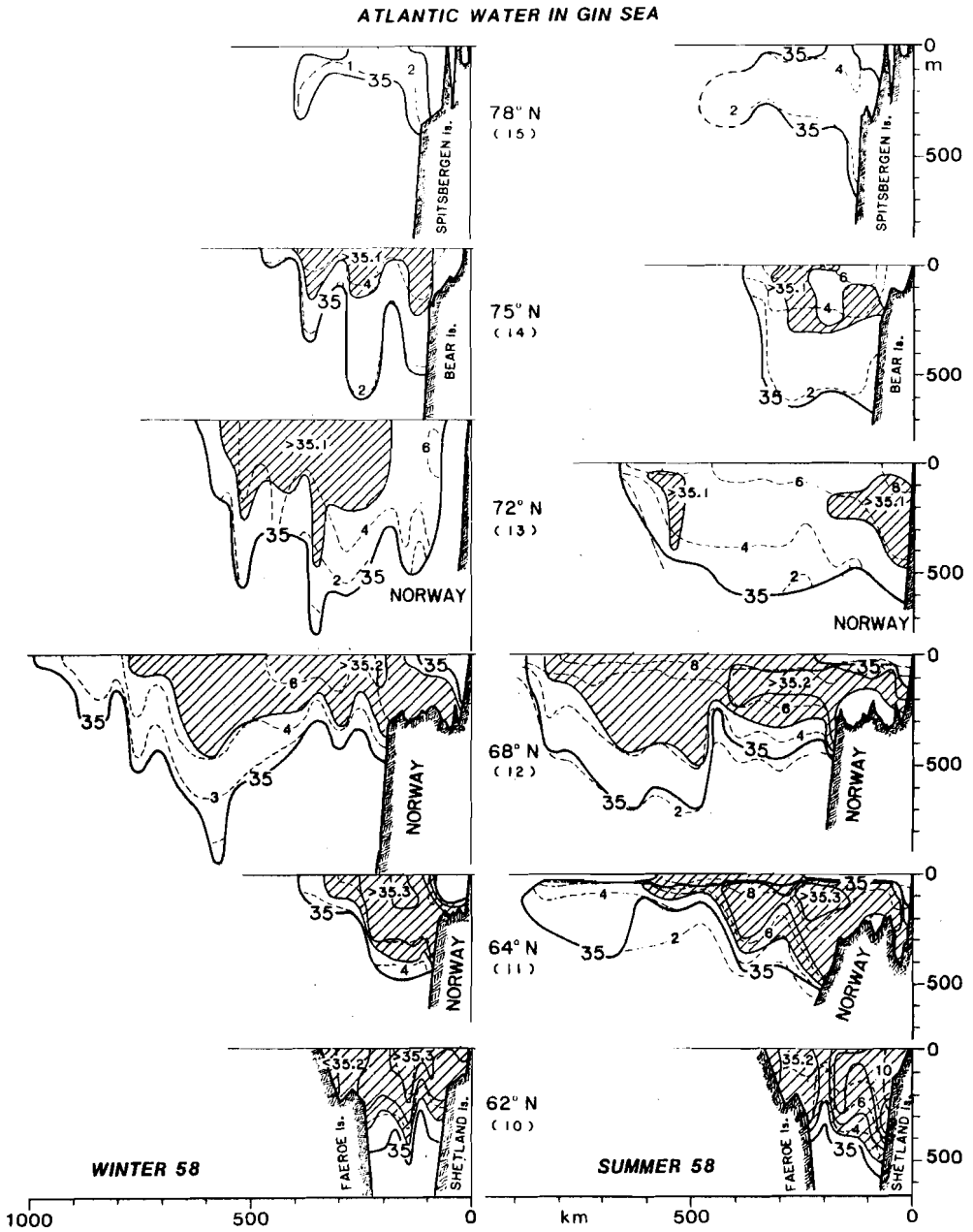

Fig. 4.7. The cross-sectional distributions of the temperature (°C) and salinity (ppt) of the Norwegian Atlantic Water at six locations (given in Fig. 4.4d) for both the winter (left panel) and summer (right panel) 1958. [From **Dietrich** (1969).]

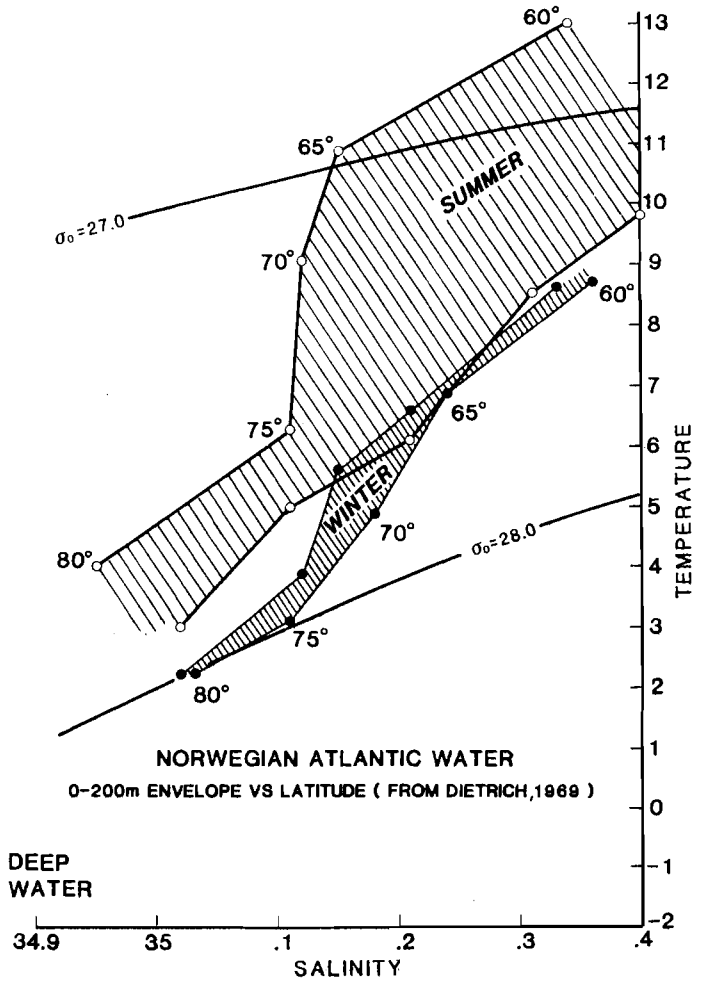

Fig. 4.8. The T-S regression of the Norwegian Atlantic Water as a function of latitude for both winter and summer 1958. At each 5° of latitude both the surface and 200 m water type is plotted with open circles for summer and solid circles for winter. [Data from **Dietrich** (1969).]

that with a complete melting during a year the GPW would have a north-to-south salinity decrease of at least 2 ppt. Instead such salinity gradients are observed and our estimates indicate, if anything, a slight increase of the mean salinity, i.e. from $S = 33.6$ to $S = 33.8$ ppt between Fram and Denmark Straits. Estimates of the southern ice export through the Denmark Strait are scant. We estimate the freshening of the GPW through melting must be roughly balanced by the salt entrainment from adjacent water masses. More detail on the salt balance is given in Subsect. 5.4.

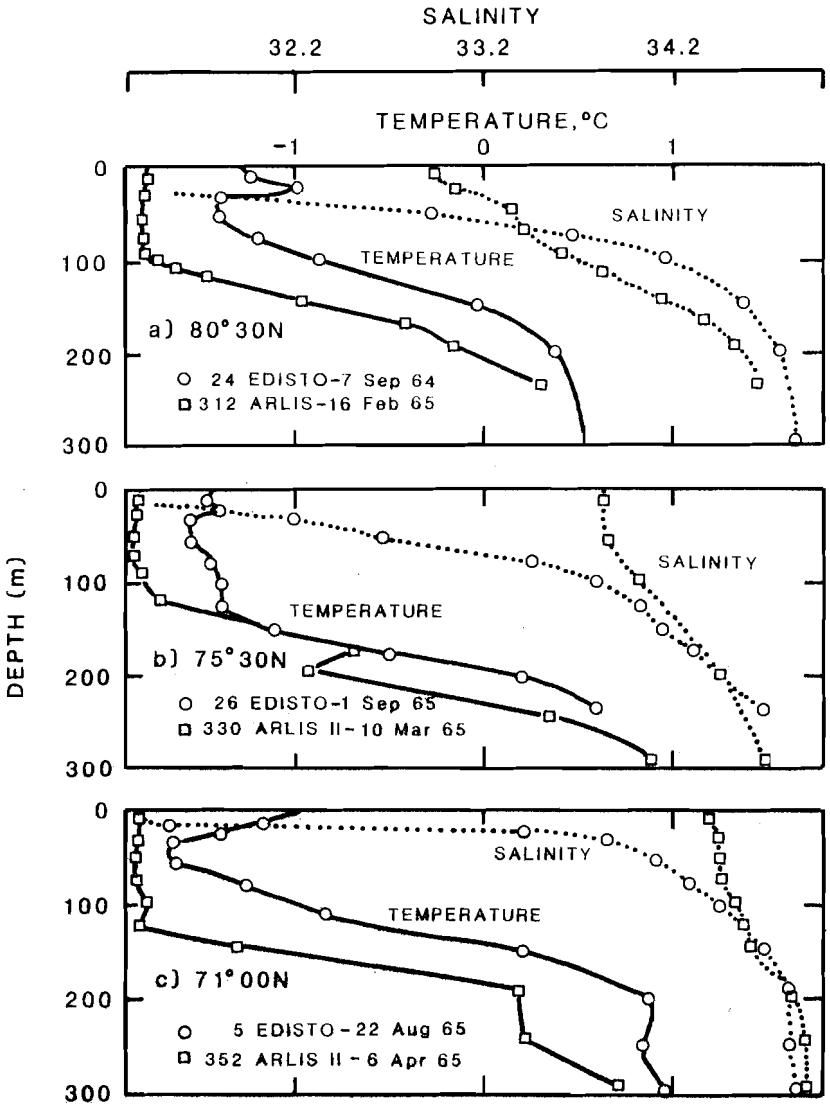

Fig. 4.9. **Vertical profiles of the GPW at three locations in the East Greenland Current for both stratified and unstratified season. [From Aagaard and Coachman (1968b).]**

The vertical distributions of T and S of the GPW from three locations are shown in Fig. 4.9. The summer halocline is much sharper as a result of the summer melt and the winter thermocline is much deeper as a result of winter convective mixing. The seasonal difference in surface layer salinities is around 1.2 ppt, and would require a $\sim$ 4.30 m of fresh water addition to a 120 m column. The result of melting this much water from ice would be a 3 K lowering of this layer's temperature from April to August. The actual change was an increase of 0.5 K, suggesting that in this case practically all of the seasonal heating was expended to satisfy the heat of fusion.

The summer T profile has a minimum at a depth of $\sim$ 50 m, which is evidence of the considerable impact of summer warming on the water column. The winter isothermal layer extends to a depth of $\sim$ 120 m, but the vertical extent of the winter convection is probably better indicated by the shallower isohaline layer. Deep convection is limited by density constraints, for example in Fig. 4.9b, the pycnoclinal density difference is $0.4\sigma_t$ units.

■ *4.1.3. Arctic Surface water (ArSW)*

The NwAtW and the GPW are the two major surface waters in the GIN Sea which are directly derived from the Atlantic and Polar Water inputs. These waters do not completely fill the surface layer of the GIN Sea. Instead they are constrained dynamically to the east and west sides of the basin, respectively. The large intervening region is occupied by what we have chosen to call the Arctic Surface Water (ArSW) which has its origin entirely within the GIN Sea, being derived from mixtures of the boundary waters exposed to atmospheric exchanges. This is essentially the same definition used by **Helland-Hansen** and **Nansen** (1909), by **Stefansson** (1962), and by **Swift** and **Aagaard** (1981). According to our water mass schematic of Fig. 4.3, the ArSW has salinities that range from 34.4 to 35.0 ppt, but the bulk of the water is found in the range 34.6 to 34.9 ppt. Its minimum temperatures run from approximatively $-1.8\,^{\circ}$C to $4\,^{\circ}$C, and the maximum temperatures are in the range of $7\,^{\circ}$C to $10\,^{\circ}$C. In the horizontal plane, the warmer waters are associated with higher salinities, which could indicate a higher proportion of NwAtW. With depth, the temperatures decrease and the salinities increase slightly. In our discussions we distinguish between the Greenland Arctic surface water (GArSW) and the Iceland Arctic Surface Water (IArSW) in recognition of an important trend between the surface waters of these two basins: those of the Greenland Sea are warmer and saltier than those of the Iceland Sea. This reflects the relatively greater exposure of the Icelandic surface waters to admixtures of GPW and/or a longer exposure to atmospheric exchange; it also reflects the relatively greater admixtures of NwAtW in the Greenland Sea. Note the ArSW water-type envelope defined here includes the Greenland Gyre Surface Water defined by of **Carmack** (1972) and the Arctic Surface Water in the Iceland Sea defined by **Swift** (1980).

The ArSW is the most seasonal of the GIN Sea water masses, all but disappearing in the winter. Autumn and winter heat losses cause the ArSW to lose its thermal stratification and to merge with the water type into that of the upper intermediate water below it. An example of the seasonal progression of vertical profiles is given in Fig. 4.10. Between summer and fall, the heat is redistributed with a surface-layer loss (0 to 100 m depth) and an intermediate-layer gain (100 to 500 m depth), which is surmised to be mostly of advective origin on the basis that there is an associated salt gain and that the profile is not suggestive of a downward heat flux through penetrative mixing. Between fall and winter, the profiles become vertical, a fact which indicates large surface heat losses and convective mixing. Note, that in Fig. 4.10 the winter profile is not from the same year. The collapse to a winter isothermal profile (at $0\,^{\circ}$C) in the surface and intermediate layers is characteristic of

the ArSW, whereas it is not typical of the GPW nor of the NwAtW each of which retain their water mass definition throughout the year.

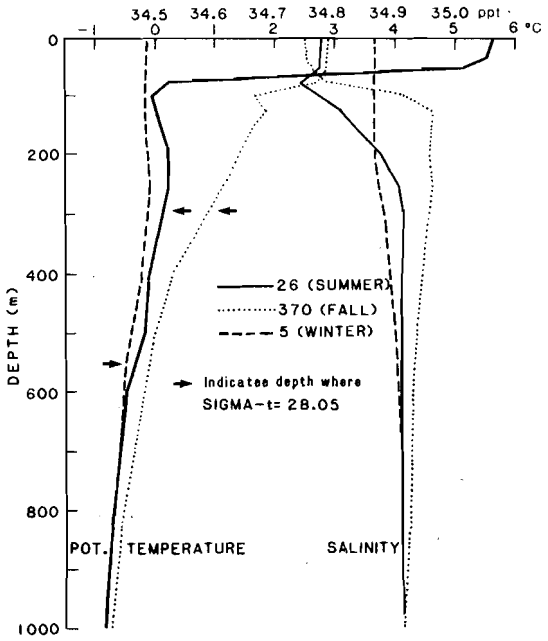

Fig. 4.10. The vertical profiles at a location (about 150 km south of Jan Mayen) in the northern Iceland Sea from: *Edisto* St. 26, 28 Aug. '74; *Bjarni Saemundsson* St. 370, 31 Oct. '74; and *Hudson* St. 5, 1 Mar. '82. [From **Swift** and **Aagaard** (1981); **Clarke, Reid** and **Swift** (1984).]

By computing the areal average over a number of stations in the eastern Icelandic Sea, **Swift** and **Aagaard** (1981) have confirmed what appears to be indicated by Fig. 4.10, i.e. that the collapse of the IArSW water type to an intermediate water type occurs during the fall-to-winter transition. For the 1974–75 season, they estimated an average temperature decrease of 1 K and a salinity increase of 0.26 ppt in the upper $\sim$ 300 m of the water column. They could account for the heat loss through atmospheric heat extraction but could not account for the salinity increase by evaporation or brine addition. They then suggested that during winter convective admixtures of the previous crop of underlying intermediate water and lateral mixtures of NwAtW combined to increase the salinity of the surface waters. The heat added by these admixtures could still have been lost through atmospheric exchange.

An increased admixture of NwAtW to the GArSW during the winter was also noted by **Carmack** and **Aagaard** (1973). This is an important point about the redistribution of salt within the system: i.e. that it occurs less as a continuous diffusive process but more as a discrete isopycnal/convective mixing event. The seasonal freshening that must follow this in spring/summer is controlled by different processes and perforce adds to the observed interannual variability of the ArSW.

The contribution of GPW to the IArSW in the north, central, and eastern Iceland Sea appears to be negligible on the basis of tritium observations (**Swift** and **Aagaard**, 1981). In this area, tritium has the same concentration ($\sim$ 6 tritium units) as that, found in NwAtW, whereas the concentration observed in the GPW is 20 tritium units. In the southern region of the Iceland Sea, some GPW influence (5–10%) was evident wherever slightly elevated tritium levels were found. However, even here the extent of the GPW influence varies considerably, as seen in the salinity distributions north of Iceland (**Malmberg**, 1984).

■ *4.1.4. Barents Sea Waters (BrW)*

We do not discuss in detail the water mass transitions occurring over the broad continental shelf region of the Barents Sea. This sea does plays a significant role in the GIN Sea thermohaline dynamics by acting as an open boundary heat sink. It also serves as a source of freshened surface water and of some deep water. We refer to the Atlantic, Polar, and Bottom categories of BrW as Barents Sea Atlantic Water (BrAtW), Barents Sea Polar Water (BrPW), and Barents Sea Bottom Water (BrBW), respectively.

An eastward branch of the NwAtC introduces NwAtW into the Barents Sea, a portion of this recirculates in the Bjornoya Trough and a portion continues eastward (see also Subsect. 5.3.6). We define the Barents Sea Atlantic Water (BrAtW) as those components of the NwAtW which are lost to and/or modified within the Barents Sea. The water type envelope is ($\sim$2–5 °C, S $\sim$34.8–35.0 ppt. The water mass boundary between the NwAtW and BrAtW does not coincide with the Spitsbergen-Bear Island-Norwegian transect, but in general bows eastward more or less conforming to the Bjornoya Trough because of the tendency for recirculation around that feature. For example, the 35 ppt contour in Fig. 4.11 generally follows the 400-m depth contour of the Bjornoya Trough. The distributions at a depth of 50 m shown in Fig. 4.11 may be considered as characteristic of the Barents Sea Opening but not as interannually invariant. In terms of a geographic boundary, the transect along the 30°E meridian is perhaps a better indicator of the cross-section of the waters entering the Barents Sea.

The Barents Sea compensates for the volume of NwAtW imported by exporting the two modified water masses BrBW and BrPW to the GIN Sea. The BrBW is the result of a local cooling of the BrAtW which produces a shelf bottom water that returns to the GIN Sea via the Bjornoya Trough. The data of **Dietrich** (1969) and that of **Dickson** and **Doddington** (1970) show water types of $T < 1$ °C and $S > 35$ ppt

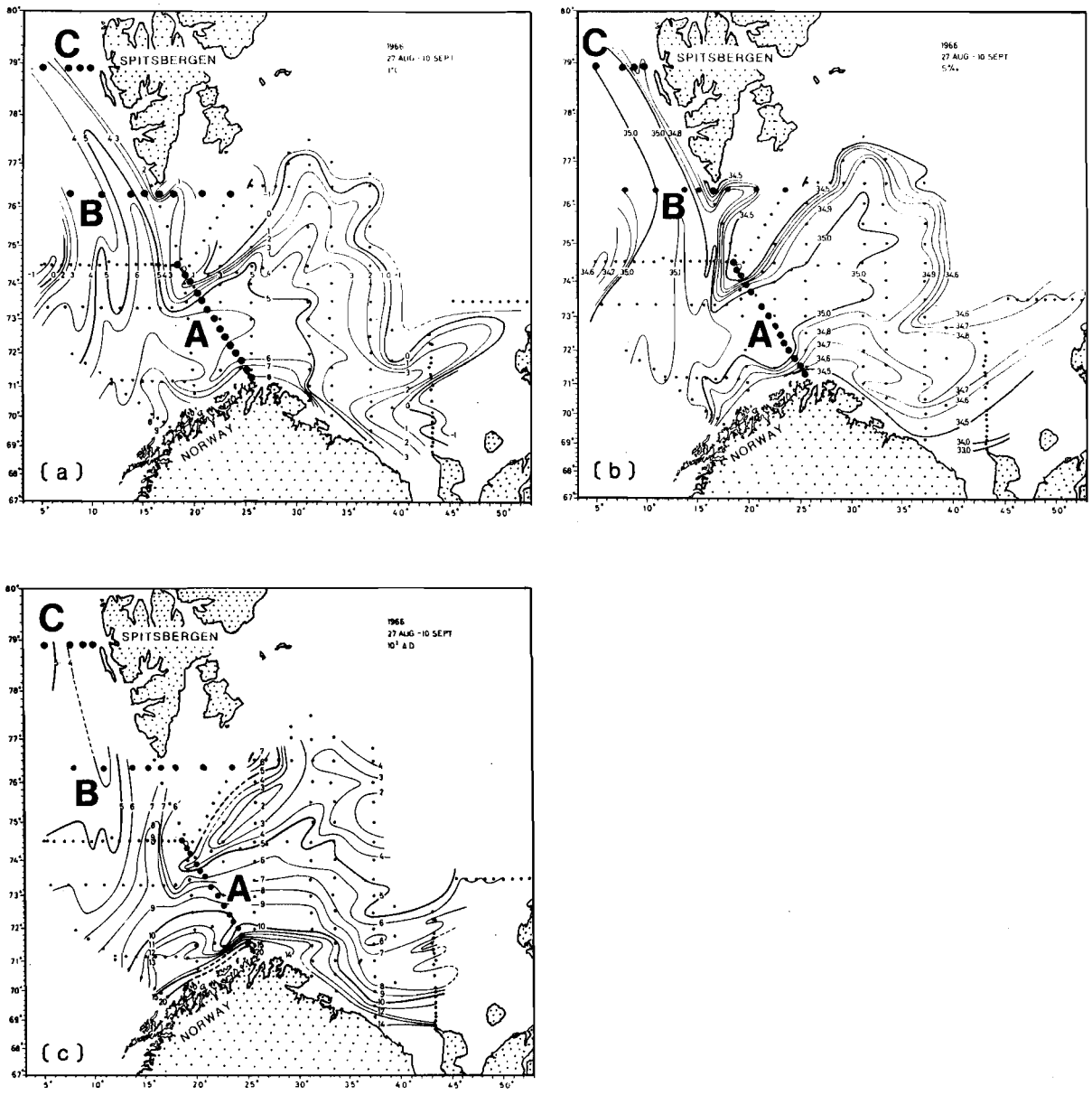

Fig. 4.11. Contours of (a) temperature and (b) salinity at 50 m and (c) dynamic height 0/200 dB in the Barents Sea Opening. [From **Dickson**, **Middtun** and **Mukhin** (1970).] The lettered sections refer to Fig. 4.12.

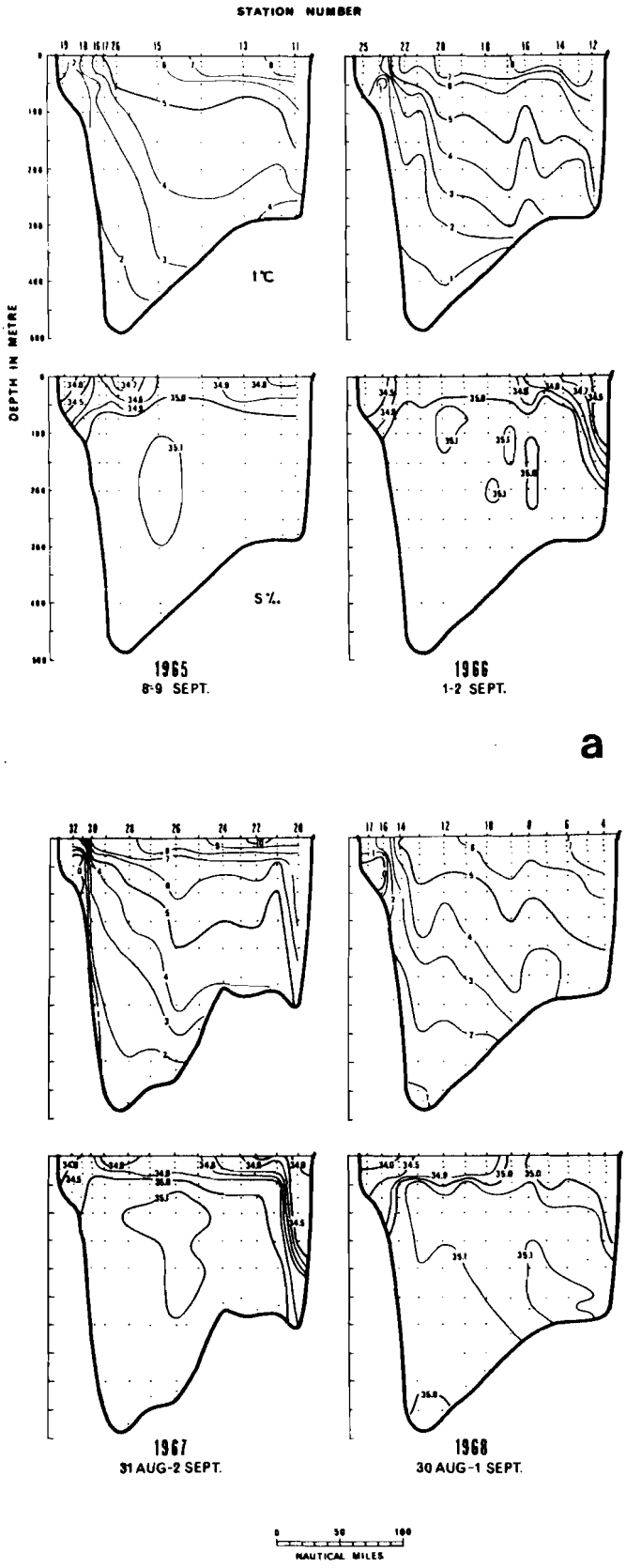

Fig. 4.12a. T and S contours across the Bjornoya Trough. The location of Sect. A is given in Fig. 4.10 with Bear Island on the left for four successive years. [From **Dickson, Middtun** and **Mukhin** (1970).]

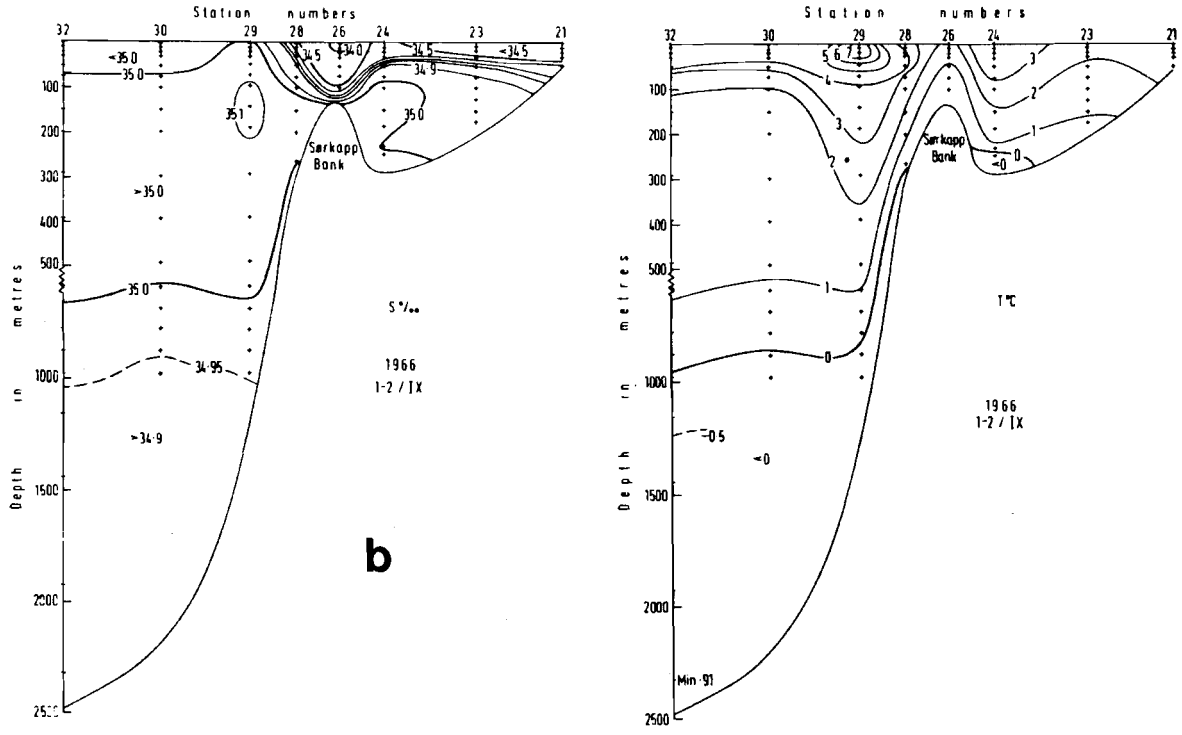

Fig. 4.12b. T and S contours corresponding to Sects. B and C in Fig. 4.10. [From **Dickson** and **Doddington** (1969).]

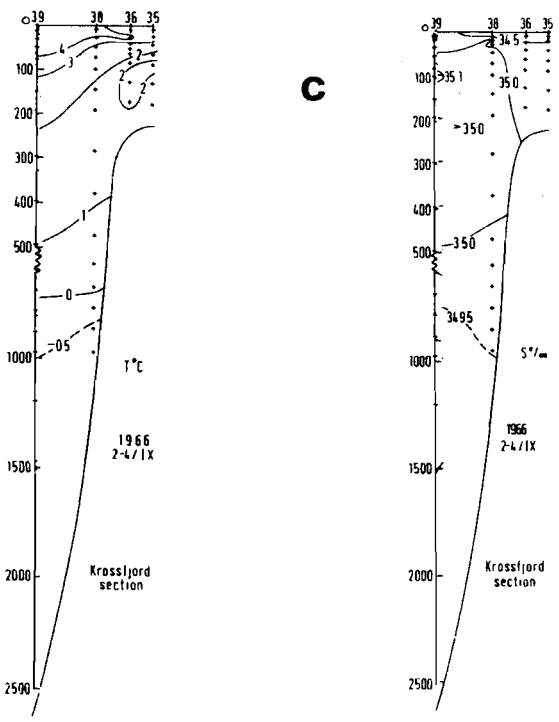

Fig. 4.12c. T and S contours corresponding to Sects. B and C in Fig. 4.10. [From **Dickson** and **Doddington** (1969).]

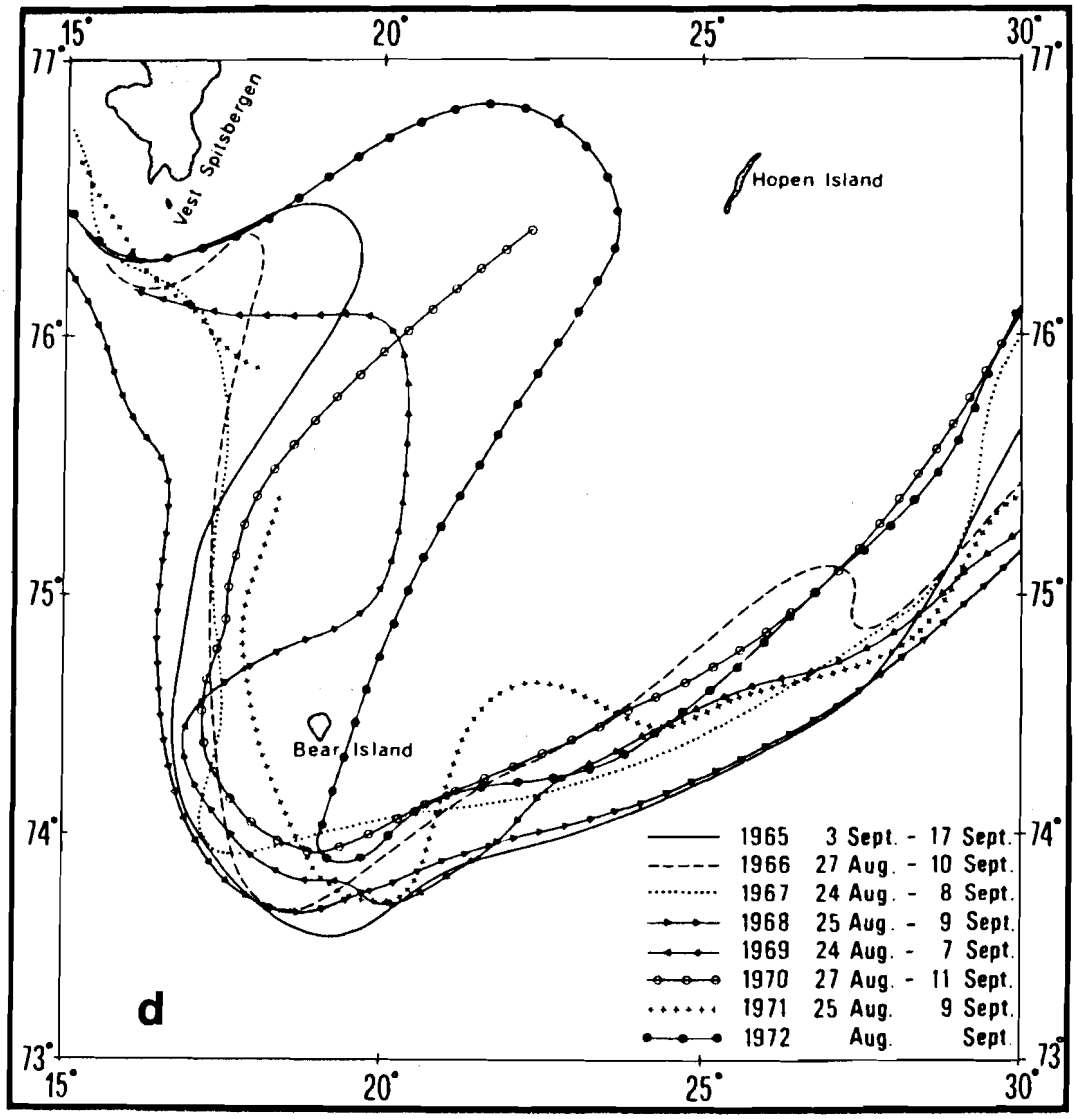

Fig. 4.12d. Variability in the 3 °C isotherm in the northern portion of the Barents Sea opening. [From **Foster, Johannessen** and **Isoppo** (1974).]

on the bottom of the northern side of the Bjornoya Trough (Fig. 4.12a). This water has potential densities of $\sigma_T \sim 28.05$ and its entry into the GIN Sea appears to be northward along the Spitsbergen continental slope at a depth dictated by its density (**Meincke**, personal communication). A similar water type was found on the 1966 transect west of South Cape shown in Fig. 4.12b at depths in the range $\sim$ 300 to 700 m. Its presence was much less apparent in the transect further to the north (Fig. 4.12c). The data of **Dickson** and **Doddington** (1968, 1970) show considerable annual variability in the amount of BrBW, implying variability in the winter cooling of BrAtW and/or in its supply. We have mentioned only the portion of the BrBW that returns to the GIN Sea. It must be noted that there is another, perhaps more significant, portion formed on the Polar Sea side of the Barents Sea Opening sill, which runs off the Barents shelf directly into the Eurasian Basin (**Swift**, **Takahashi** and **Livingston**, 1983; **Midttun**, 1985).

The BrPW is imported from the Barents Sea by the East Spitsbergen Current which transports PW with admixtures of BrW, anticyclonically to the south and west, around Spitsbergen. It has a water type of $T \sim -1\,^{\circ}\mathrm{C}$ to $3\,^{\circ}\mathrm{C}$ and $S < 34.4$ ppt. It is confined to the northwest of the Bjornoya Trough generally following the shallower contours of the continental ridge extending southwestward from eastern Spitsbergen to Bear Island. This is reflected in contours of Fig. 4.11b, where the East Spitsbergen Current (ESC) that carries this water mass first makes an anticyclonic loop north of Bear Island and then continues to the north along the coast of Spitsbergen. The boundary between the BrPW and the NwAtW to the west is distinct but variable, particularly over the continent shelf trough between South Cape and Bear Island, as shown in the position of the $3\,^{\circ}\mathrm{C}$ isotherm for the years 1965–1972 in Fig. 4.12d. The data of **Dickson** and **Doddington** show considerable variability in the amount of BrPW surviving along the western Spitsbergen shelf from their observations of the four consecutive years of 1966–1969. The BrPW is generally several tenths of σ_t units less dense than the NwAtW, and mixing with that water mass is an important aspect of the local NwAtW water-type evolution.

■ *4.1.5. Norwegian Shelf Water (NwShW)*

Between the 35 ppt isohaline and the Norwegian coast lies a water mass which we refer to as the Norwegian Shelf Water. It occupies the Norwegian Continental Shelf residing between the coast and a prograde front approximately over the shelf break and the coast. This front is referred to here as the Norwegian Shelf Front (NwShF) and it constitutes the water-mass boundary between the NwAtW and the NwShW. The 35 ppt isohaline intersects the bottom around the 150-m isobath and intersects the surface considerably seaward, often over the shelf break. The NwShW is carried north by the Norwegian Coastal Current (NwCoC) and consequently is advectively supplied from the south; in fact, it is considered to be a continuation of the relatively fresh Baltic current that emanates from the Skagerrak as the Baltic surface outflow and flows westward along the southern coasts of Sweden and Norway. The input salinity at 60°N is low, $S \sim 32$ ppt.

The northern terminus of the NwShW with respect to the GIN Sea is in the vicinity of North Cape where the NwCoC becomes the North Cape Current (NCaC) flowing west into the Barents Sea. At North Cape the salinities are around 34.5 ppt, probably as much a result of local freshening of NwAtw as to northward advective input of NwShW. **Helland-Hansen** and **Nansen** (1909) described the major features of this water mass. Their observations showed a fairly linear increase in salinity northward at 1 salinity unit/600 km. This increase, as they noted, is a result of cross frontal mixing with the NwAtW. A larger alongshore salinity gradient exists in the region of the North Sea entrance because of the greater cross-frontal current shear in the Norwegian Trench, where the adjacient NwAtW is a countercurrent flowing south and entering the North Sea (see Subsect. 5.3.5) relative to the salinity gradient in the region of North Cape where the coastal and offshore flows are both eastward tending to reduce the water mass distinction between coastal and offshore waters.

The NwShW seasonal cycles (cf. **Midttun**, 1969) show a steady increase in salinities through winter to a spring maximum, followed by a summer through-fall decrease in salinities corresponding to the local runoff supply. This dilution effect decreases northward alongshore, until east of North Cape where local run-off increases. The seasonal temperature cycle is also modified alongshore. **Midttun** (1969) observed a 4 K range at North Cape compared to a greater than 6 K range at Utsira (59°N) at a depth of 50 m. An example of the seasonal and longitudinal variation can be seen from a comparison of Figs. 4.12a, 4.13, and 5.21. The cross-sectional area, included between the coast and the 35 ppt isohaline, remains fairly constant seasonally in the south, has a winter minimum in the middle, and again is fairly constant in the north. The seasonal variation at the middle section suggests that the local salt content is more controlled by diabathic dilution and mixing than by alongshore advection. During winter the south-to-north density variation is roughly equivalent to that across the front $\sim 0.5\sigma_t$ units. This is not the case during summer, when the southern areas experience greater surface heating and greater influx of low salinity waters, which then cause the cross-frontal density gradient to be considerably larger ($\sim$3–4σ_t units) than that observed in the northern areas ($\sim 0.8\sigma_t$). This is an important difference between the water mass boundary (NwAtW and NwShW) in the North Sea entrance and that in the Barents Sea opening: to the south there is more baroclinicity and a sheared flow (see Subsects. 5.3.5 and 5.3.6).

4.2. INTERMEDIATE WATERS

Intermediate water masses are so named because they have an intermediate distribution with respect to depth. Within basins that have a negative thermohaline circulation (i.e. forming dense water) intermediate also implies an intermediate stage in formation between a surface and deep water. Intermediate waters are formed during the winter by the atmospheric buoyancy extraction processes, i.e. they are the waters that result from the heat and water vapor losses to atmosphere that increase

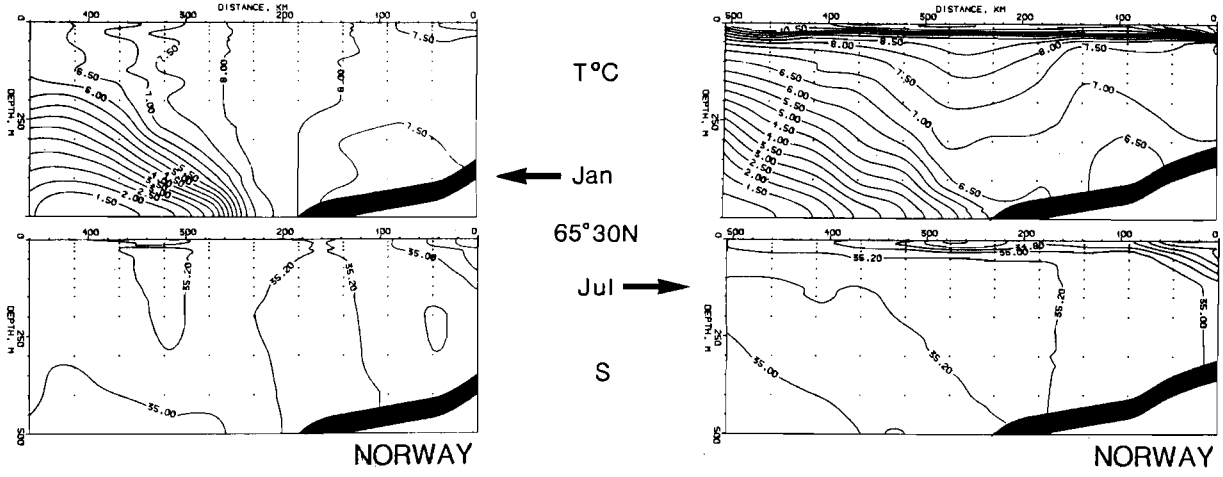

Fig. 4.13. Cross-sectional contours of T and S for January (left panel) and July (rigth panel) for a location midway along the Norwegian coast at 65°30′ N. The T and S values are historical means including 1981 from the Norwegian Oceanographic Data Centre, University of Bergen. Contours are in $\Delta T = 0.5$ K and $\Delta S = 0.2$ ppt. The offshore distance is shown from a point 35 km from the Norwegian coast. [From **Johannessen** and **Sandven** (1983).]

the density of the surface water by decreasing its temperature and increasing its salinity.

The depth to which water is affected is considerably greater during winter buoyancy extraction than during summer buoyancy addition, because of the greater efficiency of the associated transfer processes, i.e. convection versus diffusion. The effect of wind mixing on the upper $\sim$ 50 m, which occurs during both seasons, dominates over diffusion during summer. During winter, the water type of the deep convective layer is determined by the heat (and water vapor) losses acting on the existing surface water type together with mixtures of all, or portions, of the underlying (intermediate) waters. During summer, only the surface (wind mixed) portion of this is converted back to a surface water type, leaving underneath a new crop of intermediate water.

The above one-dimensional description of winter water mass production is an over-simplification, omitting the important exception that considerable lateral input is often present, so that the deepening surface layer is composed of not just a vertical mixture of surface and underlying waters but also of horizontally adjacent waters. This is particularly relevant when the production occurs within a cyclonic circulation feature, in which the surface layer is divergent and the subsurface layer is convergent, hence requiring the introduction of water laterally into the convective zone. This is thought to be important in the Greenland Sea (**Carmack**, 1972), where there is

considerable subsurface movement of NwAtW westwards toward the center of the Greenland cyclonic gyre.

It is important to note also that the extent of winter convection is not just a function of the intensity of the winter buoyancy extraction process, which in the GIN Sea is mostly thermal, but also of the 'preconditioning' of the exposed waters. This term is used to describe a previous change in water type, usually through atmospheric buoyancy extraction processis, that renders a surface water mass more susceptible to deep convection when exposed to further buoyancy losses. The NwAtW with its elevated salinities becomes a preconditioned water mass as it loses heat transversing the surface of the GIN Sea and, as a result becomes a major component of winter water mass production.

Within the GIN Sea the intermediate waters are of two origins: those formed locally (for which the water mass volume depends mostly on the severity of the previous winter but also somewhat on the mildness of the summer) and those formed elsewhere and whose local presence is only a consequence of advection. Often intermediate waters of both origins are found at the same location. The specific water type of a local intermediate water tends to vary interannually as do the conditions necessary for its winter production, viz. the intensity of the winter, the circulation, and the preconditioning of upper-layer waters. For this reason the water types cited should be regarded as somewhat qualitative. We refer to those intermediate waters derived advectively from the NwAtW as Atlantic Intermediate Waters (AtIW), and to those produced as a result of winter convection as Arctic Intermediate Waters (ArIW). We have taken $S = 34.9$ as the dividing salinity value, which implies that with respect to the GDW the AtIW is warmer and the ArIW is colder.

■ *4.2.1. Intermediate waters of the Greenland Sea*

(a) Return Atlantic Intermediate Water (rAtIW). The NwAtW becomes an intermediate water, when it submerges off of Spitsbergen as a result of its preconditioning and of being overlain with mixtures of BrPW from the East Spitsbergen Current. At approximately this juncture the flow of the NwAtIW branches, with one portion entering directly into the Polar Sea as the Polar Atlantic Intermediate Water (PAtIW), and another portion recirculating to the west and becoming incorporated into the East Greenland Current, (EGC) system. We distinguish this as the 'return' AtIW (rAtIW) because of its important return southward within the EGC. The recirculation from the West Spitsbergen Current (WSC) occurs over a large meridional extent and includes some entry into the Polar Sea, with the result that the rAtIW is vertically sorted, with its more directly recirculated portions (warmer, saltier) above those slightly denser versions arriving from further north (e.g. **Swift**, 1980). The rAtIW has a water type which lies between 0 °C and 2 °C and between 34.9 and 35.0 ppt, and it occupies the depth range of

$\sim$ 150 to 800 m (**Aagaard**, 1968) underlying the GPW where it is distinguishable by a temperature maximum, often 2 °C at a depth of 300 m. Recent more densely spaced observations have shown more detail in the structure of the rAtIW than was observed previously (cf. **Paquette** and **Bourke**, 1985); for example, the cross-sectional contours of Fig. 4.14 show, in addition to the well-defined rAtIW core, several detached parcels to the west over the Greenland Shelf. The amount of rAtIW loss to the GPW via these parcels, is not well known. In Subsect. 5.4, we have estimated that $\sim$ 1 Sv is admixed into the overlying GPW, probably through both the process of parcel entrainment and through penetrative mixing during winter convection.

(b) Jan Mayen Intermediate Water (JMAtIW). Significant advective losses occur eastward through subsidiary currents that branch from the EGC. The most important of these branch currents occurs at 73°N in the form of the Jan Mayen Current (JMC) which carries a portion of the rAtIW eastward into the Greenland Sea. This water we will refer to as the Jan Mayen AtIW (JMAtIW). During the winter season, the eastward flux of JMAtIW, is more extensive than during the summer season (Fig. 4.15). This seasonality has important implications, i.e. by prompting a source of heat/salt during the winter cooling season to the southern Greenland Sea, see also Subsect. 4.3.3.

(c) Greenland Atlantic Intermediate water (GAtIW). **Carmack** (1972) noted a strong bimodal distribution of AtIW in his volumetric T-S analysis of the Greenland Sea, as did **Carmack** and **Aagaard** (1973). These authors found submerged waters of NwAtW origin which were located within neither the WSC nor the EGC current systems. They identified these subsurface waters as having had two sources: one to the south and one to the east. The southern one was the JMAtIW. The one from the east was more extensive and had an obvious origin in the NwAtC and WSC, suggesting in fact, that it was a westward subsurface extension of NwAtW. This latter water of eastern origin we refer to as simply 'Greenland' AtIW (GAtIW). The difference between the JMAtIW and the GAtIW is slight considering the former has circuited the Greenland Sea before encountering its companion the GAtIW: the JMAtIW is cooler and fresher with $\sim$ 0.0 to 0.5 °C and 34.9 to 35.0 ppt; and the GAtIW has $T \sim$ 2.0 to 4.0 °C and $\sim$ 35.0 to 35.15 ppt (**Carmack**, 1972; **Clarke, Reid** and **Swift**, 1984). An important seasonality exists in the GAtIW whereby during winter the salinity maximums are larger than in summer and the 35-ppt isohaline, for example, extends further into the Greenland Sea (Fig. 4.15).

(d) Greenland Arctic Intermediate water (GArIW). Another type of intermediate water that is found in the Greenland Sea is less dense, colder, and fresher than the GAtIW. This is the Greenland Arctic Intermediate Water (GArIW) and is formed during winter from the GArSW and underlying intermediate waters. With these conditions of formation, its amount and water type are variable. Generally, it lies above the GAtIW and below the GArSW, and its presence is characterized by a temperature minimum. We class its water type as $T < 2$ °C and $S \sim$ 34.7 to 34.9 ppt.

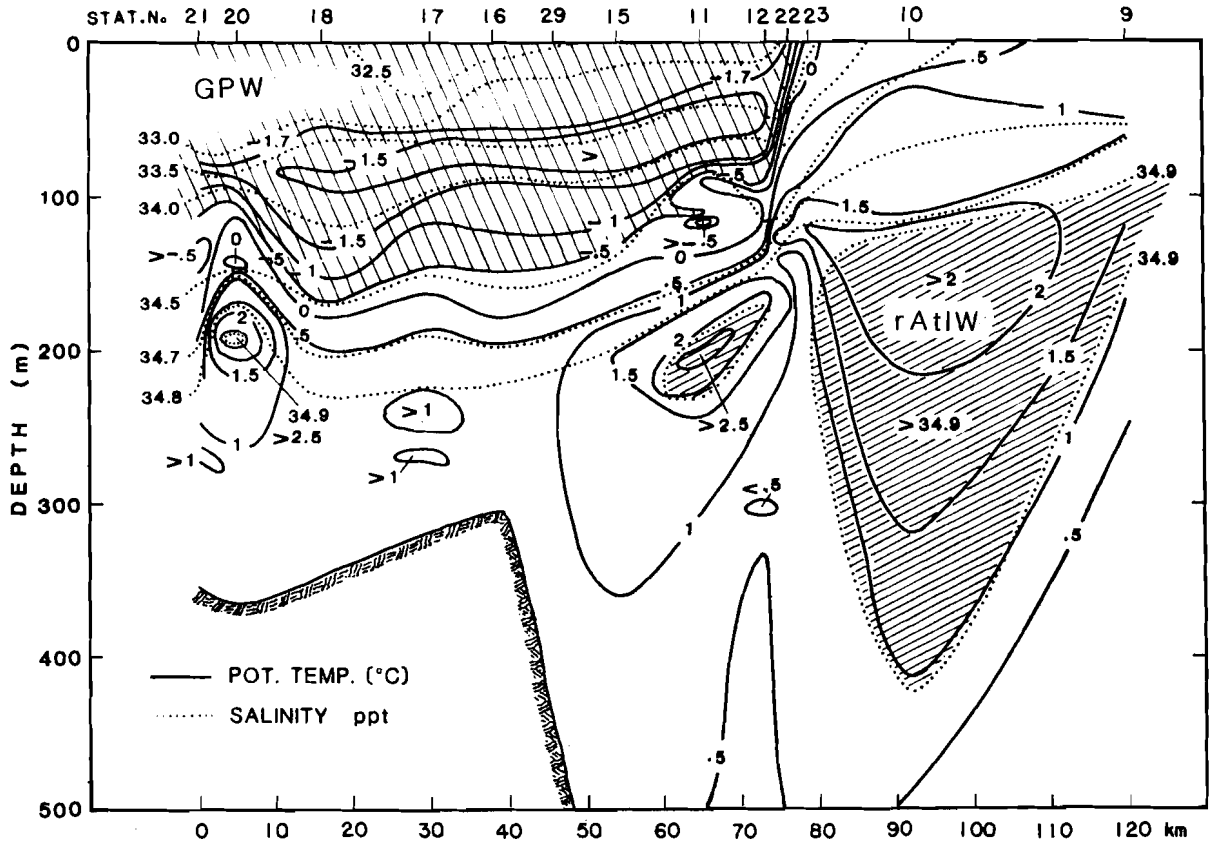

Fig. 4.14. T and S contours across the East Greenland Current at 76°30'N by the *USCGC Northwind* in October 1981. The rAtIW is hatched. [From **Paquette, Bourke, Newton** and **Perdue** (1985).]

■ *4.2.2. Intermediate waters of the Iceland and Norwegian Seas*

(a) Return Atlantic Intermediate Water (rAtIW). As mentioned in Subsect. 4.2.1(a) the rAtIW continues southward into the Iceland Sea as a subsurface component of the East Greenland Current. Initial observations indicated that the rAtIW water type underwent little modification from north to south in the EGC. For example, a comparison of the *Arlis II* profiles from the Polar Sea to Denmark Strait (Fig. 4.16) showed no trend in the rAtIW type. The variations that were present, e.g. the warmer maximum temperature at station F in the Iceland Sea than station B in the Greenland Sea, were apparently due to the fact that the *Arlis II* was not always positioned over the rAtIW

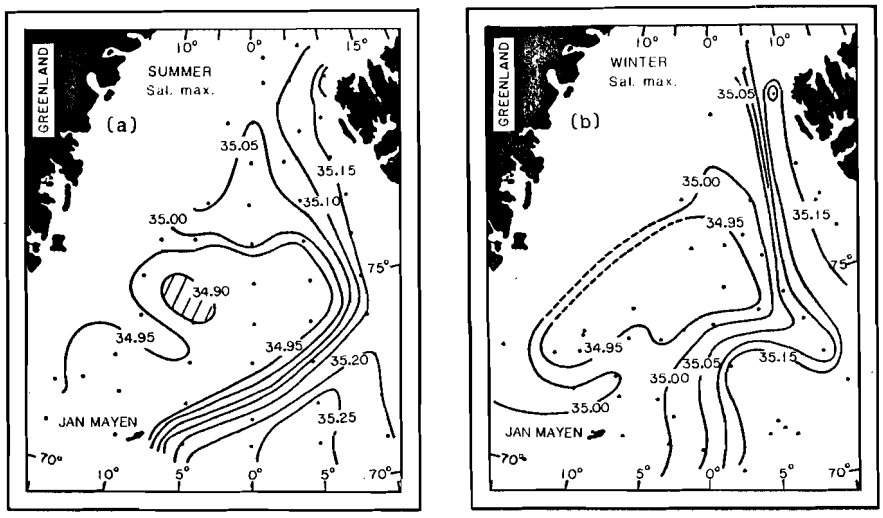

Fig. 4.15. Contours of the salinity maxima: (a) summer from *Atka*, August 1962; and (b) winter from *Atka*, January–February 1954. *G.O. Sars*, March 1954, and *Edisto*, March 1955. The shaded portion in (a) had no maximum. [From **Carmack** (1972).]

core. However, **Swift** (1980) has pointed out that this water is not completely trapped along the Greenland slope and that eastward extensions exist through the north and south gaps in the Kolbeinsey Ridge. The result is insignificant interleaving and advective losses of the rAtIW, to the more eastern portions of the Iceland sea. **Swift**'s analysis also showed a regression of the rAtIW core water type in transiting the Iceland Sea from 1.3 °C, 34.94 ppt to 0.1 °C, 34.95 ppt.

(b) Iceland Atlantic Intermediate Water (IAtIW). In the central portion of the Iceland and Norwegian Seas (between the NwAtC and EGC systems) two types of intermediate water have been described by **Swift** (1980) and **Swift** and **Aagaard** (1981). The first is found above the deep water and is identifiable by both a maximum temperature and a maximim salinity, with $0\,°C < T < 3\,°C$ and $S > 34.9$ ppt at depths of 200–300 m. This is the Icelandic Sea version of the AtIW, which we refer to as IAtIW. **Swift** postulates several sources for this water: some of it comes from the Greenland Sea, probably as JMAtIW; some from the EGC or rAtIW; and some is a direct input from the northeast (south of Jan Mayen Island) through cooling of the NwAtW.

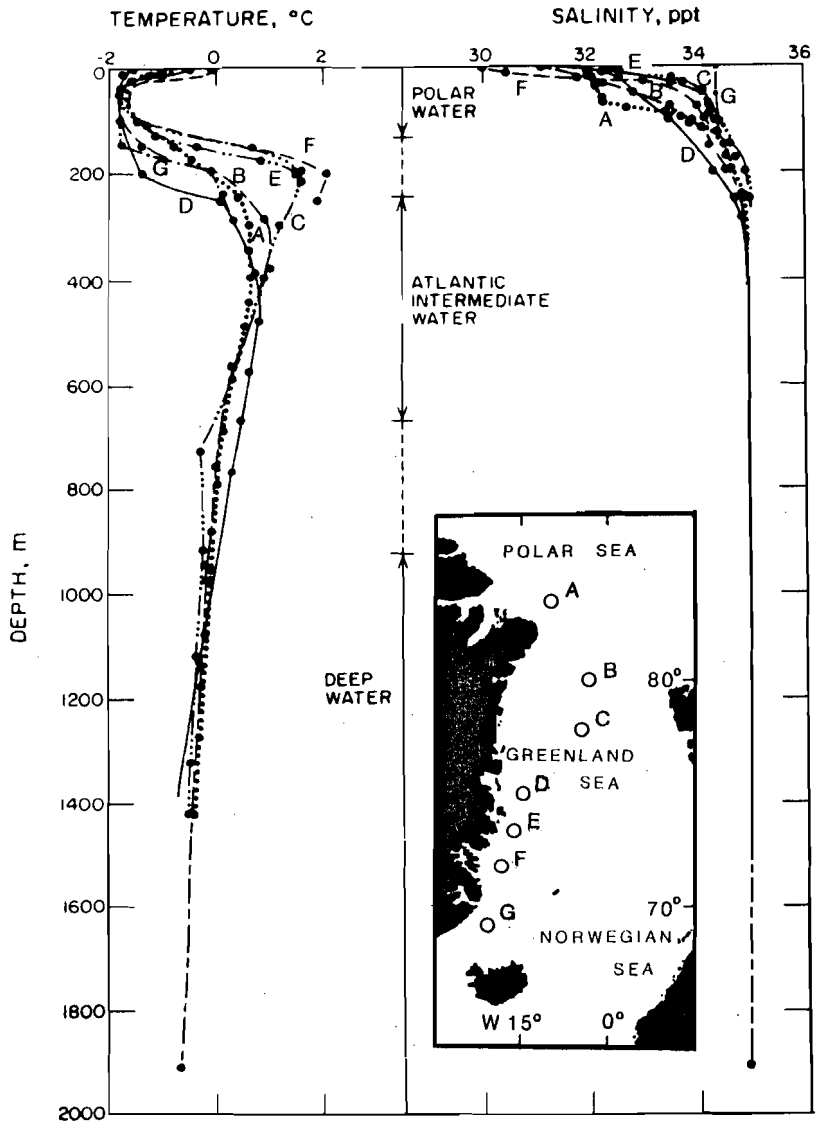

Fig. 4.16. The vertical T and S profiles from seven stations taken within the East Greenland Current, as follows: 'A' from *Belgica* St. 32, July 1905; 'B' from *Conrad Holmboe*, August 1923; 'C' from *Polarbjorn*, August 1932; 'D' from *Arlis II*, January 1965; 'E' from *Arlis II*, April 1964; 'F' from *Edisto*, September'1964; and 'G' from *Edisto*, September 1965. [From **Aagaard** and **Coachman** (1968a).]

(c) Iceland Arctic Intermediate Water (IArIW). Above the IAtIW there is a second intermediate water mass, which we refer to as IArIW as it is the Icelandic component of the ArIW. This is defined by Swift (1980) to have

$1\,°C < T < 2\,°C$ and $34.7 < S < 34.9$ ppt. In the summer it is overlain by the IArSW and, it is characterized by a temperature minimum. Winter production from the IArSW results in large seasonal variations in the volume of IArIW, since the winter thickness is $\sim$ 300 m (**Swift** and **Aagaard**, 1981). The IArIW constitutes the main winter water mass produced in the Iceland Sea. The IArIW is generally colder and always less saline than the GArIW, which itself is modified to a cooler, fresher water type by the time it reaches its more southern distributions. The fresher components of the IArIW and the GArIW would appear to be generated by lateral admixtures of GPW. On the basis of the tritium values which were observed to be high in the GPW but low in the ArIW of the northern Iceland Sea and southern Greenland Sea, **Swift** and **Aagaard** (1981) suggested that there is little GPW involved in the production of the ArIW in either Sea. They also note that local sea-ice melt may contribute to the fresher components of the IArIW. We suppose that this would be less likely along the northern boundary of the Icelandic current where contributions by GPW occur more frequently.

(d) Polar Intermediate Water (PIW). Within the East Greenland Current, a temperature minimum water is found between the GPW and the rAtIW. This has been referred to as the Polar Intermediate Water (PIW) by **Stefansson**, (1962), **Müller**, **Meincke** and **Becker** (1979) and by **Swift** (1980). It is formed as a local winter product apparently within the EGC, i.e. through convective mixing of the rAtIW and the GPW at a ratio of $\sim 2 : 1$. It is found in both the Greenland and Iceland Seas, but is a better developed feature downstream to the south where the cumulative effect of more than one winter may occur. The temperatures are less than 0 °C and the salinities range from 34.4 to 34.7 ppt, giving it some water-type overlap with the ArIW. While not contributing significantly to the internal dynamics of the GIN Sea, **Swift**, **Aagaard** and **Malmberg** (1980) identified it as a component of the Denmark outflow and presumably it may contribute to the Iceland Current in a similar fashion as does the GPW.

(e) Icelandic Current Intermediate Water (ICIW). **Stefansson** (1962) has defined the water mass of the North Icelandic Winter Water as the product of winter convective mixing between the IrAtW and the IArSW, over the north Icelandic shelf and as having the water type $\sim$ 2 to 3 °C, $\sim$ 34.85 ppt. Here we find it useful to generalize his definition to include two other intermediate water types found in the Icelandic Current system, which we define as the Icelandic Current Intermediate Water, or ICIW. Thus we include within the ICIW Stefanson's North Icelandic Winter Water, admixtures of IArIW, and a cooler fresher intermediate water formed on the north Icelandic shelf (referred to as East Icelandic Water by **Meincke** (1978). By lumping these together, we get a water type $\sim$ 1 to 4 °C and $\sim$ 34.6 to 34.9 ppt to the west narrowing to $\sim$ 2 to 3 °C, $\sim$ 34.75 to 34.90 ppt to the east. At the eastern terminus of the IC, the ICIW branches contributing both to the intermediate water output through the Færœse Channel (e.g. **Hermann**, 1967; **Meincke**, 1978) and to the NwArIW.

(f) Norwegian Arctic Intermediate Water (NwArIW). An important intermediate-water feature is the thin (< 200 m-thick) layer (evidenced by a temperature and salinity minimum) between the NwAtW and the deeper waters of the Norwegian sea. This layer is apparently a lateral extension of Icelandic Current Intermediate Water (ICIW), since its reasonably consistent water type ($\sim$ 0.5 °C and $\sim$ 34.88 ppt) falls within the water type range of the ICIW water mass. The northward flow of the NwAtC suggests a source for the NwArIW in the southern Norwegian Sea, which is perhaps the Icelandic Current (IC). Local winter production of this water along the Arctic front appears unlikely because of its homogeneous water type and lack of other evidence. For example, the winter water types observed at the surface with the correct density ($\sigma_t \sim 28.0$) are too saline (see Fig. 4.22 below). Another fact suggesting a southern advective origin is the northward disappearance of the minimum-salinity feature of the NwArIW through the Lofoten Basin, cf. **Clarke**, **Reid** and **Swift** (1984).

4.3. DEEP WATERS

■ *4.3.1. Background*

The deep waters of the GIN Sea play a very important role in the world's ocean system. However, the manner and extent of their influence is even yet not thoroughly understood. A fundamental question concerning the Arctic Ocean deep waters has been is the observation that the Greenland Sea is obviously the major location for the production of dense bottom water for the Arctic Basins, and yet the water of the Greenland Sea Deep Water (GDW) is different (colder and fresher) from that of either of the adjacent deep waters viz. the Norwegian Sea Deep Water (NwDW) and the deep waters of the Polar Basin, i.e. the Eurasian Basin Deep Water, EADW, and the Canadian Basin Deep Water, CDW.

Early observations in the GIN Sea seemed to indicate surface production of GDW when surface waters sampled during late winter and early spring in both 1901 (*R/V Capella* and *Hekla*) and 1902 (*R/V Vega*) revealed temperatures below −1 °C and salinities $\sim$ 34.9 ppt. These were recognized as being not only the coldest surface waters in the Northern Hemisphere but as also being very nearly the same water type as the GDW. On the basis of this and the fact that the adjacent deep waters were different, **Nansen** (1902) suggested that the GDW was bathymetrically restricted from entering the Polar Basin by a sill, which for roughly half a century bore his name.

Some time later **Wüst** (1942) found the potential temperature of the EADW to be the same as that at $\sim$ 1300 m depths in the Greenland Sea, seemingly providing

additional evidence for the concept of the Nansen sill at roughly that depth. **Helland-Hansen** and **Nansen** (1909) had assumed that since similar waters were observed at the surface and the bottom of the Greenland Sea that they had actually observed the production of GDW. Indeed, the phenomonological process of deep convection and bottom water formation was advanced and well described by **Nansen** (1906) on the basis of these observations. Another early concept that has seen refinement is that the NwDW is no longer considered to be the major dense water export of the Arctic system contributing to the North Atlantic Bottom Water as proposed by **Cooper** (1955). Without diminishing the value of these earlier works, it is now clear that some of their deductions were in error due to insufficient data.

Soviet bathymetric surveys have revealed (e.g. **Laktionov**, 1959) that instead of the presumed Nansen Sill a depression exists in the Greenland-Spitsbergen passage, which was then named the Lena Trough after the Soviet vessel *Lena*. The passage between Greenland and Spitsbergen is often referred to as Fram Strait after the *R/V Fram*. Between the Lena Trough and the most northern part of the Mohn Ridge are found two saddles separated by the Molloy Fracture Zone and the Molloy Deep, with depths in excess of 5600 m (**Anonymous**, 1985). The southern shallower (79°N) of these saddles constitutes the sill between the Greenland and Eurasian Basins, with a sill depth of about 2600 m (**Johnson** and **Eckhoff**, 1966). In addition to the sill, the Yermak Plateau extending $\sim$ 200 km north of Spitsbergen on the eastern side of Fram Strait acts to restrict the deeper flows ($>$ 800 m) entering the Eurasian Basin (see Subsect. 5.3.1).

Another hypothesis that has undergone modification is that there is little deep water exchange between the Greenland and the Polar Seas. In an analysis of the wind stress field, **Aagaard** (1968) observed that the wind stress curl, and hence the Sverdrup transport, is small in the Fram Strait region and suggested that, to the extent that the circulation is wind-driven, the exchange between the Greenland and the Polar Seas is restricted. This type of restriction became known as a 'dynamic barrier' and the notion, that the exchange of deep water was minimal, survived until recent data and analyses proved to the contrary, i.e. that there exists an active exchange between the two Seas down to depths of 2500 m by virtue of the Fram Strait.

This lowering of the sill, so to speak, still left the problem of the origin of the Polar Basin deep waters, for without the sill restriction one would expect these waters to more closely resemble those of the GDW. The fact that the EADW, in particular, very closely resembles the NwDW (Fig. 4.17c) has led some researchers (e.g. **Metcalf**, 1960; **Eggvin**, 1961) to suggest that the NwDW is in fact the source of deep water for the Polar Basin and, that as a source, the GDW contributes little, perhaps only through mixing. However, a look at the relative positions of the deep water types shows this still to be an unsatisfactory solution (Fig. 4.17), since, if deep water is primarily produced in the Greenland Sea in the form of GDW, not NwDW, how then do the three other Arctic deep waters gain heat and salt?

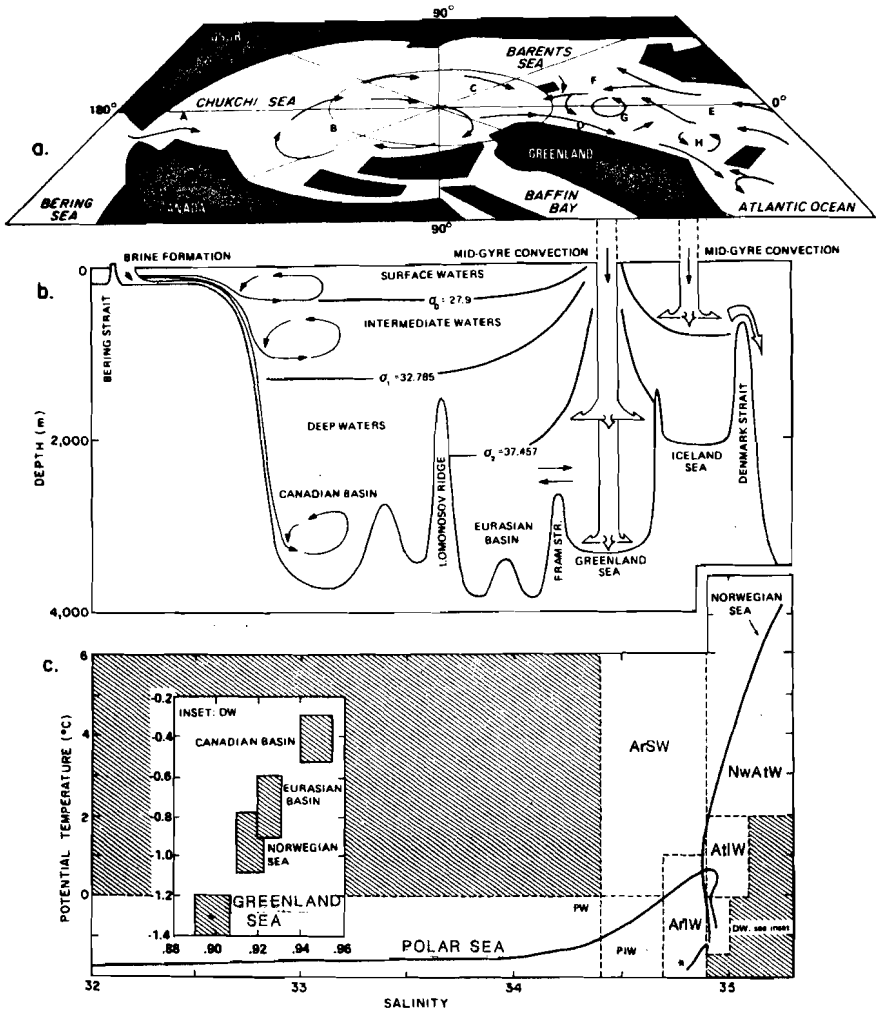

Fig. 4.17. Schematic circulation and water mass structure of the Arctic Ocean. (a) Circulation features: (A) Bearing Strait inflow, (B) the Beaufort gyre in the Canadian Basin, (C) the transpolar drift in the Eurasian Basin, (D) the East Greenland Current, (E) the Norwegian Atlantic Current, (F) the West Spitsbergen Current, and continuation into the Polar Sea, (G) the Greenland Gyre, and (H) the Iceland Gyre. (b) A vertical section along 180°–0°meridians showing vertical circulation and density structure, and (c) T-S curve with deep water insert. The asterisk is the T-S curve for the Greenland Sea Gyre. [From **Aagaard, Swift** and **Carmack** (1985).]

Aagaard, **Swift** and **Carmack** (1985) have proposed another explanation for the relationships between the four deep waters of the GIN and Polar Seas. This is summarized as follows: The GDW is the primary deep water source; it occupies the extremum position of the coldest and least saline water type, and has the greatest in-situ density. When calculated at atmospheric pressure the GDW is less dense than EADW, but when calculated at in situ pressures it is more dense (Figs. 4.17b and 4.18), because the colder waters are slightly more compressible. This would allow the GDW to flow northward pressures it is more dense (Figs. 4.17b and 4.18), because the colder waters are slightly more compressible. This would allow the GDW to flow northward into the Eurasian Basin and mix with CDW at a ratio of $\sim 1:2$ to form EADW. However, neither an overflow of CDW nor a consistent influx of GDW to the Eurasian Basin have been confirmed observationally. **Swift**, **Takahashi** and **Livingston** (1983) reported a $\sim$ 100 m thick layer of slightly modified GDW above the Fram Strait sill from summer 1981 observations. The winter 1982 observations of **Clarke**, **Reid** and **Swift** in 1984 showed only some indication of GDW near the bottom eastern side of Fram Strait (Fig. 4.19). The Lomonosov Ridge prevents the GDW from modifying the deep waters that reside within the Canadian Basin. **Aagaard et al.** (1985) answer the problem of the CDW being the warmest and the saltiest, and hence seemingly not a product of the other deep waters, by suggesting that a mixtures of cold brine-enriched shelf bottom waters combine with the relatively warm intermediate waters the PAtIW to form the CDW. In other words, deep water is made in both the Greenland Sea (cold and fresh) and in the Canadian Basin (warm and salty) by two distinctly different processes.

Aagaard, **Swift** and **Carmack** (1985) then demonstrated how the EADW exits southward through the Fram Strait on the western side at a depth of about 1500 to 2000 m, where the internal pressure has a maximum directed southward. This outflow has been observed (Fig. 4.19) and continues as a third (in depth) water mass of the EGC, but because of the bathymetric restriction leading to the Iceland Sea from the southern Greenland Sea, its flow is constrained to remain in that sea, with the important exception of flow exiting to the Norwegian Basin through the primary and secondary sills of Mohn Ridge (**Koltermann**, personal communication). As the EADW mixes (at $\sim 1:1$) with the GDW a NwDW type is formed. This explains how **Metcalf** (1960) identified this water as NwDW circumnavigating the Greenland Sea and concluded that it was enroute to the Polar Sea.

A deep advective origin for the NwDW is satisfactory in the sense that sufficient surface production of it has not been observed. The frontal production as suggested by **Metcalf** (1955) in Fig. 4.21, remains a possibility for modifying the NwDW to generate the upper NwDW (uNwDW), but is not supported by the observed oxygen concentrations, (e.g. **Metcalf**, 1955; **Clarke**, **Reid** and **Swift**, 1984). An advective origin also implies that the NwDW is an end member of the Arctic Ocean deep waters and implies a considerable age discrepancy between the GDW and the NwDW, which in fact has been supported by the Tritium analysis of **Peterson** and **Rooth** (1976) who estimated renewal times for the GDW and NwDW of 30 and 100 years, respectively.

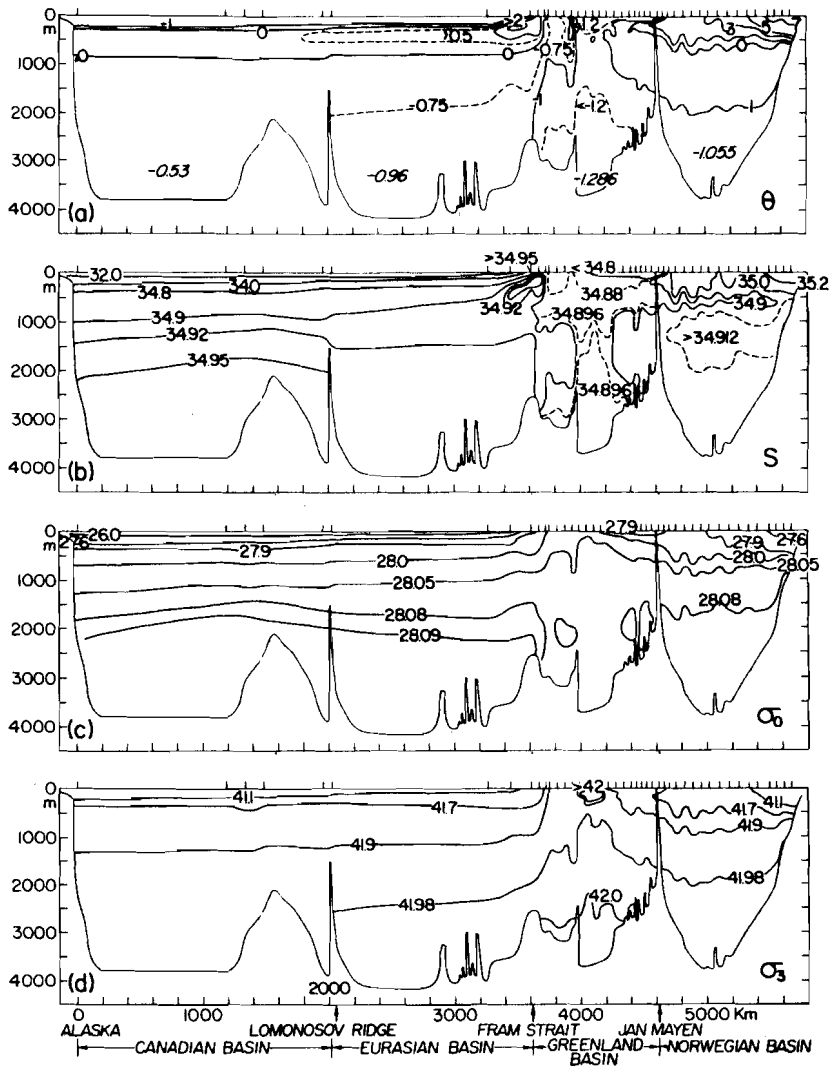

Fig. 4.18. The distributions along the 0° meridian, shown in Fig. 4.16a, of (a) potential temperature, (b) salinity, (c) σ_t and (d) σ_i at 3000 m. [From **Aagaard, Swift** and **Carmack** (1985).]

It has also been supported by a T-S volumetric analysis indicating negligible seasonal variation in the NwDW over three annual cycles (**Swift** and **Aagaard**, 1981); the implication is little winter production and a seasonally constant deep source. Constrastingly, in the Greenland Sea the largest water mass increase during winter was that of the GDW (**Carmack**, 1972; **Swift** and **Aagaard**, 1981).

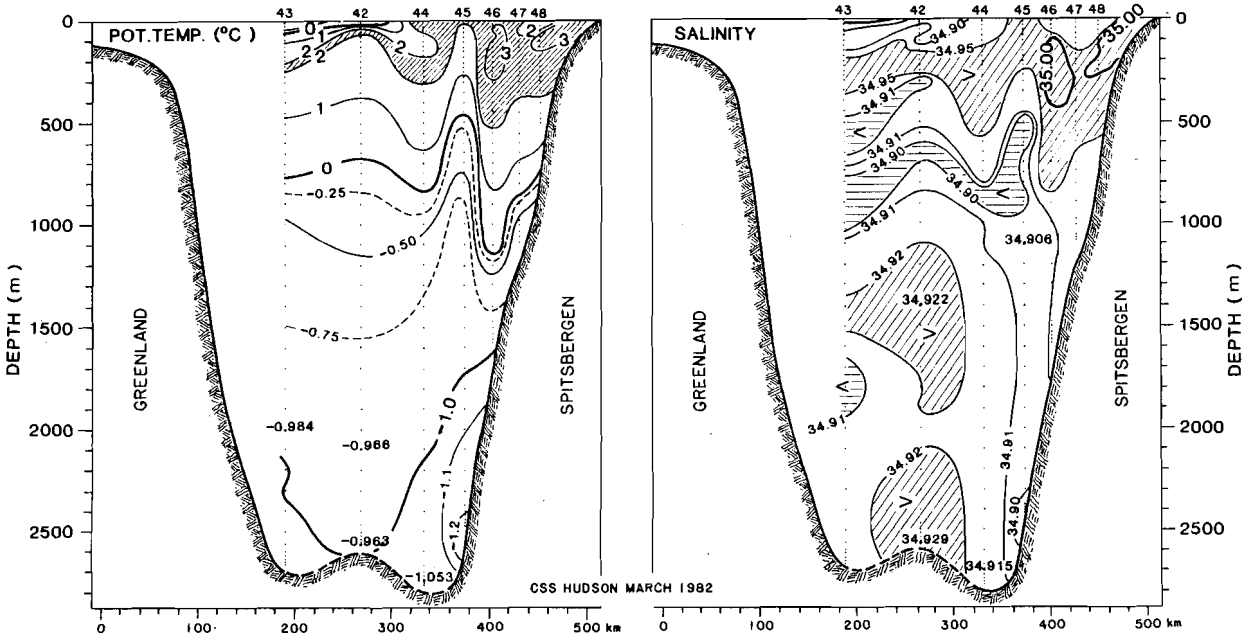

Fig. 4.19. Potential temperature (Θ) and salinity contours across Fram Strait as observed in March 1982 on *Hudson*. The water of $T = 0\,^{\circ}\mathrm{C}$ to $T = -0.75\,^{\circ}\mathrm{C}$, $S > 34.92$ is interpreted EADW existing; that over bottom at center $T = 0\,^{\circ}\mathrm{C}$ to $T = -0.96\,^{\circ}\mathrm{C}$, $S > 34.925$ as a mixture of EADW and GDW; and that in lower eastern bottom $T = 0\,^{\circ}\mathrm{C}$ to $T < -1.1\,^{\circ}\mathrm{C}$, $S < 34.90$ as GDW exiting.

■ *4.3.2. Deep water types*

The relative positions of the various deep water types are shown in Fig. 4.17c. The bottom waters of the Greenland and Canandian Basins represent water-type end members: the GDW is the freshest and coldest, while the CDW is the saltiest and warmest. The other two are considered to result from mixtures of GDW and CDW and therefore to have modified water types and be older.

The deep water masses are very homogenous, but the water types cited for these water masses vary slightly in the literature. This is because of observational error, unrepresentative sampling, different methods of averaging, and even real trends in the data. In Tables 4.1a–d we have listed representative values selected from recent works. These are spatial and temporal averages.

It is useful to look at the distribution of deep water types as observed from a single cruise, as for example those of the *CSS Hudson* Cruise 82-001 (**Clarke**, **Reid** and **Swift**, 1984) and shown in Fig. 4.20. At the 2000 m depth more scatter existed among the water types than at the 2500 m depth: the Lofoten Basin water was the warmest and saltiest while the Greenland Basin water was the least so. The

stations along Mohn Ridge were intermediate, suggesting mixing across the Ridge. Those of the Norwegian and Iceland Seas were very similar to those of the Lofoten Basin. At the 2500 m depth, the Norwegian and Lofoten Basin waters were not significantly different but were still separate from those along Mohn Ridge and those of the Greenland Basin. The three Fram Strait stations (42, 44 and 45 in Fig. 4.19) were markedly different at both depths, i.e. St. 45, which was along the Spitsbergen slope, belongs to the GDW group; and Sts. 42 and 44, which were more towards the middle of Fram Strait, appear to have been a result of mixtures of EADW, and GDW. Unfortunately there were no observations from the western part of the Greenland Sea, for these might have indicated whether or not EADW flows southward along the Greenland Slope. However, St. 103 just north of Jan Mayen does have a water type different from GDW and is indicative of EADW admixture. The presence of EADW there corroborates the suggestion (**Aagaard, Swift, Carmack**, 1985; **Koltermann** and **Machoczek**, 1985) that EADW flows southward out of the Polar Sea along the Greenland Slope and enters the Lofoten Basin via gaps in the Mohn Ridge (**Koltermann**, personal communication).

■ *4.3.3. Deep water formation*

There seemed little reason to doubt the concept of deep water formation in the center of the Greenland Sea gyre as proposed by **Nansen** (1902, 1906) and **Helland-Hansen** and **Nansen** (1909) until the **Metcalf** (1955) analysis of several winter cruises failed to reveal any evidence for deep homogenous layers even though sufficiently dense waters were present at the surface of a water type similar to the GDW. This led him to propose that sinking occurred obliquely along isopycnals as in Fig. 4.21. (We note that his station spacing was so wide (60 km) as to render his contouring ambiguous.) Later **Carmack** (1972) and **Carmack** and **Aagaard** (1973) in a thorough reassesment of historical data also could not find the exact GDW type at the surface nor could they find evidence of sinking from the surface along inclined isopycnals.

Carmack proposed an alternative mechanism for the GDW production which involved subsurface cooling of the GAtIW. Two main conditions are required for this to occur: convergence of the GAtIW toward the gyre center, and a double diffusive exchange between the GArSW and the GAtIW. Westward extensions of GAtIW, particularly from the West Spitsbergen Current (WSC), have been observed (as in the February case presented in Fig. 4.22). Such a movement which perhaps satisfies the observed Ekman divergence of the surface waters (**Aagaard**, 1968). The double diffusive exchange is seen as essential because mixing of GArSW and GAtIW would not render the GDW type. This is illustrated in Fig. 4.23a, where the GArSW and GAtIW types are connected by lines. The GDW type is too salty and cold for any linear mixtures. In fact such mixtures would need to coincide with the line denoted C in order to produce the proper density of 28.11 sigma-theta through caballing. **Carmack** has explained the process roughly as follows: The warm salty layer of GAtIW moves towards the Greenland gyre center (Fig. 4.23c); while doing so it loses heat faster than salt through the double diffusive mechanism to the GArSW and so approaches the GDW type (arrow in Fig. 3.23b). Meanwhile, the surface

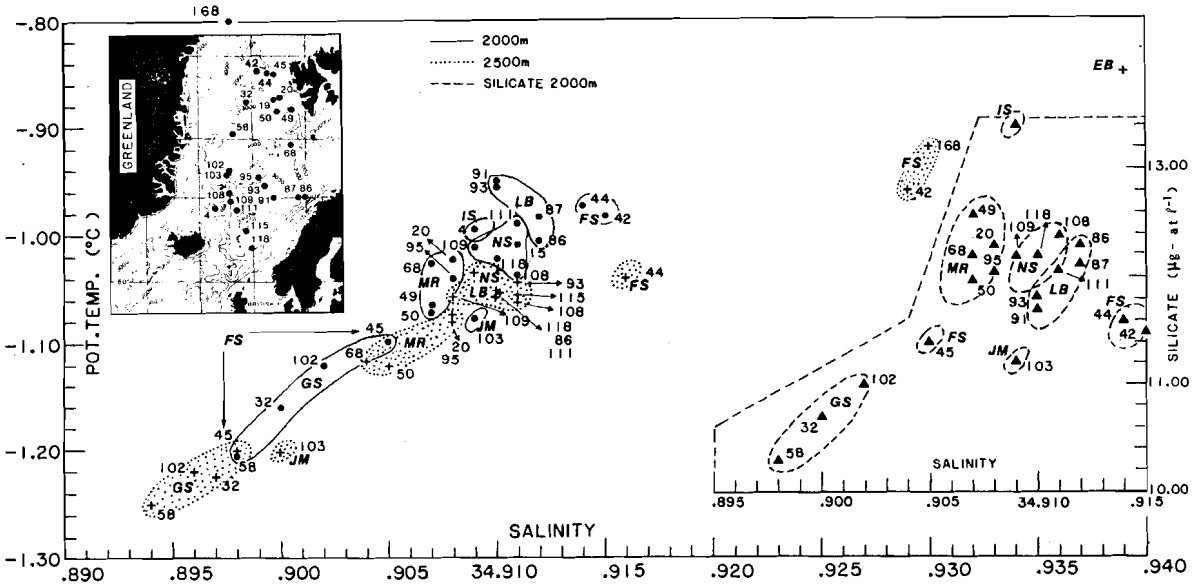

Fig. 4.20. Potential temperature, salinity and silicate values for selected stations from *Hudson* February–March 1982 (**Clarke, Reid** and **Swift**, 1984). The 2000 m T-S values are solid points (•), the 2500 m T-S values are crosses (+), and the Si-S values are solid triangles △. Regions are connected; (GS) Greenland Sea, (JM) just north of Jan Mayen, (MR) Mohn Ridge, (LB) Lofoten Basin, (NS) Norwegian Sea, (IS) Iceland Sea, (FS) Fram Strait, and (EB) Eurasian Basin. Station 168 is from *Ymer* 1980 data corrected by **Swift, Takahashi**, and **Livingston**, (1983); the EB point is from *Lorex* data at ~ 2300 m, **Moore, Lowings** and **Tan** (1983); **Aagaard, Swift** and **Carmack** (1985).

layer transfers the heat lost from the GAtIW to the atmosphere efficiently, being heated from below and cooled from above. In Fig. 4.23b, the arrow S' represents the effect of buoyancy gained by the GArSW through double-diffusive exchange and the arrow S'' the buoyancy lost to the atmosphere. The combined result is that the GArSW moves in the direction of the arrow S while the AtIW types move in the direction of I such that on reaching the gyre center, they approximate the GDW water type and redistribute themselves vertically, as shown in Fig. 4.23c.

McDougall (1983) has computed 8.4×10^4 km^3/yr as being the lateral advective transport needed to satisfy the vertical heat loss due to double diffusion. This is more than sufficient to satisfy the annual of deep water production (3.4×10^4 km^3) observed through T-S volumetric analysis (**Carmack**, 1972). However, the **McDougall** model would tend to give an overestimate because he assumed a spherical symmetry in the center convergence of GAtIW, which would increase the production over the more probable assymetric case; and he did not allow for an upward mass loss to satisfy a surface Ekman divergence.

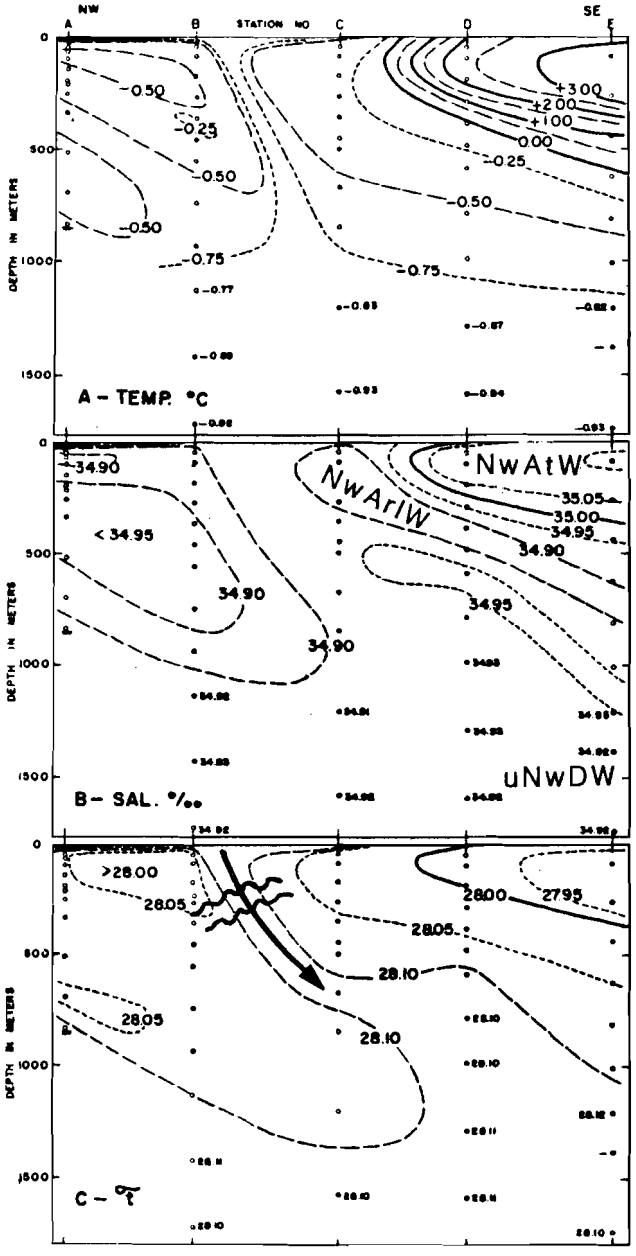

Fig. 4.21. Temperature, salinity and σ_t contours from *Edisto*, March–April 1951. Section runs NW–SE across the Jan Mayen Ridge from 70°30′N, 14°W to 66°30′N, 5°W. In the lower panel an arrow has been added to depict the supposed downward movement along isopycnals. [From **Metcalf** (1955).]

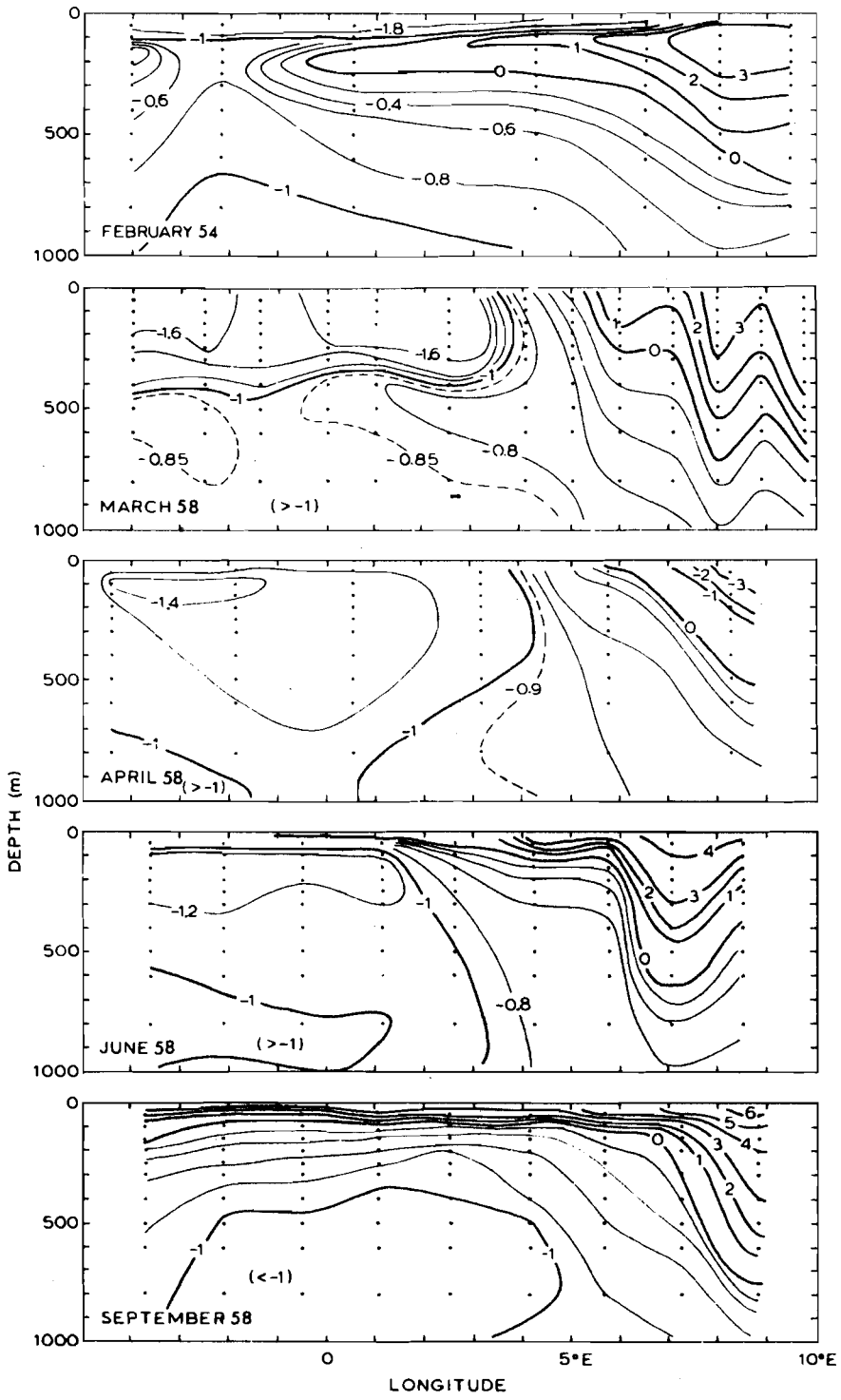

Fig. 4.22. Examples of the temperature structure from the West Spitsbergen Current to the Greenland Sea gyre at approximately 75°N: *Atka*, February 1954; *Polyarnick*, March 1958; *G.O. Sars*, April 1958; *Johan Hjort*, June 1958; *Johan Hjort*, September 1958. [From **Carmack** and **Aagaard** (1974).]

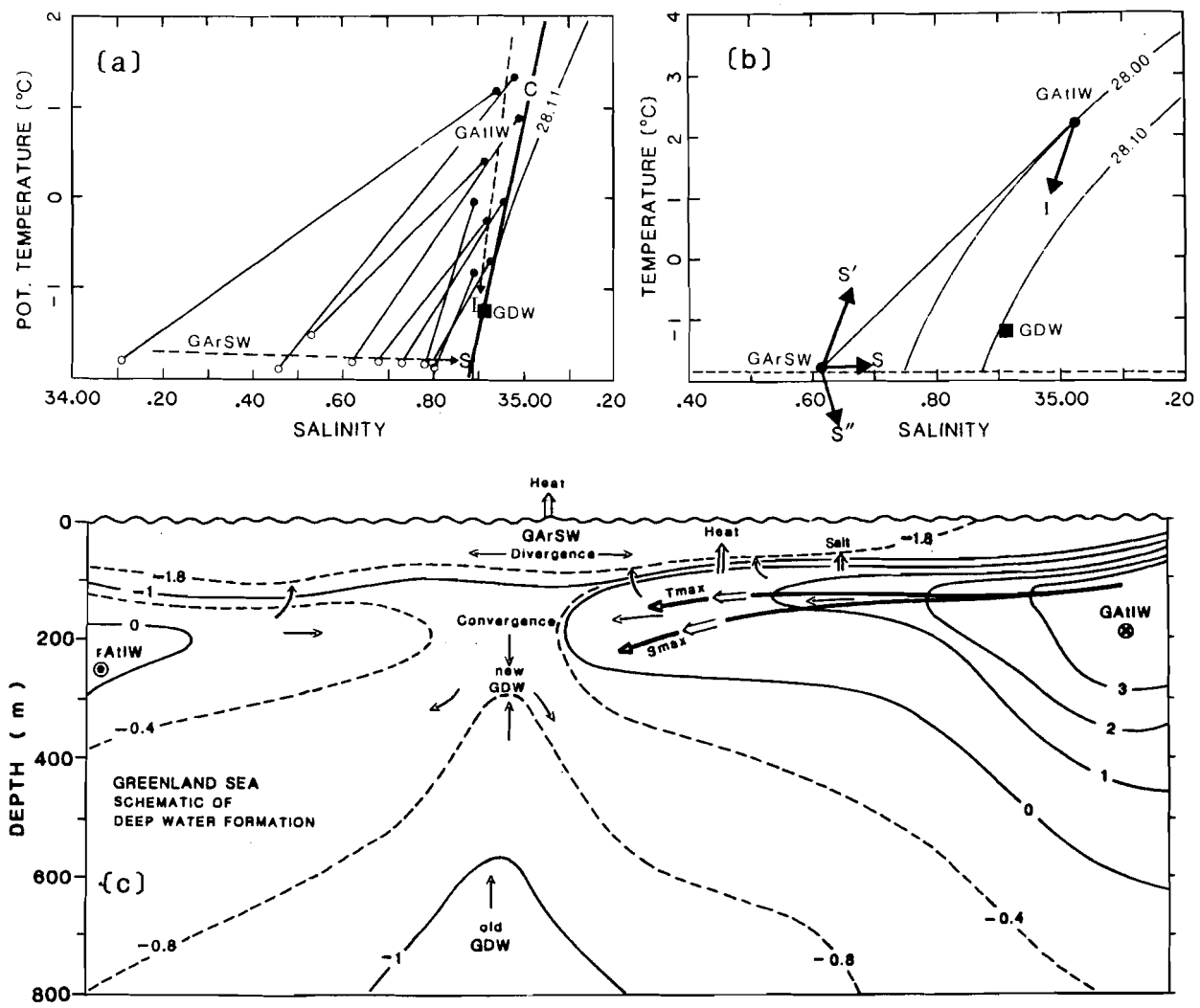

Fig. 4.23. (a) Θ-S diagram from *Atka* January–February 1954. GArSW values (o) are joined to GAtIW core values (•) by a straight line. Line C is tangent to the $\sigma_t = 28.11$-density curve at the GDW type. (◇). The T-S drift tendency of GArSW indicated by S and that of GAtIW by I. (b) The vector S is shown as the resultant of S', the drift caused by atmospheric buoyancy extraction processes and S'', the drift caused by double diffusion. (c) Schematic of GDW production. [(a) and (b) adapted from **Carmack** (1972), and (c) from **Carmack** (1972) and **McDougall** (1983).]

Confirmatory evidence on deep water production is still lacking. One can note that the February data of Fig. 4.24 shows no westward extensions of GAtIW nor are any present in the March 1958 cross-section of Fig. 4.22. **Killworth** (1979) has pointed out that the probability is very small of observing the narrow regions of intense vertical

mixing (chimneys) as have been observed in the Weddell Sea (**Gordon**, 1978). This process involves small cyclonic eddies, of the same scale as the baroclinic radius of deformation (15 km), and these promote the right conditions of surface cooling and baroclinic instability, which drive deep non-penetrative convection (no entrainment of GDW). Apart from not being observed, the chimneying would not account for the required water-type modification of the GArSW, i.e. as in Fig. 4.23a,b. **Clarke** (personal communication) has suggested another mechanism for GDW formation. He has quantified a cyclic freezing/thawing process that leads to a non-reversible water mass transition of a deep water type. The sequence is briefly as follows: (1) the surface water is already near the freezing point; (2) atmospheric heat extraction leads to freezing; (3) brine sinking leads to a convective heat (and salt) flux upwards from the GAtIW; (4) the ice cover partially melts causing a shallow melt layer; (5) the heat loss from the ocean surface increases; and (6) the cycle continues. The result is a deepening surface convective layer and production of GDW, i.e. of a water mass cooler and slightly less saline than the GAtIW.

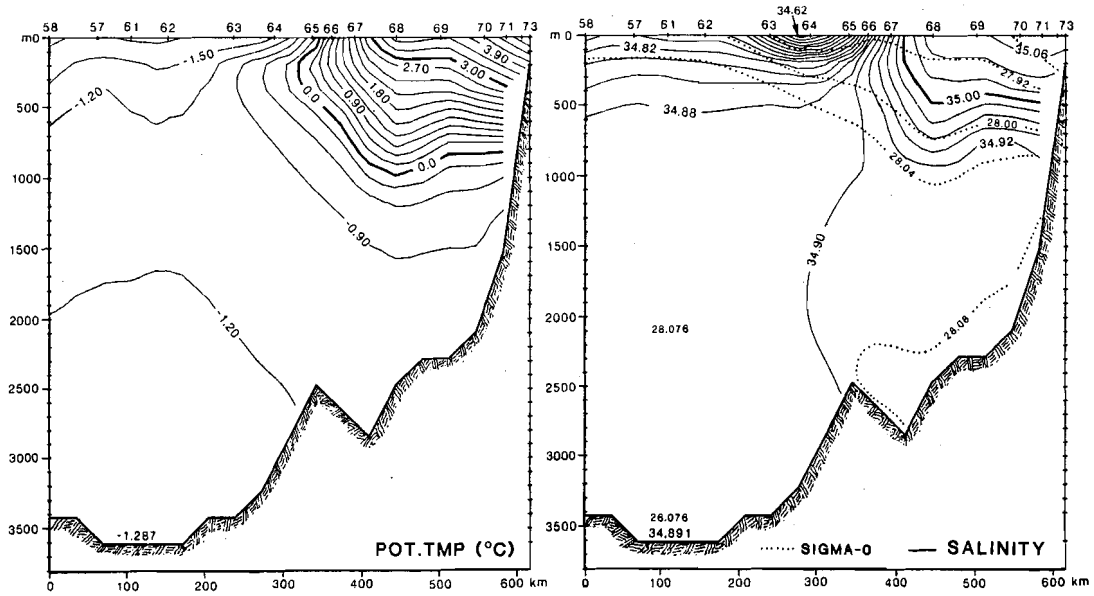

Fig. 4.24. Potential temperature (left) and salinity (right) cross sectional contours along ~ 75°N from the West Spitsbergen Current to the Greenland Gyre. [Data from **Clarke**, **Reid** and **Swift** (1984).]

5. Circulation

5.1. INTRODUCTION

The qualitative sense of the **Helland-Hansen** (1909) surface current chart for the GIN Sea has been confirmed by more recent studies, namely: the North Atlantic Water enters from the southeast, and while proceeding northward loses some flow to the Barents Sea before passing west of Spitsbergen into the Arctic, and at the same time the Polar Water enters from the northwest and proceeds southward along the Greenland shelf; additionally, these two current systems are separated by cyclonic gyres in the Greenland and Norwegian Seas which are defined also by the zonal flows along the Greenland-Icelandic-Færœ and Jan Mayen Ridges.

Alekseev and **Istoshin** (1960) have prepared a chart of the surface flow structure in greater detail from composite data (Fig. 5.1a). The two major differences between this and the 1909 chart are the greater structure in the Norwegian Atlantic Current (NwAtC) (in the form of embedded cyclonic vortices and the northwestward branching toward Jan Mayen Island) and the absence of a well-developed Norwegian cyclonic gyre. Some features, such as the double gyre in the Greenland Sea and the southeastward flow of GPW across the Iceland Sea appear suspect. **Metcalf** (1960) attempted a similar representation for winter data (Fig. 5.1b,c). In this figure both the Greenland and Iceland Sea gyres are well evident.

These generalized depictions of the circulation provoke obvious questions concerning, for example, the existence and forcing of the basin gyres, and the cause and stability of the splitting of major flows. For answers, however, one must await the convergence of modern techiques of modelling and observation. No recent attempt to generalize the circulation exists, perhaps because the acquisition of more data has demonstrated tremendous variability and acted to undermine the credibility of such representations. Further historical comment can be read in **Lee** (1963) or **Trangeled** (1974).

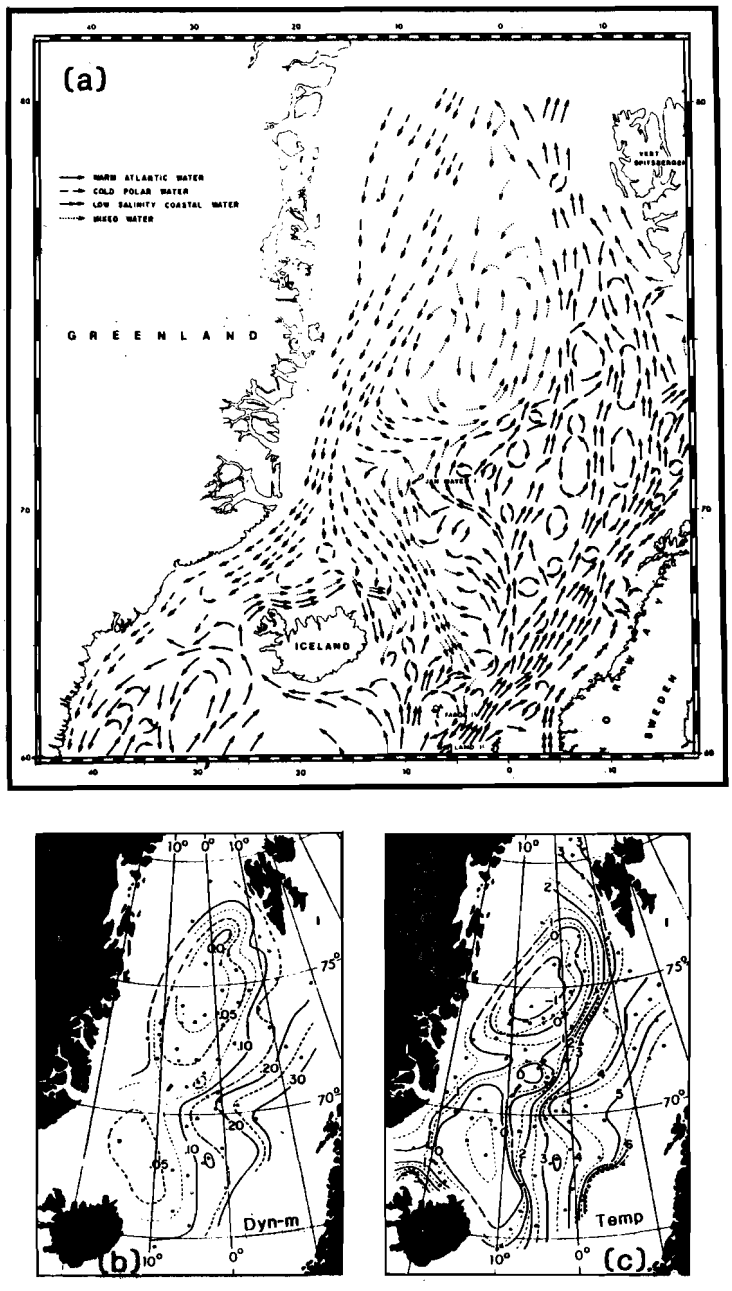

Fig. 5.1. (a) Schematic representation of the surface circulation in the GIN Sea from dynamic computations, drifters, published interpretations, and addition from **Hermann** and **Thomsen** (1946) for the area south and west of Iceland. [From **Trangeled** (1974), adapted from **Alekseev** and **Istoshin** (1956).] (b) Dynamic topography in dyn m 0/1500 dB. (c) The 200 m temperature distribution. [Both (b) and (c) are from winter composites for the years 1951 through 1955 (**Metcalf**, 1960).]

5.2. SPECIFIC CURRENT SYSTEMS

■ *5.2.1. Norwegian Atlantic Current (NwAtC)*

The NwAtC transports NwAtW northward through the Norwegian Sea from the Færœse Channel into the Greenland Sea. It was early recognized that the magnitude and consistency of this flow was essential to the thermohaline balance and circulation dynamics of the GIN Sea. Considerable observational effort has been spent in transects across the NwAtC, most notably on the Sognefjord and Ocean Weather Station *Mike* (OWS *'M'*) sections, directed to the northwest from 61°N and along 66°N from the Norwegian coast, respectively.

The Sognefjord section, which runs across the very southern extreme of the Norwegian Sea from 61°N on the Norwegian Coast to 63°N due north of the Færœs, has been occupied intermittently from 1910. **Helland-Hansen** (1934) identified the main observational problems in terms of describing the NwAtC, i.e. the flow is strongly sheared cross-stream to an extent that produces countercurrents, the transport is variable in time, and the the lower water mass interface has very large undulations. The section was reoccupied 27 times between 1947 and 1953, on each occasion during the months of May through August. In analysing these data **Saelen** (1959) confirmed **Helland-Hansen**'s findings. The transports calculated for 'in' and 'out' crossings, separated in time by $\sim$ 2 days, were equally as variable as those calculated for different years.

The mean of these NwAtW transports was 3.8 Sv with a minimum of 1.8 Sv and a maximum of 6.4 Sv, which is roughly the range of the Færœse-Channel transport. In fact, there were eight occasions in which the **Saelen** (1959) and the **Tait** (1957) analyses were preformed for the same month (between 1947 and 1952); and these gave a mean value of $\sim$3.6 Sv for the Sognefjord Section transport relative to $\sim$ 2.1 Sv for that of the Færœ-Shetland Channel. Further to the north through the OWS *'M'*-section, which was occupied 17 times during April–May 1967, transports of similar variablity and magnitude were observed by **Kvinge**, **Lee** and **Saetre** (1968). Comparisons are made in Table 5.1.

Saelen (1959) attributed the temporal variability calculated in the geostrophic flow to be a result of similar variations in the reference, or bottom layer, velocity. He gave some evidence for this from some short-term bottom current measurements, which showed sufficient variability to explain that observed in the calculated transports. Actually, the deep flow that he observed was to the south, in the opposite direction to the NwAtC. More recent moored current meter results near the Sognefjord section from (**Dorey**, 1978) confirm this with a generally southwesterly flow underneath the NwAtC and a variability of about 5 cm/s for the tidal and the 1-to-7-day periodicities. For example, all four current meters of mooring 'h' in Fig. 5.2 registered mean speeds of $\sim$ 6.5 cm/s with standard deviations of $\sim$ 4.5 cm/s and with a southern component.

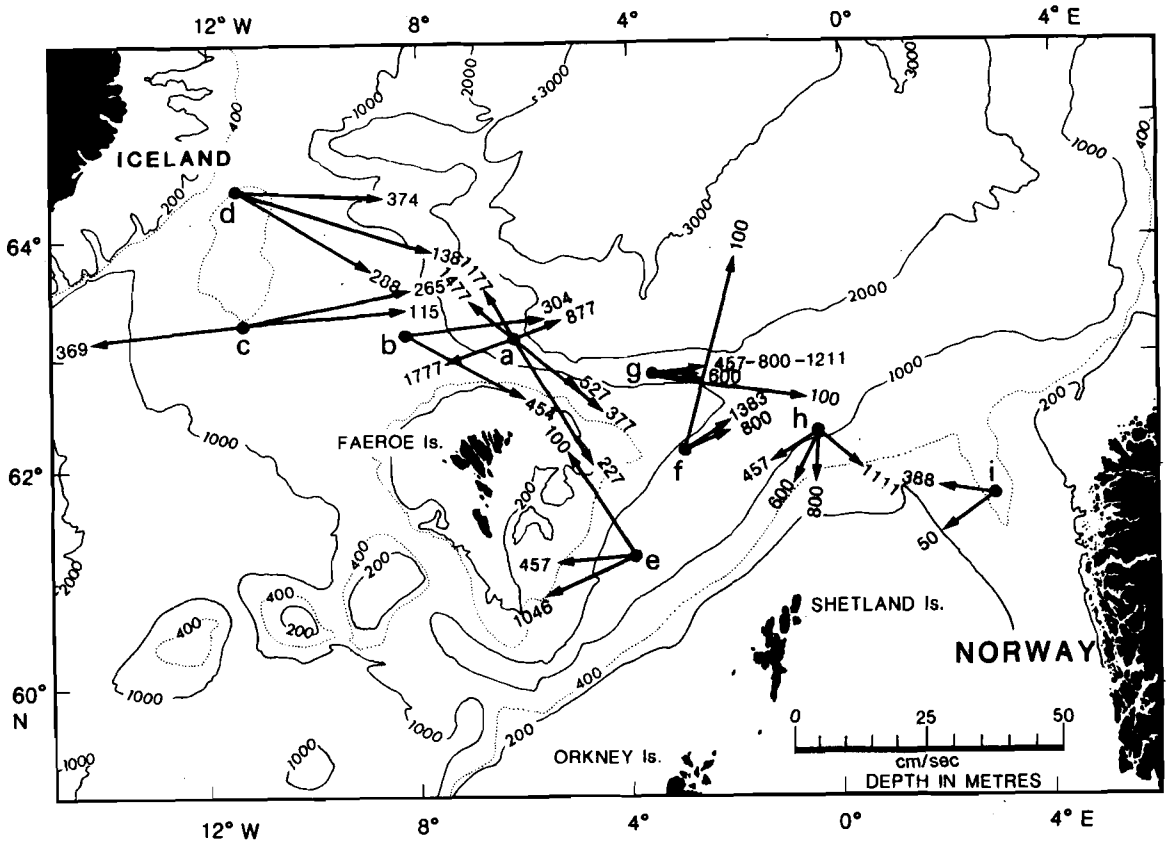

Fig. 5.2. Scalar mean velocity vector in the southern Norwegian Sea. [From **Dorey** (1978).] The number at the end of the vector indicates the current meter depths. The letter denotes the moorings: (a)–(d) from 7 June to 7 October 1975; (e)–(i) from 20 July to 27 September 1976, except for the 100 m depth on (e) which lasted only until 24 July 1976.

Helland-Hansen (1934) considered the observed horizontal variability in flow to be related to the observed large vertical undulations of the water mass interface (35-ppt). He postulated that both were evidence of the same phenomenon, to wit, elongated cyclonic vortices embedded in the NwAtC. **Saelen**'s (1963) analysis of several crossings showed that the crests of the 'waves' observed in cross section corresponded to the centers of the vortex-like structures observed in the horizontal. **Dickson** (1972) provided further evidence in this regard in his analysis of the OWS *'M'*-section summarized in Fig. 5.3. Three cyclonic gyres appear to exist across the section, the westward side of each supporting a southward transport and the eastward side a slightly larger northward transport. The local variability in T and S over 17 samplings of the cross section is also shown. The locus of variability maxima has a wave-like configuration corresponding to the cyclonic gyres. Higher interfacial variability is correlated with the more strongly northward flowing portions. **Dickson** (1972) found that these 'waves' in the isotherms were stationary over the six-week observational

period, although waxing and waning somewhat in amplitude. **Dickson** also identified a transient disturbance which actually did travel between the first two gyres at a rate of $\sim$ 6 km/day. This wave appeared to dissipate on intersecting the second offshore gyre, thereby causing considerable variablility at the place where the OWS *'M'* had been located by chance. This in part explained the disturbing variability, i.e. the 35-ppt isohaline varying by up to 400 m in depth $\sim$ 2 h, as noted at OWS *'M'* by **Mosby** (1950). We note that recent evidence on the stationarity of these features alongshore can be found in the data of the *USNS Kane* in Fig. 5.4, where repetition of at least three 'waves' is obvious over an alongshore separation of $\sim$ 75 km.

This phenomenon of elongated cyclonic eddies embedded in the NwAtC appears to be characteristic throughout its northward course. **Kislyakov** (1960) in describing similar features in the West Spitsbergen Current, has suggested that the gyres are generated by variations in cross-stream shear, which in turn is generated by barotropic interaction with the bathymetry. In support of this theory **Dickson** (1972) contoured the temperature at a depth of 400 m from the 1936 data of *R/V Armauer Hansen* (**Mosby**, 1966). This is shown in Fig. 5.5, in which the elongated eddy structure and the alignment between the eddy troughs and the bathymetry are evident.

Bathymetric control appears also to effect the branching of the NwAtC on passing the Vøring Plateau, a feature of the circulation much more definitively shown in the chart of **Alekseev** and **Istoshin** (1956) than in the earlier one of **Helland-Hansen** and **Nansen** (1909). North of the OWS *'M'*-section there are commonly two maximum-salinity cores observable in NwAtC cross sections, i.e. in Sect. 13 of Fig. 4.7. The westward branch veers northeastward on encountering the Mohn Ridge, merging with the Jan Mayen Current until it rejoins the more eastward branch of the NwAtC and becomes the West Spitsbergen Current (WSC). In this potrayal, the NwAtC is bathymetrically steered around the Lofoten Basin. Insufficient resolution in data precludes much comment on the surface circulation surface of the Lofoten Basin. The **Alekseev** and **Istoshin** chart Fig. 4.1a shows a cyclonic structure that is similar to that at the south, but expanded.

The **Alekseev** and **Istoshin** chart also suggests significant recirculation or loss along the westward limit of the NwAtC, both in the Norwegian Sea and in its Greenland Sea extension. These might be interpreted as smaller scale frontal processes rather than advective outbreaks. The amount of the NwAtW loss is very important to the internal thermohaline dynamics and is estimated in Subsect. 5.4.3.

The estimates of volume transports along the course of the NwAtC (Table 5.1) do not give a simple trend as one would expect as a result of continuous entrainment of adjacent waters. On the contrary, the center portions seem to decrease before a final increase in the Spitsbergen region.

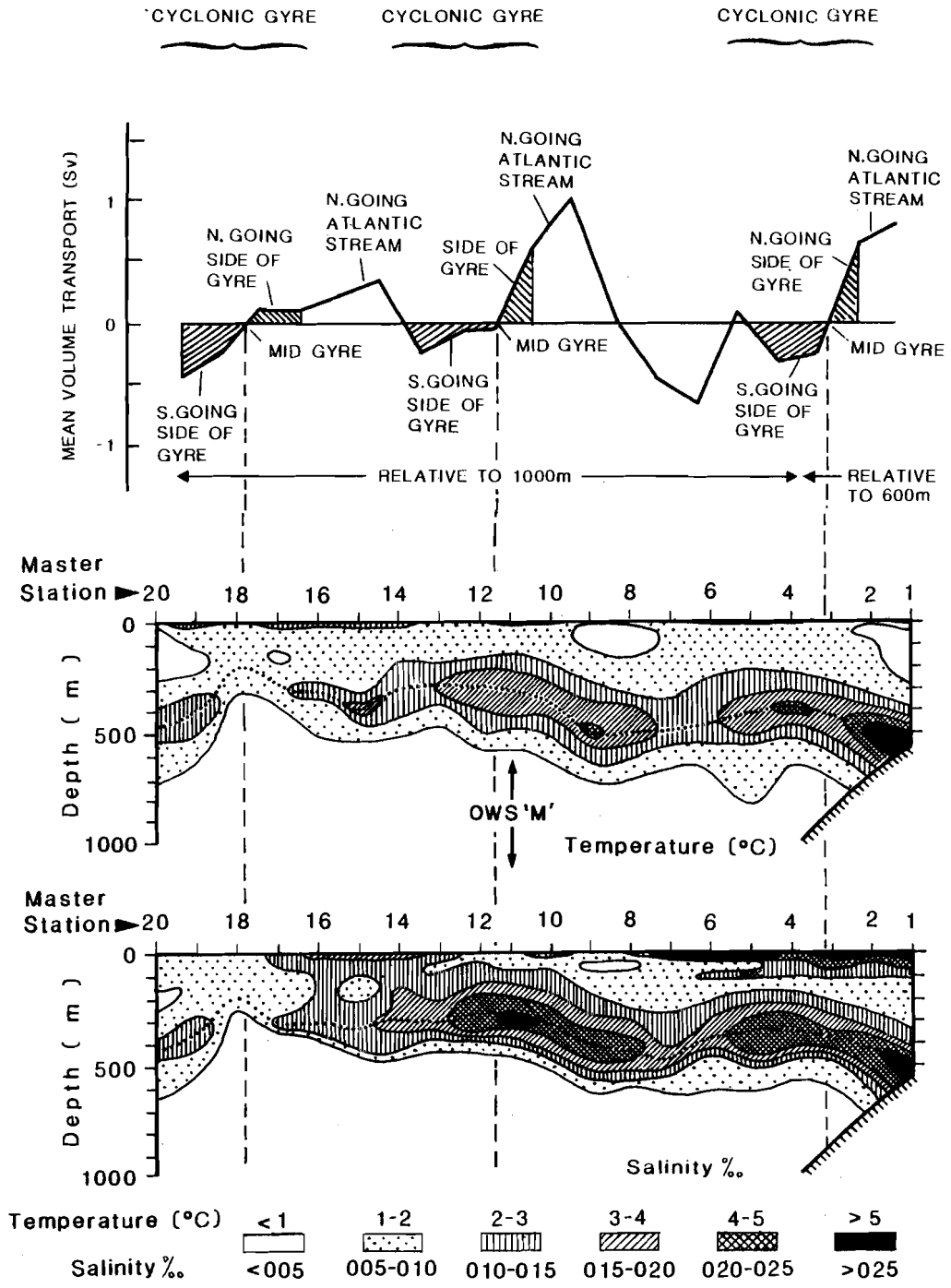

Fig. 5.3. **The mean volume transport computed relative to 1000 m depth level (and 600 m depth level inshore) for a transect along 66°N on 4 April to 18 May 1967. Below are the corresponding *T* and *S* variability observed during the 17 samplings of the section. The dotted line denotes the maximum in subsurface variability. [After Dickson, 1972.]**

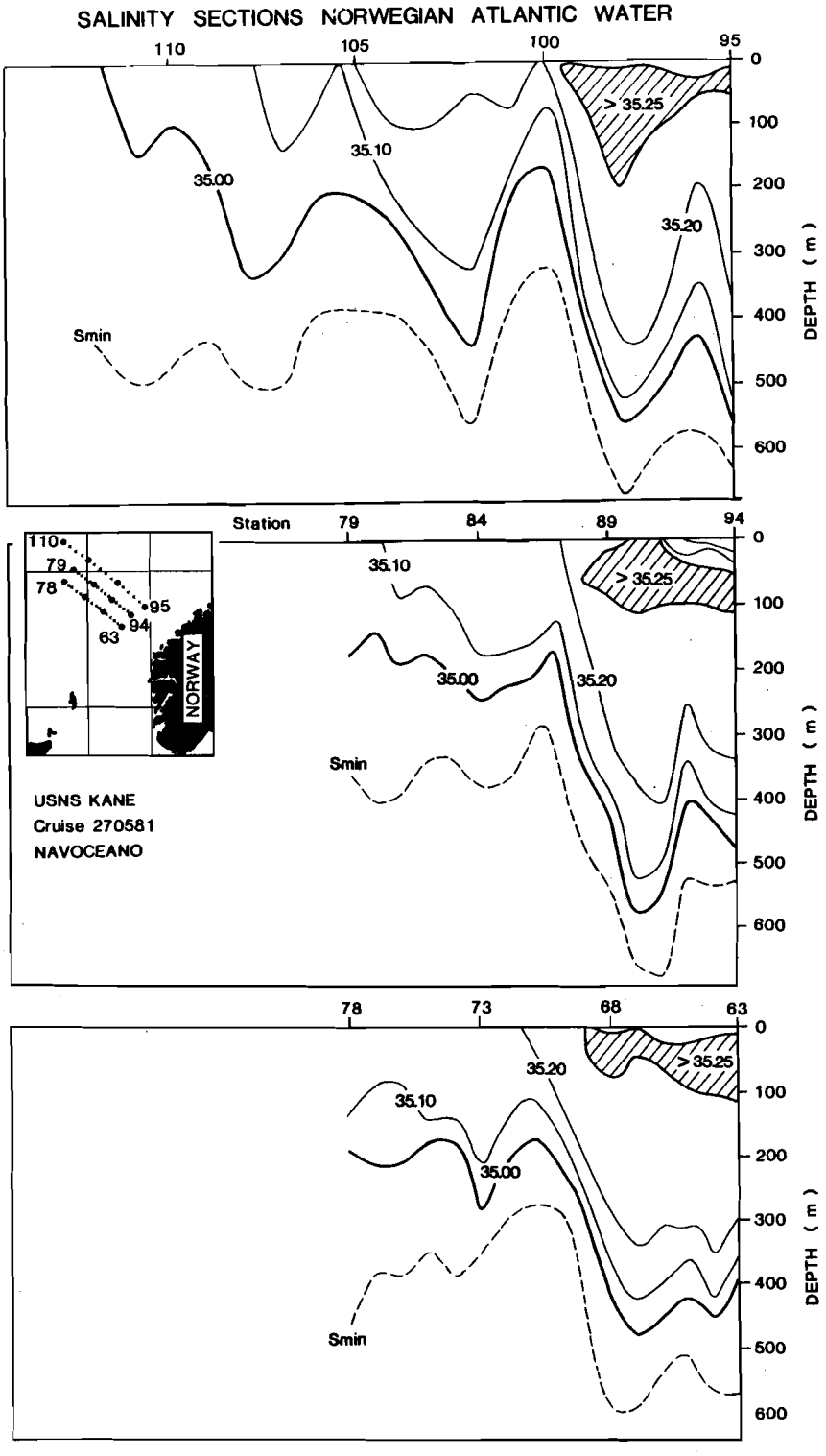

Fig. 5.4. The salinity structure of three cross-sections of the NwAtC. The dashed line marked S_{min} is the NwArIW. [Data from *USNS Kane*, May 1981 (**Teague**, 1981).]

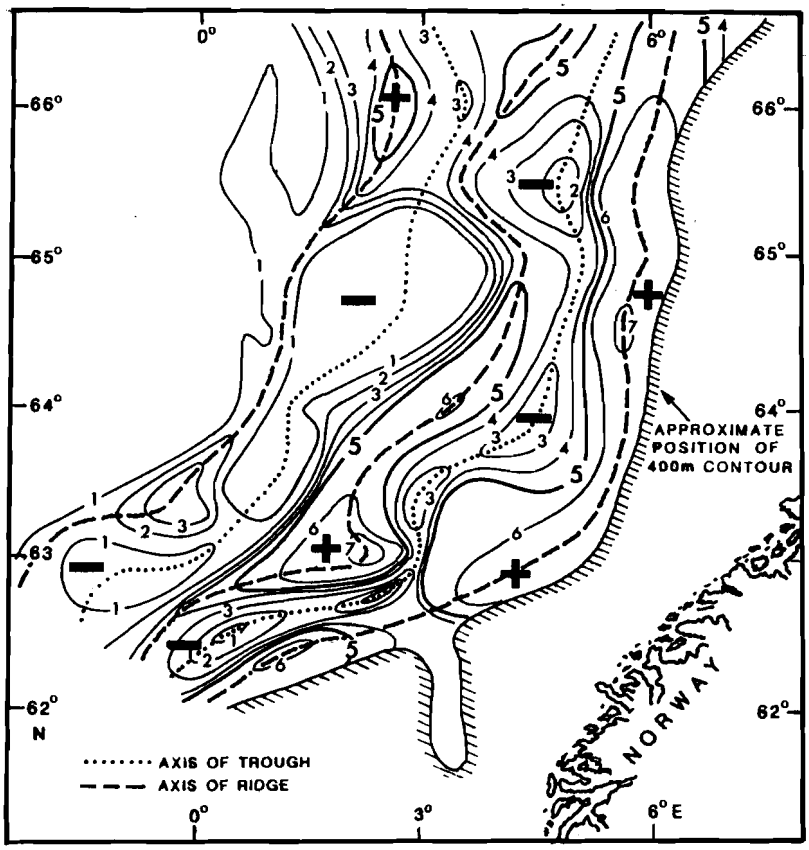

Fig. 5.5. Temperature distribution at the 400 m depth. The axes of the troughs and ridges are connected by dotted and dashed lines, respectively. The $T_{\min}$ (−) and $T_{\max}$ (+) are also indicated. [From **Dickson** (1972), data from *Armauer Hansen*, 9 June–23 July 1936.]

■ *5.2.2. West Spitsbergen Current (WSC)*

The WSC is the name given to the northernmost portion of the NwAtC that extends from the northern Lofoten basin to Fram Strait. Its transports of heat and mass are very important input quantities for the Polar Sea. For this reason, the WSC has in recent times received more observational focus than the NwAtC to the south. Nevertheless, the various observational efforts have not produced a consistent estimate of the transport, because the flow structure is complex in the same manner as the NwAtC, with counter currents and large variabilities. In this context, **Hanzlick** (1983) has presented new results and provided a good synthesis of previous results. We present the Table 5.2 as a summary of the various efforts, and refer the reader to **Hanzlick** (1983) for greater detail.

Table 5.1
Table of NwAtC transports by various researchers

Researcher	Transport (Sv)	Remarks
1. Færœse Channel		
Dooley and **Meincke** (1981)	3.3	(See Table 5.6)
2. Sognefjord Section		
Helland-Hansen (1934)	3.0	Dynamic method May 1927 and May 1929
Saelen (1959)	3.8 ± 1.3	27 estimates in months May through August 1947–53 Dynamic method
3. Ocean Weather Station 'M'		
Kvinge, **Lee** and **Saetre** (1968)	1.6	17 estimates during Spring 67
4. Bear Island Section		
Kislyakov (1960)	3.2	(See Table 5.2)
5. Spitsbergen Section		
Hanzlick (1983)	5.6	(See Table 5.2)

The last three studies listed in Table 5.2 all suggest higher transports, as a result of utilizing observed currents instead of an assumption of zero flow at some reference level. In Fig. 5.6 we give **Hanzlick**'s summary of the current observations. There are three notable characteristics: a vertical shear exists in the upper 400 m of the water column, but is not strong enough to suggest that a level of no motion exists before the bottom (moorings A and C); a lateral coherence exists between the two central moorings B and C, but not between the outer mooring A nor between the inner mooring D and the central moorings; the inner mooring has no significant reversals (southward flow) unlike those further offshore.

Hanzlick (1983) constructed a time series of the WSC transport from available current and hydrographic observations for the period of 1976–79. It is shown in Fig. 5.7 and a fairly consistent pattern of summer-fall maxima and winter-spring minima is evident in the transports. Several other researchers have noted a maximum near December and a minimum near March (cf. Table 5.2). The along stream coherence of variations in the NwAtC/WSC are not known, that is, whether or not seasonal variability is consistent from the Færœse Channel to Fram Strait, on the large scale, the two streams differ in that the WSC flows over a bathymetrically convergent bottom with streamlines of f/H converging whereas the NwAtC flows over diverging bathymetry. The WSC is also convergent in the sense of the confluence of the northward extension of the NwAtC, the Jan Mayen Current, and the East Spitsbergen Current.

Table 5.2
Table of WSC transports by various researchers

Researcher	Transport (Sv)	Remarks
Leonov (1947)	2.5	78°N section
Hill and **Lee** (1957)	1.1 3.2 max.	74°30'N section (175 km westward from Bear Island) to 400 m with 750 dB reference. From 1949–1956.
Kislyakov (1960)	3.2 ± 1.5 0.5 min. summer 5.5 max. winter	74°30'N section with 1000 dB reference. From 1954-59.
Timofeyev (1962)	3.1 ± 0.6	78°N section with 1000 dB reference. From annual estimates of the years 1933–60.
Aagaard, Darnall, and **Greisman** (1973)	8.0	79°N using current-meter data of the years 1971–72.
Greisman (1976)	7.0 11 max. Sep 3 min. Feb	79°N using current-meter data of the years 1971–72 and hydrography
Hanzlick (1983)	5.6 11.9 max. Dec −1.4 min. Mar	79°N section using current-meter data 1976–77 and hydrography

■ *5.2.3. East Greenland Current (EGC)*

In some respects the EGC appears to provide a simple symmetry to the GIN Sea circulation by transporting colder fresher water southward in constrast to the northward transport of warmer salter water of the NwAtC. This symmetry is reflected in the circulation of charts depicted in **Mohn** (1887); **Helland-Hansen** and **Nansen** (1909); and **Alekseev** and **Istoshin** (1956). However, there are also very significant asymmetries between these two systems.

The upper portion of the EGC that transports the GPW does not appear to contribute greatly to the water mass composition of the GIN Sea interior (see also Subsect. 4.1.3). In this sense; it would not be correct to consider the EGC as a boundary flow for the GIN Sea that returns water southward in compensation for the northward transport of NwAtC and the generally northward Sverdrup transports driven by the curl of the wind-stress curl (as **Aagaard**, 1970). There are two exceptions to this: the eastward advective inputs of GPW to the Jan Mayen Current and to the Icelandic Current. Neither of these losses from the EGC have been obser-

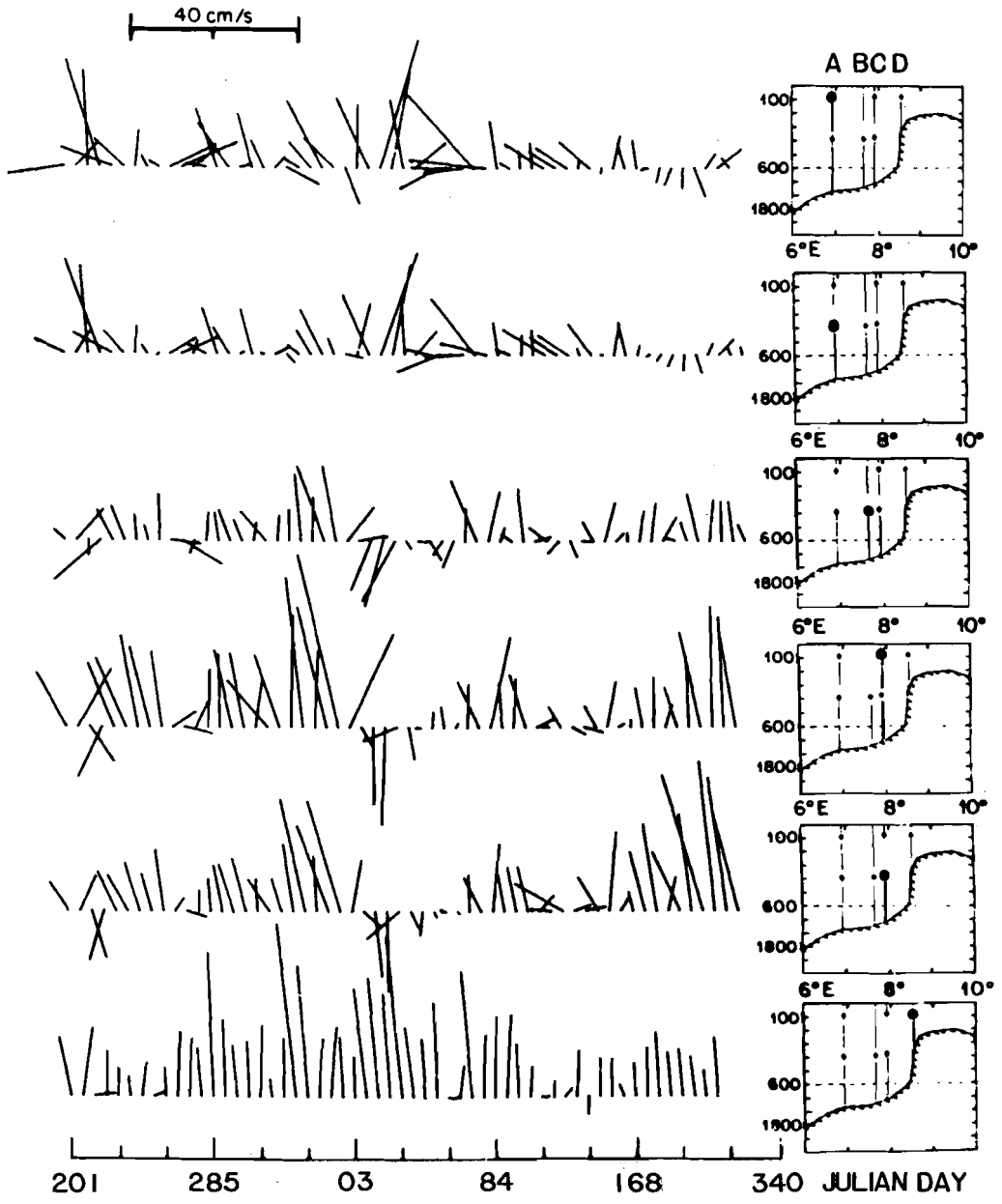

Fig. 5.6. Stick diagrams of weekly averages of the velocities observed moorings placed along 79°N from mid-July 1976 to mid-September 1977. Current-meter locations indicated at the right. [From **Hanzlick** (1983).]

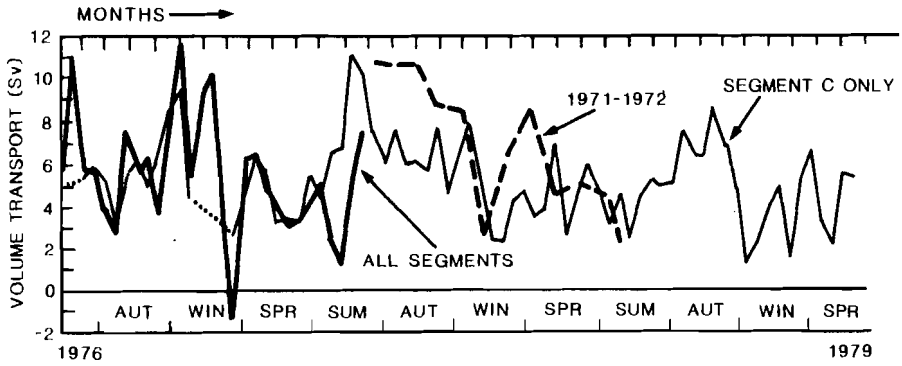

Fig. 5.7. Estimates of volume transport of the West Spitsbergen current for the period 1976–79 [from **Hanzlick** (1983)] and 1971–72 [from **Greisman**, (1976)]. Both data sets from approximately 79°N. The thin solid line indicated **Hanzlick**'s estimates from mooring C only (Fig. 5.6); the thick solid line indicates his estimates from all four moorings (A–D in Fig. 5.6); the dotted portions indicate when mooring C was not representative of the entire flow; and the dashed line indicates the transport estimates by **Greisman**. Positive values means northward transport.

vationally quantified. As a boundary flow then, the EGC has been considered to be an advective mechanism for transporting Polar Water though the system, i.e. from Fram to Denmark Straits.

Although in this context the surface movements have been more or less combined through observation of the movement of ice floes, etc., the movement of the waters underneath has been difficult to observe and is generally different than that of the ice Mitchel (1974). The *Arlis II* experiment was fortunate to acquire data along the entire trajectory of the EGC (**Tripp** and **Kusunoki**, 1965). Through their analysis of this data **Aagaard** and **Coachman** (1968a,b) greatly updated our knowledge of the EGC, with probably the most significant outcome being a revised picture of the transport and vertical structure of the EGC. Previous estimates (e.g. **Mosby**, 1962, 1959) of the transports were of the order of 2 Sv, whereas **Aagaard** and **Coachman** estimated 32 Sv. The major part of this discrepancy was attributed to the different values taken for the speed of the underlying rAIW. This had been considered to be $\sim$ 2 cm/s (according to **Aagaard** and **Coachman**, 1968a), but the *Arlis II* data showed consistently high values $\sim$ 5–10 cm/s below the halocline. In fact, the *Arlis II* data showed movement of the entire water column to depths which included the deep waters underneath the rAtIW. A summary of the mean velocity vectors is shown in Fig. 5.8. The various published estimates of the transports are given in Table 5.3.

As a continental boundary flow, the EGC is geostrophically constrained to remain

Table 5.3
East Greenland Current transports (Sv)

Researcher	Transport (Sv)	Remarks
Jakhelln (1936)	1.3	Dynamic method
Timofeyev (1963)	4.9	Total, deduced from water balance
Vowinckel and **Orvig** (1960)	3.4	
Aagaard and **Coachman** (1968)	31.5	Total, winter 1965 from *Arlis II*
	7.7	GPW (< 0 °C, < 150 m)
	21.3	rAtIW (> 0 °C, 200 to 800 m)
	2.5	DW (< 0 °C, > 800 m)
Worthington (1970)	4.0	GPW
Mosby (1962)	2.0	
Aagaard and **Greisman** (1975)	7.1	Equated to WSC
	1.8	GPW component
	5.3	rAtIW component
	0.1	Ice component

along the Greenland Continental Margin by the combination of its less dense waters and the conservation of potential vorticity. This dynamical constraint acts principally on the surface portion of the EGC, or the GPW. Note in this context that the surface flow vectors in Fig. 5.8 have large westward components, indicative of the shoreward mass flux that helps sustain the barotropic (sea level) high along the Greenland shelf which in turn drives the EGC southward. The deeper portions, which lie below the Polar Front, appear to be constrained to follow contours of f/H; and, because they are not significantly less dense than the internal waters to the east, the deeper flow vectors are more affected by the eastward extensions of the Greenland slope: the Hovgaard Fracture Zone at 78°N, the Greenland-Jan Mayen Island at 72°30′ N, and the Denmark Strait at 67°N. The 1000-m depth contour, which is below the rAtIW, does not in fact curve eastward at any of these features, except at the Denmark Strait, and an eastward component of the AtIW at these junctures is not particularly evident in Fig. 5.8. Nevertheless, water-mass analyses have indicated the existence eastward extensions of EGC waters, and although the dynamical mechanisms is not known, we assume that it is largely due to an interaction between the bathymetry of these features and the barotropic field of the EGC. The fact that eastward turnings are not always observed is explained by the interference of other forces, such as wind stress, controlling the barotropic field either in oppostion or in concurrence. In any case the deeper portions below a depth of $\sim$ 1500 m are directly affected by these bathymetric extensions, particularly by the Jan Mayen Ridge.

The eastward flow that emanates from the Greenland slope at 72°30′ N is referred to as the Jan Mayen Current (JMC). In effect, the JMC can be considered as the southern contribution to the Greenland Sea gyre. The JMC continues cyclonically on the Greenland Sea side of the Mohn Ridge until it joins the portion of the NwAtC and the WSC which lies on the eastern side of Mohn Ridge. The consistency and trajectory of the JMC, although not well described, apparently have an important bearing on the decoupling of the Greenland and Iceland Seas. The dynamic topography of **Carmack** (1972) shows less cyclonic closure of contours in summer than in winter, e.g. see Fig. 5.9a. This depiction is in conflict with the greater eastward extension of the JMAtIW during winter compared to that during summer, as shown in Fig. 5.16. The climatological average surface salinities of Fig. 6.6b also show a well-defined extension of GPW eastward. The continuity (and transport) of the JMC remains in doubt. We point out that the patches of GPW along the Mohn Ridge as in Fig. 4.6d or 4.24 may indicate seasonal discontinuity in the JMC.

There also remains some uncertainty concerning the magnitude of the rAtIW portion of the EGC. As estimated by **Aagaard** and **Coachman** (1968a), the rAtIW transport greatly exceeds that of the WSC, its source. **Aagaard** and **Coachman** partially explain this by suggesting that the *Arlis II* data (Spring in Greeland Sea) represented a seasonal maximum and therefore a much higher value than the means estimated for the WSC. In a more recent consideration, **Aagaard** and **Greisman** (1975) reduced the estimate of the rAIW transport, to that noted in Table 5.3. Previous arguments on the coupling of the WSC and the EGC were (a) that seasonal variations of the two currents were out of phase (e.g. **Laktionov**, **Shamont'ev** and **Ianes**, 1960) and (b) that they were in phase (e.g. **Timofeyev**, 1962). The more recent analysis of **Hanzlick** (1983) indicates a WSC maximum during the fall, of the order of 10 Sv, and a minimum during the spring of the order of 4 Sv (as in Fig. 5.7). The spring minimum in the WSC (Fig. 5.6) shows a definite westward veering of the velocity vectors, particularly for the more westerly moorings, and could indicate a maximum in the westward flux across the northern sections of the Greenland Sea and thus would at least be compatible with a spring maximum in the EGC. This westward link between the two systems has not been well substantiated observationally, although water mass properties indicate a very broad westward drift, beginning, according to **Aagaard** and **Coachman** (1968), as far south perhaps as 75°N. Recent current meter data at a location midway between the Spitsbergen and Greenland slopes at 78°30' N show a 41-day mean direction of south-southwestward for the upper layer flow. Less recently, a mooring placed in nearly the same location also gave a southeastward mean over a 142-day period, making reconciliation with a westward flow more difficult. Drifter buoys deployed in the upper 200 m of the WSC at this time showed a definite tendency for either westward connection to the EGC or northward entry into the Arctic (**Gascard**, personal communication). Discussion and figures on this aspect can be found in Subsect. 5.3.1.

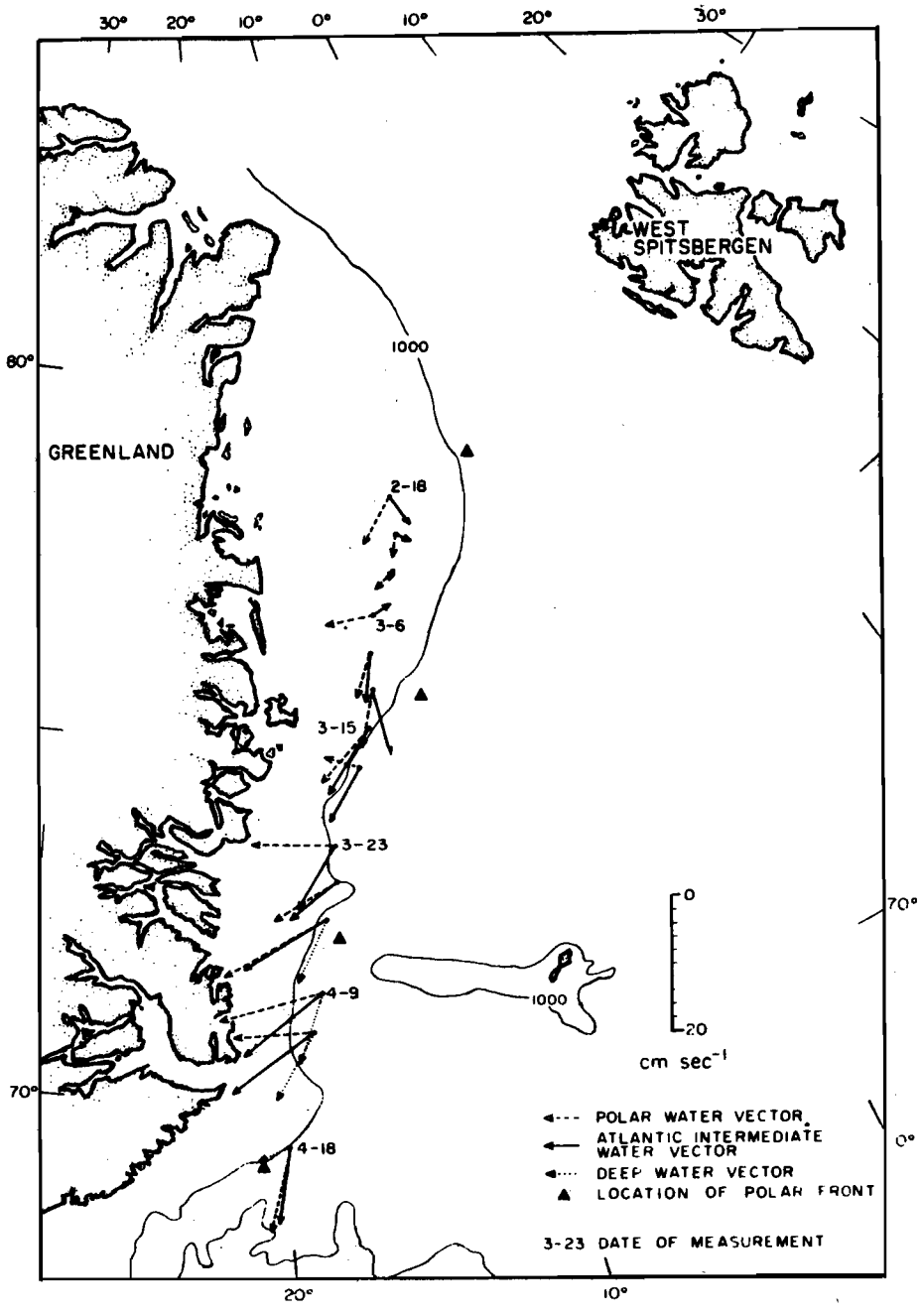

Fig. 5.8. Mean velocity vectors from *Arlis II*. Observations vectors represent depth and time averages for the layer, GPW to $T \sim 0°C$, rAtIW to ~ 800 m depth, and DW below 800 m depth. The location of the Polar Front is from **Killerich** (1945). [From **Aagaard** and **Coachman** (1968).]

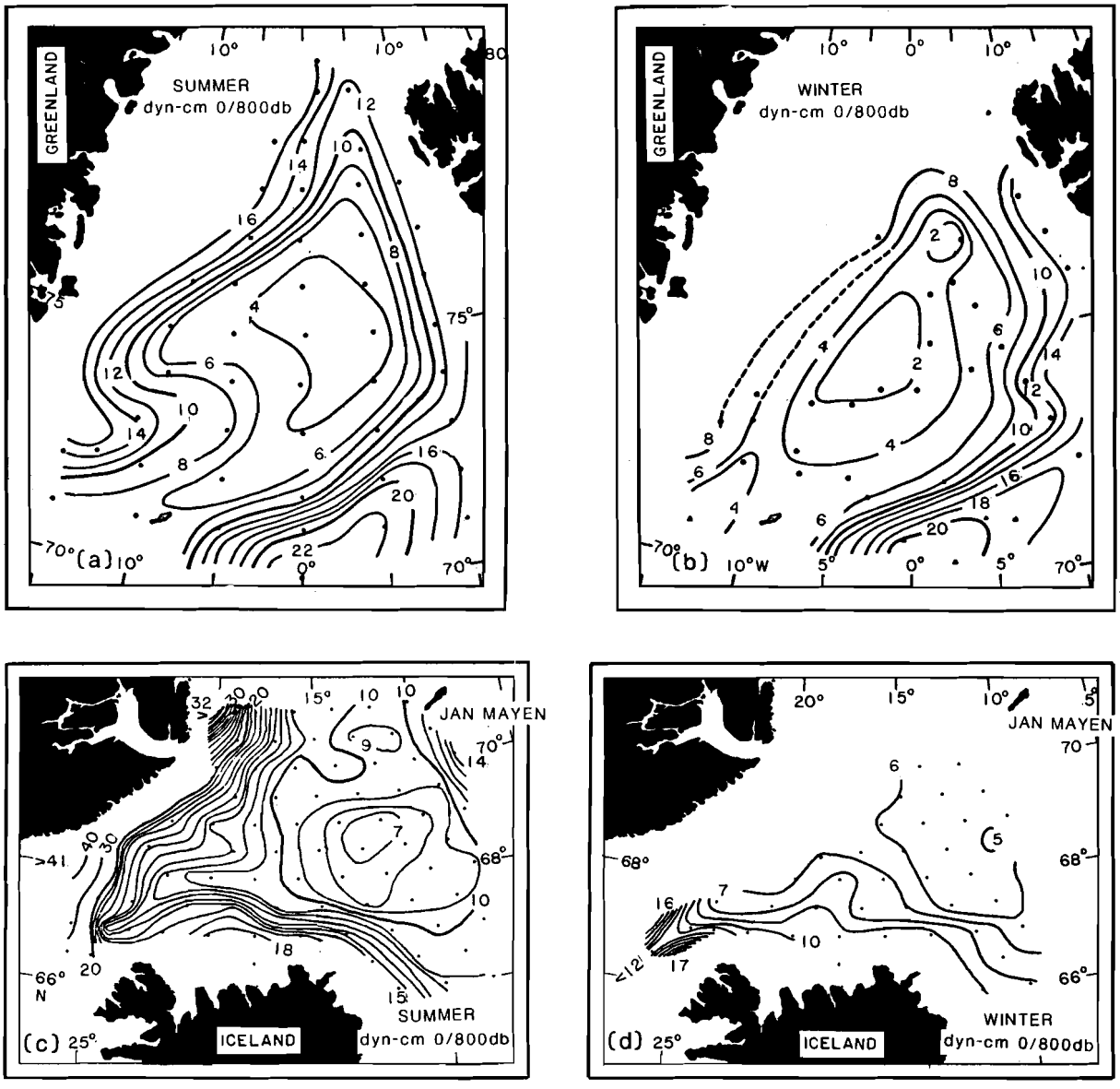

Fig. 5.9. The dynamic topography computed in dyn-cm from 800 dB: (a) August 1962 *Atka* data; (b) January–February 1954 *Atka*, March 1954 *M. Sars* data, March 1955 *Edisto* data, and March 1964 *M. Sars* data; (c) August 1974 *Edisto* and *Bjarni Saemundsson* data; (d) February–March 1975 *Bjarni Saemundsson* data. [(a) and (b) from **Carmack**, (1972); (c) and (d) from **Swift**, (1980).]

We now take up discussion of the EGC southward of Jan Mayen. The *Arlis II* velocity vectors (Fig. 5.8) show no obvious turning or dimunition at 72°N. During the

month of March when the *Arlis II* was north of 72°N, the EGC movement averaged 17.4 ± 11 cm/s, whereas during the month of April when it was south of 72°N it averaged $25.0 + 13$ cm/s. This agrees with **Swift**'s (1980) Iceland Sea estimates of 22–38 cm/s for the maximum speeds of the surface EGC relative to 800 dB (cf. Fig. 5.9c). Thus the magnitude of the flow in transit through the Greenland-Jan Mayen gap is unaffected, or increased, in transition from the Greenland to Iceland Seas, which is in conflict with the likelihood of a large volume loss eastward to the Jan Mayen Current. However, if we consider the cross-sectional area of the EGC to be proportional to the width from Greenland to the Polar Front (Fig. 5.8), then a 50% reduction in width could support a 1 Sv loss to the JMC and still support the observed speed increase to the south. The results of the thermohaline balance (Subsect. 5.4.3) estimate this loss at 0.3 Sv.

Within the Iceland Sea the distributions of the GPW and PIW masses, i.e. of those waters contained within the Polar Front or the $S = 34.7$ppt isohaline, again suggest very little coupling with the interior **Swift** (1980). The lack of significant vertical shear in the *Arlis II* velocity observations, the good correlation between water properties and bathymetry, and the existence of a $\sim$ 100 m thick bottom-mixed layer (**Swift**, 1980), all suggest that the EGC continues as a barotropic current. However, as mentioned above, bathymetric control results in some loss from the EGC, particularly of the underlying waters. Eastward movement of the rAtIW is indicated by the dynamic topography (Fig. 5.9c) at both of the bathymetric gaps in the Kolbeinsey Ridge.

■ *5.2.4. Icelandic Current*

Similar to the zonal, westward flow between the WSC and the EGC in the north of the GIN Sea, there is a zonal, eastward flow between the EGC and the NwAtC in the south. This latter flow however is more complicated, if only by virtue of its great length: from the Polar Front of the EGC to the Arctic Front north of the Færœs there is a separation of around 1000 km (as compared to the roughly 100 km across the Fram Strait). This zonal flow north of Iceland has been referred to as the East Icelandic Current, but we have shortened it to simply the Icelandic Current (IC) and mean it to refer to the entire zonal current system between the EGC and the NwAtC. However, although we describe the IC as the final link in the cyclonic boundary system of currents in the GIN Sea, we stress that a continuous cyclonic transport is not also implied. i.e. there is no implication intended that the NwAtC is an extension of the IC nor that the IC is an extension of the EGC.

We consider the westward origin of the IC to be the branch of the Irminger Current which imports Atlantic water into the Iceland Sea through Denmark Strait. This was referred to as the North Icelandic Irminger Current by **Stefansson** (1962). We refer to it here as the North Irminger Current (NIrC). The IC flows eastward along the northern continental slope of Iceland. During this course, it is exposed to the water of the central Iceland Sea to the north and to the Icelandic coastal waters to the south. The latter are basically Atlantic in origin but freshened by local runoff. According

to **Stefansson** (1962), the IC is composed of about one-third undiluted Atlantic Water and two-thirds of a mixture of essentially ArSW with small admixtures of GPW and ArIW. He found that the core of the eastward flow was most often over the shelf break and extended down to at least that depth ($\sim$ 200 m). However the bathymetry of the north Icelandic coast is quite irregular, precluding a smooth zonal flow pattern, i.e. there are southward and northward IC excursions that are consistent with the shelf bathymetry and are evident in dynamic height contours. The IC follows the Icelandic coast until it reaches the easternmost point, Gerpir, where it continues eastward rather than southward.

Swift's (1980) dynamic topography of the Iceland Sea of Fig. 5.9c,d gives some idea of the intensity of the IC but it does not show the structure over the shelf, since he used an 800-dB reference level. More detail can be found in **Stefansson** (1962), whose objective was to describe the coastal flow and therefore used the bottom as a reference level for depths less than that of the intersection with the deeper waters (at a depth of $\sim$ 300 to 400 m). To delineate the IC, **Stefansson** used the 1 °C isotherm. By doing so, he obtained a transport of 0.64 Sv off Kogur to the northwest and a transport of 1.03 Sv off Sletta to the northeast. A comparison of five sections strongly indicated that variations in the east were directly correlated with variations in the west and that the differences between the two sections were nearly constant. **Stefansson** also compared the flow speeds derived from dynamic height computations with those obtained from other methods such as drift bottle results and water mass tracking; the comparisons produced a mean flow speed of $\sim$ 6 cm/s.

Malmberg (1984) has pointed out the susceptibility of the waters north of Iceland to sea ice conditions. The variability in sea ice coverage is critically dependent on the upper ($\sim$ 100 m) layer salinity. Values less than $S = 34.70$ ppt permit ice formation or sustentation because even at freezing point the waters are not dense enough to convect; on the other hand, waters with salinity greater than $S = 34.8$ ppt sustain convection with sufficient heat flux upward to keep the surface ice-free. The eastward transport of GPW from the EGC together with the northward transport of IrAtW by the NIrC are undeniably implicated as controlling factors in the salinity of the IC and hence of the ice coverage north of Iceland.

Upon leaving the Iceland coast the IC can no longer be considered a coastal boundary current although it remains bathymetrically steered eastward along the north flank of the Iceland-Færœ Ridge (IFR). The IFR is fully defined by the 500-m depth contour (**Joseph**, 1967a) and about one-third of the Ridge has depths less than 350 m. Such depths are too great to cause direct bathymetric steering for a current as shallow as the IC, which is less than 300 m deep. The cause of this continental shelf separation of the IC has to be attributed to more complicated and larger-scaled influences.

Current measurements along the southeastern Icelandic continental shelf, south of the IFR, have shown a flow to the southwest, giving the appearance of continu-

ous anticyclonic circulation around Iceland. However the waters to the southeast are of Irminger Sea (Atlantic) origin and are not a continuation of the IC waters (**Joseph**, 1967b). There is therefore a water-mass break over the eastern Icelandic shelf corresponding to the eastward turning of the IC. This situation is well illustrated by the circum-Icelandic contours of summer temperature (and salinity) see Fig. 5.10. The water mass difference is a demonstration of the unequal exposure to admixtures north and south of Iceland. The mechanism is as follows: the NIrC introduces IrAtW to the southwest of Iceland, the IC advects it anticyclonically around the north of Iceland (where it undergoes cooling and and freshening through advective admixtures of Arctic and Polar waters) until at approximately Gerpir it re-encounters waters of the same North Atlantic origin. In circuiting Iceland to the north the original Atlantic water mixes with Arctic waters to the extent that, on rencountering the NAtW water, it is cooler, fresher, and denser by $\sim 0.2\sigma_t$ units. The alongshelf (north-south) density difference is sufficient that it re-orients the offshore geostrophic flow eastward; that is, the northward confluence of the lighter NAtW, over the southeastern Icelandic shelf and over the southern portion of the IFR, forms a sea-level high pressure ridge that extends eastward from Iceland and more or less coincides with the IFR. Consequently, the lighter NAtW on the south side tends to be forced over the IC waters but because of the Coriolis force flows to the west; the heavier IC water on the north side tends to be forced under the NAtW and flows to the east. The result is a sheared, water mass front prograde to the north, i.e. the front intersects the IFR at around the northern 500 m depth contour, titling northward.

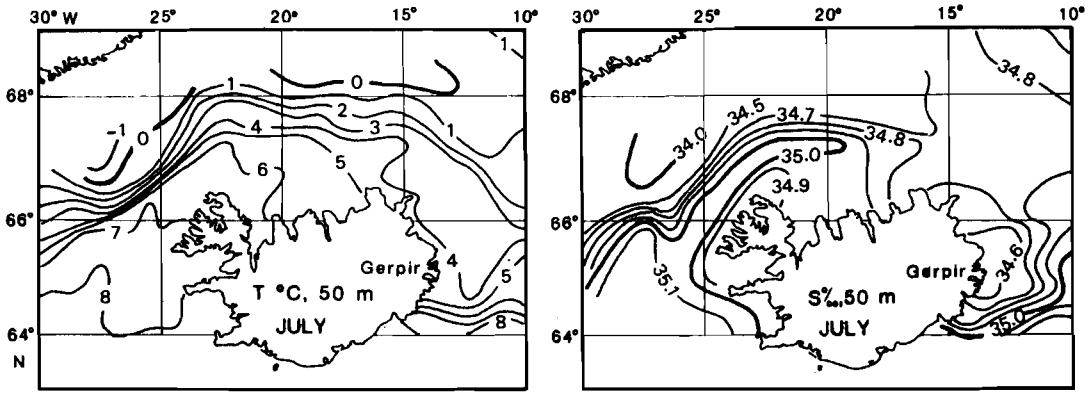

Fig. 5.10. The mean T and S distributions at 50 m depth during July from the Service Hydrographique before 1947, from the Bulletin Hydrographique for 1948–1955, and from Icelandic material for 1956–1960. [From **Stefansson** (1962).]

Considerable current-meter data has been obtained for the IFR including the eastward extensions of the IC, but no transport calculations seem to have been performed. (Note, preliminary analysis of June 1986 data indicates possible transports of up to 4 Sv, **Gould** and **Hansen** pers. comm.) The data collected in 1975/76 (**Dorey**, 1978) provides some evidence as to the structure and strength of the flow (see Fig. 5.2): the upper flow for the moorings along the north face of IFR (moorings d,b,a, and g) followed the bathymetry at speeds of $\sim$ 20 cm/s. The flow was eastwards down to a depth of approximately 1200 m, whence it reversed to westwards (mooring a). Over the crest, mooring displayed much less unidirectional motion and exhibited a reversal at the bottom due to the baroclinic shear through the front. This situation is further discussed in Subsection. 5.3.3.

5.3. COUPLING WITH ADJACENT SEAS

As a semi-enclosed sea the GIN Sea has several connections to the world ocean system, the primary one of which is through the Fram Strait where the sill is found at oceanic depths. The other connections, although wide in cross-section, are relatively shallow and therefore in contrast to the Fram Strait do not allow unrestricted exchange at oceanic depths. The sill depth, sill area, and the relative location all strongly determine the role which a strait, or opening, plays in the interior circulation. In Fig. 2.3 we have compared the profiles of all of the GIN Sea openings together with their projected sill areas in the cases where the profile does not coincide with the sill. Considerable observational effort has been focused on attempting to quantify the exchange processes that occur within these openings. Nevertheless, while the sampling effort is facilitated by the physical restriction offered by the geomorphology of a strait, it is complicated by the fact that these exchange processes are extremely sensitive to the dynamics of the adjacent seas at precisely the point of greatest restriction. Thus, while sampling in space is optimized, sampling in time is not.

■ *5.3.1. Fram Strait*

The Fram Strait opening, also called the Greenland-Spitsbergen Passage, is the only GIN Sea opening at oceanic depths: about 240 km of the 600 km wide opening at 79°N is over 2000 m deep, and the sill depth is at the depth of $\sim$ 2600 m (**Coachman** and **Aagaard**, 1974). As a consequence of this aspect of its bathymetry, the GIN Sea constitutes a very important division of the Arctic Ocean: the only portion exposed to significant atmospheric interaction causing it to play the role of a water mass buffer between the Polar Sea and the Atlantic Ocean. In recognition of these aspects, the observational focus in the Fram Strait region has been on measuring the fluxes of mass and heat through the Strait in order to better understand the difficult-to-observe water mass structure of the Polar Sea.

Recent current meter observations (Table 5.4) have assisted in coalescing opinion on the magnitude and structure of the exchange through the Strait. The magnitude of the exchange has been estimated at about four times that of the combined exchanges through the other openings of the Polar Sea (**Coachman** and **Aagaard**, 1974). This has led some investigators to assume that the volume exchange through Fram Strait is approximately balanced (e.g. **Aagaard** and **Greisman**, 1975). This assumption is supported by the fact that the inflow from the Bering Sea is approximately equal to the ouflow through the Canadian Archepelago at $\sim$ 1 to 2 Sv. The only other opening, that with the Barents Sea, is estimated to have a small net volume ($\leq$ 1 Sv). To assume, alternatively, a balance in the exchanges of salt and heat is less tenable (e.g. **Swift et al.**, 1983; **Midttun**, 1985). See Table 5.10 of Subsect. 5.4.2.

Thus, to the first order approximation the Fram Strait acts as both an entry port and an exit port for the Polar Sea. Because of its large lateral dimension the inflow and outflow are separated horizontally, rather than vertically as in narrower straits. The inflow to the Polar Sea is on the Spitsbergen side and the outflow is on the Greenland side. A horizontal separation in flow is generally accompanied by horizontal density gradients that are weaker than it would be if the separation were vertical, making it much more prone to lateral exchange between the inflows and outflows i.e. recirculation. Weak horizontal density structure is observed in the Fram Strait, except perhaps for the surface 100 m or so, where the Polar Water is less dense by $\sim 0.5\sigma_t$ units. In addition, the Strait extends from nearly 78°to 82°N (a distance of $\sim$ 450 km), enhancing the probability of recirculation. The amount of water (salt and heat) that recirculates from the WSC to the EGC within the Strait remains uncertain, but it is likely to influence the thermohaline dynamics of both the GIN and Polar Seas.

It is believed that a large portion of the east-to-west exchange occurs south of the sill as a part of what might be called the northern portion of the Greenland Sea gyre. This transport is difficult to observe but is, for example, indicated in the dynamic topography of the Greenland Sea as represented in Fig. 5.9a,b. To date the amount of westward transport occurring in the region of the sill has still not been clearly resolved, despite a series of recent measurements. We have summarized the results of Fram Strait moorings in Fig. 5.11 and the accompanying Table 5.4 with the exclusion of those of **Hanzlick** which related specifically to the WSC (Fig. 5.6). **Greisman** (1971) and **Aagaard**, **Darnall** and **Greisman** (1973) reported a consistently southeastward flow at 1360 m depth from G1 mooring at 2°E, and a predominantly southeastward flow at 116 m depth, but with some instances of northwestward flow. In this case, the southeastward surface-layer flow would imply that EGC waters extend even that far east; and the intermittent northwestward flow would suggest the presence of the WSC. Another mooring (H1) in virtually the same location, showed consistently southward flow in the surface layer (**Hunkins**, 1984). Another more recent mooring (H5) slightly to the west recorded flow to the southsouthwest at $\sim$ 10 cm/s over an 11-month mean, although the shorter series slightly to the north was similarly directed but much slower (**Hunkins**, 1986).

Table 5.4
Fram Strait current-meter data

Mooring	Depth (m)	Start	End	Speed (cm/s)	Direction (°)	Reference
G1	116	8 Sep 71	11 Aug 72	6.3	110	**Greisman**
	1360	"	"	1.6	110	(1971)
G2	148	10 Sep 71	10 Aug 72	19.2	006	"
	494	"	"	17.4	009	"
H1	52	16 Jun 83	12 Jul 83	1.8	283	**Hunkins**
	151	"	15 Jul 83	5.3	162	(1984)
H2	1015	"	27 Jul 83	4.5	166	"
H4	55	"	"	7.8	195	"
	158	"	16 Jul 83	6.8	197	"
	1014	"	27 Jul 83	5.2	175	"
	2296	"	"	7.6	171	"
H5	70	"	"	9.3	203	**Hunkins**
	185	"	"	8.3	204	(pers. comm)
H6	163	"	"	0.5	191	"
	600	"	"	0.7	225	"
A1	144	15 Jun 84	16 Jul 85	6.4	179	**Aagaard**
	424	"	"	1.4	183	**et al.** (1985)
	1069	"	"	2.6	166	"
A2	78	16 Jun 84	16 Jul 85	9.1	194	"
	378	"	"	3.8	179	"
	1378	"	"	2.3	177	"
A3	109	"	15 Jul 85	9.6	205	"
	409	"	"	6.0	201	"
	2334	"	"	0.5	150	"
A4	135	28 May 84	13 Jul 85	8.7	265	"
	635	"	"	5.3	268	"
	2320	"	"	4.8	249	"
A5	219	27 May 84	12 Jul 85	2.2	336	"
	719	"	"	0.2	216	"
	1519	"	"	1.1	204	"
	2459	"	"	5.4	230	"
A6	262	21 May 84	"	13.4	353	"
	562	"	"	9.6	353	"
A7	147	22 May 84	13 Jul 85	7.5	296	"
	647	"	"	5.3	297	"

The moorings of **Aagaard**, **Darnall**, **Foldvik** and **Tørresen** (1985) constituted the first array with instruments placed contemporaneously in the east, west and center of the Fram Strait. The instruments in the EGC (A1,A2,A3) all showed a consistent

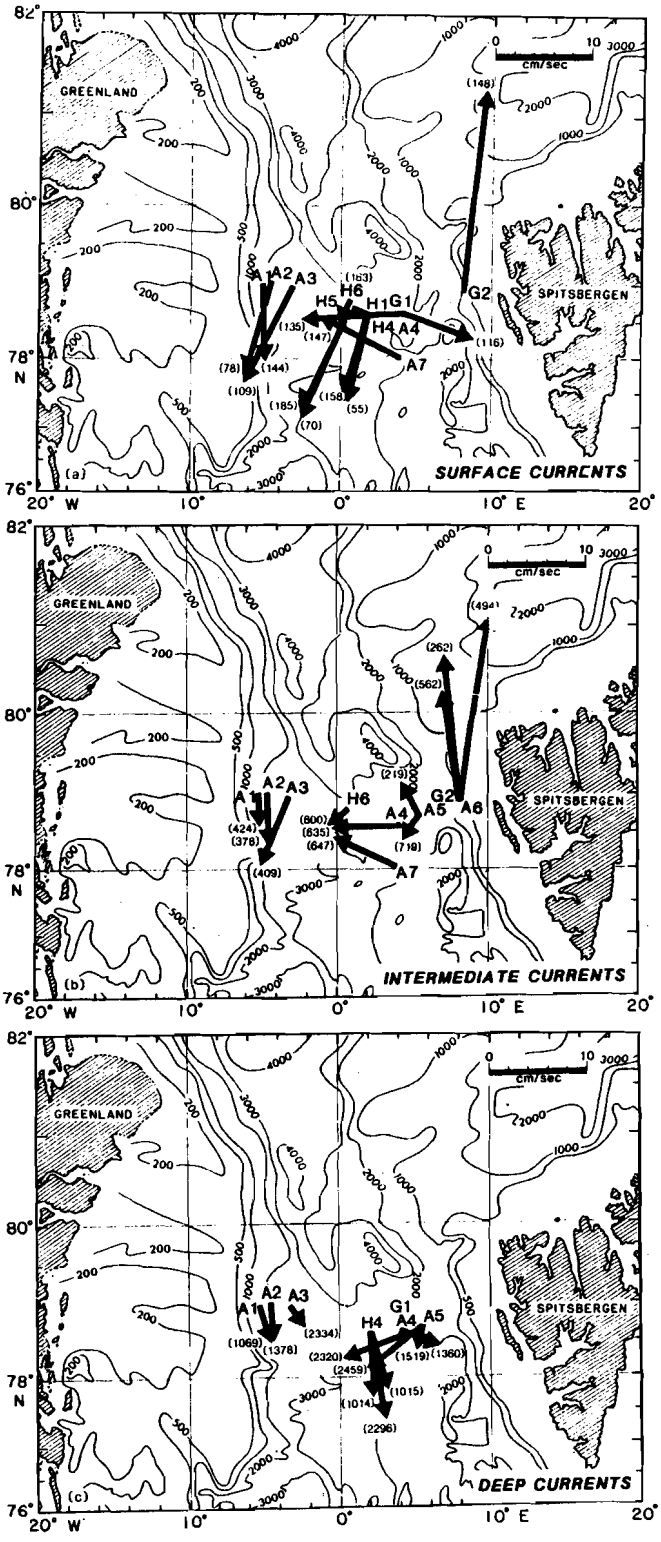

Fig. 5.11. Summary depiction of observed currents in the Fram Strait: (a) surface layer < 200 m; (b) Intermediate layer 200–1000 m and (c) deep layer > 1000 m. For the periods of observation and instrument depth see Table 5.4. (Observations of Hanzlick (1983) in Fig. 5.6 are from same latitude but not included here.)

southward flow that suggested an overall barotropic component of $\sim$ 3 cm/s with a baroclinic component increasing to the east, e.g. the flow at the 2334 m depth of A3 oscillated between northward and southward as presumably it was alternately exposed to baroclinic shear through east-west movements of the tilded isopycnals whereas the flow to the west as more consistently southward. The current-meter records within the WSC showed stronger surface flow, extending to at least the 600-m depth, and those under the western limits of the WSC (A5) showed a tendency for southwestward flow. We note that mooring A5 was virtually at the same location as St. 45 in Fig. 4.19, which was where the GDW was observed, at a depth of 2450 m, presumably the result of northward flow. However, the 6-week record of A5 at this depth registered southwestward flow (Table 5.4). The intermediate-level flow at mooring A5 was quite variable, as one might expect from the baroclinicity induced by the western boundary of the WSC. The flow at mooring A4, the only one really on the saddle of the sill, showed westward flow at all depths. It is tempting to take this observation as confirmation of the looked-for westward recirculation, because such a barotropic flow could well be driven by the higher sea levels to the north in the Eurasian Basin. However, observations taken at other times (H4 and G1) have indicated a more of a southward deep flow towards the center of the channel. The mooring A7, situated south of the sill region and possibly in the northern portion of the Greenland gyre, has registered consistent westward flow at intermediate depths.

To generalize, the surface flow through Fram Strait is bimodally directed: south in the EGC and north in the WSC. The EGC flow is broader and weaker than that of the WSC. The subsurface layers under both currents are subject to the baroclinic shears generated by the inclined water mass boundaries, the WSC more so. The flow in the central region is more variable, but generally : at the surface it flows south or north if it is within the EGC or the WSC respectively, and otherwise it flows to the west; at subsurface depths it flows either to the south or west. Away from the water-mass boundaries the center-region flow is mostly barotropic. Incidences of westward flow may be caused by a northward extension of the Greenland gyre and/or a response to the axial sea-level gradient (southward) that predominates in the center portions not strongly influenced by the diabathic sea-level pressure gradients driving the WSC or EGC flows. Incidences of southward flow may be the result of eastward extensions of the EGC, i.e. cases in which the diabathic sea-level gradient (eastward) of the EGC dominates out to the center region. The observational evidence from central region is ambiguous: either there is a net inflow from the Polar Sea or there is significant spatial variability along the axis of the Strait. A quantitative estimate of the net transport has not yet been made and further measurements will be necessary before this ambiguity is resolved. Evidence of spatial variability along the axis of the strait is found in the dynamic height computations of **Palfrey** (1967), which revealed the existence of a cyclonic feature between the WSC and the EGC, centered at about 80°N and 1.5°E in the Fram Strait. Temporal and spatial variability of such a feature would certainly complicate estimates of net flow and recirculation from a single line of cross-strait moorings.

In describing the disposition of the WSC on entering the Polar Sea, **Perkins** and **Lewis** (1984) suggested that the WSC bifurcates to the north of Spitsbergen into a coastal portion that follows the 200–400 m isobaths and another portion that continues along the deeper contours of the Fram Strait and thence around the Yermak Plateau. They also observed that water columns to the north and west of the Yermak Plateau had interleaved layers of GAtIW from the WSC (entering) and PAtIW from the Polar Sea (leaving), which suggests that a certain amount of lateral recirculation was occurring even inside the Eurasian Basin.

The GIN Sea output consists of NwAtW, GAtIW, NwDW, and GDW; and its input consists of ice, PW, PAtIW, and EADW. The upper layer components have received the most attention; their transports have been tabulated in Tables 5.2 and 5.3 for the WSC and the EGC respectively. The amount of ice has been estimated at $\sim$ 0.1 Sv by several researchers, e.g. **Timofeyev** (1958). This is a rather insignificant amount in terms of the volume budget of either Sea. However, as a component of the heat balance it is very significant: being for the Polar Sea a heat gain approximately equal to that of the WSC (see Table 5.10 in Subsect. 5.4.2). The influence of the ice within the GIN Sea is diminished by the fact that it remains confined to the surface waters of the EGC, exchanging more heat with the atmosphere than with subjacent layers through vertical mixing, as this mechanism is inhibited by the positive buoyancies of the melt water ($S \simeq 3.0$ ppt) and of the GPW.

The composition and transports of the deeper waters are less well known. **Aagaard** and **Greisman** (1975) have assumed the opposing deep in-and-out-flows to be approximately equal in magnitude, and because of their similar T-S characteristics, have taken their respective transports of heat and salt to be equal. The structures of these opposing, deeper waters are of great interest as an indicator of the large-scale dynamics in the Polar and GIN Seas. From a station centered just north of the sill **Swift**, **Takahashi** and **Livingston** (1983) found NwDW below 1000 m, except in the very bottom 100 m where they found GDW. At the same time GDW was not found east of the Mohn Ridge, which is to say under the WSC to the south of the Strait, and consequently they concluded that this bottom layer moved into the sill region directly from the Greenland Sea. Quite a different distribution is shown in Fig. 4.19, in which neither the NwDW nor the GDW were found over the central portions of the Strait but both were found to the east on the Spitsbergen side apparently flowing north as a part of the WSC. At a speed of 2 cm/s an inflow of GDW would be on the order of 0.2 Sv or 6.3×10^3 km^3/yr and would suggest a $\sim$ 600-yr residence time for the GDW component in the Eurasian Basin. The presence of GDW at St. 45 (Figs. 4.19 and 4.20) but not at St. 20 (Fig. 4.20) suggests that by March 1982 the GDW, had moved eastward to its position under the WSC within the Fram sill region and not through the gaps in the Mohn Ridge further to the south, i.e. St. 20. Over the center portion of the sill (St. 42) the water type was recorded as mostly EADW with some GDW, suggesting invasion of EADW at least to the sill. From water mass and budget arguments, we can suppose that the EADW is often likely to be found in variable amounts over the center portions of the Fram Strait, where

it would be exposed to variable north-south movements, which would facilitate the entrainment of GDW from the south and/or east, but which would not necessarily result in any large southward transport of EADW. Net transports of EADW to the south would occur primarily on the Greenland side, and for net transports of the GDW to the north primarily on the Spitsbergen side. We note that the thermohaline balance of Subsect. 5.4.2. suggests a net DW southward flow of $\sim$ 1 Sv.

■ *5.3.2. Denmark Strait*

The characteristics of the Denmark Strait, which passes southwest-northeast over the Greenland-Iceland Ridge are quite different from those of any of the other GIN Sea openings. The Strait is perhaps third in importance with respect to external water mass exchange for the GIN Sea, a status not necessarily reflected by its relative cross-sectional size (Fig. 2.2). In terms of input-output to the GIN Sea, it could be considered the reverse analogue of the Fram Strait: polar water output and atlantic water input; a large IW output and no IW input; and very little DW output and no DW input. Interestingly, there are several aspects about the Denmark Strait which given a slightly different bathymetric configuration would have changed the thermohaline dynamics of the GIN Sea considerably and to some extent those of the North Atlantic as well. For example, if the outflow of the GPW were more restricted it would force greater mixtures of polar water into the GIN Sea waters; or to the contrary if the entry of Atlantic Water were less restricted the waters of the southern Iceland Sea would be much more Atlantic in water type; or if the sill were deeper the contribution of the NwDW would be much greater.

The water mass exchange through the Denmark Strait appears to be controlled by a large-scaled circumstance, i.e. the convergence of the EGC and the NIrC, from the north and from the south, respectively. A look at the local bathymetry (Fig. 2.1) shows the Greenland Continental Slope tends southward from 68°N and the Icelandic slope tends northward from 64°N, whereas the Strait itself, at 66°N, lies along a NE–SW axis and intersects these slopes at $\sim$ 45°. As a consequence, the bathymetrically steered flows of the EGC and the NIrC converge on, and dominate, the north and south ends of the Strait respectively. The result of this convergence in conjunction with this bathymetry is a water mass interface, or a front, that runs more E–W than the channel axis and thereby causes the waters of the NIrC to fill more of the southern portion and the waters of the EGC to occupy more of the channel to the north than would otherwise be the case. Only the upper layers are affected by this skewed distribution of the water-mass interface with respect to the bathymetry, i.e. because of the 600-m sill depth.

Figure 5.12 illustrates a number of important descriptive points. The Strait is occupied by a water mass boundary. At the surface the front is formed by the confluence of Atlantic and Polar Waters, a situation unique in the GIN Sea. We note that this situation does not occur in the Fram Strait because it is wider and because its bathymetry aligns the flows through the Strait. We note also that the cross-strait T-S differences are less in the Fram Strait, because the Atlantic Water in transit

northward through the GIN Sea suffers more water-type modification in than does the Polar Water in transit southward.

South of Iceland the NIrC waters typically have little vertical structure within the upper 1200 m with $T > 4\,°C$ and $S > 35$ ppt (e.g. **Steele, Barrett** and **Worthington**, 1962 or **Stefansson**, 1968). Some seasonal temperature structure exists at the surface, but otherwise, all the way down to the depths of the Denmark Strait (600–800 m) the IrAtW brought to the Strait by the NIrC is quite homogeneous. In contrast, the waters brought to the Strait by the EGC have considerable vertical structure. As can be seen in Fig. 5.12, the vertical structures on either side of the front are different: on the Icelandic side the water columns are vertically nearly homogenous with the IrAtW type, whereas on the Greenland side the vertical structure generally consists of a polar water type down to a depth of 100 m and an intermediate water type down to the sill depth where occasionally a deep water type is found.

Swift, Aagaard and **Malmberg** (1980) describe two types of IW found in the Strait: a deeper one, which is a version of the rAtIW and arrives from the Greenland Sea via the EGC; and a shallower one, which is a version of the IArIW and arrives from the central Icelandic Sea. Both of these contain mixtures of PIW. Below them is found uNwDW with a water type of $T \sim -0.5\,°C$, $S \sim 34.92$ ppt; NwDW of the pure Icelandic Sea variety ($\sim -1.05\,°C$, ~ 34.91 ppt, **Swift**, 1984) is not actually observed in the Strait. In addition to these four water masses on the Greenland side of the front, there are also intrusions of IrAtW in the southern portions of the Strait (e.g. at $\sim$ 200 m depth in Fig. 5.12b,d). These intrusions occur at approximately the depth that the cross-axis density gradient changes sign, i.e. on the Greenland side the water is less dense at the surface and more dense at the bottom than it is at corresponding depths on the Icelandic side.

The $\sigma_t = 27.8$-isopycnal surface drops from a depth of 100 m (Fig. 5.12e) to a depth of 700 m (Fig. 5.12f) southward along the axis of the Strait. At the southern terminus the volume of water underneath this surface is nearly pinched off, surviving only in a narrow band inclined upward along the Greenland slope. It is water of this, or greater, density that is commonly defined as 'overflow' water, because such densities can reach depths of > 1500 m in the North Atlantic (e.g. **Worthington** and **Volkmann**, 1965; **Mann**, 1969). Although the volume of this water decreases southward the speed of the layer increases, as illustrated by the current vectors in on Fig. 5.12e,f and in Fig. 5.15a (below). Speed values of 50–60 cm/s are commonly observed in this layer (**Stein**, 1974) with maxima speed well in excess of 100 cm/s strongly correlated with colder temperatures (**Worthington**, 1969).

The transverse density structure tends to impart a convex shape to the front with the GPW slighty overriding the IrAtW at the surface. The severity of the inclination of the isopycnals through the lower portion of the cross section is very significant. First, the indication on Fig. 5.12e,f is that the speeds increase toward the bottom, therefore

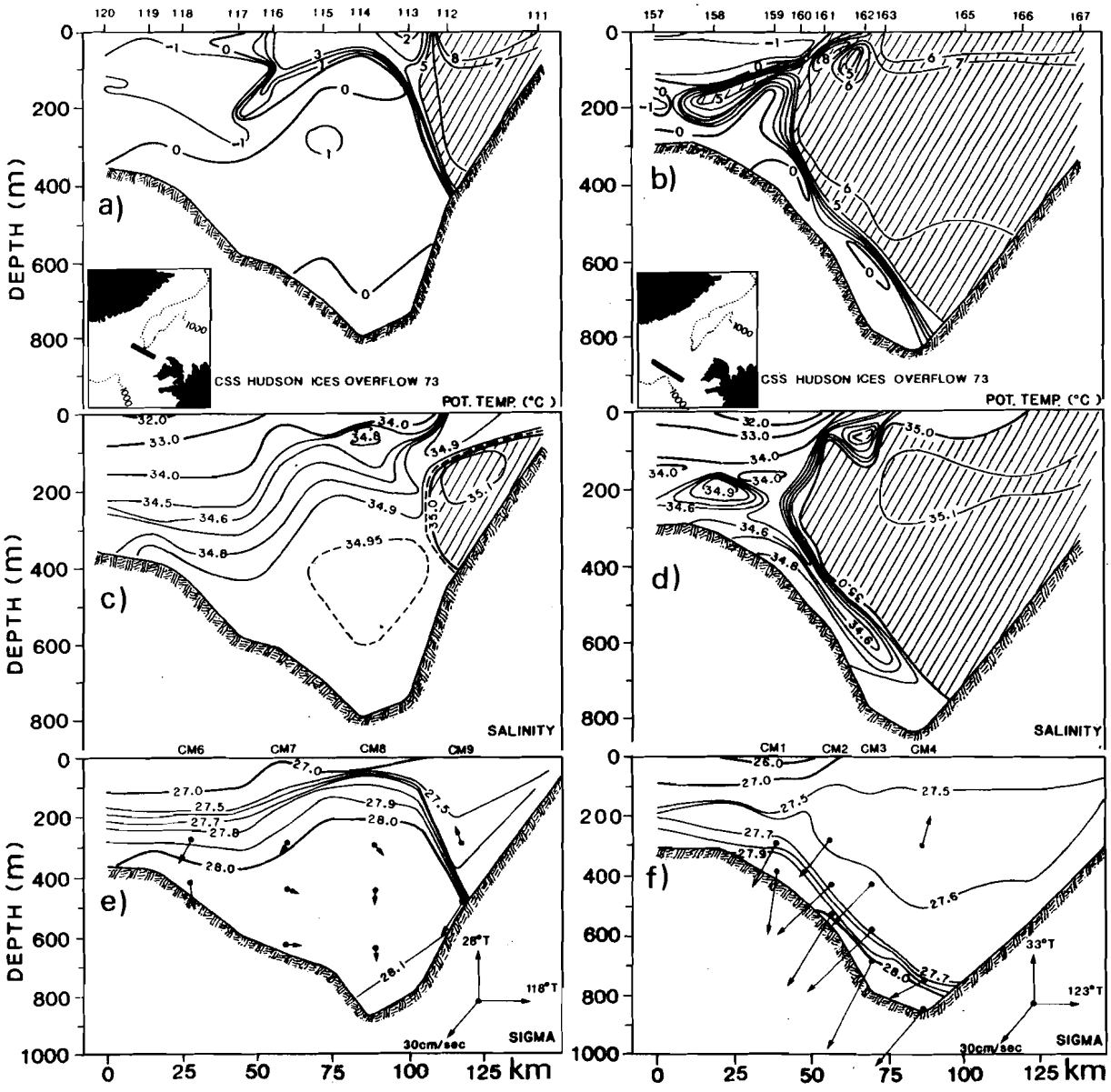

Fig. 5.12. The potential temperature (a, b), salinity (c, d), and σ_t (e, f) cross sections from a northern (left panel) and southern (right panel) transect . Both transects taken early September 1973. [From **Ross** (1982).] The vectors shown in (e, f) represent the observed mean flows from current meters positioned along the two transects for the period mid-August to mid-September. [From **Smith** (1976).] Hatched areas approximate the area occupied by IrAtW.

implying that the baroclinic shear dominates over frictional reduction. Second, the isopycnal slope on the Greenland side is contrary to that dictated by geostrophic pressure adjustment; that is: on the Greenland side a shoreward rising sea level, that drives a southward surface flow, would be compensated by shoreward deepening of the isopycnals under normal conditions of geostrophic pressure adjustment. As Fig. 5.12 shows the situation is quite the opposite, from which we conclude that a situation of strong ageostrophy exists.

A qualitative explanation for this ageostrophic situation is a consequence, we suppose, of the fact that the local sea level is controlled by larger-scaled circumstances than those determined by geostrophy in the Strait. The large-scale confluence of the EGC and the NIrC results in a sea level high that coincides roughly with the Greenland-Iceland Ridge bathymetry. The confluence is not exactly 'head on', and so the sea-level topography across the Strait is not uniformly high. Instead, the sea level rises over the Greenland and Iceland shelves, driving the EGC southward and the NIrC northward, and leaving a sea-level trough in between. On the Iceland-Sea side this can be seen in dynamic-height contours of Fig. 5.9c. This trough approximately coincides with the surface frontal interface: however, movements of the trough are controlled by local wind and the large-scale forces driving the EGC and NIrC to which the interface cannot respond adequately in a geostrophic manner (i.e. to a tilt corresponding to a balance between the sea-level and internal pressure fields). The result is large and variable bottom flows. Another important aspect of the ageostrophic response is indicated by the skewed alignment of the interface and the bathymetry and the axial pressure gradient (noted above), suggesting that the southward deep flow is both geostrophically convergent against the Greenland Slope and ageostrophically accelerated southward in response this axial pressure gradient.

In suggesting that the Denmark Strait might contribute significantly to the North Atlantic Bottom Water (NABW), **Cooper** (1955) described the overflow as occurring in intermittent boluses. Other researchers have noted significant variability in the frontal position observed in repeated samplings of stations, that were 1 to 2 days apart (e.g. **Harvey**, 1961; **Mann**, 1966), which might suggest a corresponding variability in the overflow. An analysis of repeated samplings (2 days) of the southern section shown in Fig. 5.12b,d,f revealed that the cross-sectional area between the interface and the Greenland slope decreased by 70% (from **Ross**, 1982). From a current meter record located at a depth of 760 m over the axis of the southern portion of the Strait, **Worthington** (1969) noted that as the front migrated past, the inflow of IrAtW at speeds of 25 cm/s was sharply interrupted evidenced by cold temperatures and high southwestward speeds ($>$ 75 cm/s) of the outgoing waters. These migrations occurred in bursts of 1–2 days approximately every 4 days. Consequently the mean volume flux computed at that particular current meter was apparently towards the Atlantic, even though the mean position of the front was to the west of it. **Ross**'s (1984) analysis of the mooring cross-section shown in Fig. 5.12b,d,f demonstrated that the outflow, while appearing intermittent in the Eulerian frame of a moored meter, was actually continuous in the sense that at any given time there

always existed some outflow of cold ($T < 2\,°C$) water because the migration of the front was not parallel to the Greenland slope. In other words, the outflow was never completely pinched-off.

With this same data, **Smith** (1976) found a strong spectral peak at 1.8 days, which he concluded to perhaps be a result of baroclinic instability in the front. However, **Aagaard** and **Malmberg** (1978) reported a similar frequency along the Greenland slope that lies south ($\sim$ 100 km) of the Strait, which suggests that if the responsible mechanism is a baroclinic instability then it is not controlled by the bathymetric/frontal conditions in the Strait itself.

The difficult observing conditions encountered in the Denmark Strait prevented a sufficiently comprehensive direct observation of the overflow until the highly successful *CSS Hudson* cruise during the 'OVERFLOW 73' Experiment. From this data **Ross** (1984) has computed the overflow volume from mid-August to mid-September using the section and current meters, identified in Fig. 5.12f. By computing the volume flux per T-S class, he obtained a total flux of 2.9 Sv for water at a temperature of less than 2 °C, of which 0.5 Sv was estimated to have a $T < 0\,°C$ and a $S > 34.9$ ppt, i.e. equivalent to uNwDW. In fact no incidence of NwDW was reported, substantiating **Swift**'s claim that none of it exits to the Atlantic. The **Ross** estimate, which we consider to be the most accurate, does not in fact vary much from previous estimates (see Table 5.5).

Table 5.5
Overflow estimates for Denmark Strait

Researcher	Transport (Sv)	Remarks
Worthington (1969)	2.7	$T < 4\,°C$
Mann (1969)	4-5	$T < 2\,°C$, $S > 34.7$
Timofeyev (1969)	4.0	
Swift, Aagaard and	2.3	$T < 2\,°C$
Malmberg (1980)	0.5	$T < 0\,°C$
Ross (1984)	2.9	$T < 2\,°C$

Swift, Aagaard and **Malmberg** (1980) used other information, in particular tritium concentrations to differentiate the origin of the major portion of the overflow volume, which they concluded to be essentially the IArIW. Thus, the thermohaline coupling between the Gin Sea and the North Atlantic Ocean is short-circuited, i.e. the primary contribution to the NABW is not from the oldest GIN Sea deep water, (i.e. the NwDW with residence times of less than 100 yrs), nor even from the rAtIW (with

residence times of the less than 10 yrs), but from the central Icelandic Sea component of the ArIW with residence times of the order of several years. This, as they point out, makes the NABW much more susceptible to shorter-term climatological or environmental variations, such as the low salinity anomaly or the radioactive isotope signal from the Sellafield discharge, both of which have entered the GIN Sea as a surface inflow via the Færœse Channel and exited to the North Atlantic as an overflow via the Denmark Strait.

■ *5.3.3. Iceland-Færœ Ridge*

Of the southern openings to the North Atlantic, the Iceland-Færœ Ridge (IFR) is the widest, extending about 400 km from Iceland to the Færœs (Fig. 2.2c). It is also the shallowest, with a maximum sill depth of 480 m, but it is not so shallow as to necessarily restrict any southern movement of the deeper GIN Sea water masses. The importance of the IFR relative to the exchange of waters between the GIN Sea and the Atlantic Ocean is greatly reduced by a segment of the Arctic front, called the Iceland-Færœ Front (IFF). It is useful to think of the Iceland and Færœ Islands as lying south of the Arctic Front, and that they are surrounded by Atlantic waters rather than GIN Sea waters. The temperature and salinity distributions of Fig. 4.5 substantiate this, although the water-type variability over the north Icelandic shelf tends to blur the distinction. The significant point here is that this water-mass boundary passes through the Denmark Strait and through the Færœse Channel but parallels the IFR to the north of its crest. As a consequence, the conclusion reached by many researchers has been that there is not a continuous, unmixed flow of GIN Sea water over the Ridge to the North Atlantic.

On the south side of the IFF, the fairly homogenous NAtW is found to depths much greater than those of the IFR. On the north side, the IC transporting the eastern Icelandic Shelf Water (eIShW), Icelandic Current Water (ICW) and Icelandic Current Intermediate Water (ICIW) occupies the upper $\sim$ 500 m of the water column. The upper boundary of the uNwDW often tilts up to almost to the crest of the ridge where it is has been observed (e.g. **Steele**, 1962). In cross-section the water-mass interface is well defined by strong gradients (Fig. 5.13): the temperatures decrease monotonically from 7 °C to 0 °C, the salinities decrease from $\sim$ 35.15 ppt to a mid-front minimum of $\sim$ 34.8 ppt and then increase to $\sim$ 34.9 ppt, and the densities increase monotoniocally from $\sigma_t \sim 27.5$ to > 28.0. Two components of the ICW can be identified one being warmer and more saline than the other. This is indicative of the lateral variability in the water mass composition of the IC, and in this case the warmer/saltier component was probably derived more from the southern, IrAtW-influenced portion of the IC and the cooler/fresher component was derived more from the northern, GPW-influenced portion. **Meincke** (1978) defines these as the North Icelandic Winter Water/Arctic Intermediate Water and the East Icelandic Water, respectively. Underneath these components of the ICW (Fig. 5.13), there is a layer of ICIW which touches bottom and feeds into a mixed water mass, of NAtW and uNwDW, which then extends southward into the Atlantic capping the bottom of the IFR. The distribution of these water masses is characteristic but not necessar-

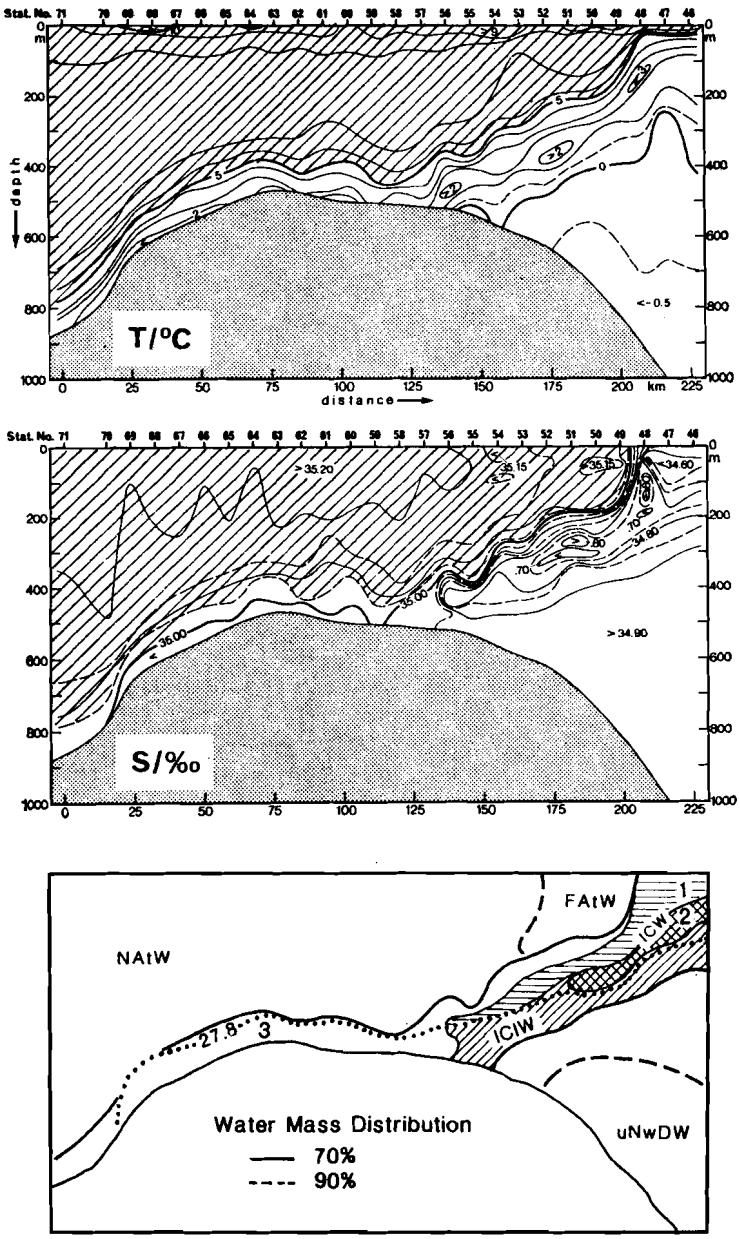

Fig. 5.13. Temperature, salinity and water mass structure from *R/V Poseidon* June 1977 transect of Iceland Færœ Ridge, (as in Fig. 5.18g). Hatched areas indicate North Atlantic Water. The dotted line in the bottom panel corresponds to the $\sigma = 27.8$ isopleth, the solid lines indicate $\sim$ 70% boundary of the water mass indicated, the dashed lines indicate $\sim$ 90%, and the numbers correspond to the following: (1) component of Icelandic Current Water containing more North Atlantic Water, (2) component containing more Greenland Polar Water and (3) mixture of Icelandic Current Intermediate Water, North Atlantic Water, and some upper Norwegian Sea Deep Water. [Adapted from **Meincke** (1978).]

ily representative in the mean (see e.g. **Lee**, 1967; **Müller**, **Meincke** and **Becker**, 1979; **Hallock**, 1985).

The surface manifestation of the IFF is highly variable in space and time. The location is often identified by the 35-ppt isohaline, as in **Hansen** and **Meincke** (1979), or by a mid-gradient isotherm, as in **Gotthardt** (1974). Fig. 5.14a shows five spring positions between 1952 and 1957 for the 35-isohaline and an envelope of the mid-gradient isotherms from five surveys between July 1971 and October 1972.

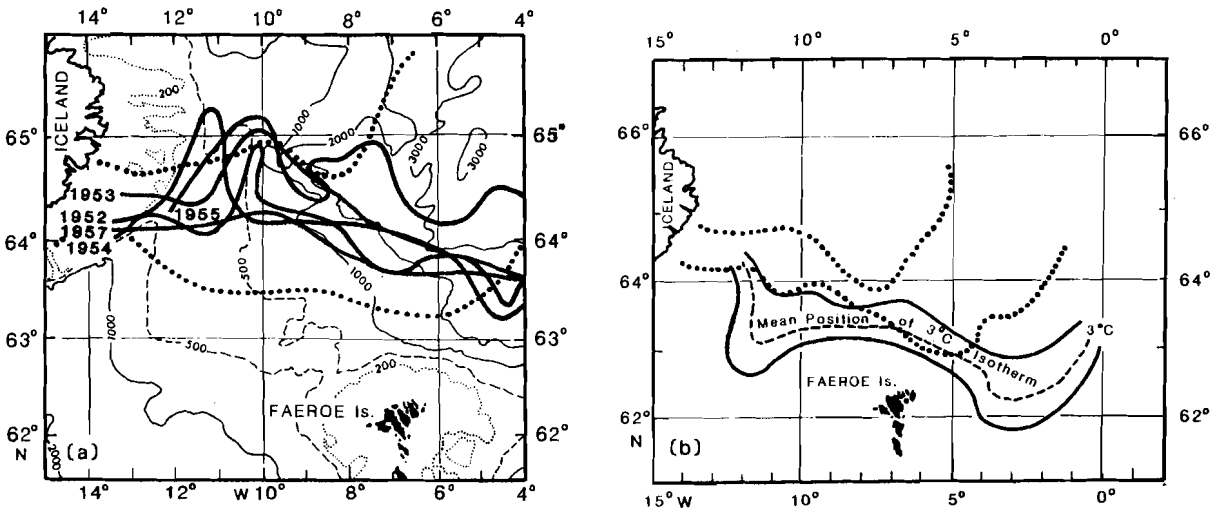

Fig. 5.14. Location of the Arctic Front over the Iceland-Færœ Ridge. (a) Solid lines mark the position of the 35-ppt isohaline at the surface (0 to 25 m) in May and June of the years indicated [from **Hansen** and **Meincke** (1979)]. The dotted lines indicate the extremes positions of the mid-gradient isoterm from 5 surveys taken between July 1971 and October 1972 [from **Gotthard** (1974)]. (b) The mid-gradient isotherm envelope for the same 5 surveys at 300 m (solid), at 100 m (dotted), and the mean position of the 3° isotherm at 300 m (dashed).

As can be seen, the definition of the IFF diminishes to the east. The 35-ppt isohaline is probably a better indicator than mid-gradient isotherms, which are more often used only because of the greater amount of temperature data available (XBTs). To the east the surface isotherms become spread apart, particularly during summer, due to surface heating and the mixing associated with large lateral excursions.

Surface mappings indicate that the lateral oscillations in the front have periodicities on the order of days rather than months. This is substantiated by moored time-series records which, according to **Willebrand** and **Meincke** (1980), have a dominant time

scale over the IFR of 10 days due to frontal baroclinic instabilities. Movement of the front perpendicular to the IFR is not equivalent to cross-frontal exchange, although severe protrusions are the most common situation in which significant exchange occurs. Erosion of the frontal boundary occurs within the surface frictional layer, resulting in a more diffuse water mass boundary. The surface waters in the frontal zone are characterized by lower vertical stabilities (**Teague** and **Von zweck**, 1982). Surface frontal mixing plays an important part in the generation of the modified Atlantic water mass, or Færœ Atlantic Water (FAtW) which, being created along the front, is advected southeastward until confluent with the NwAtWto and/or counter-clockwise around the Færœ shelf.

The IFF at greater depths has less lateral variability, as can be seen in Fig. 5.14b, which shows the extreme positions at depths of 100 m and 300 m. Because of the northward inclination of the IFF, these deeper expressions are found further south. To the east, or north of the Færœs, the IFF is also inclined to the west due to the source of NAtW entering via the Færœse Channel. Near the bottom, approximately over the (Fig. 5.14b), two important southward extensions of the frontal position are commonly found: one just east of the Iceland continental shelf break and another at the entrance to the Færœ-Shetland Channel. These extensions indicate which IFR bottom areas have a greater probability of being surface GIN-sea overflow. However, the primary mechanism for overflow is considered to be the mixing processes which occur in the frictional bottom layer and through which the uNwDW and ICIW masses leak through to the North Atlantic (Fig. 5.13).

During August and September 1973 up to 12 current meter moorings were moored on IFR mostly on the southern flank. An example of the near-bottom flow vectors is given as in Fig. 5.15b. Flow over the south flank was strong and consistent while that over the crest was more variable. A synthesis of the bottom flow over the crest is made particularly difficult by the migrating position of the front, the rugged bathymetric relief, and the associated bottom boundary-layer flow. Nevertheless, **Hansen** and **Meincke** (1979) have attempted a synthesis, by combining all available data, which yielded Fig. 5.15c,d. In this figure the flow over the north and south flanks follows the general bathymetry, to the southeast and to the northwest, respectively. On the north flank the IC appears to predominate until 600 m depth, whence a weak westward onshore flow is evident. The flow over the crest tends to be to the south over the western portion and to the north over the eastern portion. The complicated nature of the currents over the crest has also been demonstrated by the results of the year-long mooring deployed in June 1975, **Meincke** (1976) which recorded that a near-bottom flow drifting southward for the first six months and then westwards while exhibiting considerable variability at periodicities between two days and two weeks.

From observations to the south of the IFR crest **Steele** (1962) had concluded that water with temperatures 2 to 4 °C continuously crossed the IFR and that water colder than 2 °C crossed only sporadically. The incidence of some uNwDW type

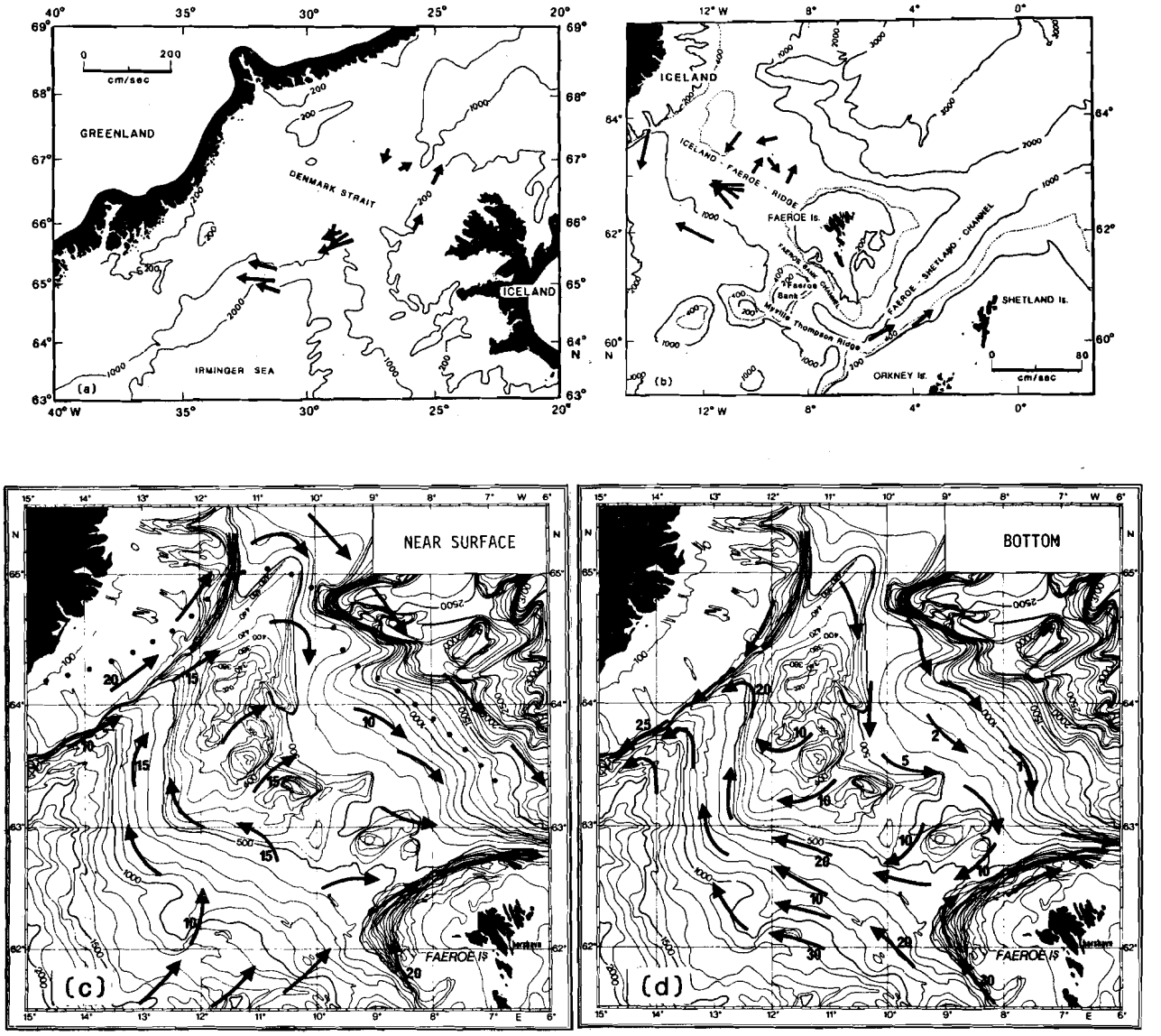

Fig. 5.15. Current vectors representing the vector average for the 25 h at 1200 h 20 August 1973 from moorings (a) in the Denmark Strait and (b) on the Iceland-Færœ Ridge. Note speed scale difference. [From **Ross** and **Meincke** (1979).] Schematic representation of the flow over the Iceland-Færœ Ridge for the (c) surface and (d) bottom layers. [From **Meincke** (1983).]

on the south flank does not necessarily imply that it crossed over the IFR since, as **Crease** (1965) documented, there is another continuous and larger source of uNwDW emanating from the Færœ Bank Channel, (also **Hermann**, 1967). In fact

Meincke (1972) found no incidence of uNwDW, or a version of ArIW, among 14 surveys of a parabathic transect at a depth of 600 m just south of the crest. He did find, however, that over the crest the maxima in flow, shear, and temperature gradient all occurred within 50 m above the bottom. Suggesting that the bottom layer may act as a conduit by which a mixed water mass is transported southward.

There is apparently considerable energy available to sustain a thick bottom-mixed layer. The crest corresponds to a nodal line of the M2 tide that generates tidal currents of 60 cm/s (**Koltermann**, 1978), and these currents provide much of the energy for the bottom-boundary-layer mixing processes. Mixing over the crest zone is also enhanced by the horizontal shear generated by the oppositely directed flows: 10 cm/s to the southeast on the north flank, and 25 cm/s to the northwest on the south flank (**Meincke**, 1978, and as shown schematically in Fig. 5.15). In fact, **Steele**'s (1961) IFR overflow estimate of 1.5–3.0 Sv was obtained by assuming a bottom layer thickness of 50–100 m and a mean diabathic speed of 13 cm/s (based on frictional arguments). This overflow appears to be an overestimate, on the basis that is too large a proportion of the source waters transported by the IC. The overestimate may have occurred because he assumed the angle between the flow and the ridge bathymetry to be 52° downslope; more recent evaluations (**Meincke**, 1972) have estimated this angle at 27°, which would reduce **Steele**'s estimate by 42%. As point of comment, all estimates for this crest based on bottom frictional arguments are likely to be subject to over-estimation: a) because they are computed to the south of the crest where the mean parabathic flow is greater than over the crest itself, and b) because they assume that the bottom-layer divergence is totally satisfied by an equivalent transport over the crest, which may not be the case since the divergence may not be satisfied locally.

More recently (**Meincke**, 1983) has estimated the overflow at 1 Sv, as shown in Fig. 5.16. Half of this occurs through a notch in the extreme western part of the IFR and the other half is distributed over various more eastern locations. The percentages of uNwDW are also indicated in Fig. 5.16; the 50% contour does not cross the IFR but is narrowest at the points where probability of overflow is highest.

■ *5.3.4. Færœse Channel*

The Færœse Channel has its narrowest horizontal constriction in the portion commonly referred to as the Færœ-Shetland Channel, and its minimum area of cross-section across the portion referred to as the Færœ Bank Channel. The projection of the transect (Fig. 2.3d) leading over the Færœ Bank Channel and the Wyville-Thompson Ridge (indicated in Fig. 5.15b) demonstrates the maximum bathymetric constriction encountered by waters passing through the Færœse Channel. If the continental shelf of the Færœ Islands were to continue south to the Færœ Bank, the bathymetry of this channel would be quite similar to that of the Denmark Strait. The existence of the Færœ Bank sill is extremely important with respect to the deep water output from the GIN Sea, but not with respect to the Færœse Channel's most important feature: its surface water input.

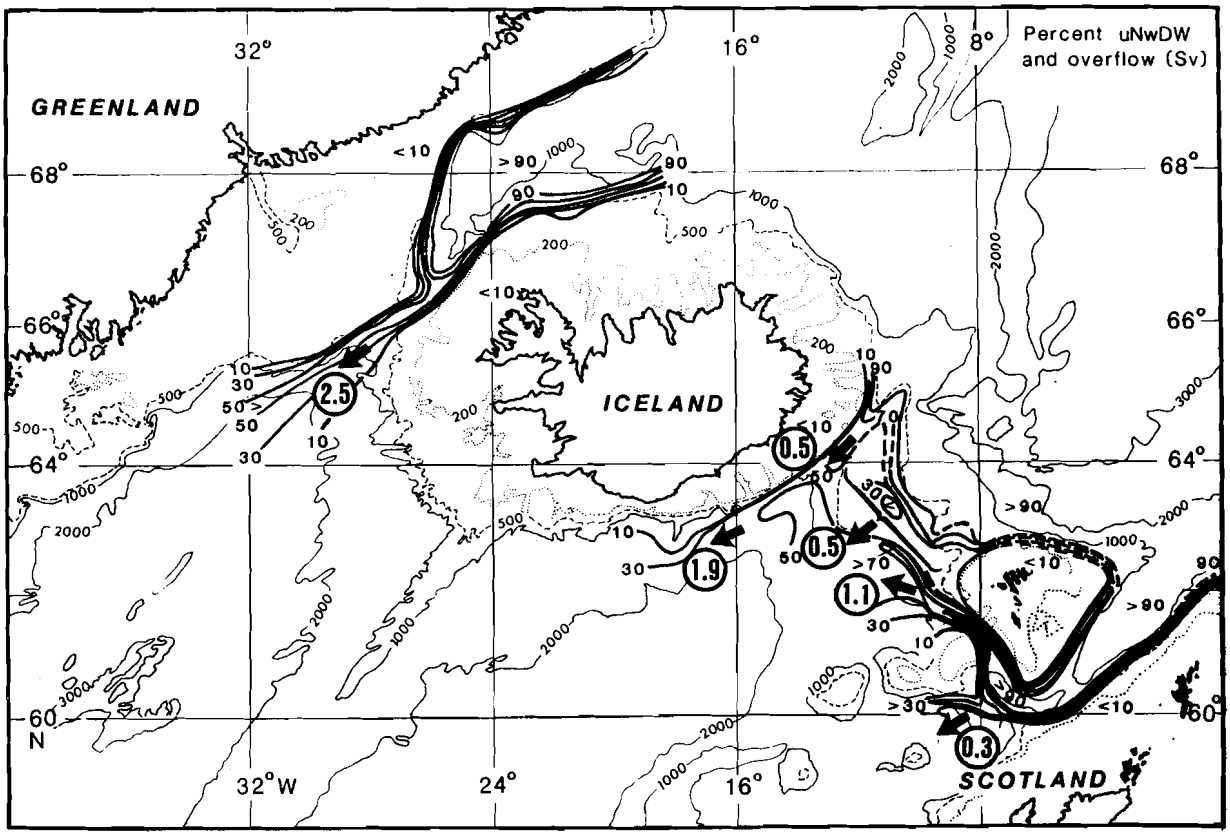

Fig. 5.16. The horizontal distribution of uNwDW. Isolines represent percentages of uNwDW found in the deep or near-bottom portion of water column. The circled numbers indicate the estimated overflow transports. [Adapted from **Meincke**, (1983).]

Whereas the Denmark Strait serves as the major southern egress of GIN Sea waters to the Atlantic, the Færœse Channel serves as the major ingress. Also while the Arctic Front, which we described as circumscribing the Iceland and Færœ Islands, is exaggerated in the Denmark Strait because of the confluence of Polar waters, it is obliterated in the Færœse Channel by the entry of Atlantic waters. **Mohn** (1887) is credited with first pointing out that the Færœse Channel is the major entrance of the warm saline Atlantic waters to the GIN Sea. The influence of these waters on the physics and biology was immediately apparent and stimmulated the obvious questions as to the amount and characteristics of this water.

The North Atlantic Current (NAtC), which has a transport estimated at 18 Sv (**Saunders**, 1982), carries warm, saline water northward along the European continental slope. The upper 1000 m of the water column consist of Eastern North Atlantic Water which varies in temperature from 5 to 12 °C, and in salinity from

35 to 35.6 ppt (**Harvey**, 1982). It contains some higher salinity admixtures from the underlying Mediterranean outflow water (**Reid**, 1979). The Wyville-Thompson Ridge with its 550 m depth sill is the first bathymetric impediment shallower than a depth of 1000 m in the northward path of the NAtC. Nonetheless, more than half of the NAtC cyclonically follows the deeper isobaths eastward as the Irminger Current, while the warmer upper layers of this water, the Wyville-Thompson Ridge separates off the warmer upper layers of this water for input to the GIN Sea and thereby limits the layer depth of the Atlantic water input. This direct input over the Wyville-Thompson Ridge has been estimated at 3 Sv by **Ellett** and **Martin** (1973).

The primary entry route of the NAtW is along the Shetland slope with a flow maximum approximately located over the 500 m isobath (Fig. 5.17), with speeds in excess of 100 cm/s (**Gould**, personal communication). The salinity and temperature maxima occur at, and to the east of, the flow maximum, indicating undiluted entry of a number of estimates of the Atlantic Water input are summarized in Table 5.6. Part of the inconsistency between these various estimates arises from the wide-ranged variability (days to years) characteristic of the inflow. **Tait**'s (1957) data perhaps provides the best evidence of the seasonal-to-interannual variability. Unfortunately, his estimates were subject to aliasing by the daily variability (time to complete a channel cross section) as noted by **Dooley** and **Meincke** (1981). This meso-scale (1–6 days) variability has amplitudes of the same order as the interannual mean and apparently is caused by both local wind forcing and the presence of quasi geostrophically-balanced eddies (of scale 30 km) that propagate with the mean flow (**Dooley**, **Martin** and **Payne**, 1976; **Dooley** and **Meincke**, 1981). Another criticism of **Tait**'s estimates, and others based on the dynamic method, is that they are subject to errors in the choice of reference level. The most apparent trend in **Tait**'s work is the seasonal one: a strong November-to-March maximum and an April-to-September minimum, with often a secondary maximum in June. However, as can be seen in Fig. 5.18, the data points are not evenly distributed throughout the year. It is primarily the lack of low values during winter that creates the trend.

The variability in summer data suggests that if there is a seasonal thermohaline signal it has an amplitude equal to or less than, that of other forcings. **Meincke** and **Kvinge** (1978) analysed the records of two near bottom current-meters, one located in the centre of the Færœ-Shetland Channel at a depth of 836 m and the other located in the centre of the north flank of the IFR at a depth of 517 m; they were investigating possible coherence with atmospheric forcing. The atmospheric energy maxima found at the period bands of 8 to 11 days 2 to 5 days were also found in oceanographic data with significant coherence. These latter data provide ample evidence of meteorological forcing other than that due to surface frictional layer response, but the specific dynamics of the mechanisms await more comprehensive observations.

The entry path shown in Fig. 5.17 is an oversimplification. The NAtC extends well westward of the British continental shelf and on encountering the Wyville-

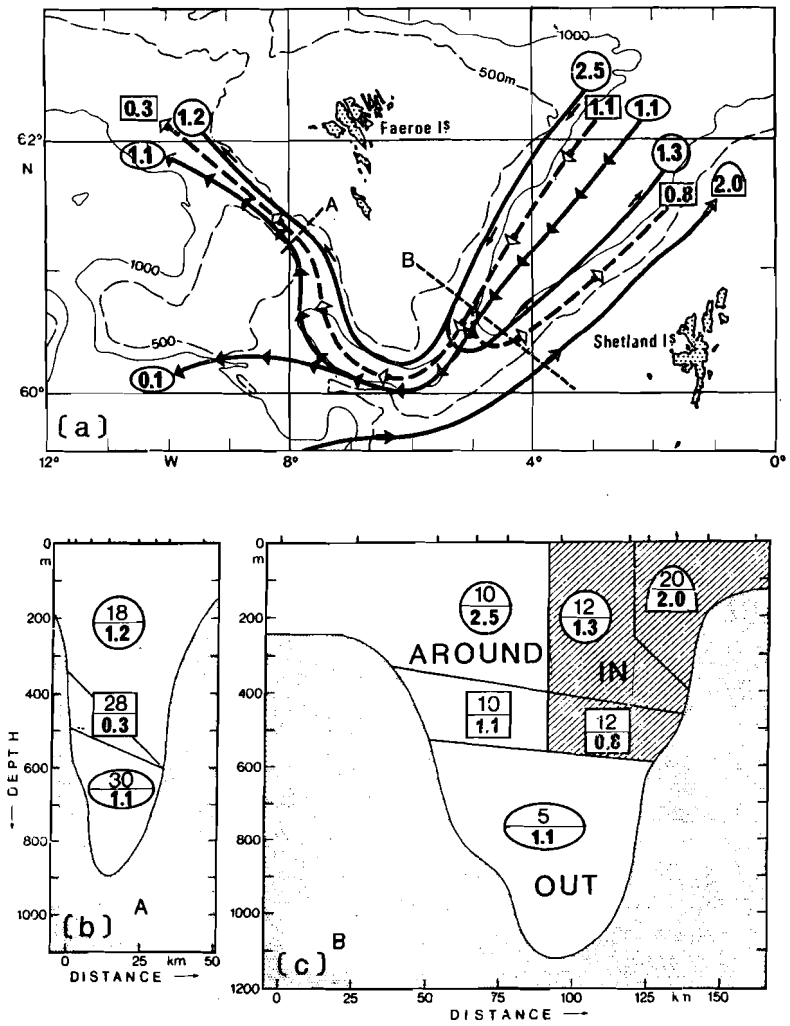

Fig. 5.17. A schematic presentation of the amounts and routes of the various water mass transports within the Færœse Channel: (a) The routes of the transports and locations of transects A and B. The figures indicate the amounts in Sv for the following water masses: Circle for Færœ Atlantic Water, square for Icelandic Current Intermediate Water an ellipse for the upper Norwegian Sea Deep Water, and semi-ellipse for the North Atlantic Water. (b) Transect A across the Færœ-Shetland Channel. In both (b) and (c) the symbols represent the same watermasses as in (a) with the upper number giving the mean speed and the lower number the transport. Both transects (b) and (c) face into the Norwegian Sea. [From **Dooley** and **Meincke** (1981).]

Table 5.6
Atlantic inflow estimates

Researcher	Transport (Sv)	Remarks
Helland-Hansen (1905)	4.0	From August 1902
Helland-Hansen and **Nansen** (1909)	4.5	From May and June 1904
Jacobsen (1943)	3.9	Average of spring and summer of many years. 800 dB reference.
Tait (1957)	2.6	Average of 69 sections from 1927 to 1952. Depth of $S = 35$ as reference.
Worthington (1970)	8.0	Based on budget calculations.
Ellett and **Martin** (1978)	3.0	Only portion crossing Wyville-Thompson Ridge.
Dooley and **Meincke** (1981)	2.0	From the 'Overflow '73' data set of hydrographic sections and current-meter observations.
	3.3	Including recirculated FAtW.

Note: Two recent works were brought to our attention at the time of final printing. Both of these provide evidence, based on current-meter observations, of considerably greater inflow of NAtW: for the transport of the entering NAtW along the Shetland shelf, **Gould**, **Loynes** and **Backhaus** (1986) estimated an annual-mean transport of $\sim$ 7.5 Sv; and for the eastward transport along the north Færœ Shelf of NAtW (at 35.2 ppt), **Hansen** (1986) estimate a $\sim$ 10-day mean transport of 2.9 Sv. The 7.5-Sv value of the former study was based on measurements only within the core of the inflow (from the 1100 to the over the 350-m isobath and therefore may be an underestimate with respect to inflow over the rest of the Færœ-Shetland section. On the otherhand, this value can not be equated to an influx of pure (35.3 ppt) NAtW since the salinities of the inflowing waters were not concurrently observed. The extensive temporal resolution of this study (9 out of 12 months) provided a clear indication of a winter maximum (January-February) of the inflow and of a 4-day peak in the spectrum of the transport.

Thompson Ridge/Færœ Bank the bathymetry turns westward, inundating the entire area including the IFR. Secondary circulations around the Færœ Plateau and the Færœ Bank introduce a slightly modified NAtW, the FAtW, into the GIN Sea. The most important of these is the anticyclonic flow, around the northern coast of the Færœ Islands and south of the IFF, which brings NAtW from IFR containing admixtures of ICW and the less saline waters from the Færœ Shelf. **Dooley** and **Meincke** (1981) estimated that 50% of this FAtW is thus recirculated in the Færœ-Shetland Channel (Fig. 5.17).

Hansen (1979) has added to the description of the circulation in the Færœse Channel, by suggesting the existence of another recirculation cell within the Færœ-Bank Channel, of NAtW which enters on the southern side and then recirculates back out to the northwest. However, there does not yet exist any direct evidence for this recirculation (**Dooley**, personal communication). Significantly, the existence of such a recirculation, would imply less export (loss) of FAtW, or rather a smaller amount of FAtW flowing around the southeastern position of the Færœ Plateau than as has been suggested by **Tait** (1957); **Müller**, **Meincke** and **Becker** (1979); **Dooley** and **Meincke** (1981) and thus a greater net influx of NAtW to the GIN Sea. The separation between the two recirculations might be bathymetrically controlled by the southeastward extension of the Færœ shelf from Sydero Island (Sydero ridge), and the existence of such a discontinuity is substantiated by gradients in temperature and salinity coincident with this ridge (**Hansen**, 1978).

The eastward disposition of the ICIW component of the IC is not well described. Its presence in the Færœ-Shetland Channel is reflected in a salinity minimum ($<$ 34.9 ppt) and it has been observed in various amounts below the incoming NAtW even in some instances displacing the entire deep layer (**Tait**, 1957). More commonly it is found as a mid-depth (300 m) band $\sim$ 100 m thick across the Channel but skewed to the Færœ side (**Meincke**, 1978). The volume appears to depend on the supply from the IC, that is, as inferred by its relative disappearance in Meincke's clockwise sequence of sections around the Færœ Islands. We note that the distributions in Fig. 5.19 are labelled as simply ICW instead of ICIW, because the water type that **Meincke** used to compute the percentage concentration was less dense than an intermediate water-type (i.e. $\sigma_t = 27.73$ instead of $\sigma_t = 27.75$). Therefore, the reader may interpret Fig. 5.19 as illustrating the percentage composition of the ICW, most of which is in fact ICIW. Clearly, the major loss occurs between the Færœ-Shetland and the Færœ Bank Channels (between e and f), with some occuring in the Færœ-Shetland Channel itself (between d and e). **Dooley** and **Meincke** (1981) suggested a similar, but much smaller, attenuation in the amount of ICIW found between the Færœ-Shetland and the Færœ Bank Channel (i.e. Fig. 5.17). Most of the attenuation appears to occur in flowing around the Sydero Bank, judging for example from the **Helland-Hansen** sections (**Müller**, **Meincke** and **Becker**, 1979), in which the ICIW lost 70% of its volume between sections that straddle this ridge 40 km apart. As an alternative to flowing around this ridge, the ICIW might exit via the Wyville-Thompson Ridge, but there has been little observational evidence of this occurring in significant amounts (**Müller** and **Meincke**, 1978; **Müller**, **Meincke** and **Becker**, 1979). The general conclusion is that unlike the Denmark Strait the Færœse Channel exports only small amounts of an IW to the Atlantic. Figure 5.16 indicates an additional outflow over the Wyville-Thompson Ridge at 0.3 Sv, in accordance with the findings of other researchers who have reported such a transport, although with an intermittent nature (e.g. **Ellett** and **Roberts**, 1973; **Ellett** and **Edwards**, 1978).

It was early recognized that a DW was exported to the Atlantic in significant amounts to affect the composition of the NAtBW. Clearly, the depth of the Færœ

Bank Channel at 800 m makes it about 200 m deeper than any other access to the North Atlantic and allows it to serve as a primary egress of the uNwDW. Most historical discussions of the Norwegian Sea outflow refer to the Norwegian Sea Deep Water without distinguishing between the uNwDW and the NwDW. **Swift** (1984) however recently made such a distinction, pointing out that the warmer version is found at depths $\geq$ 900 m and that therefore the GIN Sea export to the Atlantic is not a thermohaline end member, the pure NwDW, but a shallower, mixed version of it. **Crease** (1965) reported the results of short-term current measurements over the sill which indicated maximum speeds out of up to 100 cm/s and a transport of 0.8 Sv of uNwDW. By augmenting the same historical data that **Tait** (1957) used with newer data on other sections, **Martin** (1961) estimated the transport of the uNwDW to be 0.67 Sv for 62 sections. He noted that the deep transport was little affected by the amount of ICIW present and that there was a slight trend toward lower values in winter (Fig. 5.18). By combining hydrography and current observations, **Dooley** and **Meincke** (1981) estimated a continuous and unattenuated flow of uNwDW through the Færœse Channel at 1.1 Sv (Fig. 5.17b).

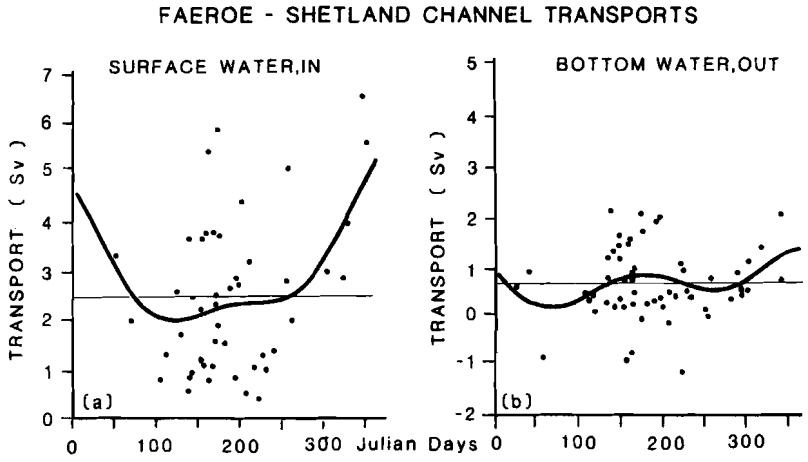

Fig. 5.18. Individual transport estimates from hydrographic transects of the Færœ-Shetland Channel: (a) North Atlantic water inflow data from 1927 to 1958 as calculated by **Tait** (1957) and **Tait** and **Martin** (1961); (b) deep and intermediate water outflow, data from 1927 to 1964 as calculated by **Martin** (1966). In both (a) and (b) the solid line represents a 8th-order polynomial fit and the ligth line the means of 2.6 and 0.75 Sv, respectively.

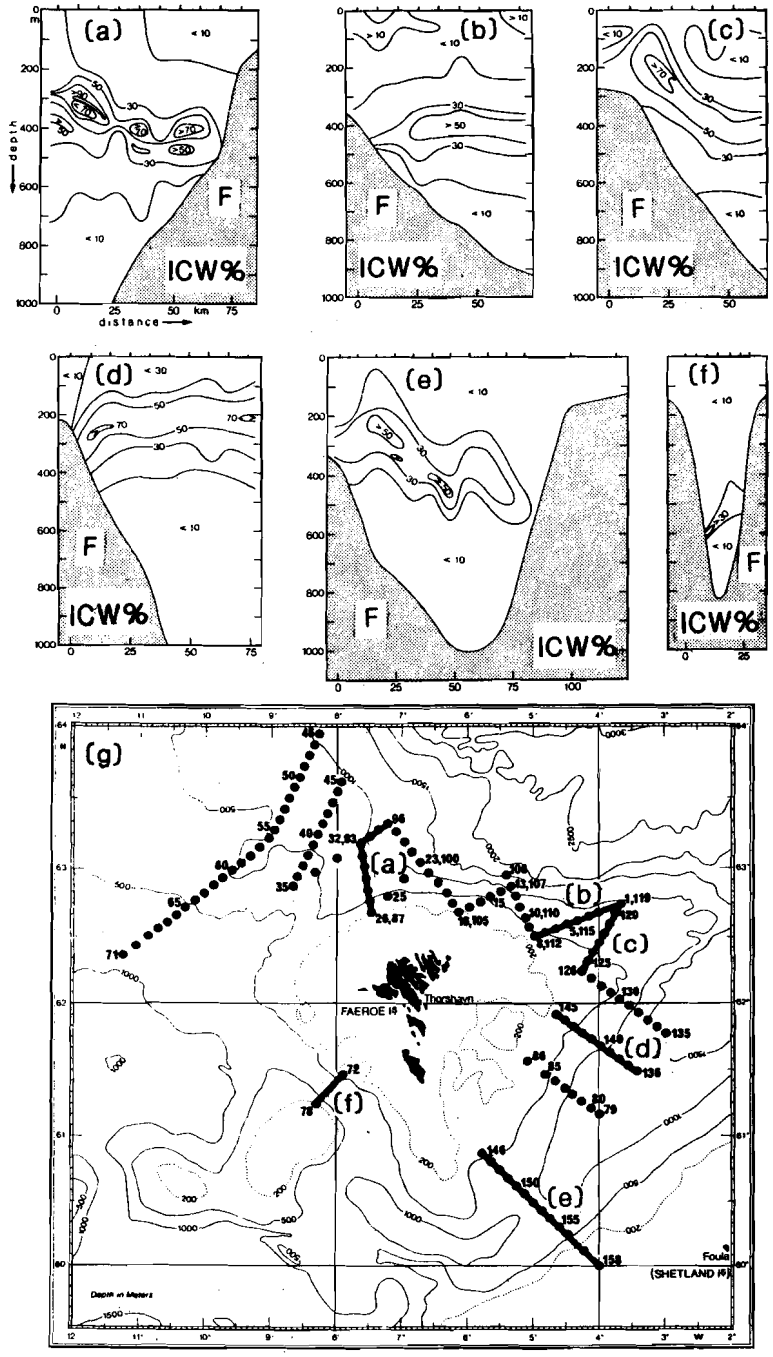

Fig. 5.19a–f Contours of percent concentration of Icelandic Current Water (taken in this case to be $T = 3°$, $S = 34.78$) in a sequence of transects taken by the *R/V Poseidon*, 24 June to 4 July 1977, as labeled in the lower panel g). The letter F designates the Færœ Island side of the transect. [From **Meincke**, (1978).]

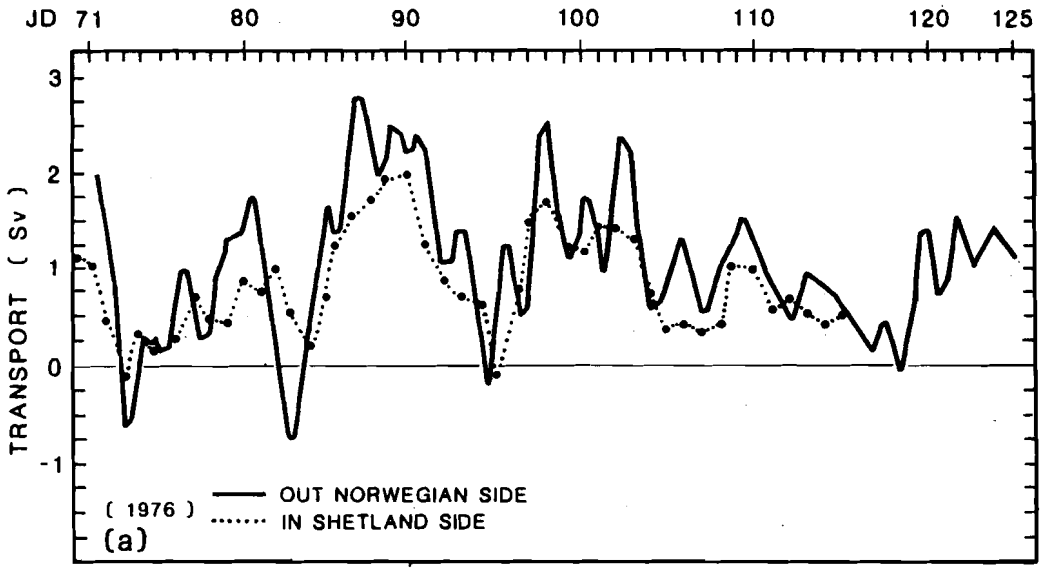

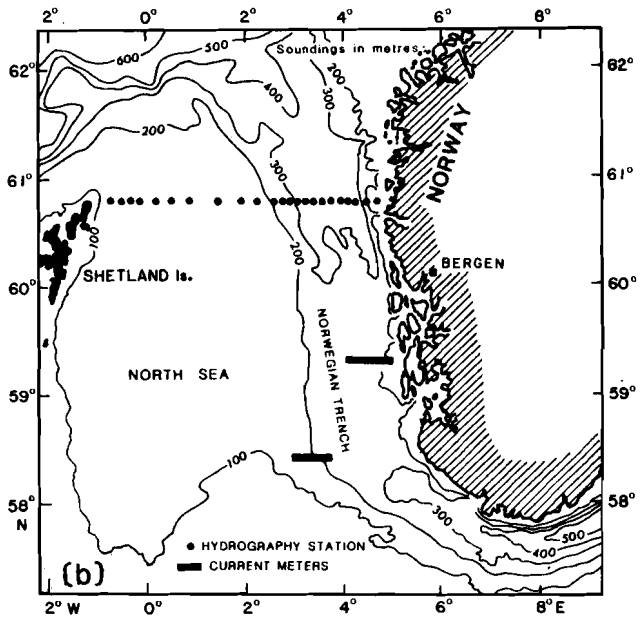

Fig. 5.20. (a) The in and out transports along the western and eastern sides, respectively of the Norwegian Trench. Measurements were from moorings deployed during the spring of 1976 at the locations indicated in Fig. 5.19b. [From **Riepma** (1978)]. (b) The bathymetry of the North Sea Entrance the moorings of Fig. 5.20a, and the hydrographic stations of Fig. 5.21.

■ *5.3.5. North Sea Opening*

The opening to the North Sea is the smallest of the GIN Sea openings (Fig. 2.3). It is largely occupied by a continental shelf depression called the Norwegian Trench, the deeper portions of which closely follow the Norwegian coast into the Skagerrak.

The 300 m-depth contour extends southward to approximately Bergen (Fig. 5.20b), and then about 200 km further south resumes its definition of the deep portion of the Skagerrak (depth > 700 m). The sill depth is 205 m, located at about 58°50'N. Historically the entrance to the North Sea has always been taken north of the sill in the vicinity of Bergen.

Thus the Norwegian Trench forms a break in the Schotland-Norwegian continental slope. As a result the upper 300 m of the NwAtC water column is not bathymetrically constrained to continue northeastwards from the Shetlands, but is free to enter the North Sea via the Norwegian Trench. However the North Sea is not a flow-through system with respect to the NwAtW. The relatively higher steric sea levels attributed to the lower salinity water resident in the North and Baltic Seas, barotropically blocks the entrance of the NwAtC and impedes any significant portion from existing via the English Channel. The portion of the NwAtW that does enter the North Sea entrance either recirculates northwards out of the Norwegian Trench to merge again with the NwAtC or is mixed into the North Sea. Both of these processes, recirculation and mixing, depend on large-scale inter-basin pressure fields, local wind stress, and local runoff, and therefore are difficult to quantify. **Furnes**, **Hackett**, and **Saetre** (1986) have concluded that the recirculation of the inflowing NwAtW is in the vicinity of the sill and is not in the Skagerrak as previously thought. They argue that the shoaling of the sill and bottom frictional transport (to the east) both divert the inflow across the Trench, and that survival of the inflow past the sill only occurs intermittently. Observations along the western side of the Trench have shown the inflow to be decreasing to the south, suggesting eastward recirculation across the Trench (**Hackett**, **Furnes** and **Saetre**, 1984); in addition a comparison with contemporaneous data from the NwAtC suggests that the entering stream undergoes decreases in temperature (T) and salinity (S), implying mixing losses (**Hackett**, **Furnes** and **Saetre**, 1984; **Clarke**, **Reid** and **Swift**, 1984).

A comprehensive current measurement program referred to as INOUT phase of JONSDAP'76 was undertaken to quantify the residual water movements of the North Sea. In Fig. 5.20 we compare the outflow from the Norwegian side of the trench as determined by **Furnes** and **Saelen** (1977) and the inflow from the western side as determined by **Riepma** (1978). The outflow is slightly larger, and the two are clearly in phase, again suggesting a strong recirculation. The comparison was not complete because the inflow was observed 100 km to the south of the outflow, and because the transport over the more western portions of the Scottish shelf were not included. **Riepma** (1978) to attempt to estimate a total inflow from other JONSDAP'76 moorings and concluded that the outflow was greater by about 0.4 Sv.

The width and meso-scale variability of the Scottish shelf make the inflow a difficult transport to measure. The variability is demonstrated by Fig. 5.20a. In general, winds from the north and northeast enhance the inflow while those from the south and southwest enhance the outflow (cf. **Furnes**, 1980). However, the lack of strong specific correlations between the time series of winds and those currents or of sea

levels is not conducive to the construction of a simple wind-forced model of the North Sea circulation.. As an example of this lack, **Koltermann** (1981) found a significant coherence between wind and current only at a periodicity of 7 days. He also found considerable energy evident at 10, 5, and 2.5-day periods, none of which could be correlated with meteorological forcing but was probably due to a natural response in the form of topographical Rossby waves.

On the basis of salt conservation one might argue that the inflow/outflow balance is more even than shown in Fig. 5.20a, i.e. perhaps smaller than the difference of 0.4 Sv computed by **Riepma**. From Fig. 5.21 we can estimate the input salinity as 35.3 ppt and the output salinity as 34.2 ppt. Even though these may be slightly in error, especially the output, their ratio is close to unity (~ 0.97) and the conservation of salt would require the ratio of the inflow/outflow transports to be the same. For example if the Baltic net outflow is 0.02 Sv, the remainder of the North Sea water balance runoff is 0.01 Sv, and the outflow is 1 Sv, then the inflow is 0.97 Sv.

The North Sea outflow includes the Norwegian Coastal Current (NwCoC), which has significantly modified water properties from those of the NwAtW, Fig. 5.21. The NwShW spreads in a wedge-shape from the Norwegian coast and as described in Subsect. 4.1.5, is shallower in summer than winter. This fresher outflow has its origin in the Baltic Sea, and so is considerably removed in a thermohaline sense from the NwAtW inflow. In addition to the NwCoC, the outflow consists of approximately the eastern half of the lower layer, which is basically the recirculated portion of the inflow. The ratio of the area of the lower portion to that of the upper portion is about 2 : 1, but corresponding the speed ratio is about 1 : 2, making the transports of the two components about equal. Thus about half of the entering NwAtW is recirculated to the NwAtC and the other half mixes into the North Sea and exits eventually via the NwCoC.

Averaged hydrography data for the Bergen-Shetland section (60°45′ N) are compared for January and July in Fig. 5.21. The inflow is quite seasonally consistent in water type at 8 °C and 35.3 ppt, which is expected since it is directly derived from NwAtW. Its presence is best seen in the July distribution as the dip in the 8.5 °C isotherm and the 35.3-ppt isohaline over the western trench slope. Indications of this water can be found further to the west over the Scottish shelf, presumably having entered the North Sea via the accesses between Scotland and the Shetland, e.g. as evidenced by the 35.3-ppt isohaline in the July section. The waters over this part of the shelf thus have a similar water type to that of the NwAtW, but are modified by local runoff and winter convective mixing, resulting in a winter, shelf-water type (**Hackett**, 1981) which we call the northern North Sea Water (nNSW). The nNSW is slightly more dense ($\sigma_t = 27.6$) than the entering NwAtW ($\sigma_t = 27.5$); it tends to move eastward into the Norwegian Trench and thence return northward to the GIN Sea. The production of nNSW is represented by the vertically homogeneous structure of January (Fig. 5.21) and the summer residual is well indicated by the $\sigma_t = 27.5$ isopleth. Seasonal variability in the nNSW type occurs because these shelf

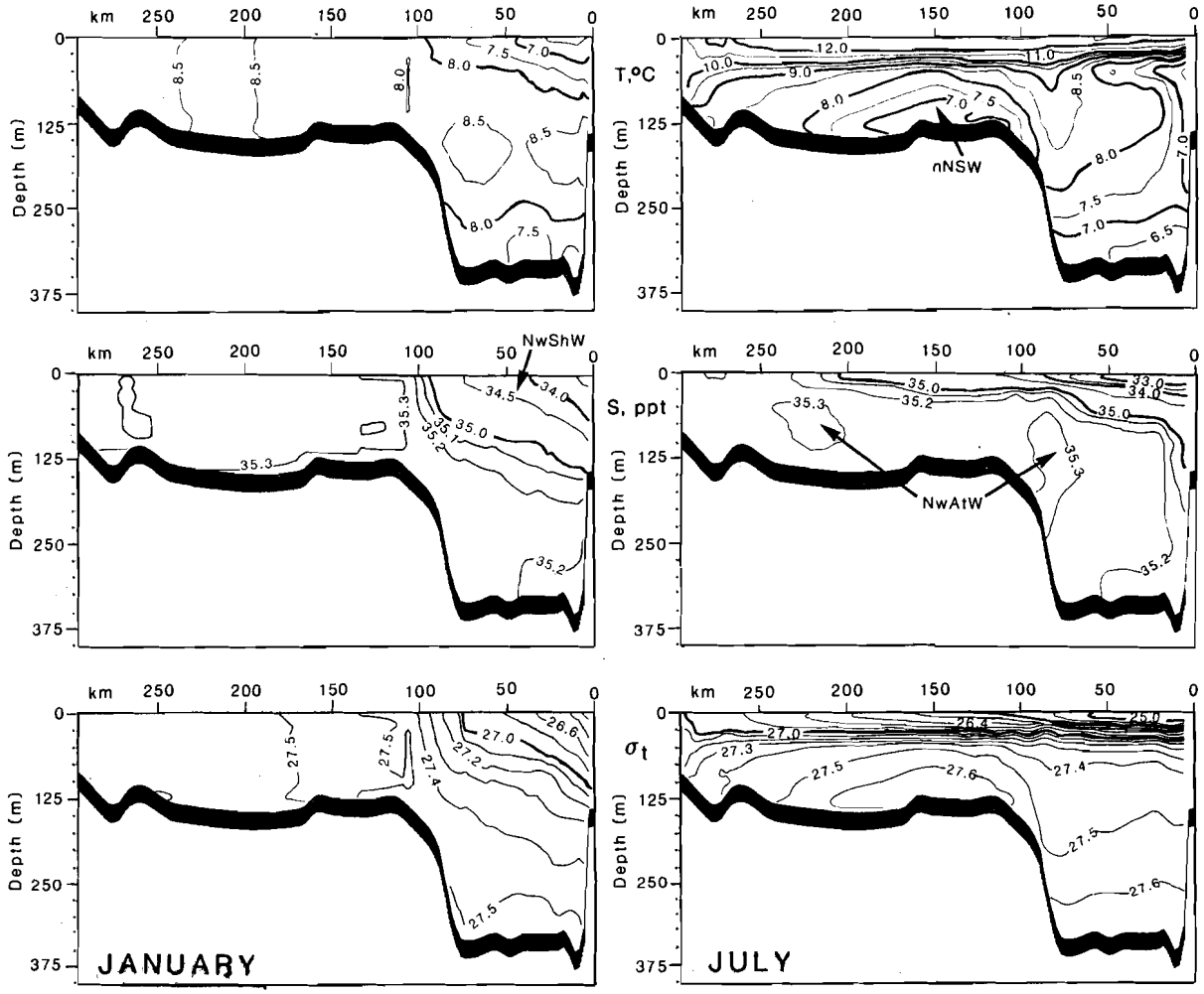

Fig. 5.21. Contours of averaged T, S and σ_t for the months of January (left panel) and July (right panel) of the Shetland-Bergen transect (Fig. 5.20b). [From **Hackett** (1981).]

waters are mostly wind-driven without an appreciable net transport, and therefore have a longer local residence time. Even in the case of the secondary entry route of NwAtW much of its volume is diverted eastward along the 100 m depth contour east of Aberdeen (**Riepma**, 1980), where it it tends to form a partial recirculation gyre over the northern North Sea shelf.

■ *5.3.6. Barents Sea Opening*

Like the North Sea, the Barents Sea is a semi-enclosed continental shelf sea, and it has openings other than those to the GIN Sea: the Spitsbergen-Franz Josef Land and the Franz Josef Land-Novaya Zemlya passages both leading to the Polar Sea. The

boundary between the Barents and GIN Seas is normally taken along the narrowest constriction, from Spitsbergen to Bear Island to Norway. Defined according to the contour of maximum-depth restriction, the boundary would lead around the Bjornoya Trough. The cross-sectional areas of these two boundaries are shown in Fig. 2.3. Although generally shallower and wider, the Barents Sea opening is roughly equivalent in area to each of the three openings to the Atlantic, but in shape it is more or less similar to the smaller North-Sea opening. For example, the Bjornoya Trough is analogous, although slightly larger, to the Norwegian Trench. A less extensive trough also leads through the South Cape-Bear Island section and extends east, but only to the 100-m deep ridge running between Bear Island and Hopen Island, Spitsbergen. This bathymetry imposes a certain symmetry on the exchange between the GIN Sea and the Arctic Ocean through the Barents Sea: primarily, an outflow from the GIN Sea north of Norway and an inflow south of Spitsbergen; and secondarily, an outflow north of, and an inflow south of, Bear Island.

Again like the North Sea, the Barents Sea is considerably freshened relative to the NwAtW, by the direct addition of runoff and by the influx of the less saline Polar Water (instead of Baltic outflow), leading to lesser densities and higher steric sea levels over the Barents shelf. The local effect of this is a tendency for recirculation around the bathymetry of the Bjornoya Trough. However, the continuous land coastline of Norway, unlike the Shetland-Orkney-Scotland island boundary entering the North Sea, is capable of sustaining a coastal, sea-level high pressure that continues to drive a coastal flow eastward. This sea level high pressure is augmented by local runoff in the summer season. Along the northern coast of Norway this flow is called the North Cape Current; as it continues further east and eventually northward along the coast of Novaya Zemlya it is called the Murman Current. The portion of the NwAtC that enters the Barents Sea via the North Cape Current either continues at 30°E with the Murman Current or else recirculates back to the west along the north side of the Bjornoya Trough. The North Cape Current must be considered as a continuation of the coalescence of the NwAtC and the NwCoC, which at the point of entry to the Barents Sea are no longer clearly distinguishable on the basis of water mass.

There is also a tendency for recirculation through the South Cape-Bear Island section, with the NwAtW entering north of Bear Island via the South Spitsbergen Current and the BrPW of the ESC exiting around South Cape. We summarize the main flows through the Barents Sea Opening from south to north as: the North Cape Current eastward along the north coast of Norway; the Bjornoya Trough Current westward along the northern slope of the Bjornoya Trough, the South Spitsbergen Current eastward north of Bear Island, and the East Spitsbergen Current westward south of South Cape.

The transports of water, heat, and salt through the Barents Sea are relevant to both the Polar and GIN Sea budgets. A considerable number of hydrographic sections of the Barents Sea Opening exist (e.g. **Adrov**, 1959; **Uralov**, 1959; **Dickson, Midttun**

and **Mukhin**, 1970) and there are some current measurements (e.g. **Agenorov**, 1946). However consensus on the transport values is rather poor. **Adrov** (1957, 1959) noted the wind-induced variability, with winds from the west and southerly quadrants assisting inflow and winds from the north and easterly quadrants impeding inflow and inducing upwelling in the Bjornoya Trough. This is somewhat supported by **Timofeyev**'s (1963) observation of a slight seasonal maximum in the outflow (eastward) during fall when southwesterly winds prevail. He estimated monthly averages of the transport through the South Cape-Bear Island section and the North Cape-Bear Island section from 45 and 131 hydrographic samplings respectively; the readings were taken between the years 1930 and 1961. For both sections he calculated (dynamic method) the individual inflows and outflows. In Fig. 5.22, we have plotted the outflow for both sections, with a net outflow: $\sim$ 1.64 Sv exiting via the southern section, and $\sim$ 0.27 Sv exiting via the northern section. He computed total inflow of 0.94 Sv making the net outflow of 0.97 Sv.

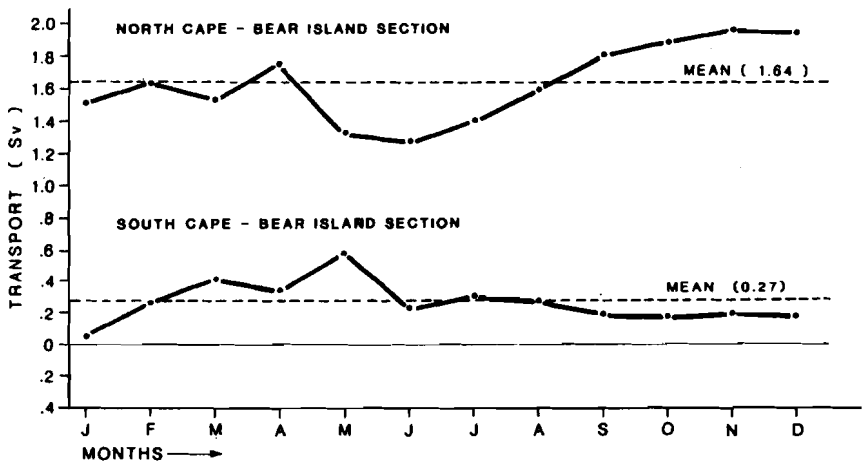

Fig. 5.22. Transport rates (outflow from GIN Sea) calculated by the dynamic method for the Barents Sea Opening, divided into two sections: the North Cape-to-Bear Island section (upper panel) and south Cape-to-Bear Island section (lower panel). [Data from **Timofeyev** (1963).]

Another analysis of just the southern section, by **Kudlo** (1967), gave 0.5 Sv net outflow (3.6 Sv out via the North Cape current and 3.1 Sv returning via the Bjornoya Trough Current). **Fletcher** (1965) used a net outflow of 0.9 Sv through the Barents Sea to the Polar Sea; and **Aagaard** and **Greisman** (1975) used a net value of 0.6 Sv for the outflow from the Barents Sea to the Polar Sea.

The distribution of the dynamic anomaly, which was shown in Fig. 4.11c, illustrates the structure of the internal field of mass in the Barents Sea Opening during September of 1966. A 200-m depth reference level for these calculations eliminated some values south of Spitsbergen, but evidence of high anomalies near Bear Island and South Cape are apparent, both favoring the general type of circulation described above. The strong gradient field of the North Cape Current is clearly shown; and the recirculation about the Bjornoya Trough is not strongly indicated but is nevertheless not excluded due to the uncertainty of the reference level. The isopleths of T and S (Fig. 4.11a,b) certainly demonstrate the presence of NwAtW in the Bjornoya Trough.

5.4. THERMOHALINE ASPECTS

For reasons of historical convention, thermohaline circulations are described as either positive or negative depending on whether or not the prevailing vertical motion is up or down, respectively. The implication is that the surface boundary condition is such as to either add or subtract buoyancy to the surface waters. An addition causes a surface high pressure with flow away at the surface and a compensatory return flow in and up underneath. An extraction causes a surface low pressure with flow in at the surface and a compensatory flow down and out underneath. A criterion for the type of thermohaline circulation for a body of water is whether or not the internal density is less or greater than the density found externally at the same depth resulting in a positive or negative circulation respectively (**Hopkins**, 1978).

The GIN Sea is a large semi-enclosed ocean basin having, in general, a negative themohaline circulation. The density contrast is much greater with the Atlantic Ocean than with the Polar Sea, because with the Polar Sea there is only a contrast between the surface layer densities of approximately one sigma-t unit; whereas with the Atlantic Ocean the contrast remains throughout the water column being more than one sigma-t unit at the surface and about a half a unit at depth. Consequently the exchange with the Atlantic is more characteristic of that of a negative circulation basin, i.e. in at the surface and out over the sill, than the exchange with the Polar Sea (cf. Subsect. 4.3).

The surface boundary condition causing the buoyancy flux can be either thermal (heat loss or gain) or haline (water added or subtracted) or both. For the GIN Sea the surface waters are made more dense primarily by loss of heat to the atmosphere, whereas for the Polar Sea the surface waters are made less dense by melting and runoff, the potential for heat lost being inhibited by the ice cover.

The gross characteristics of thermohaline circulations can be deduced by making the assumption of a steady state balance for the quantities of water, salt, and heat exchanged between local and adjoining waters (cf. **Defant** 1961). This is usually done

over an annual period in order to average over the much larger seasonal periodicity. Consequently, this assumption is not at all restrictive with respect to water volume but may be in error with respect to the balances of salt and heat in the presence of significant interannual trends in temperature and salinity. All three balances also involve exchanges with the atmosphere, which in the case of heat are particularly difficult to measure at the level of accuracy needed.

The exchanges of salt and heat that actually occur between basins are taken to be the product of the transport and a mean value of the quantity, whereas in fact, they should be considered as fluxes (a time-areal average of the product of the flow and its concentration). Significant differences between these two methods exist when the variations in water transport and the quantity are not in phase, e.g. the net flux is greatest if the variabilities are in phase. Even in the case of the simpler method, errors are introduced in the estimation of transports, which are rarely observed for an annual period nor over the entire cross section required, and in the estimation of the mean concentration of the quantity, which may not be representative for similar reasons.

The surface exchanges of heat constitute a greater portion of the heat budget than do the respective surface exchanges of the water and salt budgets. The surface heat exchange terms (Subsect. 3.2) are difficult to measure accurately particularly under the hostile environmental conditions of the GIN and Polar Seas. Consequently in the budgets presented below, we force agreement only for the balances of water and salt, except for the deep-water components for which heat is also balanced. We note also that the equations resulting from the balances intersect only when any one has an independent source of volume, salt, or heat. In general, the dilution volume (precipitation + runoff − evaporation) is small for the GIN Sea meaning that the equations for volume and salt balances are nearly parallel.

Observational information exists for all of the GIN Sea openings, as discussed in Subsect. 5.3. If we select transport estimates from each of these, we see immediately that there is an imbalance of $\sim$ 5 Sv exiting the Sea (Table 5.7).

■ *5.4.1. Arctic ocean balance*

In order to quantify the thermohaline circulation of the GIN Sea, we construct a sequence of water and salt balances to calculate the water and salt transports of the major water masses through the various openings and vertical interfaces. These results permit an estimate of the heat loss through the surface. The reader is cautioned to consider the results as an illustrative example.

First, we compute a water/salt balance for the entire Arctic Ocean, that is, as required to determine the exchanges between the Arctic Ocean and the Atlantic and Pacific Oceans. The transport through the English Channel can be ignored (between 0.06 and 0.24 Sv), **Otto** (1983), or considered as part of the NAtW transport. The

Table 5.7

Selected transport estimates (Sv) from the data reviewed in the text

Opening	In	Out
Fram Strait		
EGC	7.1	–
WSC	–	5.6
Denmark Strait		
EGC	–	2.8
overflow	–	2.9
NIrC	0.6	–
Iceland Færœ Ridge		
FAtW	1.3	–
overflow	–	1.0
Færœse Channel		
NwAtC	2.0	–
overflow	–	1.4
North Sea Entrance		
NwAtC	1.00	–
NwAtC/NwCoC	–	0.97
Barents Sea Opening		
BrAtW	–	1.9
BrPW	0.9	–
Total	11.9	16.8

values from the Canadian Archipelago and the Bering Strait have been taken from **Aagaard** and **Greisman** (1975).

Since the observed transports in and out of the GIN Sea (Table 5.7) do not balance and since we can not treat all transports as unknowns in a budget calculation, we are obliged to accept certain of the transport observations as valid in order to proceed with the calculation of the other (unknown) transports. The main problem consists of chosing between the primary inflow, that of the NAtW, and the primary outflows,

those of the WSC and the overflow to the North Atlantic. The fact that both of these outflows are independently incompatible with the observed value of the NAtW inflow (too small) has led us to select the inflow of the NAtW as one of the unknowns. For the other unknown we choose the GPW outflow as it has been the least well observed.

The various components are given in Table 5.8 including the calculated values of the AtW inflow and the GPW outflow at 8.35 and 3.49 Sv, respectively. The AtW inflow we have divied into 3 Sv of FAtW entering north of the Færœs and 5.35 entering through the Færœ Shetland Channel. In order to appreciate the sensitivity of the solution to possible errors in the other values, we have prepared Table 5.9, which essentially shows that the computed inflow (NwAtW and FAtW) remains large $\sim$ 6 Sv even when large observational errors are assumed in the other estimates. Only some drastic combination as given under item d reduces the inflow to the levels observed historically.

■ *5.4.2. Polar sea balance*

In order to segregate the GIN Sea from the rest of the Arctic Ocean, it is necessary to perform a similar balance of the Polar Sea (Table 5.10). The unknown transports were chosen to be the upper two components of the EGC (referred to as GPW and rAtIW within the GIN Sea and as PW and PAtIW within Polar sea), since the WSC outflow has been several times estimated. The deep water transports through Fram Strait were estimated independently based on the following reasoning.

(1) We assume that the EADW is composed of a mixture of CDW, NwDW, and GDW with the temperature and salinity values, respectively, of ($T = -0.7$, $S = 34.93$), ($T = -0.4, S = 34.95$), ($T = -1.0, S = 34.91$) and ($T = -1.3, S = 34.89$). This suggests a percentage composition of the EADW of 56% CDW, 33% NwDW, and 11% GDW.

(2) We assume that 1 Sv of GDW is produced annually (**Carmack**, 1972) and that some portion of this enters the Polar Sea through Fram Strait.

(3) On the basis of water type, we consider that NwDW is produced approximately as a 1 : 1 mixture of GDW:EADW (Fig. 5.23a).

(4) It is clear that some NwDW must move south to renew the waters of the deep Norwegian Basin, since the chemical properties of the NwDW do not indicate excessively longer residence times than in the Greenland Basin. Since no pure NwDW exits to the Atlantic, this southward moving component must upwell and mix with an AtIW type to form the uNwDW which does exit.

(5) A reasonable solution to the above conditions is given by the flow components in Fig. 5.23b. The amount of CDW (or water-mass equivalent) is equal to the southward moving NwDW and represents the net DW flow through Fram

Table 5.8
The various exchange terms for water, salt, and heat budgets of the Arctic Ocean

	Transport[1] (sv)	S (ppt)	Salt[2]	T (°C)	Heat[2]
Denmark Strait					
GPW	−3.49	33.8	−117.97	−1.0	3.14
ice	−0.06	3.0	−0.18	−5.0	5.09
lArIW	−1.6	34.85	−55.76	0.5	−0.96
rAtIW	−0.8	34.93	−27.94	1.0	−0.88
uNwDW	−0.5	34.92	−17.46	−0.5	0.12
IrAtW	0.6	35.1	21.06	6.0	3.66
Iceland-Færœ Ridge					
ICIW	−0.4	34.85	−13.94	2.0	−0.84
uCwDW	−0.3	34.92	−10.48	−0.5	0.12
FAtW	3.0	35.3	105.90	8.0	24.30
Færœse Channel					
ICIW	−0.2	34.85	−6.97	2.0	−0.42
uNwDW	−1.2	34.92	−41.90	−0.5	0.48
NwAtW	5.35	35.3	188.86	8.0	43.34
Canadian Archipelago					
out	−2.1	34.2	−71.82	−0.7	1.26
Bering Strait					
in	1.5	32.4	48.60	0.5	0.90
ice	–	–	–	–	−0.4
Total	0.0	–	0.0	–	78.91
dilution	0.20	–	–	–	–

[1] Calculated transport values given with two significant figures.
[2] Salt and Heat are given as their respective products.

Strait. This has the further implication that the ratio DW flushing times of the Norwegian and Eurasian Basins would be equal to the ratio of their respective DW volumes, or 1 : 2.5. We note that under the above conditions smaller assumed values for the net DW flow (1 Sv) would result in lesser salinity values for the EADW (34.93 ppt).

(6) An additional downwelling of an ArIW is required to balance the deep water

budget as shown in Fig. 5.23. This forms also an uNwDW product which could contribute to the North Atlantic overflow but not to the flushing of the NwDW.

Table 5.9

The NAtW Inflow and the GPW Outflow for variations in the solution to the water and salt budgets of the Arctic Ocean

Change	AtW inflow (Sv)	GPW outflow (Sv)
A. Overflow output reduced by half	5.0	2.6
B. Canadian Archipelago Bering Strait loss neglected	6.4	2.1
C. Twice the ice loss	7.1	2.2
D. A and B	3.0	1.3

These results indicate the deep water to be a slight source of heat and salt for the upper layers, i.e. an upward heat flux of 0.1 K–Sv and salt flux of 0.03 ppt–Sv. The salt and heat balances for the Polar Sea are not particularly sensitive to the deep water water types used in the balance because of their similarity, however, they are significantly affected by a non-zero DW exchange, as in our case. By comparison for example, **Aagaard** and **Greisman** (1975) assumed the DW fluxes through Fram Strait to be balanced.

The exchanges through the Barents Sea opening are difficult to estimate because of the large degree of recirculation and local water mass modification occurring over the Barents Shelf. We have used the transports estimates of **Timofeyev** (1963) on the basis that they are the most comprehensive. They give a net flow into the Polar Sea of 1.0 Sv, slightly larger than that used by other authors. Because of the large recirculation and mixing in the Bjornoya Trough, we chose the input salinity to be $S = 35.0$ instead of the $S = 35.1$ value found at the Bear Island-Northcape section (Subsect. 4.1.4). The output salinity we considered to be BrPW with a lower salinity of $S = 34.4$, which contrasts with the $S = 34.9$ value of **Aagaard** and **Greisman** (1975). The amount of ice leaving the Polar Sea via the Barents Sea is not wellknown; **Wadhams** (1981) suggests that **Lunde**'s (1965) estimate of 7.8 km^3/yr may be low by a factor of ten. In terms of the Polar Sea heat budget it may roughly balance the ice input of the Bering Sea (**Aagaard** and **Greisman**, 1975). We note that the heat loss via ice export from the Polar Sea to the Barents Sea probably greatly exceeds that from the Barents Sea to the GIN Sea. If true, the net heat loss figures

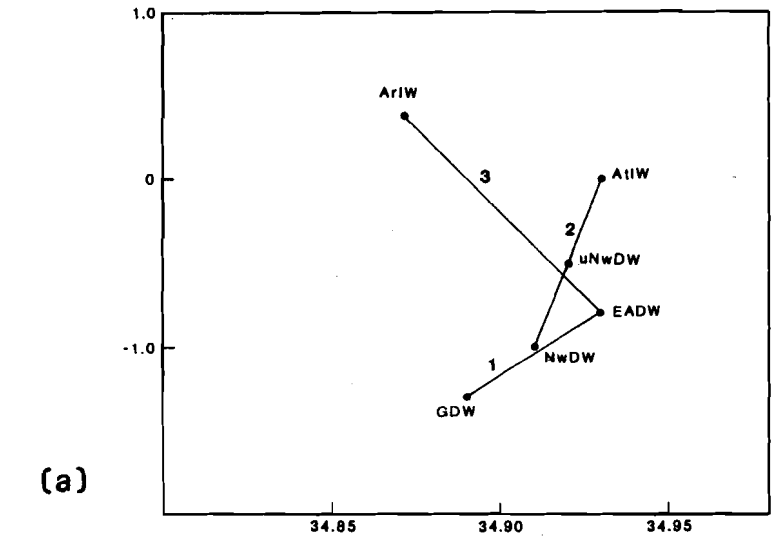

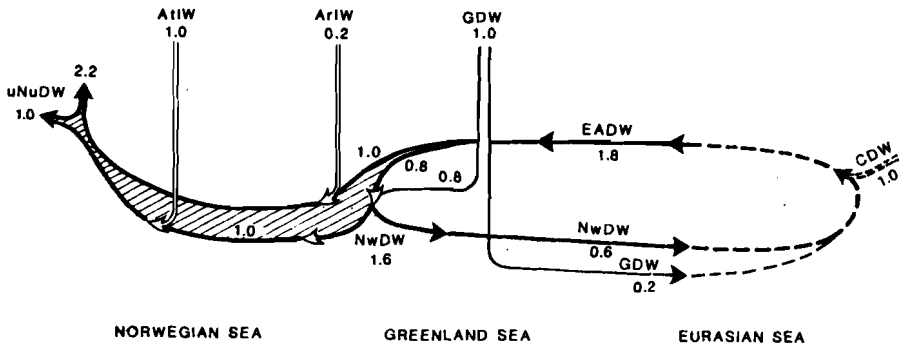

Fig. 5.23. (a) Θ–S diagram of water masses assumed to be involved in the production of uNwDW. The three labeled mixing lines indicate: (a) equal parts of EADW and GDW form NwDW; (b) equal parts of NwDW and AtIW to form uNwDW, and (c) four parts EADW with one part ArIW to form uNwDW. The water types are all reduced to a single point to simplify the illustration. The two intermediate water types are actually quite dense examples of their respective water masses. (b) A schematic of the water-mass exchanges assumed to occur in the deep layer. The numbers represent transports in Sv.

for the Barents Sea may be larger than those estimated merely from atmospheric exchange processes (Subsect. 3.2).

Table 5.10 gives the various components of the Polar Sea budget including the calculated values of the PW (2.03 Sv) and the PAtIW (3.80 Sv). The portion between the amount of PW and PAtIW, calculated as unknown in the Polar Sea balance, is

not well resolved because the two equations for volume and salt are nearly parallel. However, the combined salt flux gives a mean salinity of 34.47 ppt for a transport of 5.83 Sv. Any reasonable choice of salinities, i.e. for the PAtIW 34.94 ± 0.02 ppt, and PW < 34.0 ppt, renders a value for the PAtIW much larger than the PW, e.g. a salinity as high as 33.8 ppt for the PW would increase the transport of that water to ~ 2.4 Sv but that of the PAtIW would still be considerably more at ~ 3.5 Sv.

Table 5.10

The various exchange terms for the water, salt, and heat budgets of the polar sea and the GIN sea

Fram Strait					
Ice	−0.10	3.00	−0.30	0.10	8.99
PW	−2.03	33.6	−68.22	−1.5	2.84
PAtIW	−3.80	34.94	−132.78	1.5	−6.08
EADW	−1.8	34.93	−62.87	−0.8	1.26
WSC	4.3	35.00	150.50	2.0	9.03
WSC	2.1	34.96	73.42	0.0	0.21
NwDW	0.6	34.91	20.95	−1.0	−0.54
GDW	0.2	34.89	6.98	−1.3	−0.24
Barents opening					
BrPW	−0.9	34.4	−30.96	1.0	−0.99
Ice	negl.	–	–	–	0.2
BrAtW	1.9	35.0	66.50	4.0	7.79
Canadian Arcipelago					
out	−2.1	34.2	−71.81	−0.7	1.26
Bering Strait					
in	1.5	32.4	48.60	0.5	0.90
Ice	negl.	–	–	–	0.4
dilution	0.13	–	–	–	–
Total	0.0	–	0.0	–	25.03[1]
GIN Sea					
Total	0.0	–	0.0	–	53.82[2]

[1] Corresponds to 8.5 kcal/cm^2/yr, 23 Ly/day, or 11 W/m^2 using an area for the Polar Sea of 9.3×10^6 km^2.

[2] Corresponds to 68 kcal/cm^2/yr, 186 Ly/day, or 90 W/m^2 using an area for the Gin Sea of 2.5×10^6 km^2. Units as in Table 5.9.

Figure 5.24 illustrates the primary thermohaline transports as determined by the above budgets. The Polar Sea has a net outflow through Fram Strait. Including all components the EGC has a total outflow from the Polar Sea of $\sim$ 7.6 Sv, while on the eastern side of Fram Strait the total inflow is $\sim$ 7.2 Sv. This results, if only qualitatively correct, would have important consequences for the barotropic circulation and the heat balance of the Polar Sea. For example, this deficit could be satisfied locally by a westward compensatory movement of the excess generated by the Barents Sea inflow, in which case, about half of the heat gain of the Barents Sea imput would be recirculated out the Fram Strait. We note that this would agree with both the Arctic Circulation Models of **Semtner** (1976) and **Hibler** and **Bryan** (1984) which indicate anticyclonic flow in the Polar Sea with westward flow along the Barents slope. However, such a circulation seems unlikely on the basis of the water mass dissimularity between the BrAtW and the PAtIW. Another possibility exists: the Barents Sea inflow moves eastward as a part of a large scale cyclonic, barotropic circulation that eventually feeds the Polar Sea output at Fram Strait from the west and, in so doing, distributes the Barents Sea heat well into the Polar Sea.

The major heat sources of the Polar Sea are the WSC together with the the BrAtW and the ice export. The primary heat loss is the rAtIW component of the EGC. The total heat loss computed for the Polar Sea of 25Kcal $\times 10^9$/s, ($\sim$ 11W/m^2) which compares with the value of **Aagaard** and **Greisman** (1975) except that their estimate did not include the Barents Sea, which would have increased it. The other estimates of Table 5.10 are considerably lower and included the Barents Sea.

Table 5.11
Budget comparisons for Polar Sea from the literature

	Aagaard and **Greisman** (1975)			**Vowinckel** and **Orvig** (1970)			**Mosby** (1962)		
	(Sv)	(°C)	(ppt)	(Sv)	(°C)	(ppt)	(Sv)	(°C)	(ppt)
Bering Strait	1.5	0.5	32.4	1.0	0.9	–	1.2	2.1	32.0
Arctic Archipelago	−2.1	−0.7	34.2	−1.2	− 0.2	–	−1.1	−1.8	34.0
EGC water	−7.1	−1.2	34.0	−3.4	− 0.6	–	−2.0	−1.8	34.0
ice	−0.1	0.5	34.9	−0.1	−10.0	–	−0.4	−1.0	5.0
WSC	7.1	2.2	35.0	3.4	1.3	–	2.0	1.9	35.0
runoff	0.1	5.0	0	0.1	4.9	–	0.1	5.9	0
net heat, kcal $\times 10^9$/s		25.8			16.9			16.3	

By subtracting the Polar Sea heat loss from that of the Arctic Ocean we obtain a

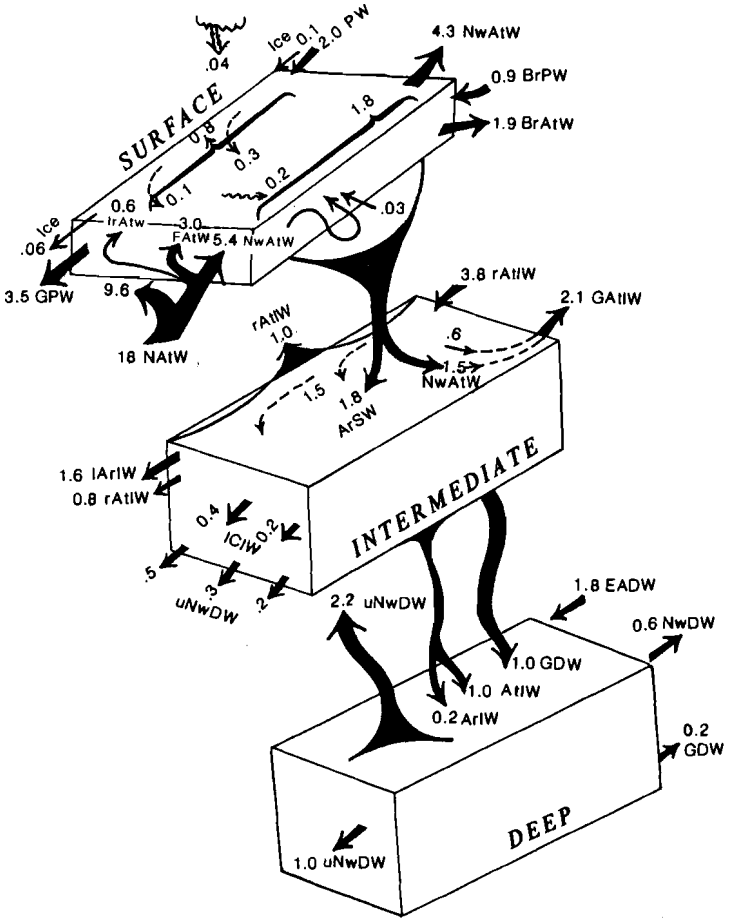

Fig. 5.24. **A schematic of the exchanges (expressed as transports in Sv) computed for the thermohaline model of the GIN Sea described in the text.**

value for the GIN Sea of $90 W/m^2$. This agrees with **Worthington**'s (1970) value of $100 W/m^2$, but is high compared to the value of $30 W/m^2$ computed by **Mosby** (1962) which also included the Barents Sea. Compared to the heat loss values computed from atmospheric exchange processes, this value agrees with **Bunker**'s (1976) value of $\sim 90 W/m^2$ (Fig. 3.6), but is somewhat more than that inferred from Fig. 3.12 of **Gorshkov** (1983).

■ *5.4.3. Vertical and horizontal exchanges*

To resolve the vertical and horizontal exchanges between the major water masses

several additional assumptions and calculations were made. The first involves an estimate of the GDW production and the subsequent deep water balance described above and depicted in Fig. 5.23b. The deep water circulates/mixes roughly as follows: Nearly half (0.8 Sv) of the entering EADW mixes with 0.8 of GDW, or that portion which does not flow into the Polar Sea, to make 1.6 Sv of NwDW. This NwDW production is split such that 0.6 Sv flows north into the Polar Sea and 1.0 Sv flows south. The southward branch of the NwDW mixes with an equal amount of an AtIW type to form uNwDW. This is equivalent to saying that the fate of the NwDW produced (in the Greenland Sea) is to either exit to the north (to the Polar Sea) or to upwell and be modified into uNwDW. It also implies a significant difference in the vertical movement of the Deep Waters: down in the Greenland Sea and up in the Norwegian Sea.

An additional production of uNwDW arises from the remainder of the EADW (1.0 Sv) which, in mixing with an ArIW type (0.2 Sv), forms (1.2 Sv) of a uNwDW type. Thus, in the simplified description given here, the two mixtures of uNwDW are independent of each other except that both require EADW. In Fig. 5.23, NwDW is formed along mixing line a. This is followed by uNwDW formation by mixing along line b. The other method of uNwDW production is shown by the mixing line c. The mixtures represented by lines a and c are likely to occur in the southern and eastern portion of the Greenland Sea as a result interaction between the circulation of these waters and the Mohn Ridge bathymetry. The production of uNwDW as indicated by line b is obviously not as simple as depicted but could, for example, suggest an upwelling of the NwDW westward onto the Icelandic Plateau and subsequent mixing with rAtIW in the Kolbeinsey Ridge or enroute to Denmark Strait. Regardless of the production mechanism, it is the uNwDW type, not the NwDW, that is eventually exported to the overflow to the Atlantic.

In this illustration, the net volume exchange through the intermediate-to-deep water interface is balanced, although upward and downward exchanges are required to satisfy the deep-water salt and heat balances. This is not true of the upper two layers: the horizontal inflows and outflows indicate that the surface layer is convergent and the intermediate layer divergent. This means that upward and downward exchanges through the surface-to-intermediate water interface amount to 2.30 Sv and a salt flux of 80.15 ppt–Sv. At this point, we subdivide the surface and intermediate layers into three horizontal divisions such that we end up with a total of six subdivisions as shown in Fig. 5.25.

A primary supposition of the thermohaline dynamics of the GIN Sea is that the Arctic waters are mixed product of Atlantic and Polar waters. It follows then that the EGC must gain salt and the NwAtC must lose salt, as the results given in Tables 5.8 and 5.10 suggest. The surface portion of the NwAtC loses $\sim$ 37% of its incoming salt in transition south to north. This loss must be partioned between downward and lateral losses. We assume that the vertical losses consist mainly of that which becomes the lower, intermediate water portion of the WSC. In order to

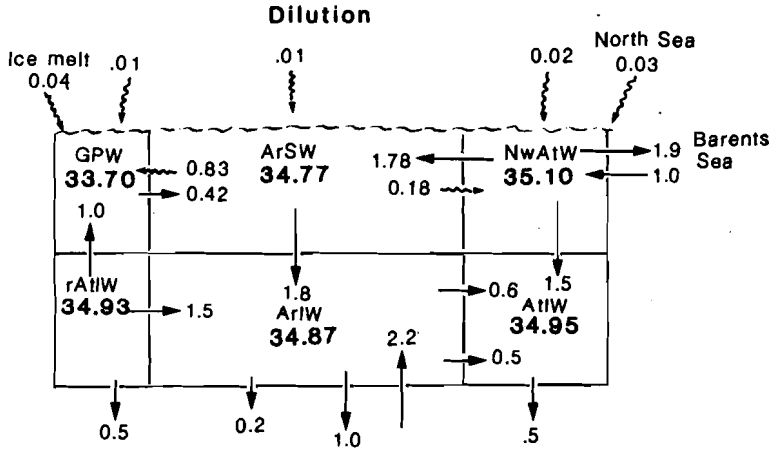

Fig. 5.25. A schematic cross section of the surface and intermediate layers of the thermohaline model (Fig. 5.24) showing the lateral and vertical exchanges (expressed as transports in Sv) and the associated salinity values (in ppt) of each component. The relative size of the water mass components is not to scale.

produce the necessary salt outflux, we require a downwelling of 1.5 Sv of NwAtW at 35.00 ppt and an entrainment of 0.6 Sv of GArIW at 34.86 ppt. We consider that this occurs to the north in the WSC, as little downward flux of NwAtW appears to occur to the south, i.e. based on the persistence of the NwArIW.

Considering the dilution of the NwAtW to be 0.05 Sv, of which 0.03 Sv enters from the North Sea, a salt balance requires a lateral loss of 56.22 Sv-ppt, which can be subdivided into a westward loss of $\sim$ 1.78 Sv and a eastward gain of $\sim$ 0.18 Sv. We consider the gain to occur primarily in the south where the IC joins the NwAtC and the loss to be the result of a turbulent-diffusive flux along the Arctic front and perhaps some direct advective loss in the northern portions of the Greenland Sea. The westward surface loss from the NwAtC represents the primary direct salting of the GIN Sea, i.e. not including the indirect salting occuring via the EADW and PAtIW outputs of the Polar Sea. The other direct source of salt is the IrAtW contribution, which is mostly restricted to the waters of the IC.

The EGC (GPW), as computed by the above Arctic and Polar Balances, is divergent, i.e. input/output $\sim$ 1.46 Sv. This result would seem to be sensitive to error since it derived from the difference between the Arctic Ocean and the Polar Sea budget calculations. Instead we find that changes in the budget of the Arctic Ocean that would create less GPW outflow at Denmark Strait, for example increasing the outflow through the Canadian Archipelago, also would create less of an outflow through the Fram Strait in the Polar Sea budget. The result is a divergence for the range

of reasonable values. However, we must note that the selection of mean salinities to compute the salt fluxes of the GPW is made difficult because of the vertical salinity gradient. Now, if we impose an additional loss to satisfy the necessary formation of the ArSW, through freshening of the NwAtW, then the GPW becomes even more divergent. We suggest that this divergence is satisfied by lateral entrainment from the ArSW and by an upward flux from the rAtIW. We assume that the lateral advective loss and the lateral gain through entraiment occur independently since they are governed by different dynamical processes: the former by the dynamics governing the large scale circulation and the latter by the dynamics associated with meso-scale mixing process across the Polar Front. The latter perhaps is assisted by the prevailing northerly winds causing the ArSW to be convergent against the GPW. The independence of these two dynamics signifies that the thermohaline solution is just an expression of the mean of these two processes.) We would ascribe the upward flux of rAtIW to a combination of the effects of interfacial entrainment (as in Fig. 4.13) and the result of the winter convection causing penetrative mixing of rAtIW and GPW.

Accordingly, if we consider a balance of the GPW, we are confronted with three unknowns: the amount up of rAtIW, the amount mixed in of ArSW, and the amount lost of GPW. The balance is such that decreasing the rAtIW upwelled has the effect of decreasing the salinity of ArSW, i.e. by increasing the lateral loss of GPW to the ArSW. We have used a value of 1 Sv for the upwelled rAtIW, a value which renders a salinity for the ArSW of 34.768 ppt. Our interpretation of **Carmack**'s (1972) and **Swift**'s (1980) results suggests that a value of 34.77 ppt, or slightly greater, would be a reasonable guess for the GIN Sea average. To maintain a greater salinity for the ArSW (with this budget) would have required a considerably larger upwelling of rAtIW, a result which we felt difficult to justify.

A salt balance of the GPW then yields a lateral salt input of 14.70 Sv–ppt, which can be partioned into a westward gain of 0.83 Sv and an eastward loss of 0.42 Sv. We presume that this loss is advective and comprises the eastward tongues of GPW observed in the JMC and in the southern Iceland Sea, which we have distributed them in Fig. 5.23 as ~ 0.3 and ~ 0.1 Sv, respectively.

Recalling that the total downward flux from the surface layer is 2.3 Sv, we find that the proportion attributable to the ArSW is 1.8 Sv and a salt flux of 62.58 Sv–ppt. This downward flux of ArSW is required to freshen the intermediate waters. The only external input to the entire intermediate level is that of the rAtIW from the Polar Sea which has a salinity above the mean for ArIW. Clearly, the rAtIW is convergent since the value of its (input–output) is 3.0 Sv. Since we have estimated an upward loss of 1 Sv, the remaining 2.0 Sv must be lost laterally or downward. We assume that the greatest portion, 1.5 Sv, is lost advectively as with the JMC and the eastward extensions of the rAtIW in the vicinity of the Kolbeinsey Ridge. This leaves 0.5 Sv to be lost downward as a part of the Deep Water requirement for

AtIW. This partioning affects the mean salinity of the ArIW, which in this case is 34.87 ppt, i.e. calculated as a mean of its three inputs is 34.87 ppt.

The above computations were meant to illustrate qualitatively, through a set of assumptions and approximate calculations, the GIN Sea thermohaline circulation. Perhaps the more significant indications are the large Atlantic inflow, the roles played by the components of the EGC, and the movement of the Deep Waters. A large NAtW inflow is apparently needed to satisfy the salt and heat requirements of the NwAtW in transit in the GIN Sea, which are summarized in the following losses:

Table 5.12

The percentages of volume, salt and heat lost by components of the NwAtC

Component to	Volume and Salt (%)	Heat (%)
Polar Sea	52	13
Barents Sea (net)	12	10
ArSW (net)	19	9
WSC, lower	18	5
Atmosphere	1	62

The importance of atmospheric heat loss over the NwAtC and the thermal, as opposed to haline, forcing of the GIN Sea is demonstrated. With regard to the magnitude of the AtW inflow, we note that if it were reduced to 4 Sv while at the same time the observed outputs to the Polar and Barents Seas were retained, the NwAtC would need to gain salt from adjacent GIN Sea waters and the heat loss would be reduced to $\sim 25 W/m^2$, conditions which clearly are not observationally supportable. We conclude therefore, that the NAtW inflow is greater than that observed, with perhaps the FAtW portion having been underestimated. This does not preclude the fact that the outflows may be overestimated, but as Table 5. demonstrates an outflow overestimation alone does not solve the problem.

Clearly the roles played by the GPW and rAtIW portions of the EGC are quite different: the GPW layer is strongly divergent and the rAtIW is strongly convergent. The GPW portion of the EGC is a sink for the GIN Sea, with the exception of its small lateral advective losses. Its salinity remains fairly constant despite quite active exchanges because the influx of salt is roughly balanced by ice melt and an accelerated outflux. The role of the rAtIW is quite the opposite: it appears to contribute greatly to the internal balances by providing lateral and vertical fluxes

with only a small ($\sim$ 20%) portion exiting to the North Atlantic. In fact, the role played by the rAtIw in providing salt to the GIN Sea interior is similar to that of the NwAtW, i.e. as calculated above the former provides 3.0 Sv at 34.93 ppt and the latter 3.1 Sv at 35.07 ppt.

The deep layer of the Greenland Sea appears to be a DW intersection where downwelling and mixing/production of water masses takes place, whereas the the deep layer of the Norwegian Sea appears to be a dead end resulting in an upwelling of the NwDW produced to the north. The production of uNwDW remains speculative as to location and mechanism. The constraint the roughly two-thirds of the NwDW produced exits via the Færœse Channel and the other one-third through the Denmark Strait suggests that the production/ distribution of uNwDW is wide spread.

5.5. WIND DRIVEN ASPECTS

The tendency for cyclonic circulation is immediately obvious in depictions of the GIN Sea surface currents (e.g. Fig. 5.1). From our present information it is doubtful that this apparently strong surface manifestation of positive vorticity is compensated by a negative vorticity elsewhere at depth. Therefore, an elemtary question concerns how much of this apparent vorticity tendency is generated locally within the GIN Sea. Since little contribution is expected to come from the basin's thermohaline circulation, the most likely source of positive vorticity would appear to be that generated by the curl of the wind stress.

A look at the wind fields shown in the climatological distributions of Figs. 3.2–3.5 reveals two important points:

(1) On a basin-wide scale, the curl of the wind stress is strongly positive because the mean wind vector changes from eastward to westward in a northward direction and from southward to northward in an eastward direction.

(2) On an inter-basin scale (separated by the atmospheric arctic front), the Norwegian Sea is exposed to a sequence of cyclones which impart cyclonic vorticity on the scales of several days and several hundred of kilometers; whereas the Greenland Sea is exposed to steadier winds that impart cyclonic vorticity at longer spacial and temporal scales. Thus, the curl of the wind stress can not be treated as consistent in space or time over the entire GIN Sea.

If the wind field is spatially inhomogenous, the horizontal transport of this frictionally driven flow develops corresponding inhomogeneities (convergences/divergences) that distort the sea-level (and/or internal stratification) causing variations in the barotropic (and/or baroclinic) pressure field. With geostrophic adjustment to this disturbed pressure field, the circulation reflects the spatial information of the wind

field. The spatial inhomogeniety of the wind field is commonly expressed as a forcing term written as the curl of the wind stress in the integrated vorticity equations. The ocean can respond to this wind-stress forcing in several ways dependent on its temporal composition (e.g. **Philander**, 1978; **Willebrand, Philander** and **Pacanowski**, 1980). The type of response can be described relative to a characteristic period, for which the b-effect and the topographic effect are both important. For the GIN Sea, given a length scale of 1000 km and a depth scale of 3000 m, this characteristic period varies from $\sim$ 2 weeks at 66°N to a month at 78°N. For shorter periodicities, on the order of days, a forced pressure field results; for periodicities on the order of weeks the response can also include the generation of Rossby waves; and for periodicities on the order of months the response is a Sverdrup balance (between meridional transport and wind-stress curl divided by the beta term). Correlations between wind and surface circulation are most likely at the low-frequency Sverdrup response, less likely at the high-frequency forced-wave response, and least likely in the mid-frequency range of free Rossby waves. From an analysis of observations in the WSC, **Hanzlick** (1983) found that only at semi-annual and larger periodicities there existed a correlation between meridional transport and the wind-stress indicative of a Sverdrup balance. The situation at the mid- and high-frequency range is complicated further by the liklehood of topographically induced Rossby waves which can be stimulated when the length scale associated with the local bathymetric slope is greater than that associated with the change in the Coriolis parameter with latitude. This is commonly the case over the mid-ocean ridges and continental slopes of the GIN Sea, and in the Norwegian Sea in particular, where there is considerable energy available at the mid-frequency range associated with the passages of cyclones.

In general, bathymetry imparts a greater signature to the vertically-averaged circulation than does the wind-stress field (cf. **Greegan**, 1976 in Subsect. 5.6). This is because the conservation of potential vorticity predominates within the internal portion (away from the surface and bottom frictional layers) of the water columns, consequently water columns conserve the ratio of their absolute vorticity to their depth by moving along isobaths when there are no changes in absolute vorticity. With a flat bottom and no stratification, the bottom friction tends to remove the vorticity put in by the wind-stress curl. With stratification, some of the surface input is dissipated internally by baroclinic shears. With variable bathymetry, the bottom-stress curl generates divergences/convergences that, because they are uncorrelated with those of the surface wind-stress curl, act to further complicate the circulation patterns. Likewise the spectrum of topographic Rossby waves induced by complicated bathymetry is broader than the spectrum of planetary Rossby waves.

Aagaard (1970) estimated the magnitudes of the Sverdrup transports from an analysis of 1965 winds derived from the six-hourly atmospheric pressure charts of the Bergen Weather Bureau (Fig. 5.26). The annual average rendered almost exclusively northward values over the entire GIN Sea with a strong maximum in the western, central region of $\sim$ 35.0 Sv. Along any meridian the Sverdrup transport has a maximum near the middle of the basin tending to cause a convergence over

the northern region and a divergence over the southern region. Also, for northern flow the bathymetry of the northern part (Greenland Sea) causes a convergence of the barotropic flow. How these inter-basin scale convergences/divergences are satisfied is not yet clear; we note, however, that the thermohaline circulation relects this tendency for downwelling in the north and upwelling in the south.

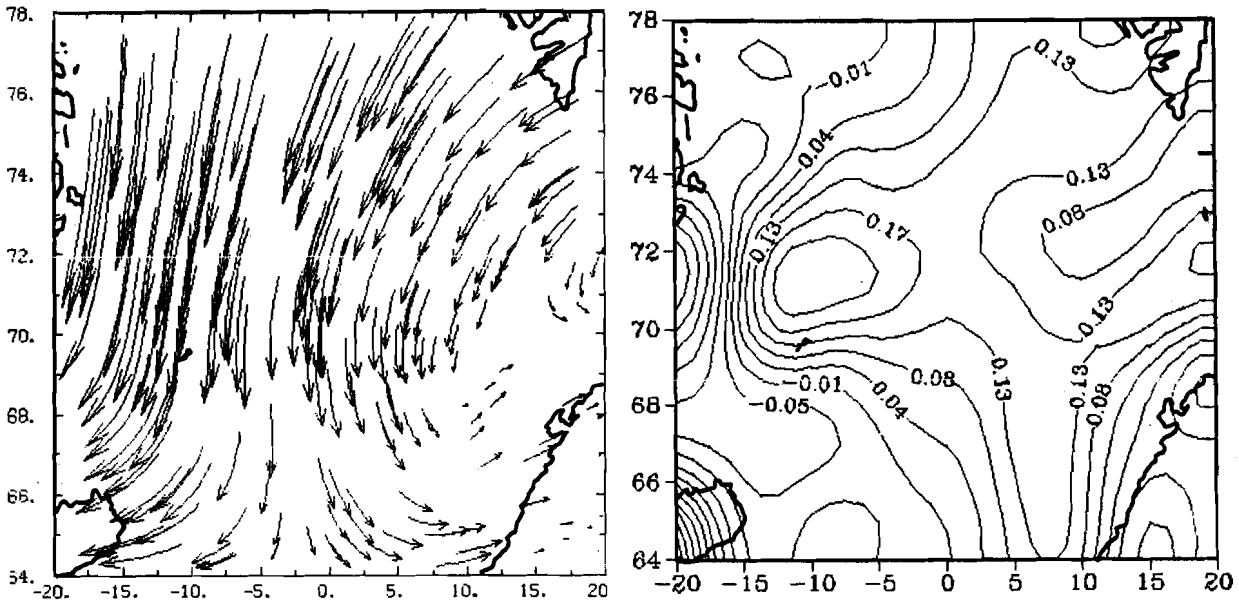

Fig. 5.26. (a) The average wind field for the 1965 winds as, reported by **Aagaard** (1970), and (b) the associated wind-stress curl replotted by **Piacsek** (using the ARROW plotting routine of NCAR and a staggered spherical grid for computing the curl).

Aagaard (1970) also demonstrated the variability in the magnitude of the wind stress curl as calculated from different averaging intervals (of the atmospheric pressure). In general, the values in the Greenland Sea decreased monotonically as the averaging interval increased from 6 h to 30 days, whereas in the Norwegian Sea they remained nearly the same (Fig. 5.27a,b). This again is indicative of the lesser spatial variability in the northeasterlies over the Greenland Sea, relative to the southwesterlies over the Norwegian Sea. Since the variance in the atmospheric pressure gradient is proportional to the wind stress (cf. **Fofonoff**, 1960), the wind stress curl will be reduced when the pressure field is averaged over longer time intervals provided the variance is correlated over the length scale used to compute the curl. **Aagaard** (1970) demonstrated this effect by calculating the wind stress curl using different averag-

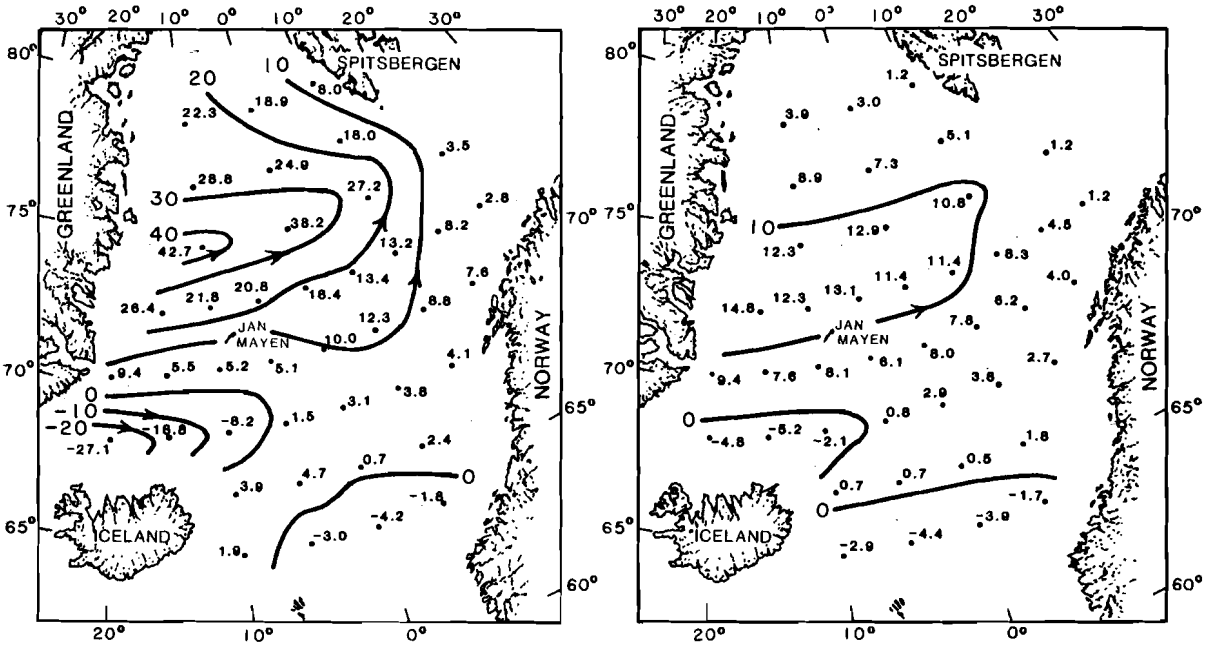

Fig. 5.27. (a) The wind-stress curl for February 1965, as reported by **Aagaard** (1960), vector-averaged from winds calculated from 6-h atmospheric pressure data and (b) from winds calculated from atmospheric pressures averaged for the month. (c) The February 1983 winds and (d) the associated wind-stress curl from the GCM data computed and plotted by **Piacsek**, as in Fig. 5.26.

ing intervals (of the atmospheric pressure) but with the same spatial spacing. In general, the values in the Greeland Sea decreased monotonically as the averaging interval increased from 6 h to 30 days, whereas they remained nearly the same over the Norwegian Sea (Fig. 5.27a,b) where the $\sim$ 300-km grid was likely too coarse to have rendered larger values of the wind-stress curl at decreased time-averaging intervals. Although this example is not conclusive, it underlines the need for caution in deriving an averaged field for the wind-stress curl and is indicative of the scale differences between the northeasterlies of the Greenland Sea and the southwesterlies of the Norwegian Sea.

Examples of daily variability are given in Fig. 5.28 in which 3-day sequences of wind patterns are given for three different but characteristic meteorological situations. The March sequence shows a large cyclone passing northeastwards and encompassing the entire GIN Sea. The August sequence is typical of the summer period in which the Arctic Front lies well north of its annual-mean location and a cyclone passes northeastwards over Greenland and the Greenland Sea leaving the Norwegian Sea exposed to consistent southwesterlies. The September sequence shows a

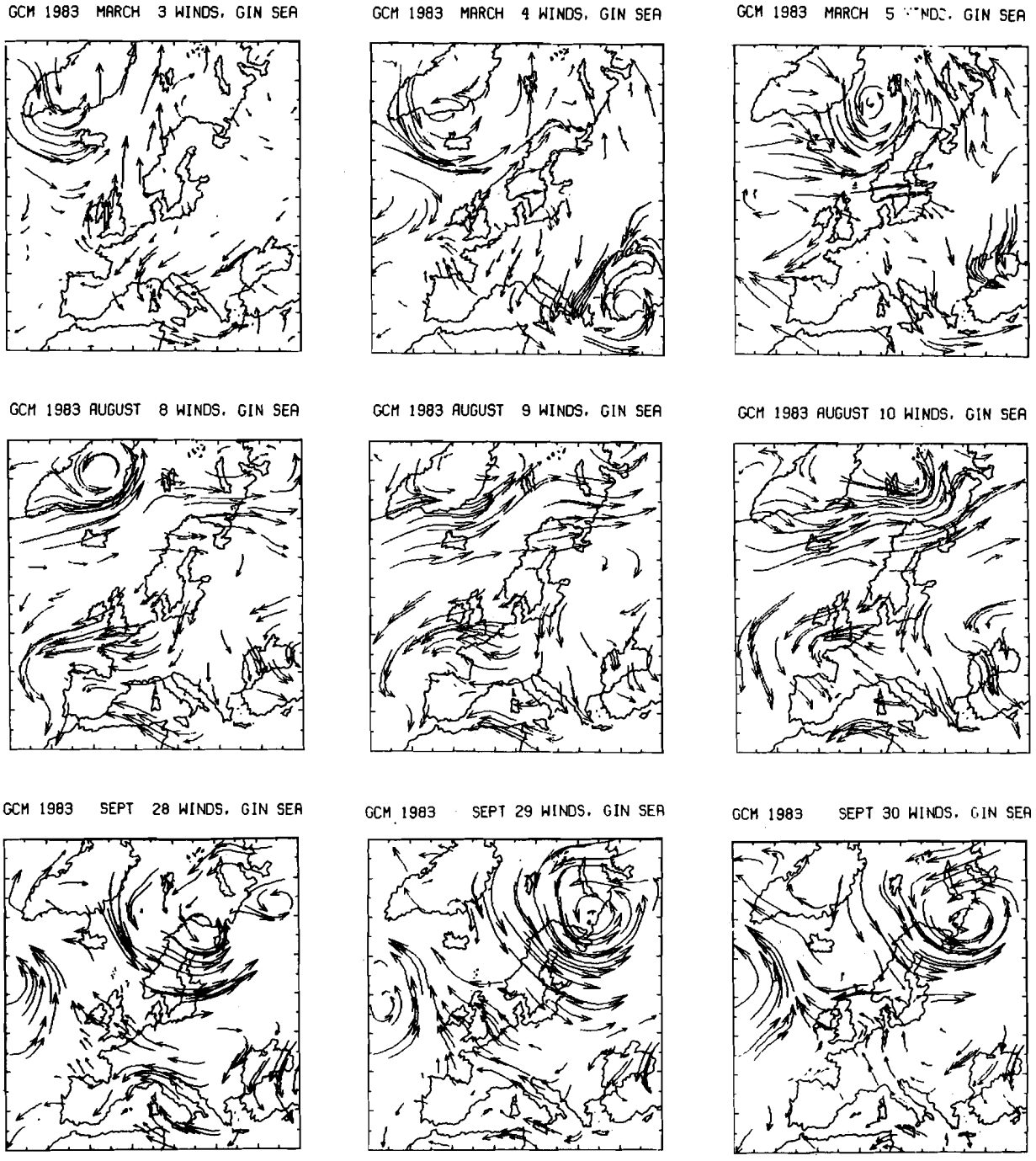

Fig. 5.28. **Three 3-day sequences of wind fields over the North Atlantic and GIN Sea area: upper 3–5 March, middle 8–10 August, lower 28–30 Sept. [Data from GCM plotted by Piacsek.]**

more unusual situation, in which the greater part of the GIN Sea is exposed to northwesterlies as a result of a stable anti-cyclone over the North Atlantic and a cyclone over the Barents Sea.

Primarily, **Aagaard** (1970) wanted to determine if the Sverdrup transports were of the same magnitude as the observed transports, particularly that of the latest estimate of the EGC transport of 35 Sv (**Aagaard** and **Coachman**, 1968). The agreement prompted the question of whether a transport balance existed between a northward driven interior flow and a southward boundary flow, the EGC. Such a conclusion could be an oversimplification, in any case the problem appears less straight forward. On one hand, the wind field derived from annual or semi-annual averages of the atmospheric pressure field would generate much smaller Sverdrup transports, i.e. in light of the above discussion. On the other hand, the more recent estimates of the EGC transport are also considerably less. It is not clear also that the EGC, or at least the upper GPW portion, serves to supply a mass divergence in the interior of the GIN Sea. We note that the circulation deduced from the thermohaline budgets (Subsect. 5.4) depicted the GPW as divergent, i.e. requiring more water from the interior, via frontal mixing, than it lost to the interior, via advection. On the other hand, the rAtIW was depicted as convergent and therefore a potential source of water for the interior, and the same is certainly true of the EADW. However, it is not clear that these deeper portions of the EGC, can be considered as GIN Sea boundary currents returning vorticity put in locally, i.e. at least to the degree that they originated in the Polar Sea.

In fact, it may not be justifiable to ascribe to the wind as the primary cause of the cyclonic circulation of the GIN Sea. Evidence of the net vorticity input is difficult to ascertain. The vorticity of the two boundary currents, the EGC and the NwAtC, tends to be cancelled if intergated zonally across the basin. The vorticity advected into and out of the basin may predominate in a vorticity balance of the Sea, i.e. in an analogous manner on which the heat budget is dominated by the the advective inputs and outputs. If more negative planetary vorticity is imported through the Fær oese Channel than is exported through Fram Strait, then the NwAtC would be considered as a source (advective) of negative vorticity which then would be compensated by any positive vorticity input from the wind stress. The wide extent of the NwAtC allows it to receive more positive vorticity from the wind while at the same time losing less as a frictional boundary current. To the north the WSC narrows exposing it to less wind vorticity and perhaps more frictionally-generated negative vorticity, possibly increasing the negative vorticity output to Polar Sea. Note that this local narrowing of the WSC may be caused by local bathymetric steering as the Mohn Ridge and the Spitsbergen shelf bathymetries converge, see the more complete discussion of **Hanzlick** (1983).

The situation is nearly the opposite for the EGC which by nature of its southward flow has a surfeit of positive vorticity. Assuming that for the upper portion of the EGC, its export is more than its input, then the EGC acts as a sink of positive

Report no. changed (Mar 2006): SR-124-UU

vorticity for the GIN Sea. The areal exposure to the wind is much less, than that of the NwAtC, and because it is generally covered by ice, the amount of positive vorticity put into the EGC via the surface interface is greatly minimized relative to that put into the NwAtC and may not constitute an adequate source. In this case, the source of vorticity may come instead from lateral inputs, i.e. from the interior. At the same time, as well defined boundary current against the Greenland Slope, it aquires an opposing negative vorticity tendency. This would suggest that a narrower, faster EGC would require more lateral positive vorticity input.

5.6. MODELS

There have been only a few attempts to numerically model the circulation of the GIN Sea, although there are several models currently under construction. The availability of data to describe the boundary conditions has been and still is a major impediment to realistic models because of the strong dependence of the circulation on the open boundary conditions. Even with this limitation, several important aspects of the circulation have been demonstrated. We will provide only a brief description of these various efforts.

Semtner (1975) adapted the **Bryan** (1969) ocean-circulation model to the Arctic Ocean using spherical coordinates with a $\sim$ 110 km wide grid and 14 vertical layers. The horizontal equations of motion included the time derivative, advective, geostrophic, and both the lateral and vertical frictional terms; the hydrostatic approximation was used to represent the vertical equation; and the advective-diffusive conservation of mass equation was used with the empirical equation of state of **Bryan** and **Cox** (1972). The bathymetry of **Smith, Menard** and **Sharman** (1965) was used. At the solid boundaries no-slip and no-flux conditions were imposed and at the open boundaries fluxes of mass, heat, and salt were estimated from observations. The initial conditions were taken from climatological data. The wind stress field was taken from an annual mean of the atmospheric pressure field with a scalar multiplier. A surface heat flux of $85 W/m^2$ was specified over the ice-free portions.

For the GIN Sea, a basin-wide cyclonic circulation was generated at all vertical levels (Fig. 5.29a) In cross section (Fig. 5.29b) the distributions are fairly symmetrical with somewhat greater gradients in flow on the Greenland side and in temperature and salinity on the Norwegian side. These results are not surprising given the strong and balanced inflow and outflow (7 Sv) at the Færœse Channel and Denmark Strait, respectively. Also the wind-stress field was cyclonic on a basin-wide scale but much stronger on the Greenland side, a consequence of the averaging technique. The coarse grid, the poor spatial representation of the wind stress, and the rough estimates of the inflow/outflow all prevented the model from providing more realistic detail in the results.

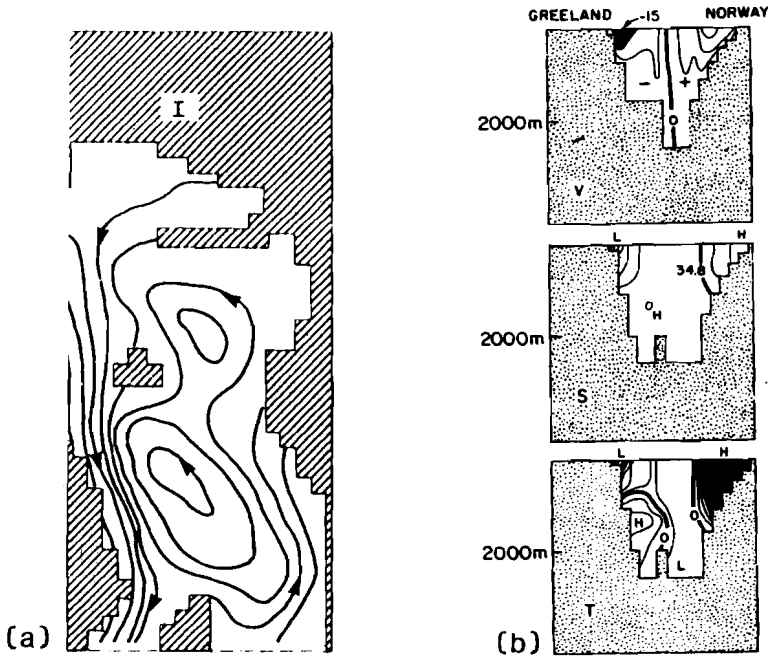

Fig. 5.29. (a) The predicted pressure field at 20 m for the GIN sea from **Semtner**'s (1976) model of the Arctic Ocean. The countour interval is 0.08 dynamic meters. (b) Vertical cross sections of velocity (upper) with contour interval 2 cm/s, of salinity (middle) with contour interval 0.02 ppt, and of temperature (lower) with contour interval 0.2 K.

Rzheplinskiy (1975) used a steady state diagnostic model to investigate the winter circulation around Iceland. A large computational grid of 1° latitude by 2° longitude was used from 50°N to 75°N and from the continental slopes of Greenland to Europe with a 50% smaller grid in the vicinity of Iceland. His results demonstrated a greater varability in transport for the baroclinic/real-bathymetry case relative to the barotropic/flat-bottom case. For example in the latter case, there was little evidence of anticyclonic flow around Iceland whereas in the baroclinic/real bathymetry case it was well developed with the exception of the eastward separation of the IC, as observed. In other respects the model failed to represent well the Denmark Strait outflow and the Færœse Channel inflow.

Greegan (1976) investigated the effects of wind, inflow, and bathymetry on the surface circulation of the GIN Sea. Using an explicit finite difference scheme, she integrated the linearized equations of motion over two layers: the upper 500 m of the water columns and a lower layer from 500 m depth to a scaled bottom topography. She

considered the basin to be bounded at approximated the 500-m depth contour except at the position of the Fram Strait and the Færœse Channel through which she specified a mass flux. She used a spin-up time of about a month, instead of the several years needed to bring the barotropic flow into steaty state, rendering the model results valid only for the upper layer.

With a flat bottom, the forcing of the wind stress primarily determined the circulation, e.g. with the cyclonic wind-stress distribution depicted by **Aagaard**'s (1970) average of 1965 winds, a basin-wide cyclonic circulation cell resulted that was centered around Jan Mayen Island with a westward intensification and that resembled the Sverdrup transport results of **Aagaard**. The inclusion of bathymetry (scaled by 30%) greatly modified this by dividing the circulation into two cells, each around the deeper portions of the Norwegian and Greenland Basins, and by reducing the transport magnitude (Fig. 5.30a). The addition of a northward directed inflow (5.5 Sv) at the location of the Færœ-Shetland Channel produced northward flowing boundary currents along both the Norwegian and Greenland Coasts (Fig. 5.30b). The latter result, even if contrary to observed conditions of the IC, served to demonstrate the sensitivity of the modelled circulation to the inflow boundary condition.

Zaripov and **Rzheplinskiy** (1977) have computed the winter and summer circulations in the southern GIN Sea and Northern Atlantic using a steady state diagnostic model. Zero mass-flux conditions were imposed at the solid boundaries and at the open boundaries the mass flux was computed by the dynamical method for the corresponding seasonal density distribution. The net northward flux was adjusted to be 1 and 2 Sv for the summer and winter seasons, respectively. The wind and density fields were taken from climatological atlases.

The results showed that both the wind-stress curl term and the Jacobian (bottom pressure, depth) term strongly influenced the flow. The latter dominated in regions of abrupt bathymetry, as in the straits and along continental shelves. The integrated flow generally followed the bathymetry (Fig. 5.31), showing a well defined IC feeding into the NwAtC and a weak EGC that joins the IC rather than exiting the Denmark Strait. The strong seasonal differences, e.g. the nearly twice as great a transport around Iceland in the summer as in the winter, the authors attribute to the stronger baroclinic signal during the summer. They are probably also an artifact of the net flux condition imposed at the open boundaries.

Hibler and **Bryan** (1984) coupled the sea-ice model of **Hibler** (1979, 1980) with the ocean model of **Bryan** (1969) to investigate the effects of the circulation on sea ice in the Arctic Ocean. The ocean model was weakly forced below the first level depth (30 m) with observed data from (**Levitus**, 1982) and for the first level from the ice model. The ice model calculated the momentum, heat, and salt fluxes through the upper layer, i.e. from the first level of the ocean model to the air-sea interface; while the ocean model provided the advective heat exchange information to the ice model at the first level interface. The ice model results provided information on the the

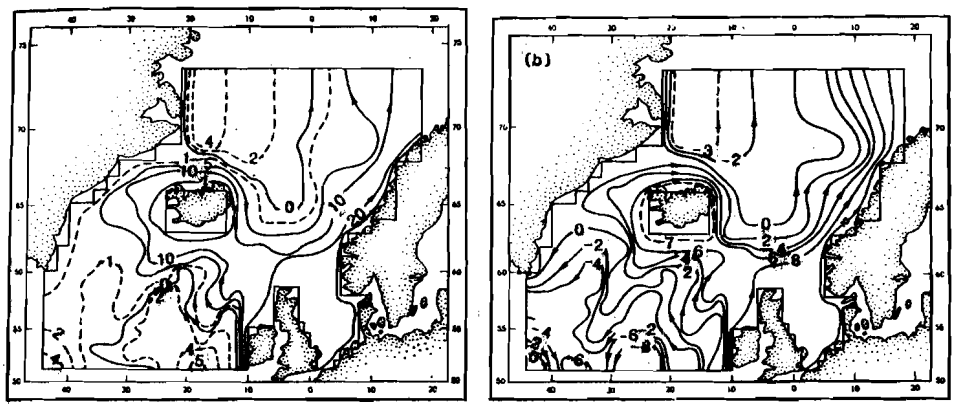

Fig. 5.30. The vertically-averaged flow vectors of **Creegan**'s (1976) model annually averaged winds of **Aagaard** (1970), (Fig. 5.26) and with bathymetry reduced by 70% and (b) the same except with the open boundary conditions of 5.6 Sv entering through the southern opening (dashed boundary).

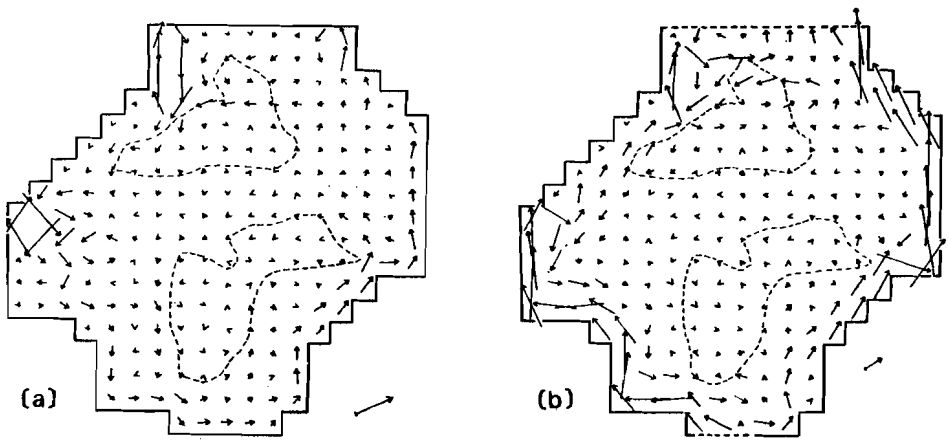

Fig. 5.31. The vertically integraded flow field as calculated by **Zaripov** and **Rzheplinskiy** (1977) for (a) winter and (b) summer. Isolines are given in 10^5 m^3/s.

ice characteristics (drift, thickness, and compactness) and on the energy exchanges with the atmosphere. The results demonstrate the complications in the sequence of momentum transfer from wind to ice to water and the reverse from water to ice. In Fig. 5.32a,b the ice drift is compared with the second level flow field. The results also demonstrate the importance of advective heat in any ice cover calculation. The ice cover calculated with out the ocean-model heat input is much too exstensive, whereas that calculated from the coupled model conforms will with the observed ice limit (Fig. 5.32c). Their computed net heat gained by the upper layer from below can be compared with Fig. 5.32 in Subsect. 5.4.2, which shows the net heat lost to the atmosphere.

Peggion (1986) has developed an inverse model which uses a variational method for deriving the flow field from hydrographic data within a ocean region of variable bathymetry. The model equations are written with the geostrophic, hydrostatic, Boussinesq, and beta-plane approximations. The effects of the surface and bottom frictional layers and of the turbulent transfers of mass and momemtum are neglected. This inverse model was developed to investigate the meso-to-large-scale internal flow structure in the Norwegian Sea utilizing recent hydrographic data, as that of SACLANTCEN GIN Sea Project (1985).

The model computes the internal flow field from the baroclinic geostrophic velocity referred to an unknown velocity field at the bottom (defined as the surface above the frictional bottom layer). This bottom velocity field is expressed in terms of the pressure (geostrophic) on the bottom surface. The bottom pressure field is represented by a partial differential equation from the approximated equations of motion and the conservation of mass equations (density and/or other conservative property). The solution would be exact under the conditions that the distribution of the data corresponded exactly to the flow structure represented by the equations. Since this is not the case, i.e. mostly due to non-synoptic and observational errors in the data and due to approximations inherent in the equations, there remains a residual error to the solution. This residual is an additional unknown component to the problem, and the solution is given by that bottom pressure field which corresponds to a minimization of the residual. Application of the model to data in the Norwegian Sea is planned in early 1987.

Piacsek and **Grillaki** (1986) are constructing a barotropic model using an explicit time ingegration scheme to study the circulations induced in the GIN Sea by various wind stress fields and open boundary conditions. The wind stresses are derived from the monthly-averaged and daily wind data of the Fleet Numerical Oceanographic Center (USA) and are taken from the July, September, and annual 1965 winds of **Aagaard** (1970). The open boundary mass fluxes are taken from the literature, including those of Subsect. 5.4. This modelling effort includes the testing of an implicit code for the conservation of mass, which at present has only been conducted for a flat bottom version. Model runs using the bathymetry of **Piacsek** are expected in 1987.

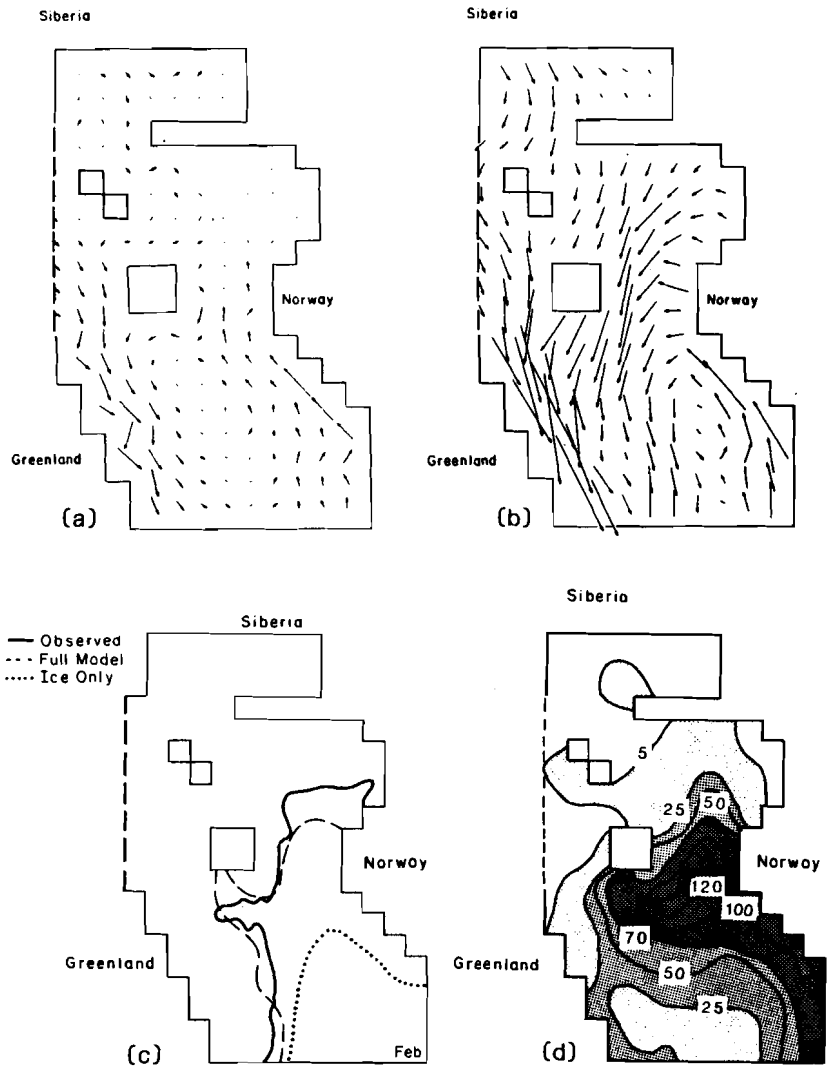

Fig. 5.32. (a) The mean annual currents for the second vertical level (30 to 76 m) of the **Hibler** and **O'Brien** (1984) model. (b) The mean annual drift. (c) The 50% ice concentration limits for February 1979 as observed (solid line) as given by the ice-ocean model (dashed line) and by the ice-only model (dotted line). (d) Advection heat gain in W/m^2.

Legutke (1986) has constructed a three-dimensional, primitive-equation model of the GIN Sea using a finite difference scheme over a grid with a horizontal spacing of 20 km and a vertical spacing of 12 vertical layers. The fluxes of momentum, heat and salt are specified at the surface and at the open boundaries of the Fram and Denmark

Report no. changed (Mar 2006): SR-124-UU

Straits and the Færœse Channel. The model uses an initial climatological density structure (**Levitus**, 1982). During spin up, the annual mean winds and constant inflow were used. The results were expressed as integrated flow for any of the vertical layers. In general, they showed that the Sverdrup balance predominated only in certain localities and that the interaction between the bottom pressure and the batymetry was important nearly everywhere.

6. Summary

The GIN Sea plays an unique and vital role in the circulation of the worlds oceans. It is in effect a small intermediate ocean coupling the Polar Ocean to the Atlantic Ocean. The manner and degree of this coupling are determined by its geomorphology and by its surface boundary conditions that determine the fluxes of heat, momentum, and water.

The GIN Sea Basin is comprised of two major basins, the Norwegian and Greenland Basins. These two Basins are separated by the mid-ocean ridge system which, apart from restricting deep water movements between them, exerts an important control on the local circulation through its interaction with the pressure field. The GIN Sea Basin itself is connected to the remainder of the Arctic Ocean, or the Polar Sea, through Fram Strait and is separated from the Atlantic Ocean by the Greenland-Scotland continental ridge. The areal size of the access to the Atlantic is less than half of that to the Polar Sea, but more importantly, it is restricted in depth: i.e. below 400 m to less than 50 km^2 in area and below 600 m to less than 4 km^2. This means, for example, that the entire volume of water in the Arctic Ocean deeper than 600 m would require around 200 yr to exit to the Atlantic at a speed of 50 cm/s. It means also that the adjacient deep waters of the Norwegian Sea must upwell more than 2000 m to flow over the Færœ Bank sill ($\sim$ 830 m). The access between the GIN and Polar Seas is much less restrictive in depth, over the $\sim$ 2600 m Fram Strait sill, so that the deeper waters can pass relatively unrestrictedly.

The meteorology controlling the atmospheric exchanges of heat momentum and water does not lend itself well to averaging or simple description. This is because the GIN Sea lies under an atmospheric transition from the midlatitude westerlies to the polar easterlies, and because its sea surface is partially ice covered. This transition corresponds to the average position of the atmospheric Arctic Front, which runs diagonally northeast-southwest and roughly paralleling the division between the Norwegian and Greenland Seas. Consequently the Norwegian Sea is exposed to a sequence of northeastward moving cyclones that are more frequent and greater in scale during winter than summer; and the Greenland Sea is exposed to seasonally persistent northeasterlies that wane somewhat during summer.

The division with respect to heat exchange is more complicated. The southeastern portion of the Norwegian Sea, which might be considered an extension of the North Atlantic from the point of view of surface waters, manifests nearly the same net heat loss ($\sim$ 90 W/m^2) as the North Atlantic region just to the south with the southern Norwegian Sea receiving less solar input but also losing less heat through evaporation. The net heat loss increases strongly to the north as the warm waters of the Norwegian Atlantic Current flow northward under the polar easterlies. The

maximum values west of Spitsbergen are more than twice that to the south ($\sim$ 180 W/m^2) due to increased back radiation and sensible heat loses and decreased solar input. To the west, and generally over the ice covered portions of the East Greenland Current, the net heat loss values are greatly reduced to values of about 15 W/m^2, because the effect of ice inhibition of the evaporative and sensible heat losses is much greater than the increased back radiation losses underneath the clearer dryer atmosphere found along the east coast of Greenland.

The intermediate and deep waters of the GIN Sea (and the rest of the Arctic Ocean) are more dense than those at equivalent depths in the Atlantic. This classifies it as a basin having a negative thermohaline circulation, that is, one in which dense waters are formed within the basin at the surface, sink, and feed a dense water ouput over the sill. Thus the forcing for this type of circulation is the buoyancy extraction occurring at the surface through losses in heat and/or water. However, the estimates for the heat loss are not unusually high and those for the water balance are even slightly positive. Why then is the GIN Sea considered such an important area of dense water production?

The answer, we suggest, is more related to the degree of deep water isolation than to the intensity of the buoyancy extracted at the surface. The deep waters of the Arctic Ocean are the most isolated of the worlds oceans (with the exception of those of the Mediterranean). It is the lack of a horizontal advective heat source that allows the relatively small heat loss to maintain such a large volume of cold deep water. We note that if the entire Arctic Ocean were filled with 8 °C Atlantic water and closed off, it would take around 50 yr to reduce its temperature to 0 °C at a heat loss rate diminishing with temperature from a maximum of 200 W/m^2 to 10 W/m^2. On the other hand, if the Iceland-Færœ Ridge were a deep opening similar to that of Fram Strait, an inflow of the entire North Atlantic current at 18 Sv would be sufficient to flush the Arctic Ocean in about 40 yr. Thus, from these rough estimates, it appears that without the circumstance of the Greenland-Scotland Ridge the Arctic Ocean would not be able to maintain its deep water product.

In an approximate way then, the thermohaline circulation is determined by two factors: the restriction of the opening and the intensity of buoyancy extraction processes (cf. **Hopkins**, 1978). While the former remains fixed, the latter is subject to considerable variation, as for example those occurring with meteorological cycles. We recall that the extent of the ice cover varied as much between successive years as between longer-termed weather cycles. This suggests that there exists some self-regulatory processes that provide a low-frequency compensation for annual variability. Variations in either the amount of surface heat advected in or the amount of heat lost to the atmosphere are fairly strongly damped due to the nonlinearity of the heat exchange process itself. For example, if the input of warm North Atlantic Water is increased then (a) the resulting increase in the rate of atmospheric heat loss, particularly evaporative, is greater than the corresponding increase in surface temperature; and (b) the ice-free area over which this loss occurs is extended. In

the opposite event, that of an increase in ice-cover due to a severe winter or a reduction in the Atlantic input, there follows a correspondingly greater decrease in the atmospheric heat loss.

Another self-regulating dynamic controls the amount of water entering the basin. The negative thermolhaline circulation of the basin interior requires that the exchange across the sill with the external ocean be governed by opposing flow: an inflow at the surface accelerated by a barotropic (sea level) horizontal pressure gradient directed into the basin at the surface, and an outflow at and above the sill depth accelerated by a baroclinic (internal) horizontal pressure gradient directed out of the basin. The sea level difference is steric, that is, due to the fact that the less dense waters external to the sill form higher water columns than those formed by the more dense waters inside the basin. The corollary response is an internal pressure gradient increasing with depth caused by the increasing weight of the internal water columns relative to those outside. In the simplest case that the inflow must balance the outflow, the two opposing pressure gradients balance well above the sill depth and the speed at sill depth exceeds that at the surface. The self-regulation with respect to the thermohaline circulation is effected by the following cycle: with the event of a greater heat loss within the basin, the upper layers become colder creating a lower internal steric height and more warm external water flows in which then in turn reduces the steric height difference and impedes further convective overturn. With the contrary event of a reduction in the heat loss, less warm waters enter and convection is facilitated. Again the corollary internal response is that with the greater heat loss more dense water is produced, the convective sinking of which causes an increase in the internal pressure gradient and the outflow is increased balancing the increased inflow; and vice versa for less production and a weaker outflow.

The over-the-sill exchange between the Atlantic and the Arctic Oceans is, of course, much more complicated than that depicted above. One of these complications is the effect of geostrophy which causes the inflow to be concentrated under a sea level rising to the right-hand side of the channel (looking in). Likewise, the outflow is concentrated on the left-hand side and the interface separating the upper and lower waters tilts up to he left. The exchange through the Færœse Channel, being narrower and deeper, most closely resembles this flow structure. However, the thermohaline requirement that the outflow equal the inflow, need not apply strickly to the Færœse Channel because of the existence the other two openings. In fact, our estimates gave 5.4 Sv in and 1.4 Sv out.

Denmark Strait is shallower, wider, and its water-mass interface intersects the surface. At the depth of the sill the internal pressure gradient that can develop is less than that which can develop at the depth of the Færœse sill. In this sense then, the amount and the depth of the outflow is limited relative to that of the Færœse Channel. However, this is not quite valid with respect to the amount for an important reason, one having to do with the presence of the East Greenland Current.

The Polar Sea has a mixed thermohaline circulation: that is, it has primarily a positive circulation that exports a less dense water mass, but with some negative circulation associated with the saline bottom water produced on its continental shelves. The East Greenland Current remains constrained to the Greenland continental margin, except for the $\sim$ 20% which is lost laterally to the Arctic Surface Water and thereby inhibits the efficiency of dense water production in the GIN Sea. Thus, the primary thermohaline output of the Polar Sea is delivered directly to the Atlantic Ocean via the Denmark Strait, the negative thermohaline circulation of the GIN Sea is enhanced, and the outflow of Denmark Strait is complicated.

The Denmark Strait is wide enough to accomodate the surface countercurrents of the Polar Sea output on the west side and a GIN Sea input on the east side. Because these two very different surface water masses have nearly the same density their confluence is marked by a watermass interface that intersects the surface. Another interface separates the fresher waters of the surface Polar Sea output (Greenland Polar Water) and a lower layer GIN Sea ouput (primarily Iceland Arctic Intermediate Water). This lower output is accelerated out of the basin by the outward internal pressure gradient and is concentrated by the effect of geostrophy against the Greenland Slope, where it incurs an additional barotropic outward component because of the presence of the overlying sea level gradient (rising toward Greenland) geostrophically driving the Polar output. Denmark Strait serves primarily as an output port for Arctic Ocean waters with $\sim$ 3.5 Sv of Greenland Polar Water mostly from the Polar Sea and with $\sim$ 2.9 Sv of various GIN Sea intermediate water mass products; and secondarily, it serves as an input port of only $\sim$ 0.6 Sv of Atlantic Water.

Without bathymetric constraints forcing it to satisfy the input/output requirements nearly met by the other two openings, the opening over the Iceland-Færœ Ridge is the least important in terms of exchange with the Atlantic Ocean. For example, if the Denmark Strait were closed, the Greenland Polar Water would be constrained to exit east of Iceland and, in doing so, would extend the ice cover over the entire Iceland Sea. Furthermore, a complete blockage of the Wyville-Thompson Ridge would cause the Atlantic Water to enter west of the Færœs. As it is, the same type of pressure gradient forces exist across the Ridge as force the flow through the Færœse Channel, but with the difference that the bathymetry on the north side continues unimpeded past the bounds of the opening. This configuration allows a countercurrent geostrophically adjusted to the pressure changes across the front to flow parallel to the sill instead of transversing it. The actual alignment of the front is oblique to the bathymetry resulting in a situation not quite symmetric east and west, that is, very little outflow occurs east of Iceland whereas considerable inflow does occur west of the Færœs. We have estimated this Færœ inflow to be $\sim$ 3 Sv. The outflow of mostly intermediate water products is $\sim$ 0.7 Sv.

The two shelf seas, the North Sea and the Barents Sea, contribute in specific ways to the thermohaline circulation. The North Sea plays the lesser role, mostly acting to freshen the Norwegian Atlantic Current with the Baltic Sea outflow. Much of this

fresh water volume, along with the Norwegian Coastal runoff, is contained within the Norwegian Coastal Current and/or is mixed into the eastern portions of the Norwegian Atlantic Current which ultimately provides the input to the Barents Sea.

The Barents Sea primarily represents a heat and salt sink for the GIN Sea, that is by providing an outflow port for the Norwegian Atlantic Current. The Barents Sea also represents a region very important in terms of water mass modification, but this is mostly relevant to the Polar Sea, even though nearly the entire western portion encompassing the Bjornoya Trough bathymetrically belongs to the GIN Sea. As mentioned, the Barents Sea location is conducive to high evaporative and sensible heat losses as the warm waters of the Norwegian Atlantic Current enter the region of the Polar Easterlies. Another important factor in the loss of heat is the insolation from the heat stored in deeper waters provided by the broad shallow shelf bathymetry. Also, the saline Norwegian Atlantic Water is readily converted to a dense water product upon cooling. As the extent of the cooling is a function of the residence time on the shelf, this dense water production appears to be more important with regard to the Polar Sea which receives waters that have transversed the shelf as opposed to the the GIN Sea which receives recirculated waters. The actual amount of the Barents Shelf Bottom Water input to the Gin Sea has not been well observed. Its contribution to the main body of GIN Sea waters may be minimized by the same fate that minimizes the effect of other Barents Sea inputs: that is, that return flows from the Barents Sea become incorporated into the West Spitsbergen Current and for the most part are returned to the Polar Sea through Fram Strait. Hence, the significance of these Barents Sea inputs remains uncertain. However, it appears that of them both the least dense and the most dense have the better probability of becoming mixed into other GIN Sea water masses: that is, the least dense by surface frictional transport across/over the West Spitsbergen Current and the most dense by cross-isobath sinking under the West Spitsbergen Current. Included in these uncertainties with regard to the Barents Sea inputs to the GIN Sea must be the amount of ice transport and its role played in modifying the heat and salt content that the West Spitsbergen Current exports to the Polar Sea. In the case that we consider the Barents Sea inputs, amoung which we must include the ice transport, as serving primarily to modify the heat and salt content of the West Spitsbergen Current, then clearly even the GIN Sea portion of the Barents Sea has an important indirect effect on the Polar Sea.

Because of its depth, the Fram Strait acts more as a lateral restriction than a bathymetric barrier to the circulation of the Arctic Ocean. Consequently the large two-way flow through the Strait is more an extension of the internal circulations in the GIN and Polar Seas than a response to the differential thermohaline forcing between them. Nevertheless, the thermohaline response is compatible with the flow structure and the water mass products have a staggered vertical structure within the two counterflows. The general thermohaline situation of water columns more dense south of the Strait than north of it supports a southward surface Polar flow (favoring the west side) and a northward deep GIN flow (favoring the east side);

however, the specific situation is a little more complex. The upper portion of the Polar Sea, which has a positive thermohaline circulation due to its positive water balance, exports as a surface output the low-saline Polar Water and imports as a subsurface input the Norwegian Atlantic Water. Underneath this the slightly less dense Polar products (Polar Atlantic Intermediate Water and the Eurasian Basin Deep Water) exiting southward on the Greenland side and the slightly more dense GIN products (Norwegian and Greenland Deep Waters) exiting northward on the Spitsbergen side. Our thermolhaline transport estimates for Fram Strait show the Polar Sea as having a net outflow of 0.5 Sv; however, if the Barents Sea exchange is included, the situation is reversed so that the GIN Sea has a net outflow of 0.5 Sv.

The combined result of these exchanges through the various openings and with the atmosphere determines the gross thermohaline circulation and the water mass structure within the basin. The exchanges through the openings can also be forced by higher frequency sea-level forcing in a manner which is not necessarily correlated one from another, and the internal circulation is also controlled by the momentum exchange occurring within the basin over a broad range of frequencies. In addition interannual variations exist in the salt and heat content of the exchanges and/or in the atmospheric conditions governing the exchange of heat and water with the sea. Even the self-regulatory tendencies that dampen the effect of these variations have their own intrinsic response times; for example, the barotropic response at Fram Strait to a sea level pulse through the Færœse Channel will begin after 8 hr, but the amplification of the net heat loss due to a greater flux of warm water through the Færœse Channel may occur on a seasonal time scale.

In order to illustrate the water mass structure, we construct the following account of the transport and transformation of the major water masses through the GIN Sea system based on our model of the thermohaline budget (Figs. 5.23b, 5.24, 5.25 refer).

The Atlantic Water enters the system at $\sim$ 8.4 Sv, which is sufficient to flush the resident volume of the NwAtW in less than 2 yr. Immediately on entry it encounters the waters of the IC confluent from the west. The extent of mixture of these waters into the NwAtC is not well known, although it is assumed that they are the source for the NwArIW that constitutes the underlying salinity-minimum layer that gradually mixes out in traversing the southern half of the Norwegian Sea. Also just after entry, $\sim$ 1 Sv NwAtWcirculates into the North Sea/Baltic Sea approximately half of which recirculates within the Norwegian Trench and rejoins the NwAtC only slightly freshened and cooled. The other half returns as a distinct water mass (NwShW), freshened by the Baltic Sea outflow, transported northward along the Nowrwegian contental shelf in the NwCoC. At the Barents Sea Opening, $\sim$ 1.9 Sv branches eastward, with a main part of approximately 1.4 Sv continuing to form, together with the remnants of the NwCoC, the North Cape Current. and a second part of $\sim$ 0.5 Sv mixing with $\sim$ 0.4 Sv of PW to return to the WSC.

The NwAtC appears to lose only a small portion of its volume through mixing downward ($\sim$ 0.5 Sv), but does lose about 1.8 Sv laterally. This lateral loss constitutes the direct entry of Atlantic Water into the Arctic Waters. It appears that most of this occurs north of Jan Mayen Island, i.e. into the Greenland Sea. A small portion of this, $\sim$ 0.1 Sv, is involved in the winter formation of GDW.

Approximately 6.4 Sv of NwAtW leaves the GIN Sea submerging under the Polar Water to become the PAtIW. Already by the latitude of Spitsbergen the lower one third has become cool enough to be classified as an intermediate water mass. This is the source water for the rAtIW entering the GIN Sea on the other side of Fram Strait at about 3.8 Sv. A portion of this recirculates in the vicinity of Fram Strait and the rest within the Polar Sea. This suggests that about 2.6 Sv are available for salting the Polar Waters, both surface and deep.

The surface Polar Water that exits at about 2 Sv is derived from the Bering Sea input, from ice melt and runoff, and from the upwelled PAtIW. Within the GIN Sea the GPW primarily adsorbs lateral admixtures of ArSW and convective (vertical) mixtures of rAtIW. It does contribute 0.4 to the ArSW, probably in lateral flows that branch from the EGC as in the JMC and the IC. The combination of this lateral loss, that from the NwAtC, the input from the IrAtW constitute the approximate renewal rate of 2.8 Sv and a renewal time on the order of 4 yr for the ArSW.

The primary fate of the ArSW is a conversion to intermediate water ($\sim$ 1.8 Sv) including a small portion involved in the GDW production. A slightly larger source of intermediate water derives from the rAtIW which is convergent within the GIN Sea: of the $\sim$ 3.8 Sv that enters about 1.8 Sv leaves with he EGC and $\sim$ 2 Sv contributes to the intermediate and deep waters. These results suggest that nearly as much Atlantic Water enters the body of Arctic Waters within the GIN Sea indirectly through return flow from the Polar Sea than directly from the NwAtW.

The entire deep water circulation of the Arctic is primed by the annual production of GDW at a rate of $\sim$ 1 Sv. This does not imply that the cessation in GDW would stop the horizontal circulation of the deep waters. They would decay over a much longer period since they are driven by the intergrated pressure differences between the various basins. On the otherhand, the vertical circulation would be arrested accordingly. This distinction is made because in the case of the GIN Sea there is a rough equivalency between the horizontal and vertical transports. From the point of view of oxygen, or other component introduced via exposure to the atmosphere, distinction between horizontal or vertical renewal would make a large difference since the horizontal transports have a very much longer history within the Arctic deep water system. We give some examples.

The vertical renewal time for the GDW based on its annual production is about 30 yr, but the physical flushing time—considering the horizontal input of EADW — is $\sim$ 15 yr. However, this EADW has come from the Eurasian basin, which itself has

a physical flushing time on the order of 70 yr (using a volume of 4.0×10^6 km^3 and 1.8 Sv). This is complicated because of the age difference between the components of the EADW coming from the Canadian Basin versus those from the Greenland Basin. More than half of the EADW does not mix into the GDW but flows into the Norwegian Basin whence it upwells to overflow into North Atlantic. The vertical renewal time for the NwDW based only on the amount derived from the annual GDW production ($1/1.6 \times 0.8 = 0.5$ Sv) is also about 30 yr, but including the horizontal input of the EADW (0.5 Sv), gives a physical renewal time of$\sim$ 15 yr, i.e. similar to the GDW. However, if we consider the uNwDW volume ($\sim 1.1 \times 10^6$ km^3) and its total supply (3.2 Sv), we get $\sim$ 10 yr physical flushing time for that water mass. Vertical renewal of the uNwDW is about 15 yr, which is less than that calculated for the underlying NwDW. This does not imply that the uNwDW would reflect a more recent equilibration with the atmosphere, because only one of the three water masses mixing in vertically would have had recent atmospheric exposure, i.e. the ArIW. In fact, this component alone would render a $\sim$ 175 yr vertical renewal. One implication of this vertical structure would be the tendency to create an oxygen minimum layer within the uNwDW of physical (rather than biological) origin. Note, a slight minimum is found in the *CSS Hudson* data at $\sim$ 1000 m, **Clarke**, **Reid**, and **Swift** (1984).

Although the specific numerical values in the above examples are only approximate, they serve to potray the GIN Sea as having both an active vertical circulation and an active horizontal circulation. More accurate descriptions will clearly need better quantification of the horizontal input fluxes and of the atmospheric exchanges.

Appendix A

Categorization of works since 1972

An attempt has been made to categorize works on the GIN Sea since 1972 to provide an update of the bibliography of **Trangeled** (1974). The format of our approach differs somewhat so that in addition to an alphabetical listing, we provide functional grouping of the works. This was done in an information data base on a VAX 750 computer with VAX 11 Datatrieve software, which together with the database is available on request. The database consists of a data file for each work with the following information:

(a) *A sequential number.* These are used for the purposes of this report, namely to provide a simple identification. The numbers correspond to the works with the same number in the Bibliography.

(b) *Author(s).* (See Bibliography.)

(c) *Publication year.* (See Fig. A.1.)

(d) *Period of data acquisition.* (See Table A.1.)

(e) *Type of data.* The types of data are subdivided into the following groups: hydrographic, currents meter, chemical, model, waves, ice, satellite, meteorological, historical, and combinations. (See Table A.2.)

(f) *Geographic area.* This includes the following subdivisions: Greenland Sea, Norwegian Sea, Iceland Sea, North Atlantic, Polar Sea, Fram Strait, Denmark Strait, Iceland Færœ Ridge, Barents Sea, Færœse Channel and North Sea. For broader regions combinations of these subdivisions were used.

(g) *Type of study.* Data reports are distinguished in Table A.2 from analysis works by an asterisk after the accompanying sequence number.

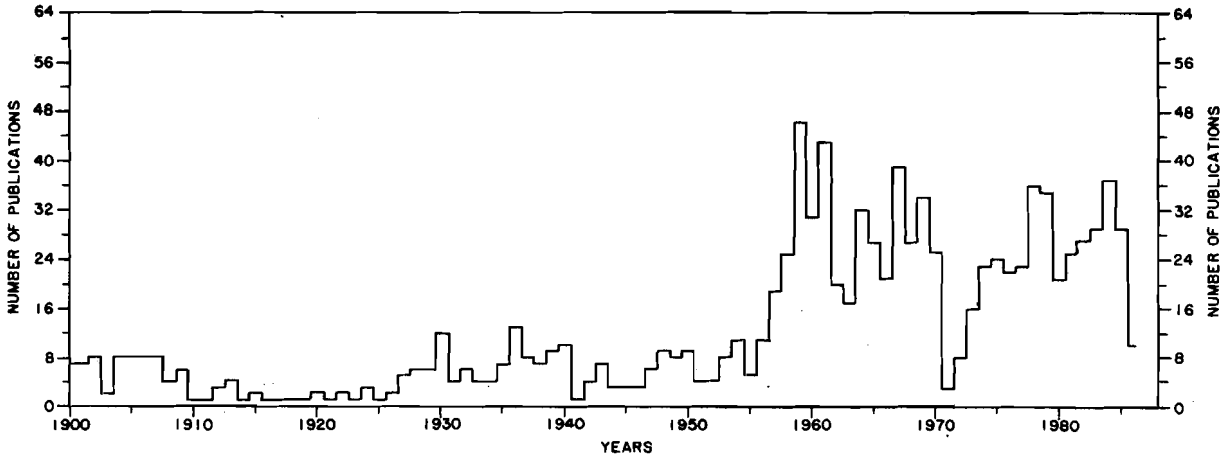

Fig. A.1. **A histogram showing the number of published works (physical oceanography) on the GIN Sea since 1900.**

Report no. changed (Mar 2006): SR-124-UU

Table A.1
Major cruises after 1972

Country	Ship	Period	Area
Canada (Overflow '73)	*CSS Hudson*	2/8–26/9 1973	Denmark Strait
UK (Overflow '73)	*Challenger*	21/8–14/9 1973	Færœse Channel
UK	*Cirolana*	21/8–14/9 1973	Færœse Channel
UK	*Explorer*	14/8–16/9 1973	Færœse Channel
UK	*Shackleton*	7/8–14/9 1973	Færœse Channel
UK	*O.W.S. Weather Adviser*	8/8–3/9 1973	Northeast Atlantic
UK	*O.W.S. Weather Monitor*	5/9–26/9 1973	Northeast Atlantic
Denmark (Overflow '73)	*Dana*	23/8–9/9 1973	Irminger Sea
Denmark/Færœs (Overflow '73)	*J.C. Svabo*	15/8–25/8 1973	Færœse Channel
USSR (Overflow '73)	*Boris Davydov*	14/8–13/9 1973	Iceland Sea
USSR	*Professor Viese*	7/8–22/9 1973	Denmark Strait
Norway (Overflow '73)	*Helland Hansen*	12/8–11/9 1973	Færœse Channel
Germany (Overflow '73)	*Walter Herwing I*	9/8–5/9 1973	Iceland-Færœ Ridge
	Walter Herwing II	8/9–19/9 1973	Denmark Strait
	Meerkatze 2	28/7–2/9 1973	Iceland-Færœ Ridge
	Meteor	5/8–26/9 1973	Iceland-Færœ Ridge
Iceland (Overflow '73)	*Bjarni Saemundsson*	10/8–10/9 1973	Iceland Sea Iceland-Færœ Ridge
Iceland	*B. Saemundsson*	Summer–1974	Iceland Sea–East Greenland Sea
		Winter–1975	Denmark Strait
Iceland	*Edisto*	Winter–1975	Denmark Strait

Table A.1. (Cont'd)
Major cruises after 1972

Country	Ship	Period	Area
USA	*USNS Kane*	Summers 1974, 1975	Between Iceland and Norwegian Sea
Norway	*R/V Polarsirkel*	Nov./Dec. 1977	North of Spitsbergen
Denmark	*R/V Polarsirkel*	1979–1983	Færœse Channel
UK	*R/V Polarsirkel*	1979–1985	Færœse Channel
USA	*USNS Kane*	14/8–3/11 1980	Færœse Channel
USA	*USNS Kane*	Sept.–Nov. 1980	Iceland-Færœ-Shetland and Norwegian Sea
Norway	*USNS Kane*	1981–1984	Greenland Sea
Denmark	*USNS Kane*	1982	Greenland Sea
Denmark	*USNS Kane*	1983–1984	Færœse Channel
USA	*CSS Hudson*	Feb.–Apr. 1982	Norwegian and Greenland Seas
Norway/Denmark	*CSS Hudson*	1982–1984	Norwegian and Greenland Seas
Iceland	*CSS Hudson*	1982–1984	SW of Iceland
Norway (MIZEX 83)	*R/V Polarbjorn*	18/6–2/8 1983	Eastern Fram Strait, Greenland Sea
USA (MIZEX 84)	*Lynch*	18/5–28/6 1984	Eastern Fram Strait, Greenland Sea
Norway (MIZEX 84)	*HU Sverdrup*	1–25/6 1984	Eastern Fram Strait, Greenland Sea
Norway	*MS Hakon Mosby*	12/6–30/7 1984	Eastern Fram Strait, Greenland Sea
USA (MIZEX 84)	*MV Polarqueen*	29/5–29/7 1984	Eastern Fram Strait, Greenland Sea
USA	*MV Kvitbjorn*	30/5–30/7 1984	Eastern Fram Strait, Greenland Sea
Germany (MIZEX 84)	*FS Polarstern*	11/6–18/7 1984	Eastern Fram Strait, Greenland Sea
Germany (MIZEX 84)	*FS Valdivia*	20/6–18/7 1984	Eastern Fram Strait, Greenland Sea
USA	*FS Valdivia*	1982–1984	Arctic Ocean
Germany	*FS Valdivia*	1982–1984	Arctic Ocean
Norway	*FS Valdivia*	1982–1984	Arctic Ocean

Table A.2
Listing of references according to type of data and geographic area

(a) Type of data

Hydrographic

8, 1*, 9, 5*, 7, 10, 13*, 19*, 20, 21*, 22*, 24*, 26*, 28, 27, 29, 30, 31*, 32*, 34, 35, 39*, 47*, 48, 49, 51, 50, 53, 52, 55*, 56, 63, 62, 64, 66, 68, 69*, 73*, 77*, 78, 80, 79*, 84, 85*, 81*, 86, 88, 89, 93, 94, 105*, 103, 106*, 102*, 110, 109, 111, 112, 117, 119, 121, 122, 123, 129, 130, 131, 133, 134, 135*, 138, 139, 140, 146, 152, 148, 153, 150, 147, 151, 154, 156, 158, 159, 161, 162*, 160, 163, 165*, 166, 167*, 169, 171, 172, 176, 180, 184, 199*, 190*, 193, 195, 196, 197, 198, 202, 203*, 204, 207, 206, 208*, 209, 210, 212, 215, 218, 213, 216, 214, 217, 221*, 222*, 223*, 227, 231, 234, 242, 243*

Currents

8, 1*, 11, 3*, 5*, 7, 6, 30, 40, 42, 47*, 48, 49, 51, 50, 52, 54, 55*, 63, 67, 60, 69, 74*, 76, 77*, 78, 79, 82, 86, 88, 98, 105*, 103, 106*, 102*, 104*, 109, 112, 114, 115, 116, 118, 123, 143, 145, 146, 148, 153, 150, 147, 149, 151, 161, 160, 163, 166, 174, 183, 185, 186, 190*, 189, 193, 191*, 203*, 207, 206, 201, 211, 215, 242

Chemical (nutrients + trace elements)

15, 19*, 28, 30, 31*, 32*, 34, 35, 37*, 47*, 56, 79*, 81*, 89, 93, 133, 151, 168, 176, 184, 206, 215, 218, 213, 216, 214, 220*

Modelling

14, 41, 42, 67, 93, 101, 111, 137, 148, 144, 141, 176, 206, 226, 235

Wave

13*, 79, 102

Ice

12, 106*, 104*, 113, 137, 172, 205, 238

Satellite

78, 103, 85*, 102, 124, 125, 126, 141, 157, 165*, 181, 188

Meteorological

5*, 13*, 14, 75, 40, 42, 47*, 67, 72*, 82, 85*, 86, 105*, 103, 106*, 102*, 116, 119, 118, 125, 137, 139, 146, 150, 149, 157, 182, 183, 187, 189, 196, 202, 210, 226, 235, 239, 242

Historical

5*, 10, 14, 28, 27, 29, 33, 34, 75, 45, 53, 54, 62, 66, 76, 77*, 82, 84, 85*, 86, 87, 88, 93, 101, 112, 113, 117, 121, 123, 131, 134, 135*, 137, 138, 139, 140, 148, 144, 145, 146, 153, 147, 159, 163, 184, 187, 196, 197, 201*, 202, 208*, 209, 218, 224, 227, 235, 238, 239, 240

Report no. changed (Mar 2006): SR-124-UU

Table A.2. (Cont'd)
Listing of references according to type of data and geographic area

(b) Geographysical area

Greenland Sea

1*, 3*, 5*, 10, 19*, 28, 27, 29, 31*, 32*, 33, 75, 56, 76, 77*, 86, 103, 111, 117, 119, 124, 125, 126, 135*, 137, 145, 157, 165*, 167*, 168, 171, 172, 176, 182, 187, 196, 202, 204, 216, 217, 220*, 224, 226, 231, 234, 238, 242

Norwegian Sea

5*, 10, 13*, 14, 19*, 21, 22*, 26*, 28, 31*, 32*, 33*, 75, 41, 42, 47 *, 49, 66, 67, 68, 69*, 77*, 80, 79*, 89, 93, 101, 102*, 110, 109, 116, 117, 119, 118, 121, 123, 139, 142, 143, 144, 141, 156, 159, 167*, 168, 169, 171, 176, 183, 184, 185, 187, 196, 197, 198*, 202, 204, 208*, 212, 221*, 223*, 224, 242

Iceland Sea

19*, 31*, 32*, 33, 54, 56, 94, 114, 117, 119, 130, 135*, 137, 169, 172, 187, 203*, 204, 209, 211*, 215, 213, 216, 224, 226, 227, 238

North Atlantic

41, 42, 49, 67, 115, 116, 183, 185, 186, 197

Polar Sea

8, 9, 5*, 24*, 33, 34, 35, 56, 101*, 106*, 104*, 112, 129, 154, 165*, 173, 201, 202, 217, 220*, 235

Fram Strait

1*, 11, 3*, 28, 29, 75, 76, 86, 105*, 106*, 104*, 122, 137, 165*, 177, 205, 226, 235

Denmark Strait

5*, 6, 37*, 113, 134, 140, 145, 153, 149, 166, 192*, 190*, 189, 193, 198*, 207, 206, 210, 215, 218, 216, 214, 227

Iceland-Færœ Ridge

7, 6, 15, 21*, 26, 75, 50, 53, 52, 54, 55*, 73*, 80, 79*, 82, 84, 89, 98, 138, 140, 148, 153, 150, 147, 161, 162*, 160, 182, 191, 204, 218, 221*, 222*, 223*, 243*

Barents Sea

5*, 13*, 14, 45, 66, 98, 121, 156, 198, 202, 217, 224

Færœ Channel

22, 31*, 32*, 36, 47*, 48, 49, 51, 50, 53, 54, 55*, 73*, 74*, 80, 79, 82, 85*, 81*, 89, 138, 152, 151, 162*, 181, 182, 184, 204, 223*

North Sea

31, 67, 68, 69, 77, 78, 116, 185

Appendix B

Gloassary of acronyms

AOG	Applied Oceanography Group
ARSW	Arctic Surface Water
ArIW	Arctic Intermediate Water
AtW	Atlantic Water
AtIW	Atlantic Intermediate Water
BrAtW	Barents Sea Atlantic Water
BrPW	Barents Sea Polar Water
BrBW	Barents Sea Bottom Water
BrW	Barents Sea Water
CDW	Canada Basin Deep Water
DW	Deep Water
EGC	East Greenland Current
EADW	Eurasian Basin Deep Water
eIShW	eastern Icelandic Shelf Water
ESC	East Spitsbergen Current
FAtW	Færœ Atlantic Water
GArSW	Greenland Arctic Surface Water
GAtIW	Greenland Atlantic Intermediate water
GArIW	Greenland Arctic Intermediate Water
GCM	Global Climatic Model
GDW	Greenland Sea Deep Water
GIN	Greenland-Iceland-Norwegian Sea
GPW	Greenland Polar Water
ICES	International Council for the Exploration of the Sea
ICW	Icelandic Current Water
ICIW	Icelandic Current Intermediate Water
IArIW	Iceland Arctic Intermediate Water
IArSW	Iceland Arctic Surface Water
IAtIW	Iceland Atlantic Intermediate Water
IC	Iceland Current
IFR	Iceland-Færœ Ridge
IrAtW	Irminger Atlantic Water
IW	Intermediate Water
JMAtIW	Jan Mayen Atlantic Intermediate Water
JMC	Jan Mayen Current
JMPW	Jan Mayen Polar Water
JONSDAP	Joint North Sea Data Acquisition Programme
MIZEX	Marginal Ice Zone Experiment
NABW	North Atlantic Bottom Water
NAtDW	North Atlantic Deep Water
NAtW	North Atlantic Water
NAtC	North Atlantic Current
NCaC	North Cape Current
NIIW	North Icelandic Winter Water
NIrC	North Irminger Current
nNSW	northern North Sea Water
NORSEX	Norwegian Remote Sensing Experiment
NwArIW	Norwegian Arctic Intermediate water
NwAtC	Norwegian Atlantic Current
NwAtW	Norwegian Atlantic Water
NwDW	Norwegian Sea Deep Water
NwCoC	Norwegian Coastal Current
NwShW	Norwegian Shelf Water
PAtIW	Polar Atlantic Intermediate Water
PIW	Polar Intermediate Water
PW	Polar Water
rAtIW	return Atlantic Intermediate water
uNwDW	upper Norwegian Deep Water
ShW	Shelf Waters
SW	Surface Water
WSC	West Spitsbergen Current

intentionally blank page

Bibliography

AAGAARD, K. Circulation of the Greenland Sea. *In*: UNITED STATES NAVY. Proceedings of the fifth Symposium on military oceanography, Panama City, Fl., volume I. Alexandria, VA, Oceanographer of the Navy, part I, 1968: 335–363.

AAGAARD, K. and COACHMAN, L.K. The East Greenland current north of Denmark Strait, part I, *Arctic*, **21**, 1968a: 181–200.

AAGAARD, K. and COACHMAN, L.K. The East Greenland current north of Denmark Strait, part II, *Arctic*, **21**, 1968b: 267–290.

AAGAARD, K. Wind-driven transports in the Greenland and Norwegian Seas. *Deep-Sea Research*, **17**, 1970: 281–291.

[1] AAGAARD, K. Greenland Sea currents, Technical Report. Seattle, University of Washington, 1972.

[2] AAGAARD, K. On the drift of the Greenland pack ice. *In*: Karlsson, T. *ed.* Sea Ice. Reykjavik, National Research Council of Iceland, 1972.

[3] AAGAARD, K., DARNALL, C. and GREISMAN, P. Year-long current measurements in the Greenland-Spitsbergen passage. *Deep-Sea Research*, **20**, 1973: 743–746.

[4] AAGAARD, K. and GREISMAN, P. Greenland Sea studies, TR–M75–98. Seattle, University of Washington, 1974.

[5] AAGAARD, K. and GREISMAN, P. Toward new mass and heat budgets for the Arctic Ocean. *Journal of Geophysical Research*, **80**, 1975: 3821–3827.

[6] AAGAARD, K. and MALMBERG, S.-A. Low-frequency characteristics of the Denmark Strait overflow. ICES C.M. C:47, 1978. (Unpublished document)

[7] AAGAARD, K. and MALMBERG, S.-A. OVERFLOW working Group. ICES observational summary, Mona 5–Mona 6. ICES '73 Expedition'. Contribution No. 50, 1978.

[8] AAGAARD, K. On the deep circulation in the Arctic Ocean. *Deep-Sea Research*, **28**, 1981: 251–268.

[9] AAGAARD, K., COACHMAN, L.K. and CARMACK, E.C. On the halocline of the Arctic Ocean. *Deep-Sea Research*, **28**, 1981: 529–545.

[10] AAGAARD, K., SWIFT, J.H. and CARMACK, E.C. Thermohaline circulation in the Arctic Mediterranean Seas. *Journal of Geophysical Research*, **90**, 1985: 4833–4846.

[11] AAGAARD, K., DARNALL, C., FOLDVIK, A. and TØRRESEN, T. Fram Strait current measurements, 1984–1985. Ref. No. 63. Bergen, University of Bergen, Department of Oceanography, Geophysical Institute, 1985.

ADROV, M.M. Hydrological investigations in the Kopytov area. *Trudy Poliarnyi Nauchno-Issledovatel'skii Institut Morskogo Rybnogo Khoziaistva i Okeanografii*, **10**, 1957: 198–211.

Report no. changed (Mar 2006): SR-124-UU

ADROV, M.M. Recent data concerning the hydrology of the north-eastern portion of the Barents Sea. *Trudy Poliarnyi Nauchno- Issledovatel'skii Institut Morskogo Rybnogo Khoziaistva i Okeanografii*, **11**, 1959: 5–25.

ADROV, M.M. Dissolved oxygen in the waters of the Iceland-Færœ Ridge area, June 1960. *Rapport et Procès-Verbaux des Réunions, Conseil International pour l'Exploration de la Mer*, **157**, 1967: 184–195.

AGENOROV, V.K. The dynamics of the waters of the Barents Sea. Moscow, Gidrometeoizdat, 1946. (In Russian).

ALEKSEEV, A.P. and ISTOSHIN, B.V. Scheme of constant currents in the Norwegian and Greenland Seas. *Trudy Poliarnyi Nauchno-Issledovatel'skii Institut Morskogo Rybnogo Khoziaistva i Okeanografii*, **9**, 1956: 62–68. [Translation: US Fishery Wildlife Service, Special Scientific Report 1956: 69–76.]

ALEKSEEV, A.P.and ISTOSHIN, B.V. Some results of oceanographic investigations in the Norwegian and Greenland Seas. *In*: Soviet Fisheries investigations in northern European seas. Moscow, The Polar Research Institute of Marine Fisheries and Oceanography (PINRO), 1960: 23–36.

[12] ANONYMOUS. Bathymetric map, Molloy Fracture Zone, Seabeam survey August 1984, *DPVFS POLARSTERN*. Bremerhaven, Alfred-Wegener Institut für Polarforschung, Hannover, Prakla-Seismos GmbH, Kiel, Geologisch-Paläontologisches Institut, 1985.

BALAKSIN, L.L. The water circulation and relief of the Northern part of the Greenland sea. International Oceanographic Congress, 1st, (preprints of abstracts: 1959: 430–431).

[13] BARSTOW, S.F., BJERKEN, S. and EIDNES, G. Environmental data collection along the Norwegian Coast. Wave and meteorological measurements on Haltenbanken. April–June 1985, ODAP Report No. 64. Okeanografisk Senter. Trondheim-NTH, Norway, SINTEF Gruppen-NHL, 1985.

[14] BATTEN, E. Sea ice conditions in the Norwegian, Barents and White Seas, DAHC15–73–C0181. Arlington, VA. Defense Advanced Research Project Agency, Department of Defence, 1976.

BEAL, M.A. Bathymetry and Structure of the Arctic Ocean. PH. D. Thesis, Oregon State University, 1968.

[15] BECKER, G.A. Is there a correlation between nutrients and water in the Iceland-Færœ Ridge area? ICES C.M. C:7, 1978. (Unpublished Document.)

BERGTHORSSON, P. An estimate of drift ice and temperature in Iceland in 1000 years. *Jokull*, **19**, 1969: 945–1001.

[16] BERGTHORSSON, P. Advection of climate by ocean currents. *In*: Karlsson, T. *ed.* Sea Ice. Reykyavik, National Research Council of Iceland, 1972.

[17] BERLIAND, T.G. and STROKINA, L.A. Global distribution of the total amount of cloudiness. Leningrad, Hydrometeorology Publishing House, 1980. (In Russian)

[18] BLINDHEIM, J. and LJÖEN, R. On the hydrographic conditions in the West Spitsbergen current in relation to ice distribution during the years 1956–1963. *In*: Karlsson, T. *ed.* Sea Ice. Reykjavik, National Research Council of Iceland, 1972.

BOISVERT, W.E. Major currents along the coast of Norway and the USSR to Kurils, NAVOCEANO SR–193. Washington D.C., Naval Oceanographic Office, 1970.

[19] BOCK, M., BECKER, G.A. and KOLTERMANN, K.P. First results from the *'Meteor'* deep water cruise in May–July 1982. ICES C.M. C:9, 1982. (Unpublished Document.)

BOWEN, I.S. The ratio of heat losses by conduction and by evaporation from any water surface. *Physical Review*, **27**, 1926: 779–787.

BOURKLAND, M.T. Oceanographic cruise summary western Greenland Sea, August–September 1965, IR–68–10. Washington D.C., Naval Oceanographic Office, 1968.

[20] BOYUM, G. Short-term variations in temperature and salinity off the west coast of Norway. Bergen, Geophysical Institute, Division A, Physical Oceanography, University of Bergen, 1975.

[21] BROOME, R.D. XBT profiles in the northeast Atlantic and Norwegian Sea. April–May 1981, data summary, ocean measurements program. NSTL Station, MS., US Naval Oceanographic Office, 1982.

[22] BROOME, R.D. XBT profiles in the northeast Atlantic and Norwegian Sea. September–November 1980, data summary, ocean measurements program. NSTL Station, MS., US Naval Oceanographic Office, 1982.

BRYAN, K. A numerical method for the study of the circulation of the world ocean. *Journal of Computational Physics*, **4**, 1969: 347–376.

[23] BRYAN, K. and COX, M.D. An approximate equation of state for numerical models of ocean circulation. *Journal of Physical Oceanography*, **2**, 1972: 510–514.

[24] BUCKLEY, J.R., EVJEN, A., GAMMELSROD, O.M., JOHANNESSEN, O. M., ROED, L.P. and ROYSET, H. Hydrographic observations from the cruise north of Spitsbergen. December 1977. Rep. 48. Bergen, Geophysical Institute, Division A, Department of Oceanography, University of Bergen, 1978.

[25] BUNKER, A.F. Computations of surface energy flux and annual air-sea ineraction cycles of the North Atlantic Ocean. *Monthly Weather Review*, **104**, 1976: 1122–1140.

[26] BURNS, D.A. and LOMBARD, N.V. XCP profiles in the vicinity of the Færœ Islands during october 1980, data summary. NSTL Station, MS, Naval Ocean Research and Development Activity, 1982.

[27] CARMACK, E.C. and AAGAARD, K. The formation of bottom water in the Greenland Sea. Colloques internationaux du CNRS No. 215. Processus de formation des eaux océaniques profondes. Paris 4–7 October 1972: 65–42.

[28] CARMACK, E.C. On the hydrography of the Greenland Sea. Ph. D. Thesis, University of Washington, 1972.

[29] CARMACK, E.C. and AAGAARD, K. On the deep water of the Greenland Sea. *Deep-Sea Research*, **20**, 1973: 687–715.

[30] CLARKE, R.A. and HILL, H. Current system south and east of the Grand Banks of Newfounland. *Journal of Physical Oceanography*, **10**, 1980: 25–65.

Report no. changed (Mar 2006): SR-124-UU

[31] CLARKE, R.A., REID, J.L. and SWIFT, J.H. *'CSS Hudson'* Cruise 88–001. 14 September–6 April 1982, volume 2: CTD data plots, SIO 84–14. La Jolla, CA., University of California, Scripps Institution of Oceanography, 1984.

[32] CLARKE, R.A., REID, J.L. and SWIFT, J.H. *'CSS Hudson'* Cruise 82–001. 14 February–6 April 1982, volume 1: Physical and chemical data, SIO 84–14. La Jolla, CA., University of California, Scripps Institution of Oceanography, 1984.

[33] COACHMAN, L.K. and AAGAARD, K. Physical oceanography of Arctic and Subarctic Sea. *In*: Herman, Y. *ed.* Marine Geology and Oceanography of the Arctic Seas. New York, NY, Springer, 1974.

CODISPOTI, L.A. Some results of an oceanographic survey in the northern Greenland Sea, summer 1964, NAVOCEANO TR–202. Washington D.C., US Naval Oceanographic Office, 1968.

[34] CODISPOTI, L.A. and LOWMAN, D. A reactive silicate budget for the Arctic Ocean. *Limnology and Oceanography*, **18**, 1973: 448–456.

[35] CODISPOTI, L.A. and OWENS, T.G. Nutrients transports through Lancaster Sound in relation to the Arctic ocean's reactive silicate budget and the outflow of Bering Strait waters. *Limnology and Oceanography*, **20**, 1975: 115–119.

[36] COLLAR, P.G. and CARTWRIGHT, D.E. Open sea tidal measurements near the edge of the northwest European continental shelf. *Deep-Sea Research*, **19**, 1972: 673–689.

COOPER, L.H.N. Deep water movements in the north Atlantic as a link between climatic changes around Iceland and biological productivity of the English Channel and Celtic Sea. *Journal of Marine Research*, **14**, 1955: 347–362.

[37] COOTE, A.R. and HILTZ, R.S. 'OVERFLOW'73' Denmark Strait, volume I: Oxygen and nutrient sections, BI–D–78–4, Data Series, Bedford Institute of Oceanography, 1978.

COUNTRYMAN, K.A. Oceanographic cruise summary, Denmark Strait April–May 1966, NAVOCEANO NOO–IR–68–37. Washington D.C., US Naval Oceanographic Office, 1968.

COUNTRYMAN, K.A. Some summer oceanographic features of the Norwegian Sea, Summer 1963, NAVOCEANO TR–216. Washington D.C., US Naval Oceanographic Office, 1968.

[38] COX, S.K. Measurements of cloud emissivity in the 8 to 13 micrometer wave band. *Journal of Applied Meteorology*, **10**, 1973: 260–265.

CREASE, J. The flow of Norwegian Sea water through the Færœ Bank Channel. *Deep-Sea Research*, **12**, 1965: 143–150.

[39] CURRIE, R.I., EDWARDS, A. and ELLETT, D.J. R.R.S. *'Challenger'* cruise 10/1973. Report and data list. ICES, Expedition 'OVERFLOW'73'. SMBA Internal reports C.R. Series No. 1, 1974: 1–23.

[40] DANIAULT, N., BLOUCH, P. and FUSEY, F.X. The use of free-drifting meteorological buoys to study winds and surface currents. *Deep-Sea Research*, **32**, 1985: 107–113.

[41] DAVIES, A.M. A numerical model of the North Sea and its use in choosing locations for the deployment of off-shore tide gauges in the JONSDAP'76 oceanographic experiment. *Deutsche Hydrographische Zeitschrift*, **29**; 1976: 11–24.

[42] DAVIES, A.M.,and HEAPS, N.S. Influence of the Norwegian Trench on the wind-driven circulation of the North Sea. *Tellus*, **32**, 1980: 164–175.

DEFANT, A. Physical Oceanography. Volumes. I and II. Oxford, UK, Pergamon Press, 1961.

DICKSON, R.R. and DODDINGTON, T.C. Hydrographic conditions of Spitsbergen in the summer of 1966 and 1967. *Annales biologiques*, **24**, 1968: 24–29.

DICKSON, R.R. and DODDINGTON, T.C. Hydrographic conditions of Spitsbergen in the summer of 1968 and 1969. *Annales biologiques*, **26**, 1970: 26–32.

DICKSON, R.R., MIDTTUN, L.S. and MUKHIN, A.I. The hydrographic conditions in the Barents Sea in August–September 1965–1968. Coop. Res. Report No. 18, 1970: 3–24.

[43] DICKSON, R.R. Variability and continuity within the Atlantic current of the Norwegian Sea. *Rapport et Procès-Verbaux des Réunions, Conseil International pour l'exploration de la Mer*, **162**, 1972: 167–183.

[44] DICKSON, R.R., LAMB, H.H., MALMBERG, S.-A. and COLEBROOK, J.H. Climatic reversal in Northern North Atlantic. *Nature*, **256**, 1975: 479–481.

[45] DICKSON, R.R. and BLINDHEIM, J. On the abnormal hydrographic conditions in the European Arctic during 1970s. *Rapport et Procès-Verbaux des Réunions, Conseil International pour l'exploration de la Mer*, **185**, 1984: 201–215.

[46] DICKSON, R.R., GOULD, W.J., GRIFFITHS, C., HEDLER, K.J. and GMITROWICZ, E.M. Seasonality in currents of the Rockall Channel. Ministry of Agriculture, Fisheries and Food, Directorate of Fisheries Research, Fisheries Laboratory, Lowestoft, 1986.

DIETRICH, G. A new atlas of the northern North Atlantic Ocean. *Deep-Sea Research*, **16**, 1969a: 31–34.

DIETRICH, G. Atlas of the hydrography of the northern North Atlantic Ocean. Based on the Polar survey of the International Geophysical Year, winter and summer 1958. ICES Outside Series, 1969b.

[47] DIETRICH, G. and HORN, W. Norwegian Sea expedition 1969. *METEOR Forschungsergebnisse*, **12**, 1973: 1–10.

[48] DOOLEY, H.D. Features of hydrography and currents in the Færœ-Shetland Channel during OVERFLOW'73. ICES C:31, 1975. (Unpublished Document.)

[49] DOOLEY, H.D. Hypotheses concerning the circulation of the Northern North Sea. *ICES, Journal du Conseil*, **36**, 1974: 54–61.

[50] DOOLEY, H.D., MARTIN, J.H.A. and PAYNE, R. Flow across the continental slope off northern Scotland. *Deep-Sea Research*, **23**, 1976: 875–880.

[51] DOOLEY, H.D. and CREASE, J. Observed and geostrophic currents south and east of Færœ during OVERFLOW'73. ICES C.M. C:53, 1978. (Unpublished Document.)

Report no. changed (Mar 2006): SR-124-UU

[52] DOOLEY, H.D. and MEINCKE, J. Circulation and water masses in the Færœse Channels during OVERFLOW'73. *Deutsche Hydrographische Zeitschrift*, **34**, 1981: 41–55.

DOOLEY, H.D. Seasonal variability in the position and strength of the Fair Isle current. *In*: Sünderman, L. *ed.* North Sea Dynamics, Heidelberg, Springer-Verlag, 1983.

DOOLEY, H.D., MARTIN, J.H.A. and ELLETT, D.J. Abnormal hydrographic conditions in the northeast Atlantic during the 1970s. *Rapport et Procès-Verbaux des Réunions, Conseil Permanent pour l'Exploration de la Mer*, **185**, 1984: 179–187.

[54] DOREY, S.W. A summary of current observations between Iceland and Norway, NAVOCEANO TN–6120–01–75. Washington D.C., US Naval Oceanographic Office, 1975.

[55] DOREY, S.W. Current-meter data report for observations between Iceland and Norway during 1975 and 1976, NAVOCEANO TN–3431–01–78. Washington D.C., US Naval Oceanographic Office, 1978.

[56] DORSEY, H.G. and PETERSON, W.H. Tritium in the Arctic ocean and east Greenland current. *Earth and Planetary Science Letters*, **32**, 1976: 342–350.

EGGVIN, J. Some results of the Norwegian hydrographical investigations in the Norwegian Sea during the International Geophysical Year. *Rapport et Procès-Verbaux des Réunions, Conseil International pour l'exploration de la Mer*, **149**, 1961: 212–218.

EGGVIN, J. Bathymetric chart of the Norwegian Sea and adjacent areas. Bergen, Fiskeridirektoratets Havforskings Institut, 1963.

EINARSSON, T. The ice in the North Polar Basin and in the Greenland Sea, and the general causes of occasional approach of the ice to the coast of Iceland. *Jokull*, **19**, 1969: 2–6.

[57] EINARSSON, T. Sea currents, ice drift, and ice composition in the East Greenland current. *In*: Karlsson, T. *ed.* Sea Ice. Reykjavik, National Research Council of Iceland, 1972.

[58] ELLETT, D.J. and MARTIN, J.H.A. The physical and chemical oceanography of the Rockall Channel. *Deep-Sea Research*, **20**, 1973: 585–625.

ELDER, R.B. Oceanographic observations between Iceland and Scotland. July–November 1965, Report No. 28–CG 373–28. Washington D.C., US Coast Guard Oceanographic Unit, 1970.

[62] ELLETT, D.J. and ROBERTS, D.G. The overflow of Norwegian Sea deep water across the Wyville–Thomson Ridge. *Deep-Sea Research*, **20**, 1973: 819–835.

[63] ELLETT, D.J. and EDWARDS, A. A volume transport estimate for Norwegian Sea overflow across the Wyville-Thomson Ridge. ICES C.M. C:19, 1978. (Unpublished Document.)

[64] EROFEEVA, E.S. Geostrophic currents of the north-eastern part of the Atlantic. *Trudy Institut Okeanologii Akademii Nauk*, **114**, 1972: 96–108.

Report no. changed (Mar 2006): SR-124-UU

[65] ESBENSEN, S.K. and KUSHNIR, Y. The heat budget of the global Ocean: an atlas based on estimates from surface marine observations, Climate Research Institute, Rep. No. 29. Corvallis, Oregon, Oregon State University, 1981.

FLETCHER, J.O. *ed.* The heat budget of the Arctic Basin and its relation to climate, RM 5233-NFS. Santa Monica, California, The Rand Corporation, 1966.

[66] FOSTER, L.A., JOHANNESSEN, O.M. and ISOPPO, C. Oceanographic summary of the Barents Sea south of Bear Island in the summer, SACLANTCEN SM-52. La Spezia, Italy, SACLANT ASW Research Centre, 1974.

[67] FURNES, G.K. Wind effects in the North Sea. *Journal of Physical Oceanography*, **10**, 1980: 978-984.

[68] FURNES, G.K., HACKETT, B. and SAETRE, R. Retroflection of Atlantic water in the Norwegian Trench. *Deep-Sea Research*, **33**, 1986: 247-265.

[69] FURNES, G.K. and SAELEN, O.H. Currents and hydrography in the Norwegian Coastal Current off Utsira during JONSDAP'76. The Norwegian Coastal Current Project, Report 2-77, 1-18, 1977.

[70] GATHMAN, S.G. Climatology. *In*: Hurdle, B.G. *ed.* The Nordic Seas. New York, NY, Springer, 1986.

[71] GORDON, A.L. Deep Antarctic convection west of Maud Rise. *Journal of Physical Oceanography*, **8**, 1978: 600-612.

[72] GORSHKOV, S.G. *ed.* World Ocean Atlas, volume 3. Arctic Ocean. New York, NY, Pergamon Press, 1983.

[73] GOTTHARD, G.A. Observed variations of the UK-Iceland GAP front, NAVOCEANO TN-6150-20-74. Washington D.C., US Naval Oceanographic Office, 1974.

[74] GOULD, W. MIAS current-meter data. Inventory of data series for sites between 57-63N 0-12W. Wormley, Godalming, Surrey, Marine Information-Advisory Service I.O.S., 1984.

GRASSHOFF, K. Some results of hydrographic investigations in the Iceland-Færœ Ridge area in March 1963. *Annales Biologiques*, **20**, 1963: 23-24.

[75] GREEGAN, A. A numerical investigation of the circulation in the Norwegian Sea. *Tellus*, **28**, 1976: 451-459.

[76] GREISMAN, P.E. Current measurements in the Eastern Greenland Sea. Ph. D. Thesis, University of Washington, Seattle, 1975.

[77] HACKETT, B. The Feie-Shetland section: A hydrographic atlas, Report No. 3-81. Bergen, Geophysical Institute, University of Bergen, 1981.

[78] HACKETT, B., FURNES, G.K. and SAETRE, R. Observations of the Atlantic inflow to the Norwegian Trench: January-March 1982. Report 59, Bergen, Geophysical Institute, Department of Physical Oceanography, University of Bergen, 1984.

[79] HALLOCK, Z.R. USNS Kane. Northeast Atlantic and Norwegian Sea survey operation 270980. Phases I, II, III, 16 September-28 November 1980. Ocean measurements program. NSTL Station, MS, US Naval Oceanographic Office, 1981.

[80] HALLOCK, Z.R. Variability of frontal structure in the Southern Norwegian Sea. *Journal of Physical Oceanography*, **15**, 1985: 1245–1254.

[81] HANSEN, B. and NIELSEN, A. Data report for the *'I.C. Svabo'* Cruises in the Færœ-Shetland Channel in connection with OVERFLOW'73, Rep. No. **27**. Institute of Physical Oceanography, University of Copenhagen, 1974.

[82] HANSEN, B. Sea level variations and currents on the Færœ Plateau and their relation to the hydrography, Institute of Physical Oceanography, Rep. No. 39. University of Copenhagen, 1978.

[83] HANSEN, B. Residual flow and temperature on the Færœ Plateau during the first half of 1978 in relation to the circulation. ICES, C.M. C: 18, 1979. (Unpublished Document.)

HANSEN, B. and MEINCKE, J. Eddies and meanders in the Iceland-Færœ Ridge area. *Deep-Sea Research*, **26**, 1979: 1067–1082.

[85] HANSEN, B. and MEINCKE, J. Long-term coastal sea surface temperature observations of the Færœ Islands. *Rapport et Procès-Verbaux des Réunions, Conseil International pour l'Exploration de la Mer*, **185**, 1984: 162–169.

[86] HANZLICK, D.J. The West Spitsbergen current: transport, forcing and variability. Ph. D. Thesis, University of Washington, Seattle, 1983.

HARVEY, J.G. OVERFLOW of cold deep water across the Iceland Greenland Ridge. *Nature*, **189**, 1961: 911–913.

HARVEY, J.G. The topography of the south-western Færœ Channel. *Deep-Sea Research*, **12**, 1965: 121–127.

[87] HARVEY, J.G. T–S relations and water masses in the eastern-north Atlantic. *Deep-Sea Research*, **29**, 1982: 1021–1033.

HASTINGS, H.D. Surface climate of the Arctic Basin, Rep. 7R–71–5. Fort Belvoir, VA. US Army Engineer Topographic Laboratories, 1971.

[88] HEAPS, N.S. A mechanism for local upwelling along the European continental slope. *Oceanologica Acta*, **3**, 1980: 449–454.

HELLAND-HANSEN, B. Report on hydrographical investigations in the Færœ-Shetland Channel and the northern part of the North Sea in 1902. Report on Fishery Hydrographic Investigation in the North Sea and Adjacent Waters, 1905a.

HELLAND-HANSEN, B. and NANSEN, F. The Norwegian Sea, its physical oceanography. Based on the Norwegian researches 1900–1904. Report on Norwegian Fishery and Marine-Investigations, Bergen, 2(2), 1909.

HELLAND-HANSEN, B. The Sognefjord section. Oceanographic observations in the northernmost part of the North Sea and the southern part of the Norwegian Sea. James Johnstone Memorial Volume. Liverpool, University Press, 1934: 257–274.

HERMANN, F. The T–S diagram analysis of the water masses over the Iceland-Færœ Ridge and in the Færœ Bank Channel. *Rapport et Procès-Verbaux des Réunions, Conseil International pour l'Exploration de la Mer*, **157**, 1967: 139–149.

[89] HERR, F.L., SCRANTON, M.I. and BARGER, W.R. Dissolved hydrogen in the Norwegian Sea: mesoscale surface variability and deep-water distribution. *Deep-Sea Research*, **28**, 1981: 1001–1016.

[90] HIBLER, W.D.III. A dynamic thermodynamic sea ice model. *Journal of Physical Oceanography*, **9**, 1979: 815–846.

[91] HIBLER, W.D.III. Modelling a variable thickness sea ice cover. *Monthly Weather Review*, **108**, 1980: 1943–1973.

[92] HIBLER, W.D.III. and BRYAN, K. A large-scale ice/ocean model for the marginal ice zone. *MIZEX Bulletin*, III, April 1984. HILL, H.W. and LEE, A.J. The effect of the wind on water transport in the region of the Bear Islands fisheries. *Proceedings of the Royal Society*, **148**, 1959: 104–116.

[93] HOFFERT, M.I. and BROECHER, W.S. Apparent vertical diffusion rates in the pycnocline of the Norwegian Sea as determined from the vertical distribution of tritium. *Geophysical Research Letters*, **5**, 1978: 502–504.

[94] HOJERSLEV, N. and LUNGREN, B. Inherent and apparent optical properties of Icelandic waters, *'Bjarni Saemundsson'* 'OVERFLOW'73'. Copenhagen, Institute of Physical Oceanography, University of Copenhagen, 1977.

HOPKINS, T.S. Physical processes in the Mediterranean Basin. *In*: Kjerfve, B. *ed.* Estuarine Transport Processes. Columbia, University of South Carolina Press, 1978.

[95] HOPKINS, T.S. and GARFIELD, III N. Physical origins of Georges Bank water. *Journal of Marine Research*, **39**, 1981: 465–500.

[96] HUNKINS, K. Current and temperature data from instrument moorings in Fram Strait during MIZEX 83', TR-LDGO-84-1. Palisades, New York, Lamont Doherty Geological Observatory of Columbia University, 1984.

[97] HURDLE, B.G., *ed.* The Nordic Seas. New York, NY, Springer, 1986.

[98] HUTHNANCE, J.M. Large tidal currents near Bear Island and related tidal energy losses from the North Atlantic. *Deep-Sea Research*, **28**, 1981: 51–70.

[99] ICES Working Group OVERFLOW'73. OVERFLOW'73 Inventory ICES Oceanographic Data Lists and Inventories, No. 29. ICES OVERFLOW'73 Expedition Contribution No. 18, 1976.

[100] ICES (SMEDS, J. *ed.*) JONSDAP'76 Inventory. ICES Oceanographic Data Lists and Inventories, No. 107, 1984.

JACOBSEN, J.P. The Atlantic current through the Færœ-Shetland Channel and its influence on the hydrographical conditions in the northern part of the North Sea, the Norwegian Sea and the Barents Sea. *Rapport et Procès-Verbaux des Réunions, Conseil International pour l'exploration de la Mer*, **112**, 1943: 5–47.

JAKHELLN, A. Oceanographic investigations in the East Greenland waters in the summer of 1930–1932. *Skrifter om Svalbard og Ishavet*, **67**, 1936.

[101] JAMES, I.D. and McCLIMANS, T.A. Coastal current whirls in laboratory and numerical models. *Ocean Modelling*, **53**, 1983: 1–3.

Report no. changed (Mar 2006): SR-124-UU

[102] JOHANNESSEN, O.M. and MORK, M. Remote sensing experiment in the Norwegian coastal waters, spring 1979, Report 3–79. Bergen, Geophysical Institute, University of Bergen, 1979.

[103] JOHANNESSEN, O.M. and JOHANNESSEN, J.A. Oceanographic conditions in the marginal ice zone north of Svalbard in early fall 1979 with an emphasis on mesoscale processes. *Journal of Geophysical Research*, **88**, 1983: 2755–2769.

[104] JOHANNESSEN, O.M., SANDVEN, S., JOHANNESSEN, J.A. and MYKING, S. Current, temperature and salinity measurements from drifting ice floes. Bergen, Geophysical Institute, Division A, Physical Oceanography, University of Bergen, 1984.

[105] JOHANNESSEN, J.A., JOHANNESSEN, O.M. et al. A CTD data report from the marginal ice zone experiment (MIZEX) in the Fram Strait—East Greenland Sea region in June–August 1983. Bergen, Geophysical Institute, Division A, Physical Oceanography, University of Bergen, 1984.

[106] JOHANNESSEN, O.M., JOHANNESSEN, J.A. and SANDVEN, S. MIZEX Ocea nography. Ice, ocean eddies and internal waves. Preliminary results. Bergen, Geophysical Institute, Division A, Physical Oceanography, University of Bergen, 1985.

[107] JOHANESSEN, O.M. Brief overview of the physical oceanography. *In*: Hurdle, B.G. *ed.* The Nordic Seas. New York, NY, Springer, 1986: 103–127.

JOHNSON, G.L. and ECKHOFF, O.B. Bathymetry of the north Greenland Sea. *Deep-Sea Research*, **13**, 1966: 1161–1173.

JOSEPH, J. The bottom topography of the Iceland-Færœ Ridge region. *Rapport et Procès-Verbaux des Réunions, Conseil International pour l'exploration de la Mer*, **157**, 1967a: 16–17.

JOSEPH, J. Current measurements during the international Iceland-Færœ Ridge expedition, 30 May to 18 June 1960. *Rapport et Procès-Verbaux des Réunions, Conseil International pour l'exploration de la Mer*, **157**, 1967b: 157–172.

JOSEPH, J. Observations of the depth of visibility, vertical temperature and turbidity recordings in the sea between Iceland and the Færœs during the ICES Iceland-Færœ Ridge expedition, May-June 1960. *Rapport et Procès-Verbaux des Réunions, Conseil International pour l'exploration de la Mer*, **157**, 1967c: 223–237.

[108] KAGAN, B.A. Global interaction of ocean an terrestrial tides. (In Russian), Leningrad, Gidrometeoizat, 1976.

[109] KARABASHEVA, E.I., POZDYNIN, V.D. and SHKURENKO, V.I. Small-scale turbulence in the Norwegian Sea and in the Gulf Stream. *Oceanology*, **15**, 1976: 27–30.

[110] KARABASHEVA, E.I. and POZDYNIN, V.D. Statistical description of horizontal surface temperature gradients in the north Atlantic and the Norwegian Sea. *Oceanology*, **18**, 1979: 405–407.

[111] KILLWORTH, P.D. On 'chimney' formation in the ocean. *Journal of Physical Oceanography*, **9**, 1979: 531–554.

[112] KILLWORTH, P.D., and SMITH, J.M. A one-and-a-half dimensional model for the Arctic halocline. *Deep-Sea Research*, **31**, 1984: 271–293.

KISLYAKOV, A.G. Fluctuations in the regime of the Spitsbergen current. *In*: Soviet Fisheries Investigations in the northern European seas. Moscow, The Polar Research Institute of Marine Fisheries and Oceanography (PINRO), 1960: 39–49. (In Russian).

[113] KOGAN, B.A. Variability of ice conditions in the Danish Strait. *Problemy Arktiki i Antarktikti Sbornik Statei*, **50**, 1977: 129–133.

KOCH, L. The East Greeland Ice. *Meddelelser om Gronland*, **130**(3), 1945: 1–373.

[114] KOLTERMANN, K.P. The tidal current constituents during OVERFLOW'73 . ICES C.M. C:8, 1978. (Unpublished document.)

[115] KOLTERMANN, K.P. Examples of flow pattern of the northern North Sea during JONSDAP '76. ICES C.M. C:39, 1978. (Unpublished Document.)

[116] KOLTERMANN, K.P. Low-frequency variations of currents and water levels in the northern North Sea during JONSDAP'76. *In*: The Norwegian Coastal Current. Proceedings from the Norwegian Coastal Current Symposium, Geilo, 9–12 September, **1**, 1981: 72–92.

[117] KOLTERMANN, K.P. and MACHOCZEK, D. On the climatological mean state distribution of temperature and salinity in the Greenland Sea. ICES C.M., C:39, 1985. (Unpublished Document.)

[118] KORT, V.G., TITOV, V.B. and OSADCHIY, A.S. Kinematics and structure of currents in a study area in the Norwegian Sea. *Oceanology*, **17**, 1977: 505–508.

[119] KORT, V.G. and TARASENKO, V.M. Synoptic variability of the Norway current. *Oceanology*, **17**, 1977: 379–382.

[120] KOZO, T.L. and TUCKER, W.B. Sea ice bottomside features in the Denmark Strait. *Journal of Geophysical Research*, **79**, 1974: 4505–4511.

[121] KUDLO, B.P. Some data on the water exchange between the Barents and Norwegian Seas, NAVOCEANO NOO-Trans-350. Washington D.C., US Naval Oceanographic Office, 1961.

KUDLO, B.P. and ERSHTADT, T.A. On the adaptability of the dynamic method of calculating current elements in the Barents Sea. *GOIN, Trudy*, **86**, 1965: 100–111.

[122] KULLENBERG, J.G. Observations of light-scattering distributions in the transition zone to the Arctic Ocean. *Rapport et Procès-Verbaux des Réunions, Conseil International pour l'Exploration de la Mer*, **185**, 1984: 102–110.

[123] KUSHNIR, V.M., PARAMONOV, A.N. and ZABURDAYEV, V.I. The structure of thermocline oscillations in the Norwegian Sea. *Oceanology*, **17**, 1977: 387–390.

KVINGE, T., LEE, A.J. and SAETRE, R. Report on study of variability in the Norwegian Sea, April–May 1967. Bergen, Geophysical Institute, University of Bergen, 1968.

LACOMBE, H. Physical Oceanography of the eastern boundary current of the Atlantic ocean. ICSU/SCOR working part 3, symposium, Cambridge. London, Institute of Geological Sciences, 70/13, 1970: 47–65.

LAKTIONOV, A.F. Bottom topography of the Greenland Sea in the region of the Nansen' sill. *Priroda*, **10**, 1959: 95–97.

LAKTIONOV, A.F., SHAMONT'EV, V.A. and IANES, A.V. Oceanographic characteristics of the north Greenland Sea. *In*: Soviet Fisheries investigations in north European Seas. Moscow, The Polar Research Institute of Marine Fisheries and Oceanography (PINRO), 1960: 51–65.

LAPPO, S.S. Deep currents in the north Atlantic Ocean. *Deep-Sea Research*, **11**, 1964: 435–439.

[124] LA VIOLETTE, P.E. and DIACHOK, O.I. The use of APT satellite imagery in a subarctic airborne oceanographic survey. *Journal of Arctic Institute of North America*, **27**, 1974: 306–308.

[125] LA VIOLETTE, P.E. and HUBERTZ, J.M. Surface circulation patterns off the east coast of Greenland as deduced from satellite photographs of ice floes. *Geophysical Research Letters*, **2**, 1975: 400–402.

LEE, A.J. The variability of the Atlantic current in the Norwegian Sea. *Annual Report and Proceeding of the Challenger Society. Edinburgh*, **4**, 1969: 54–55.

LEE, A.J. and HILL, H.W. The effect of the wind on water transports in the region of the Bear Islands fishery. *Proceedings of the Royal Society*, **148**, 1959: 104–116.

LEE, A.J. The hydrography of the European Arctic and Subarctic Seas. *Oceanography Marine Biology Annual Review*, **1**, 1963: 47–76.

LEE, A.J. Temperature-depth records by the research vessel *'Ernest Holt'*. *Rapport et Procès-Verbaux des Réunions, Conseil International pour l'exploration de la Mer*, **157**, 1967: 223–237.

LEONOV, A.K. Experimental quantitative computation of the transport of water, heat and salts into the Arctic Basin by the Atlantic and Pacific currents. *Meteorologiya i Hidrologiya*, **5**, 1955.

[126] LEPPARANTA, M. Investigations of the ice dynamics in the marginal ice zone. Helsinki, Institute of Marine Research, 1984.

[127] LEVITUS, S. Climatological atlas of the world ocean. NOAA Publ. 13, Washington D.C., US Department of Commerce, 1982.

[128] LEWIS, E.L. and PERKIN, R.G. Supercooling and energy exchange near the Arctic Ocean surface. *Journal of Geophysical Research*, **88**, 1983: 7681–7685.

[129] LIND, R.J and KATSAROS, K.B. A model of longwave irradiance for use with surface observations. *Journal of Applied Meteorology*, **21**, 1982: 1015–1023.

LUNDE, T. Ice conditions in the Svalbard region 1946–1963. *Arbok, Norsk Polar Institutt*, 1963: 61–80.

[130] LUNDGREN, B. and HOJERSLEV, N. Inherent and apparent optical properties of Icelandic waters. *'Bjarni Saemundsson* 'OVERFLOW'73'. ICES. C.M. C:25, 1977. (Unpublished Document.)

[131] MAILLARD, C. Mean circulation in the north east Atlantic from historical data. Brest, France, Centre Océanologique de Bretagne, 1981.

MALMBERG, S.-A., GADE, H.G. and SWEERS, H.E. Report on the second joint Iceland-Norwegian expedition to the area between Iceland and Greenland in

August–September 1965. Reykjavik. NATO Subcommitte on Oceanographic Research. TR–41. Irminger Sea project, 1967.

[132] MALMBERG, S.-A., GADE, H.G. and SWEERS, H.E. Current velocities and volume transports in the East Greenland current off Cape Nordenskjold in August–September 1965. *In*: Karlsson, T. *ed.* Sea Ice. Reykjavik, National Research Council of Iceland, 1972.

[133] MALMBERG, S.-A. A note on the deep water south of Iceland OVERFLOW'73. ICES. C.M. C: 32, 1974. (Unpublished Document.)

[134] MALMBERG, S.-A. On the hydrography of the Denmark Strait overflow. ICES. C.M. C: 48, 1978. (Unpublished Document.)

[135] MALMBERG, S.-A. Hydrographic conditions in the East Icelandic current and sea ice in north Icelandic waters, 1970–1980. *Rapport et Procès-Verbaux des Réunions, Conseil International pour l'exploration de la Mer*, **185**, 1984: 170–178.

MANN, C.R. Temperature and salinity characteristics of the Denmark Strait overflow. *Deep-Sea Research*, **16**, supplement, 1969: 125–137.

[136] MANTYLA, A. and REID, J.L. Abyssal characterisics of the world ocean water. *Deep-Sea Research*, **30**, 1981: 805–833.

[137] MARKHAM, D.G. Ocean mixing and circulation response in the marginal Ice zone. Master's Thesis, Naval Postgraduate School Monterey, California, 1983.

[138] MARTIN, J.H.A. Long term changes in the Færœ-Shetland Channel associated with intrusions of Iceland-Færœ Ridge water during the period 1955–1975. ICES. C.M. C: 22, 1976. (Unpublished Document.)

[139] McCARTNEY, M.S. and TALLEY, L.D. Warm water to cold water conversion in the northern north Atlantic and its relation to the general circulation. *Journal of Physical Oceanography*, **14**, 1984: 922–935.

[140] McCARTNEY, M.S. and TALLEY, L.D. The subpolar mode water of the north Atlantic Ocean. *Journal of Oceanography*, **12**, 1982: 1169–1188.

[141] McCLIMANS, T.A. and NILSEN, J.H. Whirls in the Norwegian coastal current. *In*: Gade, H.G., Edwards, A. and Svendsen, H. *ed.* Coastal oceanography. New York, NY, Plenum, 1982.

[142] McCLIMANS, T.A. Laboratory simulation of river plumes and coastal currents. ASME Symposium on modelling of environmental flow systems, Boston, 1983.

[143] McCLIMANS, T.A. and LONSET, L. Oscillations of frontal currents. *Continental Shelf Research*, **4**, 1985: 609–707.

[144] McCLIMANS, T.A., VINGER, A. and MORK, M. The role of FROUDE number in models of baroclinic coastal currents. *Ocean Modelling*, **62**, 1985: 14–17.

[145] McDONNEL, S. Surface currents, Greenland Sea including Denmark Strait.

[146] McDOUGALL, T.J. Greenland sea bottom water formation: a balance between advection and double-diffusion. *Deep-Sea Research*, **20**, 1983: 1109–1117.

MEINARDUS, A. Periodic variation in the ice drift around Iceland. *Annales Hydrographiques*, **34**, 1906.

Report no. changed (Mar 2006): SR-124-UU

[147] MEINCKE, J. The hydrographic section along the Iceland-Færœ Ridge carried out by R.V. *'Anton Dohrn'* in 1959–1971. *Berichte der Deutschen Wissenschaftlichen Kommission für Meeresforschung*, **22**, 1972: 372–384.

[148] MEINCKE, J. OVERFLOW'73. Large scale features of the overflow across the Iceland-Færœ Ridge. ICES. C.M. C:7, 1974. (Unpublished Document.)

[149] MEINCKE, J. OVERFLOW'73. Evidence for atmospheric forcing of Arctic water overflow events. ICES. C.M. 29, 1975. (Unpublished Document.)

[150] MEINCKE, J. Coupling between bottom currents and weather pattern in the Iceland-Færœ Ridge. ICES. C.M. C:30, 1976. (Unpublished Document.)

[151] MEINCKE, J. and KVINGE, T. On the atmospheric forcing of overflow events. ICES. C.M. C: 9, 1978. (Unpublished Document.)

[152] MEINCKE, J. On the distribution of low salinity intermediate waters around the Færœs. *Deutsche Hydrographische Zeitschrift*, **31**, 1978: 50–64.

[153] MEINCKE, J. The modern current regime across the Greenland Scotland Ridge. *In*: Bott, M.H.P., Saxov, S., Talwani, M. and Thiede, J., *eds*. Structure and Development of the Greenland Scotland Ridge, new methods and concepts, proceedings of a NATO Advanced Research Institute held at Padua University, 11–15 May,1981. New York, NY, Plenum Press, 1983.

[154] MELLING, H. and LEWIS, E.L. Shelf drainage flows in the Beaufort Sea and their effect on the Arctic Ocean pycnocline. *Deep-Sea Research*, **29**, 1982: 967–985.

[155] MESERVE, J.M. US Navy marine climatic atlas of the world. volume I. North Atlantic ocean, Rep. 50–1C–528. Washington D.C., Naval Air Systems Command, 1974.

METCALF, W.G. On the formation of bottom water in the Norwegian basin. *Transactions, American Geophysical Union*, **36**, 1955.

METCALF, W.G. A note on water movement in the Greenland and Norwegian Seas. *Deep-Sea Research*, **7**, 1960: 190–200.

MIDTTUN, L. Variability of temperature and salinity at some localities off coast of Norway. *Progress in Oceanography*, **5**, 1969: 41–54.

[156] MIDTTUN, L. Formation of dense bottom water in the Barents Sea. *Deep-Sea Research*, **32**, 1985: 1233–1241.

[157] MITCHELL, P.A. Ice drift in the east Greenland sea as derived from satellite imagery, NAVOCEANO TN–6150–23–74. Washington D.C., US Naval Oceanographic Office, 1974.

MOHN, H. The north Ocean, its depths, temperature and circulation. The Norwegian North Atlantic expedition 1876–1878, 2(2), 1887.

[158] MOLINA-CRUZ, A. and THIEDE, J. The glacial eastern boundary current along the Atlantic Eurafrican continental margin. *Deep-Sea Research*, **25**, 1978: 337–355.

MOSBY, H. Recherches océanographiques dans la Mer de Norvège à la Station météorologique 'M'. *Cahiers du Centre de Recherches et d'Etudes Océanographiques*, Paris, 1950.

MOSBY, H. Water, salt and heat balance of the North Polar Sea and the Norwegian Sea. *Geophysiske Publikationer* 24(11), 1962c.

MOSBY, H. *'Armauer Hansen'* in the Norwegian Sea, 1935, tables. Bergen, Norway. Geophysical Institute, University of Bergen, 1966a.

MOSBY, H. *'Armauer Hansen'* in the Norwegian Sea, 1936, tables. Bergen, Norway. Geophysical Institute, University of Bergen, 1966b.

MOSBY, H. Norwegian Atlantic current March and December 1965, tables. Bergen, Norway. Geophysical Institute, University of Bergen, 1969: 1–54.

[159] MOSBY, H. Diffusion of bottom water in the Norwegian Sea. *Colloques Internationaux du CNRS* No. 215. Processus de formation des eaux océaniques profondes, Paris 4–7 October 1972, 1972: 59–64.

[160] MÜLLER, T.J., SCHOTT, F.A., SIEDLER, G. and KOLTERMAN, K.P. OVERFLOW'73. Observations in a small scale overflow event on the Iceland-Færœ Ridge. ICES. C.M. C:6, 1974. (Unpublished Document.)

[161] MÜLLER, T.J., SCHOTT, F.A. and SIEDLER, G. Observations of overflow on the Iceland-Færœ Ridge. *Meteorologische, Rundschau*, 1974: 49–55.

[162] MÜLLER, T.J., MEINCKE, J. and BECKER, G.A. ICES-expedition OVERFLOW'73. The distribution of water masses on the Greenland-Scotland Ridge in August–September 1973. ICES expeditions OVERFLOW'73, Contribution. No. 62. Kiel, Institut für Meereskunde, Kiel, 1979.

[163] MYSAK, L.A. and SCHOTT, F. Evidence for baroclinic instability of the Norwegian current. *Journal of Geophysical Research*, **82**, 1977: 2087–2095.

NANSEN, F. The Arctic ocean. Encyclopedia Britannica, **31**, 1902a: 808–812.

NANSEN, F. Oceanography of the Polar Basin. Norwegian North Polar expedition, 1893–1896, Scientific results, 3(9), 1902b.

NANSEN, F. Northern waters. Captain Roald Amudsen's oceanographic observations in the Arctic Seas in 1901 with a discussion of the origin of the bottom waters in the Northern Seas. *Videnskabsselskabets Skrifter, Matematisk-Naturvidenskabelig Klasse*, 3(1), 1906.

NANSEN, F. Blant Sel og Bjorn. Min forste Ishavsferd. (Between Seal and Bear. My first voyage to the Polar Sea.) Oslo, Cristiania, 1924.

[164] NIILER, P.P. and MYSAK, L.A. Barotropic waves along and eastern continental shelf. *Geophysical Fluid Dynamics*, **2**, 1971: 273–288.

[165] NORSEX ARCTIC WORKING GROUP. The Norwegian remote sensing experiment (NORSEX) in a marginal ice zone. *Journal of Geophysical Research*, (Submitted July 1981).

[166] OAKEY, N.S. and ELLIOTT, J.A. The variability of temperature gradient microstructure observed in the Denmark Strait. *Journal of Geophysical Research*, **85**, 1980: 1933–1944.

ORVIG, S. *ed.* World Survey of Climatology. volume 14. Climate of the Polar Regions. Amsterdam, Elsevier, 1970.

OTTO, L. Currents and water balance in the North Sea. *In*: Sünderman, J. and Lenz, W. *ed.* North Sea Dynamics. Berlin, Springer, 1983: 26–43.

[167] OSTERHUS, S., LARS, G. and SAELEN, O.H. Report from cruise whith R/V *'Hakon Mosby'* to the Norwegian-Greenland seas. July 1984, Report No. 62. Bergen, Norway, University of Bergen, 1985.

[168] OSTLUND, H.G., DORSEY, H.G. and ROOTH, C.G. Geosecs North Atlantic radiocarbon and tritium results. *Earth and Planetary Science Letters*, **23**, 1974: 69–86.

PALFREY, K.H. Physical oceanography of the Northern part of the Greenland Sea in the summer of 1964. Master's Thesis, University of Washington, Seattle, 1967.

[169] PAQUETTE, R.G. BOURKE, R.H. NEWTON, J.F. and PERDUE, W.F. The east Greenland Polar front in autumn. *Journal of Geophysical Research* **90**, 1985: 4866–4882.

[170] PEGGION, G. A method for determining absolute velocities from hydrographic data. SACLANTCEN SR–114, La Spezia, Italy, SACLANT ASW Research Centre. 1987.

[171] PENIN, V.V. On the question of current dynamics in the Norwegian and Greenland Seas, NRL–Trans. 1257. Washington D.C., US Naval Research Laboratory, 1972.

[172] PERDUE, W.F. Oceanographic investigation of the east Greenland Polar front in autumn. Master's Thesis, Monterey, Naval Postgraduate School, 1982.

[173] PERKIN, R.G. and LEWIS, E. Mixing in the west Spitsbergen current. *Journal of Physical Oceanography*, **14**, 1984: 1315–1325.

[174] PERRY, R.K., FLEMING, H.S. et al. Bathymetry of the Norwegian-Greenland and Western Barents Seas. Naval Research Laboratory, Acoustic Division, Environmental Sciences Branch, 1980.

[175] PERRY, R.K. Bathymetry. *In*: Hurdle, B.G. *ed.* The Nordic Seas. New York, NY, Springer, 1986: 211–234.

[176] PETERSON, W.H. and ROOTH, C.G. Formation and exchange of deep water in the Greenland and Norwegian Seas. *Deep-Sea Research*, **23**, 1976: 273–283.

[177] PERKIN, R.G. and LEWIS, E. Mixing in the west Spitsbergen current. *Journal of Physical Oceanography*, **14**, 1984: 1315–1325.

[178] PHILANDER, S.G.M. Forced oceanic waves. *Reviews of Geophysics and Space Physics*, **16**, 1978: 15–46.

[179] PIACSEK, S. and GRILLAKI, D. Terra Cognita, **6**, 1986: 369.

[180] PINGREE, R.D. and MORRISON, G.K. The relationship between stability and source waters for a section of the north east Atlantic. *Journal of Physical Oceanography*, **13**, 1973: 280–285.

[181] PINGREE, R.D. Cyclonic eddies and cross-frontal mixing. *Journal of Marine Biology*, **58**, 1978: 955–963.

[182] PULS, K.E. and MEINCKE, J. General atmospheric circulation and weather conditions in the Greenland-Scotland area for August–September 1973. *Berichte aus dem*

Institut für Meereskunde an der Christian-Albrechts-Universität, Kiel, **14**, 1975: 1–24.

[183] RAMSTER, J.W. North Sea oceanography: the current situation and possible future developments. *In*: Watt, D.C. *ed.* The North Sea: a New International Regime. Guildford, England, Wesburg House, 1980.

[184] REID, J.L. On the contribution of the Mediterranean Sea outflow to the Norwegian-Greenland sea. *Deep-Sea Research*, **26**, 1979: 1199–1223.

[185] RIEPMA, H.W. Residual currents in the North Sea during the in/out phase of 'JONSDAP 76'. (First results extended) ICES C.M., C:48, 1978. (Unpublished Document.)

[186] RIEPMA, H.W. Short time temperature variations and tidal current constants in the North Sea south east of the Dogger Bank. *Deutsche Hydrographische Zeitschift*, **33**, 1980: 82–89.

[187] ROGERS, J.C. and VAN LOON, H. The seasaw in winter temperatures between Greenland and Northern Europe. Part II: Some oceanic and atmospheric effects in middle and high latitudes. *Monthly Weather Review*, **107**, 1979: 509–519.

[188] ROSS, C.K. OVERFLOW '73. Transport of overflow water through Denmark Strait. ICES C.M. C:16, 1976. (Unpublished Document.)

[189] ROSS, C.K. OVERFLOW '73. Denmark Strait, volume 2. (Moored instrument time series). Institute of Oceanography, Data Series, B1–D–77–5, 1979.

[190] ROSS, C.K. OVERFLOW variability in Denmark Strait. ICES. C.M. C:21, 1978. (Unpublished Document.)

[191] ROSS, C.K. and MEINCKE, J. Near bottom current vectors observed during ICES OVERFLOW '73 experiment, August–September 1973, B1–79–8. Bedford Institute of Oceanography, 1979.

[192] ROSS, C.K. OVERFLOW'73. Denmark Strait. volume 3. (Temperature, salinity, and sigma–T sections). *Canadian Technical Report of Hydrology and Ocean Sciences*, **16**, 1982: 1–62.

[193] ROSS, C.K. Temperature-salinity characteristics of the overflow in Denmark Strait during OVERFLOW'73. *Rapport et Procès-Verbaux des Réunions, Conseil International pour l'exploration de la Mer*, **185**, 1984: 111–119.

[194] RUDELS, B. and ANDERSON, L. Observations of the mass, heat and salt exchange through Fram Strait. Okeanografiska Institutionen, Report No. 42, Goteborgs Universitet, 1982.

[195] RUDDINAM, W.F.and MCINTYRE, A. Time-transgressive deglacial retreat of polar waters from the north Atlantic. *Quaternary Research*, **3**, 1973: 117–130.

[196] RZHEPLINSKIY, D. Calculations and investigations of oceanic circulation features in the vicinity of Iceland. *Izvestiya Atmospheric and Oceanic Physics*, **11**, 1975: 175–185.

SAELEN, O.H. Studies in the Norwegian Atlantic current. Part I: The Sognefjord section. *Geophysica Norwegica*, **20(13)**, 1959: 1–28.

Report no. changed (Mar 2006): SR-124-UU

SAELEN, O.H. Studies in the Norwegian Atlantic current. Part II: Investigations during the years of 1954–1959 in an area west of Stad. *Geophysica Norwegica*, **23(6)**, 1963: 1–82.

[197] SAETRE, R. The Atlantic inflow to the North Sea and the Skagerrak indicated by surface observations. ICES C.M., C:17, 1978. (Unpublished Document.)

[198] SANDVEN, S. and JOHANNESSEN, O.M. Temperature and salinity in the Norwegian continental shelf. Geophysical Institute, Division A, Bergen, Physical Oceanography, University of Bergen, 1983.

SARKISYAN, A.S. Deficiencies of barotropic models of oceanic circulation. *Izvestiya Atmospheric and Oceanic Physics*, **5**, 1969: 818–835.

[199] SAUNDERS, P.M. Circulation in the Eastern North Atlantic. *Journal of Marine Research*, **40 suppl.**, 1982: 641–657.

[200] SCHWIDERSK, E.W. Tides. *In*: Hurdle, B.G. *ed.* The Nordic Seas. New York, NY, Springer, 1986.

[201] SCOR WORKING GROUP 58. The Arctic ocean heat budget. SCOR Working Group 58' No. 52. Bergen, Geophysical Institute, Division A, Physical Oceanography, University of Bergen, 1979.

[202] SEMTNER, A.J.Jr. Numerical simulation of the Arctic ocean circulation. *Journal of Physical Oceanography*, **6**, 1976: 409–425.

[203] SHOR, A., MULLER, D. and JOHNSON, D. Transport of Norwegian Sea overflow. Preliminary results of Atlantis II Cruise 94, June–July 1977. ICES C.M. C:44, 1977. (Unpublished manuscript)

SKOV, N.A. The ice cover of the Greenland Sea: an evaluation of oceanographic and meteorological causes for year-to year variations. *Meddeleeser om Gronland*, **188**, 1970: 178–219.

[204] SMART, J.H. Spatial variability of major frontal systems in the north Atlantic-Norwegian Sea area: 1980–1981. *Journal of Physical Oceanography*, **14**, 1984: 185–192.

SMITH, S.M., MENARD, H.W. and SHARMAN, G. World-wide ocean depths and continental elevations averaged for areas approximating one degree square of latitude and longitude. Ref. Rep. 65–8. Scripps Institution of Oceanography, 1965.

[205] SMITH, IV D.C., MORISON, J.H. et al. Topographic generation of an eddy at the edge of the east Greenland current. *Journal of Geophysical Research*, **89**, 1984: 8205–8208.

[206] SMITH, P.C. The dynamics of bottom boundary currents in the ocean, Ph. D. Thesis. Report No.73–4. Cambridge, Mass., Massachussets Institute of Technology, 1975.

[207] SMITH, P.C. Baroclinic instability in Denmark Strait overflow. *Journal of Physical Oceanography*, **6**, 1976: 355–371.

[208] SOLONITSINA, L.R. Hydrographic conditions in Norwegian Sea water in 1978. *Annales Biologiques*, **35**, 1978: 64–67.

STEELE, J.H. Observations of deep water overflow across the Iceland-Færœ Ridge. *Deep-Sea Research*, **6**, 1959: 69–72.

STEELE, J.H., BARRETT, J.R. and WORTHINGTON, L.V. Deep currents south of Iceland. *Deep-Sea Research*, **9**, 1962: 465–474.

STEELE, J.H. Notes on the deep water overflow across the Iceland-Færœ Ridge. *Rapport et Procès-Verbaux des Réunions, Conseil International pour l'Exploration de la Mer*, **149**, 1961: 84–88.

STEFANSSON, U. North Icelandic water. *Rit Fiskideildar*, **3**, 1962.

STEFANSSON, U. Dissolved nutrients, oxygen and water masses in the northern Irminger Sea. *Deep-Sea Research*, **15**, 1968a: 541–575.

STEFANSSON, U. Nitrate - Phosphate relationship in the Irminger Sea. Journal du Conseil, ICES 32(2), 1968b.

STEFANSSON, U. Temperature variations in the North Icelandic coastal area during recent decades. *Jokull*, **19**, 1969: 18–28.

[209] STEFANSSON, U. Near-shore fluctuation of the frontal zone southeast of Iceland. *Rapport et Procès-Verbaux des Réunions, Conseil International pour l'Exploration de la Mer*, **162**, 1972: 201–205.

[210] STEIN, M. Observations on the variability of the outflow of Greenland Sea through the Denmark Strait. *Berichte der Deutschen Wissenschaftlichen Kommission*, **23**, 1974: 337–351.

[211] STEIN, M. Profiling current meter measurement on board of R/V *'Bjarni Saemundsson'* during OVERFLOW '73. ICES C.M. C: 43, 1974. (Unpublished Document.)

[212] STEIN, M. Fine-structure contamination of internal wave data in the Norwegian Sea. *Meteor Forschungsergebnisse*, **19**, 1977: 18–23.

STOKS, T. The depth conditions of the Northern Seas. *Deutsche Hydrographische Zeitschrift*, **3**, 1950: 93–100.

[213] SWIFT, J.H. and AAGAARD, K. The role of the Denmark Strait overflow in the circulation of the North Atlantic. ICES C.M. C:46, 1978. (Unpublished Document.)

[214] SWIFT, J.H., AAGAARD, K. and MALMBERG, S.A. The contribution of the Denmark Strait overflow to the deep north Atlantic. *Deep-Sea Research*, **27**, 1980: 29–42.

[215] SWIFT, J.H. Seasonal processes in the Iceland Sea, with especial reference to their relationship to the Denmark Strait overflow. Ph. D. Thesis, University of Washington, 1980: 1–296.

[216] SWIFT, J.H. and AAGAARD, K. Seasonal transitions and water mass formation in the Iceland and Greenland Seas. *Deep-Sea Research*, **28**, 1981: 1107–1129.

[217] SWIFT, J.H., TAKAHASHI, T. and LIVINGSTON, H.D. The contribution of the Greenland and Barents Seas to the deep water of the Arctic Ocean. *Journal of Geophysical Research*, **88**, 1983: 5981–5986.

[218] SWIFT, J.H. The circulation of the Denmark Strait and Iceland-Scotland overflow waters in the north Atlantic. *Deep-Sea Research*, **31**, 1984: 1339–1355.

[219] SWIFT, J.H. The Arctic waters. *In*: Hurdle, B.G. *ed.* The Nordic Seas. New York, NY, Springer, 1986: 124–153.

TAIT, J.B. Recent oceanographycal investigations in the Færœ-Shetland Channel. *Proceedings of the Royal Society of Edinburgh*, **64 (A)**, 1957: 239–289.

TAIT, J.B. and MARTIN, J.H.A. The Atlantic current and water masses in the Færœ-Shetland Channel and over the Iceland-Færœ Ridge during the I.G.Y. *Rapport et Procès- Verbaux des Réunions, Conseil International pour l'exploration de la Mer*, **149**, 1961: 60–83.

[220] TAN, F.C., DYRSSEN, D. and STRAIN, P.M. Sea ice meltwater and excess alkalinity in the east Greenland current. *Oceanologica Acta*, **6**, 1983: 283–288.

[221] TEAGUE, W.J. CTD profiles in the northeast Atlantic and Norwegian Sea. September–November 1980, data summmary, volume II. NSTL Station, MS, US Naval Oceanographic Office, 1981.

[222] TEAGUE, W.J. CTD profiles in the northeast Atlantic and Norwegian Sea. April–May 1981, data summary, volume I. NSTL station, MS, US Naval Oceanographic Office, 1981.

[223] TEAGUE, W.J. and VON ZWECK, O.H. Variability in the mixed layer depth near the Iceland Færœ-Polar front during spring 1981, TR–289, NSTL Station, MS, US Naval Oceanographic Office, 1982.

TIMOFEYEV, V.T. An approximate determination of the heat balance of the Arctic Basin water. *Problemy Arktiki*, **4**, 1958: 23–28. [Translation: American Meteorological Society TR–164.]

TIMOFEYEV, V.T. The movement of Atlantic water and heat into the Arctic sea basin. *Deep-Sea Research*, **9**, 1962: 358–361.

TIMOFEYEV, V.T. Interaction of the Arctic ocean waters with Atlantic and Pacific waters. *Okeanologiya*, **3**, 1963: 569–578.

[224] TRANGELED, S. Oceanography of the Norwegian and Greenland Seas and adjacent areas. volume I. Bibliography. SACLANTCEN SM–4. La Spezia, Italy, SACLANT ASW Research Centre, 1973.

[225] TRANGELED, S. Oceanography of the Norwegian and Greenland Seas and adjacent areas. volume 2: Survey of 1870–1970 literature. SACLANTCEN SM–4, La Spezia, Italy, SACLANT ASW Research Centre, 1974.

TRIPP, R.B. and KUS UNOKI, K. Physical, chemical and current data from Arlis II: eastern Arctic Ocean, Greenland Sea, and Denmark Strait area, February 1964–May 1965, TR 186. University of Washington, Department of Oceanography, 1967.

[226] TUCKER, W.B .III. A comparison of sea ice mode results using three different wind forcing fields. CRREL–SR–82–16 US Army Cold Regions Research and Engineering Laboratory, Hanover, New Hampshire 03755, 1982.

[227] TYAGUNOVA, O.V. Large-scale temporal variations of hydrological conditions in the Denmark Strait and adjacent areas. ICES C.M. C:19, 1979. (Unpublished Document.)

[228] VILMUNDARSON, T. Evaluation of historical sources on sea ice near Iceland. *In*: Karlsson, T. *ed.* Sea Ice. Reykjavik, National Research Council of Iceland, 1972.

[229] VINJE, T.E. Sea ice studies in the Spitsbergen-Greenland area. Springfield, VA., National Technical Information Service, 1977a.

[230] VINJE, T.E. Sea ice conditions in the European sector of the marginal seas of the Arctic, 1966–75. *Arbok, Norsk Polarinstitutt*, 1977b: 163–174.

VOWINCKEL, E. and ORVIG, S. Water balance and heat flux of the Arctic Ocean. *McGill University Publication in Meteorology*, **44**, 1961.

VOWINCKEL, E. and ORVIG, S. Incoming and absorbed solar radiation at the ground in the Arctic. *Archiv für Meteorologie, Geophysik, und Bioklimatologie*, **13 B** 1964a: 352–377.

VOWINCKEL, E. and ORVIG, S. Long wave radiation and total radiation balance at the surface in the Arctic. *Archiv für Meteorologie, Geophysik, und Bioklimatologie*, **13 B**, 1964b: 451–479.

VOWINCKEL, E. and ORVIG, S. Radiation balance of the troposphere and of the Earth atmosphere in the Arctic. *Archiv für Meteorologie, Geophysik, und Bioklimatologie*, **13 B**, 1964c: 451–502.

VOWINCKEL, E. and ORVIG, S. The climates of the North Polar Basin. *In*: Orvig, S., *ed.* World Survey of Climatology, volume 14. Climate of the Polar regions, New York, NY, Elsevier, 1970: 129–226.

URALOV, N.S. On the influence of the North Cape current on the freezing of the Barent Sea. GOIN, Trudy, 37, 1959: 14–33.

[231] WADHAMS, P., GILL, A.E. and LINDEN, P.F. Transects by submarine of the East Greenland Polar Front. *Deep-Sea Research*, **26**, 1979: 1311–1327.

[232] WADHAMS, P. A comparison of sonar and laser profiles along corresponding tracks in the Arctic ocean. *In*: Pritchard, R.S., *ed.* Sea Ice Processes and Models. Seattle,University of Washington Press, 1980: 283–289.

[233] WADHAMS, P. The ice cover in the Greenland and Norwegian Sea. *Review of Geophysics and Space Physics*, **19**, 1981: 345–393.

[234] WADHAMS, P. and SQUIRE, V.A. An ice-water vortex at the edge of the east Greenland Current. *Journal of Geophysical Research*, **88**, 1983: 2770–2780.

[235] WADHAMS, P. Arctic Sea ice morphology and its measurement. *ed.* Arctic Technology and Policy. Proceedings Second Annual MIT Sea Grant College, Program, Lecture and Seminar. New York, NY, McGraw-Hill, 1983: 179–195.

[236] WADHAMS, P. The ice cover. *In*: Hurdle, B.G. *ed.* The Nordic Seas. New York, NY, Springer, 1986: 21–84.

[237] WALKER, E.R. and WADHAMS, P. Thick sea-ice floes. *Arctic*, **32**, 1979: 140–147.

[238] WEECKS, W. Physical properties of the ice cover of the Greenland Sea, CRREL–SR–82–28. Hanover, NH, US Army Cold Regions Research and Engineering Laboratory, 1986.

WEYL, P.K. The role of the oceans in climate change: a theory of the ice ages. (Unpublished Document) Corvallis, Oregon State University, 1966.

WICHETT, W.P. Transport computations for the Norvegian Sea 1950–1954. TR 71. Nanaimo, B.C., Fisheries Research Board of Canada. Biological Station, 1968.

[239] WILLEBRAND, J. Temporal and spatial scales of the wind field over the north Pacific and north Atlantic. *Journal of Physical Oceanography*, **8**, 1978: 1080–1094.

[240] WILLEBRAND, J. and MEINKE, J. Statistical analysis of fluctuations in the Iceland-Scotland frontal zone. *Deep- Sea Research*, **27**, 1980: 1047–1066.

[241] WILLEBRAND, J., PHILANDER, S.G.H. and PACANOWSKI, R.C. The oceanic response to large-scale atmospheric disturbances. *Journal of Physical Oceanography* , **10**, 1980: 411–429.

WORTHINGTON, L.V. An attempt to measure the volume transport of Norwegian Sea water through the Denmark Strait. *Deep-Sea Research*, **16**, supplement, 1969: 421–432.

WORTHINGTON, L.V. and VOLKMANN, G.H. The volume transport of the Norwegian Sea OVERFLOW water in the North Atlantic. *Deep-Sea Research*, **12**, 1965: 667–676.

WORTHINGTON, L.V. The Norwegian sea as a Mediterranean Basin. *Deep-Sea Research*, **17**, 1970: 77–84.

WÜST, P.J. The morphological and oceanographic relations in the North Polar Basin. *Arktis*, **6**, 1942: 1–21.

ZAITSEV, G.N. The heat balance of the Norwegian and Greenland seas and factors of its formation. Soviet Fisher. Invest. North European Seas, 1960: 46–52.

ZAITSEV, G.N., FEDOSOV, M.V., ILJINA, N.L. and ERMACHENKO, I.A. Components of the water, thermic and chemical budget of the Greenland and Norwegian seas. *Rapport et Procès-Verbaux des Réunions, Conseil International pour l'Exploration de la Mer*, **149**, 1961: 46–52.

[242] ZARIPOV, B.R. and RZHEPLINSKIY, D.G. Long term average seasonal water circulation of the northeastern Atlantic and of the Norwegian, Greenland and north Seas. (Diagnostic calculations). *Oceanology*, **17**, 1977: 520–524.

ZLOBIN, V.S., SAPRONETSKAYA, N.G. and ALEKSEYEVA, A.G. Some data on the hydrochemical regime and primary production in Norwegian Sea. PINRO, volume XI, 1968: 133–144. (Trans. No. 500 US Naval Oceanographic Office, Washington D.C. 20390, 1970.

ZUBOV, N.N. Arctic ICE . (In Russian). Izdatel'stvo Glavsermorputi, Moscow (English translation by US Naval Oceanographic Office, Bay St. Louis, Miss, 1945.

[243] ZWECK, VON O.H. and TEAGUE, W.J. Towed CTD measurements in the northeast Atlantic and Norwegian Sea, data summary, measurements program. NSTL Station, MS, US Naval Oceanographic Office, 1981.